

THESIS

**HYDRAULIC MODELING AND MEANDER MIGRATION OF THE
MIDDLE RIO GRANDE, NEW MEXICO**

Submitted by

Michael J. Sixta

Department of Civil Engineering

In partial fulfillment of the requirements

For the Degree of Master of Science

Colorado State University

Fort Collins, Colorado

Spring 2004

COLORADO STATE UNIVERSITY

November 7, 2003

WE HEREBY RECOMMEND THAT THE THESIS PREPARED UNDER OUR SUPERVISION BY **MICHAEL J. SIXTA** ENTITLED **HYDRAULIC MODELING AND MEANDER MIGRATION OF THE MIDDLE RIO GRANDE, NEW MEXICO** BE ACCEPTED AS FULFILLING IN PART REQUIREMENTS FOR THE DEGREE OF MASTER OF SCIENCE.

Committee on Graduate Work

Adviser

Department Head

ABSTRACT OF THESIS

HYDRAULIC MODELING AND MEANDER MIGRATION OF THE MIDDLE RIO GRANDE, NEW MEXICO

The dynamic characteristics of the Middle Rio Grande (MRG) in central New Mexico have been of both interest and concern for the regulatory agencies involved with its management. The MRG has experienced sedimentation problems, prompting the development and implementation of sediment detention and flood control features, including the construction of Cochiti Dam in 1973, whose effects have been significant and extensively studied.

The San Felipe Reach was examined for a hydraulic modeling analysis (HMA), driven by the understanding of historic, current and potential future geomorphic characteristics of the channel. Analysis of water and suspended sediment data, aerial photographs, cross section surveys and bed material size, reveal the temporal and spatial changes in the processes that act on the channel.

Geomorphic analyses indicated that the general trends of the San Felipe Reach included a decrease in width, width-to-depth ratio, wetted perimeter and cross sectional area and an increase in velocity and depth during the 1962-1998 time period, while the channel planform remained straight with a sinuosity close to 1.2. The reach average active channel width decreased from 580 feet in 1918 to 219 feet in 2001. Since construction of Cochiti Dam, the channel bed degraded by approximately 4 feet, resulting in a coarsening of the bed material from a fine sand to a coarse gravel. Calculated transport capacities were comparable to the incoming bed material load of

1,900 tons/day, indicating the channel slopes in 1992 and 1998 were able to transport the incoming bed material load at a channel forming discharge of 5,000 cfs.

The Galisteo Reach was utilized in performing a meander migration analysis (MMA). This work involved the development and analysis of datasets to identify trends in curvature and migration rates of isolated bends over a 20-year time period (1972-1992), to ultimately predict future migration trends to aid in restoration efforts. Research was conducted based on the variables that most influence bend migration rates while at the same time examining such previous studies as Hickin and Nanson (1984), and Rozovskii (1957).

Trends in bend curvatures on the Galisteo Reach were not readily apparent due to the reach having non-typical meandering characteristics. Small secondary flow deviation angles (<15 degrees) indicated a channel in a state of equilibrium. Sine curves indicated greater channel curvature after Cochiti Dam was in place. Higher, more frequent discharge peaks were observed during a period that did not consistently exhibit higher migration rates indicating additional dominant forces outside of discharge. Specific stream power calculations indicated a medium-energy floodplain. Positive increasing trends were found between migration rates and width-to-depth ratios.

To make a definitive claim of where the channel will be in the future would be presumptuous. However, through analyzing results from both analyses, rates of lateral movement are expected to slow in the future as the channel approaches a state of quasi-equilibrium. This prediction assumes future hydrologic and sediment regimes to be similar to those of the past 30 years.

Michael Joseph Sixta
Civil Engineering Department
Colorado State University
Fort Collins, CO 80523
Spring 2004

ACKNOWLEDGEMENTS

First and foremost, I would like to express my deepest appreciation to my adviser Dr. Pierre Julien for his continual guidance not only with this study, but also with my entire graduate school program. I would also like to thank the U.S. Bureau of Reclamation, in particular Drew Baird, for the opportunity to work on the Rio Grande, and for contributing the topic for my thesis work. In addition, I would like to extend my thanks to my other committee members, Dr. Chester Watson of the Civil Engineering Department and Dr. Sara Rathburn of the Geosciences Department.

Thanks to Claudia Leon for the development of the Rio Grande database, help with the Bureau reports, your guidance, support and answers to my constant questions. I would also like to extend a special thanks to the rest of the team; Rosalia, Mark, John and Jason. I'm extending special thanks to Mark for help with class and thesis work, workouts, lunches and your continual encouragement; and to Jason for help with the reports, keeping the office atmosphere fun and exciting and for being a great roommate.

I would like to thank other friends/co-workers including Brian, Jamis, Chance, Sarah, Patrick (Tex) and Jeff (Precious) for lots of good times and memories. I would like to make a special acknowledgment to Mark (Baller) Tiaht for being more than just a friend, roommate and landlord; your character, friendship and support is something that I will always remember.

Finally, I would like to thank my parents Dave and Sue for their continual support both emotionally and financially throughout my studies. And thanks to my brother Rob and my sister Anne for their unconditional love. I love you all.

I have never seen a river that I could not love. Moving water... has a fascinating vitality. It has power and grace and associations. It has a thousand colors and a thousand shapes, yet it follows laws so definite that the tiniest streamlet is an exact replica of a great river.

– Roderick Haig-Brown

TABLE OF CONTENTS

ABSTRACT OF THESIS	iii
ACKNOWLEDGEMENTS	v
TABLE OF CONTENTS	vii
LIST OF FIGURES	ix
LIST OF TABLES	xii
LIST OF EQUATIONS.....	xv
LIST OF SYMBOLS	xvi
LIST OF ACRONYMNS	xviii
CHAPTER 1: INTRODUCTION.....	1
CHAPTER 2: LITERATURE REVIEW.....	4
2.1 Introduction.....	4
2.2 Hydraulic Modeling Analysis (HMA)	6
2.2.1. Site Background	6
2.2.2. Hydrology and Climate	11
2.3 Meander Migration Analysis (MMA)	13
2.3.1. Background.....	13
2.3.2. Terminology	14
2.3.3. Equilibrium versus Stability.....	15
2.3.3.1. Equilibrium	16
2.3.3.2. Stability	17
2.3.4. Causes of Migration.....	19
2.3.5. Studies and Analysis Work.....	21
2.3.5.1. Bend Curvature (Hickin and Nanson)	21
2.3.5.2. Secondary Flow (Rozovskii)	24
2.3.5.3. Additional Analyses.....	26
2.4 Available Data	28
2.5 Summary	30
CHAPTER 3: HYDRAULIC MODELING ANALYSIS (HMA)	31
3.1 Introduction.....	31
3.2 Reach Background	32
3.2.1. Reach Definition	32
3.2.2. Available Data.....	32
3.2.3. Channel Forming Discharge	33
3.3 Geomorphic Characterization.....	35
3.3.1. Channel Classification	35
3.3.2. Sinuosity	39
3.3.3. Longitudinal Profile	40
3.3.4. Channel Cross Sections	42
3.3.5. Channel Geometry.....	43
3.3.5.1. Width.....	45
3.3.6. Bed Material.....	46
3.4 Suspended Sediment and Water History	50
3.4.1. Single Mass Curves.....	50
3.4.1.1. Discharge Mass Curve.....	50
3.4.1.2. Suspended Sediment Mass Curve	51
3.4.2. Double Mass Curves	52
3.5 Sediment Transport Analysis.....	54
3.6 Summary and Conclusions.....	62

CHAPTER 4: MEANDER MIGRATION ANALYSIS (MMA)	67
4.1 Introduction	67
4.2 Reach Background	67
4.2.1. Reach Definition	67
4.2.2. Bend Definition	68
4.2.3. Available Data	70
4.2.4. Photograph Error Analysis	71
4.3 Dataset Development (GIS Methodology)	74
4.3.1. Radius of Curvature Dataset (3-point Methodology)	74
4.3.2. Radius of Curvature Dataset (Nanson and Hickin Methodology)	78
4.3.3. Migration Dataset	79
4.3.4. HEC-RAS® Dataset	83
4.4 Data Analysis and Results	83
4.4.1. Curvature Analysis (Hickin and Nanson – 1984)	83
4.4.2. Secondary Flow Analysis (Rozovskii – 1957)	85
4.4.3. Sine Curve Analysis	87
4.4.4. Hydrological Analysis	88
4.4.5. Stream Power/Specific Stream Power Analysis	91
4.4.6. Additional Analyses	92
4.5 Summary and Conclusions	94
CHAPTER 5: SUMMARY AND CONCLUSIONS	98
5.1 Introduction	98
5.2 HMA	98
5.3 MMA	99
5.4 Conclusions	100
REFERENCES	102
APPENDIX A: Aerial Photograph Data	110
APPENDIX B: Location Maps (San Felipe Reach)	133
APPENDIX C: Available Data (San Felipe Reach)	139
APPENDIX D: Cross Sections (San Felipe Reach)	142
APPENDIX E: Annual Peak Mean Discharges	146
APPENDIX F: HEC-RAS® Modeling Results	148
APPENDIX G: Bed Material Histograms and Statistics	150
APPENDIX H: Double Mass Curve (1956-1999)	155
APPENDIX I: Sediment Transport Work	157
APPENDIX J: Location Maps (Galisteo Reach)	183
APPENDIX K: Radius of Curvature Dataset (3-Point Methodology)	190
APPENDIX L: Radius of Curvature Dataset (Nanson and Hickin Methodology)	211
APPENDIX M: Migration Dataset	222
APPENDIX N: Curvature Plots	247
APPENDIX O: Sine Generated Curves	252
APPENDIX P: Migration (M) and Width-to-Depth (W/h) Ratio Trends	256

LIST OF FIGURES

Figure 2-1: Location of study subreaches in relation to Cochiti Reach, Rio Grande, NM showing locations of pertinent USGS gaging stations.....	5
Figure 2-2: Annual suspended sediment yield in the Rio Grande in tons/year at Otowi gage (upstream of Cochiti Dam), Cochiti gage (just downstream of Cochiti Dam) and Albuquerque gage (downstream of Cochiti gage) from 1974 to 2000. Cochiti gage record ends in 1988.....	8
Figure 2-3: 1995 Rio Grande spring runoff hydrographs.....	12
Figure 2-4: Terminology depiction.....	15
Figure 2-5: Relative migration rates (Hickin and Nanson, 1984).....	22
Figure 3-1: Maximum mean daily annual discharge in cfs on the Rio Grande at San Felipe (1927-1999).....	34
Figure 3-2: Maximum mean daily annual discharge frequency histograms on the Rio Grande at San Felipe (1927 – 2001).....	35
Figure 3-3: Non-vegetated active channel of the San Felipe Reach. 1918 planform from topographic survey. All other planforms from aerial photographs.	36
Figure 3-4: Time series of sinuosity of the San Felipe Reach as measured from the digitized aerial photographs.	39
Figure 3-5: Longitudinal mean bed elevation profile to San Felipe Reach for 1962, 1972, 1992 and 1998.	41
Figure 3-6: Cross section CO-22 (San Felipe Reach) representing pre-dam and post-dam construction.....	42
Figure 3-7: Average main channel geometry from HEC-RAS® results for Q = 5,000 cfs. (a) Velocity, (b) Cross-sectional area, (c) Depth, (d) W/h, (e) Wetted perimeter.....	44
Figure 3-8: Active channel width from digitized aerial photographs.....	46
Figure 3-9: Comparison of bed material gradation curves for 1961, 1972, 1992 and 1998.	48
Figure 3-10: Histogram depicting the D ₅₀ and D ₈₄ change with time for CO-20.....	49
Figure 3-11: Discharge mass curve at the San Felipe gage (1927 – 2000).....	51
Figure 3-12: Suspended sediment mass curve at Bernalillo and Albuquerque gages (1956 – 1999).....	52
Figure 3-13: Cumulative discharge at San Felipe gage vs. cumulative suspended sediment load at Bernalillo and Albuquerque gages (1956 – 1999).....	53
Figure 3-14: Sediment transport capacity and supply curves (Julien, 1998).....	54
Figure 3-15: Albuquerque gage sand load rating curve for the spring and summer seasons from 1978 to 1999.....	57
Figure 3-16: Example of bed material load estimation methodology from 1992 BI-line surveys.....	61
Figure 4-1: Subreach time series of sinuosities along Cochiti Reach.	68
Figure 4-2: Bend selection along Galisteo Reach used in the MMA.....	69
Figure 4-3: Radius of curvature features used in 3-point methodology.....	76
Figure 4-4: Example of 3-point methodology used in radius of curvature calculation.....	77

Figure 4-5: Example of mean radius of curvature calculation using the Nanson and Hickin (1983) methodology.....	79
Figure 4-6: Example of migration rate calculation from bend 3 for the 1972-1985 time period.	81
Figure 4-7: Bend averaged relative migration rate versus r_m/W	84
Figure 4-8: Sine-generated curves for bend 2.	88
Figure 4-9: Mean daily flow (cfs) at San Felipe (1972-1992).	89
Figure 4-10: M versus W/h for 1972-1985 time period (Galisteo Reach).....	93
Figure B-1: 2001 river planform of the San Felipe Reach displaying locations of the agg/deg lines.	134
Figure B-2: 2001 river planform of the San Felipe Reach displaying locations of the CO-lines.	135
Figure B-3: Aerial photograph of San Felipe Reach (photo 1 of 3).	136
Figure B-4: Aerial photograph of San Felipe Reach (photo 2 of 3).	137
Figure B-5: Aerial photograph of San Felipe Reach (photo 3 of 3).	138
Figure D-1: Cross sections CO-17 and CO-18 (San Felipe Reach) representing pre-dam and post-dam construction.	143
Figure D-2: Cross sections CO-19 and CO-20 (San Felipe Reach) representing pre-dam and post-dam construction.	144
Figure D-3: Cross sections CO-21 and CO-23 (San Felipe Reach) representing pre-dam and post-dam construction.	145
Figure E-1: Annual peak discharge in cfs at Bernalillo (1941-1969).	147
Figure E-2: Annual peak discharge in cfs at Albuquerque (1942-1999).....	147
Figure F-1: Active channel widths from HEC-RAS® modeling.	149
Figure G-1: Histograms depicting the D_{50} and D_{84} change with time for CO-17 and CO-18 (San Felipe Reach).	151
Figure G-2: Histograms depicting the D_{50} and D_{84} change with time for CO-19 and CO-21 (San Felipe Reach).	152
Figure G-3: Histograms depicting the D_{50} and D_{84} change with time for CO-22 and CO-23 (San Felipe Reach).	153
Figure H-1: Double mass curve from Rio Grande at Bernalillo and Rio Grande at Albuquerque (1956 – 1999).....	156
Figure I-1: Bed material and suspended material gradation curves from BI-survey lines for 1992.	176
Figure I-2: Bed material and suspended material gradation curves from BI-survey lines for 1993.	177
Figure I-3: Bed material and suspended material gradation curves from BI-survey lines for 1994.	178
Figure I-4: Bed material and suspended material gradation curves from BI-survey lines for 1995.	179
Figure J-1: 2001 river planform of the Galisteo Reach displaying locations of the agg/deg lines.	184
Figure J-2: 2001 river planform of the Galisteo Reach displaying locations of the CO-lines.	185
Figure J-3: Aerial photograph of Galisteo Reach (photo 1 of 4).....	186
Figure J-4: Aerial photograph of Galisteo Reach (photo 2 of 4).....	187
Figure J-5: Aerial photograph of Galisteo Reach (photo 3 of 4).....	188
Figure J-6: Aerial photograph of Galisteo Reach (photo 4 of 4).....	189
Figure M-1: Migration of bend 1 (1972-1992).	223
Figure M-2: Migration of bend 2 (1972-1992).	224

Figure M-3: Migration of bend 3 (1972-1992).	225
Figure M-4: Migration of bend 4 (1972-1992).	226
Figure M-5: Migration of bend 5 (1972-1992).	227
Figure M-6: Migration of bend 6 (1985-1992).	228
Figure M-7: Migration of bend 7 (1972-1992).	229
Figure N-1: Relative migration rate versus r_m/W (apex area averaged).	248
Figure N-2: Relative migration rate versus R_{min}/W (bend averaged).	248
Figure N-3: Relative migration rate versus R_{min}/W (apex area averaged).	249
Figure N-4: Migration rate versus r_m/W (bend averaged).	249
Figure N-5: Migration rate versus r_m/W (apex area averaged).	250
Figure N-6: Migration rate versus R_{min}/W (bend averaged).	250
Figure N-7: Migration rate versus R_{min}/W (apex area averaged).	251
Figure O-1: Sine generated curves for bend 1 (1972, 1985 and 1992).	253
Figure O-2: Sine generated curves for bend 3 (1972, 1985 and 1992).	253
Figure O-3: Sine generated curves for bend 4 (1972, 1985 and 1992).	254
Figure O-4: Sine generated curves for bend 5 (1972, 1985 and 1992).	254
Figure O-5: Sine generated curves for bend 6 (1985 and 1992).	255
Figure O-6: Sine generated curves for bend 7 (1972, 1985 and 1992).	255
Figure P-1: M versus W/h for 1985-1992 time period (Galisteo Reach).	257
Figure P-2: M versus W/h for 1972-1985 time period (apex area).	257
Figure P-3: M versus W/h for 1985-1992 time period (apex area).	258
Figure P-4: M versus W/h for 1972-1985 time period (bends 1,2,3,4,5 and 7).	258
Figure P-5: M versus W/h for 1985-1992 time period (all bends).	259
Figure P-6: M versus W/h for 1985-1992 time period (bends 1,2,3,5 and 7).	259
Figure P-7: M versus W/h for 1985-1992 time period (bends 1,2,5 and 7).	260

LIST OF TABLES

Table 3-1: Channel pattern classification for 1962, 1972, 1992 and 1998.....	38
Table 3-2: Percentages of total load that behave as washload and bed material load at flows close to 5,000 cfs; taken from BI-line surveys.....	55
Table 3-3: Summarized sediment transport results for 1962 and 1972.....	64
Table 3-4: Summarized sediment transport results for 1992 and 1998.....	64
Table 4-1: Average depth (feet) of each bend based on HEC-RAS® analysis.....	83
Table 4-2: Bend averaged deviation angles.....	86
Table 4-3: Average specific stream power for each bend during two time periods.....	92
Table A-1: Aerial Photograph Data (Source: Richard et al. 2001).....	111
Table A-2: Aerial photograph dates and mean daily discharge on those days.....	112
Table C-1: Periods of record for discharge and continuous suspended sediment data collected by the USGS.....	140
Table C-2: Periods of record for bed material particle size distribution data collected by the USGS.....	140
Table C-3: Surveyed dates for bed material particle size distribution data at CO-lines and SFP-lines collected by the USBR.....	140
Table C-4: Surveyed dates for the Cochiti range lines collected by the USBR.....	141
Table F-1: HEC-RAS® results.....	149
Table G-1: Median grain size statistics from material samples at Bernalillo gage, San Felipe gage, and CO-lines.....	154
Table I-1: Bed material and suspended material gradation data for BI-286, BI-291 and BI-296 (1992-1995).....	158
Table I-2: Bed material load analysis summary utilizing results from the Modified Einstein Procedure (MEP).....	180
Table I-3: Suitability of bedload and bed material load transport equations (Stevens and Yang, 1989).....	181
Table I-4: Hydraulic input data for sediment transport capacity computations from 1962, 1972, 1992 and 1998 HEC-RAS® runs at 5,000 cfs.....	181
Table I-5: Bed material load and bedload transport capacity for 1962 and 1972.....	182
Table I-6: Bed material load and bedload transport capacity for 1992 and 1998.....	182
Table K-1: Radius of curvature calculations for bend 1 (1972).....	191
Table K-2: Radius of curvature calculations for bend 1 (1985).....	192
Table K-3: Radius of curvature calculations for bend 1 (1992).....	193
Table K-4: Radius of curvature calculations for bend 2 (1972).....	194
Table K-5: Radius of curvature calculations for bend 2 (1985).....	195
Table K-6: Radius of curvature calculations for bend 2 (1992).....	196
Table K-7: Radius of curvature calculations for bend 3 (1972).....	197
Table K-8: Radius of curvature calculations for bend 3 (1985).....	198
Table K-9: Radius of curvature calculations for bend 3 (1992).....	199
Table K-10: Radius of curvature calculations for bend 4 (1972).....	200
Table K-11: Radius of curvature calculations for bend 4 (1985).....	201
Table K-12: Radius of curvature calculations for bend 4 (1992).....	202

Table K-13: Radius of curvature calculations for bend 5 (1972).....	203
Table K-14: Radius of curvature calculations for bend 5 (1985).....	204
Table K-15: Radius of curvature calculations for bend 5 (1992).....	205
Table K-16: Radius of curvature calculations for bend 6 (1985).....	206
Table K-17: Radius of curvature calculations for bend 6 (1992).....	207
Table K-18: Radius of curvature calculations for bend 7 (1972).....	208
Table K-19: Radius of curvature calculations for bend 7 (1985).....	209
Table K-20: Radius of curvature calculations for bend 7 (1992).....	210
Table L-1: Mean radius of curvature calculation for bend 1 (1972).....	212
Table L-2: Mean radius of curvature calculation for bend 1 (1985).....	212
Table L-3: Mean radius of curvature calculation for bend 1 (1992).....	213
Table L-4: Mean radius of curvature calculation for bend 2 (1972).....	213
Table L-5: Mean radius of curvature calculation for bend 2 (1985).....	214
Table L-6: Mean radius of curvature calculation for bend 2 (1992).....	214
Table L-7: Mean radius of curvature calculation for bend 3 (1972).....	215
Table L-8: Mean radius of curvature calculation for bend 3 (1985).....	215
Table L-9: Mean radius of curvature calculation for bend 3 (1992).....	216
Table L-10: Mean radius of curvature calculation for bend 4 (1972).....	216
Table L-11: Mean radius of curvature calculation for bend 4 (1985).....	217
Table L-12: Mean radius of curvature calculation for bend 4 (1992).....	217
Table L-13: Mean radius of curvature calculation for bend 5 (1972).....	218
Table L-14: Mean radius of curvature calculation for bend 5 (1985).....	218
Table L-15: Mean radius of curvature calculation for bend 5 (1992).....	219
Table L-16: Mean radius of curvature calculation for bend 6 (1985).....	219
Table L-17: Mean radius of curvature calculation for bend 6 (1992).....	220
Table L-18: Mean radius of curvature calculation for bend 7 (1972).....	220
Table L-19: Mean radius of curvature calculation for bend 7 (1985).....	221
Table L-20: Mean radius of curvature calculation for bend 7 (1992).....	221
Table M-1: Migration rate input data for bend 1 (1972).....	230
Table M-2: Migration rate input data for bend 1 (1985).....	230
Table M-3: Migration rate input data for bend 1 (1992).....	231
Table M-4: Migration rate input data for bend 2 (1972).....	231
Table M-5: Migration rate input data for bend 2 (1985).....	232
Table M-6: Migration rate input data for bend 2 (1992).....	232
Table M-7: Migration rate input data for bend 3 (1972).....	233
Table M-8: Migration rate input data for bend 3 (1985).....	233
Table M-9: Migration rate input data for bend 3 (1992).....	234
Table M-10: Migration rate input data for bend 4 (1972).....	234
Table M-11: Migration rate input data for bend 4 (1985).....	235
Table M-12: Migration rate input data for bend 4 (1992).....	235
Table M-13: Migration rate input data for bend 5 (1972).....	236
Table M-14: Migration rate input data for bend 5 (1985).....	236
Table M-15: Migration rate input data for bend 5 (1992).....	237
Table M-16: Migration rate input data for bend 6 (1985).....	237
Table M-17: Migration rate input data for bend 6 (1992).....	238
Table M-18: Migration rate input data for bend 7 (1972).....	238
Table M-19: Migration rate input data for bend 7 (1985).....	239
Table M-20: Migration rate input data for bend 7 (1992).....	239
Table M-21: Migration rate calculations for bend 1 (1972-1992).....	240
Table M-22: Migration rate calculations for bend 2 (1972-1992).....	241

Table M-23: Migration rate calculations for bend 3 (1972-1992).....	242
Table M-24: Migration rate calculations for bend 4 (1972-1992).....	243
Table M-25: Migration rate calculations for bend 5 (1972-1992).....	244
Table M-26: Migration rate calculations for bend 6 (1985-1992).....	245
Table M-27: Migration rate calculations for bend 7 (1972-1992).....	246

LIST OF EQUATIONS

Equation 2-1: Lane's relationship.....	16
Equation 2-2: Migration rate regression.....	23
Equation 2-3: Deviation angle calculation.....	25
Equation 2-4: Stream power calculation.....	27
Equation 3-1: Mean bed elevation calculation.....	40
Equation 4-1: Calculations used in 3-point methodology.....	76
Equation 4-2: Calculations used in migration rate determination.....	82
Equation 4-3: Migration rate calculation.....	82
Equation 4-4: Minimum radius of curvature calculation.....	85
Equation 4-5: Sinuosity calculation.....	87
Equation 4-6: Critical shear stress calculation.....	90
Equation 4-7: Equation 4-6 rewritten to solve for critical discharge.....	90

LIST OF SYMBOLS

Q – flow discharge
Q_{2Y} – 2-year instantaneous peak discharge
g – acceleration due to gravity
n – Manning’s roughness coefficient
Fr – Froude number
h – flow depth
V – flow velocity
W – active channel width
Tw – active channel top width
A – channel cross-sectional area
S – channel slope
S_f – friction slope
L – channel length along centerline
P – sinuosity
H – hydraulic depth (= A/Tw)
WP – wetted perimeter
ρ – density of water
γ_w – specific weight of water
R_h – hydraulic radius (= A/WP)
τ_c – critical shear stress
τ_{rR} – radial shear stress
τ_θ – downstream bed shear stress
Ω_R – ratio of centrifugal force to shear force
D_s – material grain size (particle diameter)
D₁₀ – effective size (particle diameter corresponding to 10% finer)
D₃₅ – effective size (particle diameter corresponding to 35% finer)
D₅₀ – effective size (particle diameter corresponding to 50% finer)
D₈₄ – effective size (particle diameter corresponding to 84% finer)
M – migration rate
M/W – relative migration rate
R – radius of curvature
R_{min} – minimum radius of curvature
R_m – mean radius of curvature
r’ – radius of inner circle (Nanson and Hickin methodology)
r’’ – radius of outer circle (Nanson and Hickin methodology)
r_m – mean radius of curvature (Nanson and Hickin methodology; = (r’ + r’’)/2)
λ – deviation angle
θ_m – maximum orientation angle
Ω – stream power
ω – specific stream power (= Ω/W)
x₁, x₂, x₃, y₁, y₂, y₃ – centerline coordinates (x_{CL}, y_{CL})

x_{BL}, y_{BL} – bankline coordinates
 x_{mid}, y_{mid} – centerline/bankline midpoint coordinates
 x_c, y_c – centroid coordinates
 m, p – midpoint line slopes
 a, c – tangent line slopes
 b, d – tangent line intercepts
 Δr – movement of right bank
 Δl – movement of left bank
 ΔW – change in width ('+' indicates widening, '-' indicates narrowing)
 Δt – time period span

LIST OF ACRONYMNS

HMA – Hydraulic Modeling Analysis
MMA – Meander Migration Analysis
MRG – Middle Rio Grande
CO – Cochiti survey lines
BI – Bernalillo Island survey lines
SFP – San Felipe Pueblo survey lines
USBR – United States Bureau of Reclamation
USGS – United States Geological Survey
USACE – United States Army Corps of Engineers
SCS – Soil Conservation Service
NRCS – National Resources Conservation Service
GIS – Geographic Information Systems
HEC-RAS® – Hydraulic Engineering Center – River Analysis System
MBE – Mean Bed Elevation
WSE – Water Surface Elevation
MEP – Modified Einstein Procedure
ADR – Advanced Digital Rectification
RMS – Root Mean Square
NMAS – National Map Accuracy Standards
NAD – North American Datum
NAD27 – 1927 North American Datum
cfs – cubic-feet-per-second (ft^3/s)
pcf – pounds-per-cubic-foot (lb/ft^3)
psf – pounds-per-square-foot (lb/ft^2)
a.k.a. – “also known as”

CHAPTER 1: INTRODUCTION

The Middle Rio Grande (MRG) is one of the most historically documented rivers in the United States. It is also 100 percent engineered, under constant supervision from regulatory agencies such as the U.S. Bureau of Reclamation (USBR) and U.S. Army Corps of Engineers (USACE). Located in north-central New Mexico, the MRG stretches approximately 143 miles between White Rock Canyon and Elephant Butte Reservoir (Lagasse, 1994). The Cochiti Reach, located on the MRG, starts just downstream of the Cochiti Dam and spans approximately 28 miles downstream to Highway 44 in Bernalillo. Utilized by Richard (2001) in quantifying and predicting lateral channel adjustments, four subreach delineations were developed based on channel characteristics and the existence of natural or manmade controls. This study focused on two of those subreaches: 1) Galisteo Reach, spanning 8.1 miles from the mouth of Galisteo Creek (agg/deg 98) to the mouth of the Arroyo Tonque (agg/deg 174); 2) San Felipe Reach, spanning 6.2 miles from the mouth of the Arroyo Tonque (agg/deg 174) to the Angostura Diversion Dam (agg/deg 236). For a complete discussion of agg/deg lines, refer to Section 2.4.

Historically, the Cochiti Reach was characterized as an aggrading sand bed channel with extensive lateral movement. Because of the flood and safety hazards posed by channel movements, the USBR and USACE initiated efforts to reduce these risks in the 1920's. Efforts included the construction of numerous diversion structures, levees and dams, culminating with the construction of Cochiti Dam, which closed in November of 1973. This dam caused significant changes downstream. The main focus

of this study was to analyze the impacts of these changes with the aim of forecasting future river conditions. Predicting how the river channel is expected to change will aid in management issues by letting agencies know how and where to focus restoration efforts. Restoration efforts in this region are particularly important due to the specific habitat needs of local endangered species such as the silvery minnow and the southwestern willow flycatcher. In attaining this objective, the approach taken was to focus research efforts on two main areas: 1) hydraulic modeling analysis (HMA); and 2) meander migration analysis (MMA).

Performed on the San Felipe Reach, the objective of the HMA was to analyze historic data to estimate pre-dam and post-dam characteristics of the reach. In achieving this objective, numerous analyses were performed including the identification of spatial and temporal trends in channel geometry by evaluation of cross section data. Also, planform classifications were performed through analyses of aerial photographs and channel geometry data. Next, temporal trends in water and sediment discharge and concentration were analyzed using U.S. Geological Survey (USGS) gaging station data. In addition, temporal trends in bed material were identified through analyses of gradation curves and histograms. This was later used in the second phase of analysis (MMA). Finally, the equilibrium state of the river was evaluated through applications of hydraulic geometry methods, empirical width-time relationships and sediment transport analyses using a Modified Einstein Procedure (MEP).

Performed on the Galisteo Reach, the objective of the MMA was to develop a group of datasets and, through the analysis of those datasets, analyze trends in curvature characteristics and migration patterns of seven isolated bends over a 20-year time period (1972-1992). Numerous analyses were executed in achieving this objective including the relationship between migration rates (M) and radius of curvature-to-width ratios (R/W) based on the study performed by Hickin and Nanson (1984). According to

this study, “channel migration rates are strongly controlled by bend curvature.” Also, secondary flow characteristics were identified through deviation angle calculations based on work from Rozovskii (1957). Next, the development of sine-generated curves was utilized to quantify the curvature of each bend as well as to see how closely each bend follows an idealized meandering planform. In addition, to try an link higher and lower points in the flow regime with higher and lower rates of migration, a hydrological analysis was conducted. Also, a stream power (Ω) analysis was performed to relate magnitudes of stream power and migration rates. A specific stream power (ω) analysis was also conducted to estimate the energy level of the floodplain. Finally, additional relationships including such variables as migration rates (M) and relative migration rates (M/W) compared with depth-to-radius of curvature (h/R) ratios and width-to-depth (W/h) ratios were inspected for possible trends.

This thesis has been developed in five chapters. Chapter 1 presents the introduction. A review of pertinent literature was performed, which is summarized in Chapter 2. As for the HMA, the literature review discusses past geomorphological studies in addition to a historical background of the MRG. As for the MMA, topics including terminology, equilibrium versus stability, causes of migration and relevant past studies are discussed. Chapter 3 presents all the analysis methodologies and results from the HMA. Chapter 4 focuses on the MMA by showing the development of the datasets, the analyses performed with those datasets and the results of those analyses. Finally, Chapter 5 summarizes the conclusions from both analyses.

CHAPTER 2: LITERATURE REVIEW

2.1 Introduction

The Rio Grande originates in south-central Colorado, flows southward through central New Mexico, and continues flowing southeast between Texas and Mexico to the Gulf of Mexico (Rittenhouse, 1944). The MRG, located in central New Mexico, comprises a reach of the river that spans approximately 143 miles between White Rock Canyon and Elephant Butte Reservoir (Lagasse, 1994). The reaches of interest for this study include the Galisteo Reach and San Felipe Reach, both of which are subreaches of the Cochiti Reach located along the MRG (see Figure 2-1). Also shown in Figure 2-1 are the locations of the pertinent gaging stations utilized in this study. The Galisteo Reach spans 8.1 miles from the mouth of Galisteo Creek (agg/deg 98) to the mouth of the Arroyo Tonque (agg/deg 174). The San Felipe Reach spans 6.2 miles from the mouth of the Arroyo Tonque (agg/deg 174) to the Angostura Diversion Dam (agg/deg 236). These reach delineations are consistent with those developed and used by Gigi A. Richard (2001). For a complete discussion regarding agg/deg lines, refer to Section 2.4.

As described in the introduction, two analyses were performed for this study. A hydraulic modeling analysis (HMA) was performed on the San Felipe Reach, and a meander migration analysis (MMA) was performed on the Galisteo Reach. A review of literature was performed to aid in the development and understanding of the analyses undertaken.

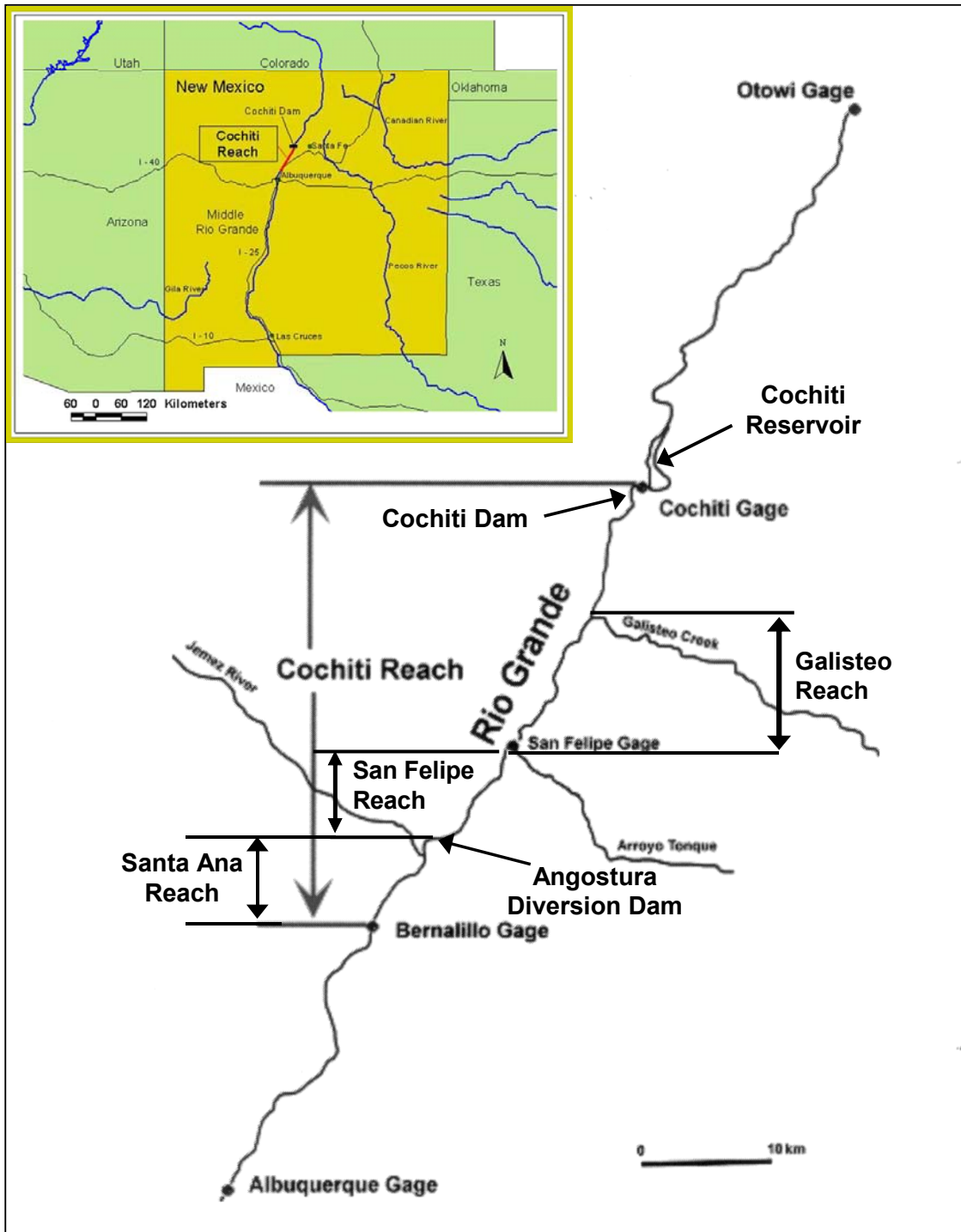


Figure 2-1: Location of study subreaches in relation to Cochiti Reach, Rio Grande, NM showing locations of pertinent USGS gaging stations.

2.2 Hydraulic Modeling Analysis (HMA)

2.2.1 Site Background

The MRG is one of the most historically documented rivers in the United States. The Embudo gaging station, located 27 miles upstream of the Otowi gage, began recording stream flow data in 1889 representing the longest running measurement site in the United States (Graf, 1994). The Cochiti Reach can be historically described as aggrading sand bed channel with extensive lateral mobility. This aggradational trend is thought to have commenced as early as 11,000 years ago (Sanchez and Baird, 1997). Increasing sedimentation of the river bed began after 1850 due to water shortages and increasing sediment input from tributaries and arroyos (Scurlock, 1998). The aggradation of the river induced severe flooding, waterlogged lands and failing irrigation facilities (Scurlock, 1998). The amount of irrigated lands reached a maximum development by 1880, with a cultivated area of approximately 124,000 acres (Lagasse, 1980). This was reduced to approximately 40,000 acres by 1925.

In the efforts of saving irrigated lands and reducing flood risks, a major regulation of the river began in the 1920's which included the construction of numerous diversion structures, dams, levees and channelization works (Scurlock, 1998). The Middle Rio Grande Conservancy District was formed in 1925 by the State of New Mexico. The purpose of the district was to improve drainage, irrigation and flood control in the middle valley (Woodson and Martin, 1962). A floodway was constructed in 1935 in the efforts of providing flood protection to the adjacent irrigated and urban areas (Woodson, 1961). The floodway averaged 1,500 feet wide and was located between a system of levees approximately 8 feet high (Lagasse, 1980). The floodway was designed to carry a 40,000 cubic-feet-per-second (cfs) flow with an extra levee height provided for the city of Albuquerque to increase the design capacity to 75,000 cfs (Woodson and Martin, 1962).

A major flood with a mean daily discharge of 22,500 cfs took place in 1941 for a 2 month duration, breaching the levees in 25 places along the river causing extensive flood damage (Woodson and Martin, 1962). The bed of the channel rose to an elevation above the surrounding floodplain as a direct result of this flood, leading to its perched characteristic that is still existent today. This event prompted the USACE and USBR together with other Federal, State and local agencies to recommend a comprehensive plan of improvement for the Rio Grande in 1948 (Pemberton, 1964). The plan consisted of constructing a system of reservoirs on the Cochiti Reach of the Rio Grande and its tributaries (Abiquiu, Jemez and Galisteo) in addition to the rehabilitation of the damaged floodway (Woodson and Martin, 1962). The rehabilitation of the floodway reduced the design capacity to 20,000 cfs with the exception of the area surrounding the city of Albuquerque where the design capacity was reduced to 42,000 cfs.

The 1940's – 1960's period was characterized by extensive management practices including bank stabilization efforts such as Jetty-jack lines, which protect the banks from erosion by slowing velocities and inducing sedimentation behind the jetties. The culmination of these efforts to stabilize the channel was with the construction of Cochiti Dam. Cochiti Dam, which began impounding water and sediment in November 1973, was built for flood and sediment control as well as for reversing the aggradational trend and inducing degradation of the main stem (Lagasse, 1980). Based on a sediment transport analysis, the USBR predicted that the channel downstream of Cochiti Dam could degrade by more than a meter (Woodson and Martin, 1962). The degradation was expected to extend as far downstream as the Rio Puerco. It was further predicted that the channel bed material would coarsen, which would inhibit further degradation.

Cochiti Dam and Reservoir provide the single largest source of flood control storage space on the main stem of the Rio Grande (Bullard and Lane, 1993). The Dam traps virtually all (99%) of the sediment entering the reservoir from upstream. This has

caused significant changes downstream of the dam, such as the observed degradational trend as a result of clear water scour. The change in annual suspended sediment yield from upstream of Cochiti Dam (Otowi) to downstream (Albuquerque) is shown in Figure 2-2. The major sources of sediment to the MRG downstream from Cochiti Dam are tributary inputs and erosion of the channel bed and banks. It is evident from Figure 2-2 that there is an increase in sediment yield between Cochiti Dam and the Albuquerque gaging station.

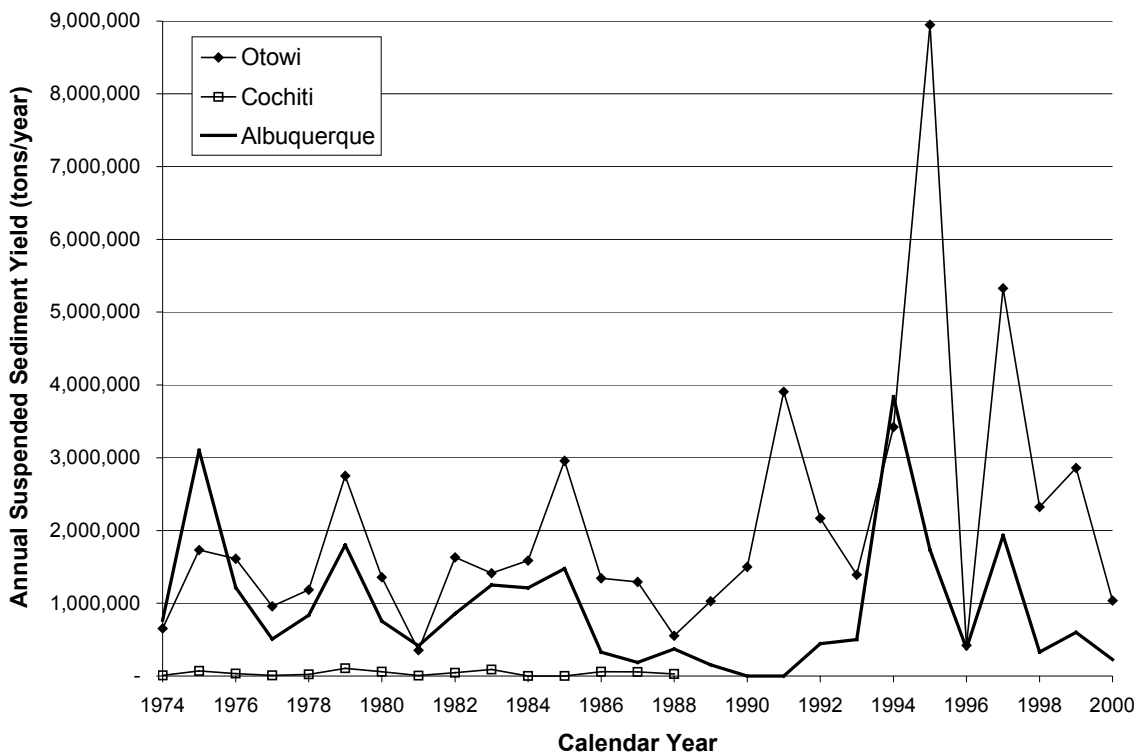


Figure 2-2: Annual suspended sediment yield in the Rio Grande in tons/year at Otowi gage (upstream of Cochiti Dam), Cochiti gage (just downstream of Cochiti Dam) and Albuquerque gage (downstream of Cochiti gage) from 1974 to 2000. Cochiti gage record ends in 1988.

There were several studies conducted since the construction of Cochiti Dam that have explored the changing morphology of the reach. Lagasse (1980) performed a geomorphic analysis of the MRG during 1971 to 1975 from Cochiti Dam to the Isleta Diversion Dam. It was concluded that the response of the reach to the dam construction

was dominated by the inflow of tributaries and arroyos (Leon, 1998). It was further suggested that the reach located between the dam and the Jemez River approached a stable condition more rapidly than the river downstream of the Jemez confluence, due to an armor layer development coupled with local base level control that was established by tributaries and arroyos (Leon, 1998). It was also speculated that the reach located between the dam and Galisteo Creek may have already completed the adjustments underwent after closure of the dam (Richard, 2001). Finally, Lagasse noted that evidence of armoring had progressed to locations as far downstream as Albuquerque by 1979 (Richard, 2001). The geomorphic analysis conducted by Lagasse (1980) documented the channel adjustments to the dam construction through a qualitative analysis of planform, profile, cross section and sediment data. The data analysis methodology used for this study was utilized as a guide for the HMA, for which some of the same analyses were performed.

Morphological changes in the Cochiti Reach since 1918 have been documented by Sanchez and Baird (1997). A trend showing a decrease in channel width was observed with no acceleration in the rate of channel narrowing noted since the closure of Cochiti Dam. It was also shown that the sinuosity increased since the construction of the dam, but has not reached the peak level of 1949. These observations will be discussed in more detail in the HMA of the San Felipe Reach (Chapter 3).

The Santa Ana Reach (Figure 2-1), located between the Angostura Diversion Dam and the Highway 44 Bridge in Bernalillo was studied by Mosley and Boelman (1998) - Draft. One of the main conclusions from this study was that the reach moved from a braided to a meandering channel pattern with a high width-to-depth ratio, pool/riffle channel that was dominated by gravel material. Data indicate the width-to-depth ratio decreased since construction of the dam.

Similar morphological trends were observed in reaches located sporadically along the MRG. These trends were documented in reports written for the USBR. All research and writing of these reports was conducted at Colorado State University under the guidance of Dr. Pierre Y. Julien and through funding from the USBR. The reaches researched to date include the following:

- Rio Puerco Reach (Richard et al., 2001). This reach spans 10 miles from just downstream of the mouth of the Rio Puerco (agg/deg 1101) to the San Acacia Diversion dam (agg/deg 1206).
- Corrales Reach (Leon and Julien, 2001b), updated by Sixta et al. (2003b). This reach spans 10.3 miles from the Corrales Flood Channel (agg/deg 351) to the Montano Bridge (agg/deg 462).
- Bernalillo Bridge Reach (Leon and Julien, 2001a), updated by Sixta et al. (2003a). This reach spans 5.1 miles from New Mexico Highway 44 (agg/deg 298) to cross-section CO-33 (agg/deg 351).
- San Felipe Reach (Sixta et al., 2003c). This reach spans 6.2 miles from the mouth of the Arroyo Tonque (agg/deg 174) to the Angostura Diversion Dam (agg/deg 236).

As mentioned earlier, the HMA portion of this thesis focuses on the San Felipe Reach for which the latest listed report was written. Some of the detailed analysis results of this report will therefore be discussed in Chapter 3 of this study.

The MRG has some uniquely definable characteristics. Currently the Cochiti Reach is perched, meaning that the channel bed is at an elevation higher than the surrounding floodplain (Baird, 2003). It will be shown that the current state of this reach is degradational, which is counterintuitive to its perched behavior. This condition is

extremely rare, shared only with one other river in the world; the Yellow River in China (Baird, 2003). This makes the analysis of this reach quite challenging and interesting.

2.2.2. Hydrology and Climate

The MRG Valley has a complex hydrologic system (Bauer, 2000). Water flows through a system of sub-basins where the surface water and groundwater are interrelated (Lagasse, 1980). Two types of flows in the valley are distinguished as a result of precipitation seasonal variations. During April through June flows are generated in spring and early-to-mid summer due to melted snow and rain from the mountains; July through October is characterized by mid-to-late summer and fall flows caused by short intense local rains on one or more of the tributary areas (Rittenhouse, 1944). The hydrograph for the spring and early-to-mid summer flows is characterized by a gradual rise to a moderate rate of discharge that is maintained for an approximate 2-month period. The peak flows are generally of short duration with high volumes or runoff (Leon, 1998). The mid-to-late summer and fall flows are characterized by a sharp hydrograph, representing a quickly receding peak discharge (short duration), with low volumes of runoff. For the Cochiti Reach, flows above 5,000 cfs are considered to be flood flows (Woodson, 1961).

Typical spring runoff hydrographs in the MRG can be seen in Figure 2-3. The Otowi gaging station is located upstream of the Cochiti Dam, while the Cochiti and Albuquerque gages are located on the downstream side of Cochiti Dam (Figure 2-1). Attenuation of the spring runoff peak between Otowi and the gages downstream is evident in the hydrographs (Figure 2-3). Peak outflows from Cochiti Dam can historically occur as much as 62 days after, or as much as 225 days prior to the peak inflows to the reservoir (Bullard and Lane, 1993).

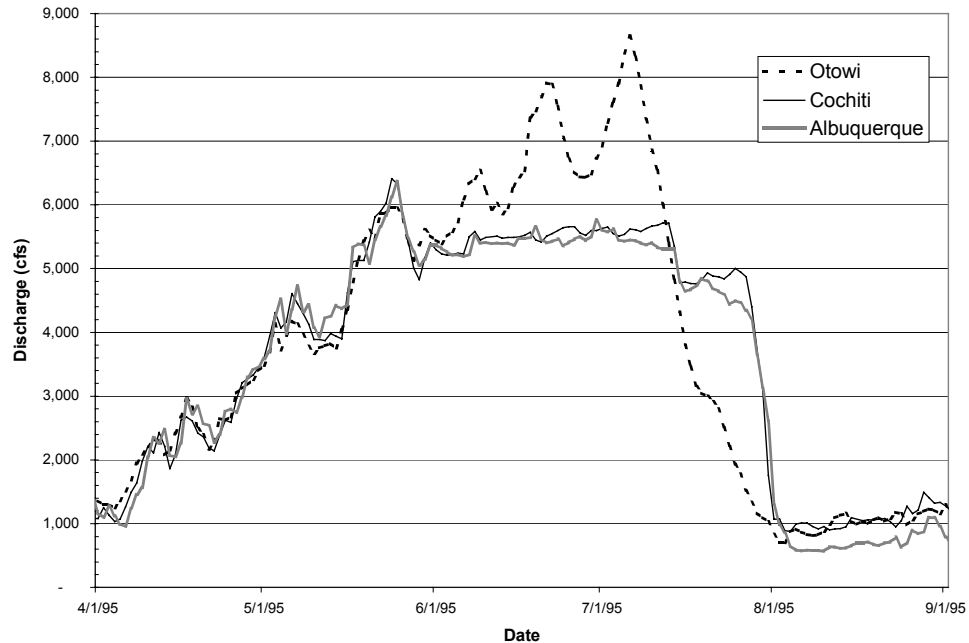


Figure 2-3: 1995 Rio Grande spring runoff hydrographs.

Besides flood regulation, climate changes seem to have a strong influence in the flow regime of the Rio Grande. Richard (2001) observed that the magnitude of the annual peak flows at the Otowi and Cochiti gages declined with time since 1895, prior to the construction of main dams in the Rio Grande system. Cochiti gage data show a dry period from about 1942 to about 1978 (Richard, 2001). Richard (2001) also determined that peak flows between 1943 and 1973 (pre-Cochiti dam) are not statistically different from those between 1974 and 1996 (post-Cochiti dam).

Molnár (2001) analyzed trends in precipitation and streamflow in the Rio Puerco, one of the largest tributary arroyos of the Rio Grande downstream from the San Felipe Reach. It was concluded that a statistically significant increasing trend in precipitation in the basin at the annual timescale occurred between 1948 and 1997. This increase is due to increases in non-summer precipitation, in particular in the frequency and intensity of moderate rainfall events (Molnár, 2001). It was also concluded that there is a strong

relationship between the long-term precipitation trends in the Rio Puerco Basin and the sea surface temperature anomalies in the Northern Pacific (Molnár, 2001).

Also, annual maximum precipitation events seem to produce lower annual maximum runoff events in the last 50 years, most likely due to vegetation cover and the hydraulic characteristics of the basin (Molnár, 2001). Even though this type of analysis has not been performed in other sub-basins of the Rio Grande, it is likely that the same trends occur in nearby areas along the Rio Grande.

2.3 Meander Migration Analysis (MMA)

2.3.1. Background

The second part of this study focuses on the meander migration of the Galisteo Reach. The areas of concern with meander migration are many. The channel migration could be eroding valuable land, posing a safety risk, or threatening nearby structures. It is important to note also that while lateral movements may pose threats to human-made structures, they can enhance the channel diversity that is vital to healthy riverine habitat (Richard, 2001). The tendency of natural rivers to migrate actively across floodplains in a state of dynamic equilibrium, coupled with the tendency for floodplains to be densely populated, cultivated and otherwise exploited, has led to conflict between nature and humankind (Darby, 2001).

Frequently, rivers are mistakenly considered to be static; that is, unchanging in its shape and form. An alluvial river however, in its natural state, is generally changing its position and shape because of hydraulic forces acting on its bed and banks (Richardson et al., 2001). Rivers are fed by water and sediment, and therefore respond to the inherent fluctuation of these inputs, often resulting in a continuous dynamic state. These fluctuations can occur naturally (droughts, floods), or be human induced (dams, hydraulic control structures). The work of Brookes (1992) illustrates how these driving

variables (discharge and sediment supply) act on boundary conditions (channel bed and bank) to form the channel characteristics (cross section, longitudinal profile, and planform).

2.3.2. Terminology

It is important to define a few terms that will be used throughout this thesis as terminology in this field is not completely standardized. The terminology used in this thesis is consistent with that of Jones and Harper (1998). Meander growth occurs from the removal of material from one side of the channel (cut bank) together with the deposition of material on the opposite side (point bar). The removal and deposition of material occur at relatively the same time and results in an increase in channel length and sinuosity (Figure 2-4:A). The lateral translation of preexisting meanders, either upstream or downstream and parallel to the general channel trend is referred to as meander migration (Figure 2-4:B). Generally, channel length and sinuosity are much less affected by meander migration than with meander growth (Jones and Harper, 1998).

The processes of meander migration and meander growth, acting together or separately, lead to the development of a meander belt (Jones and Harper, 1998). The meander belt is defined by the active flood plain area and is approximately equal to the amplitude of the meanders (Leopold and Wolman, 1960). Another interpretation for defining this area is the distance between lines drawn tangent to the extreme limits of successive fully developed meanders (Richardson et al., 2001).

The term avulsion refers to a process by which a river channel shifts to a new, separate channel at a different location on the flood plain (Schumm, 1977). This usually occurs when a river breaks through its banks; therefore this process is usually associated with a flood or catastrophic event (Richardson et al., 2001). It can be seen in

Figure 2-4:C that an avulsion can result in the abandonment of a single meander loop or numerous meanders (Jones and Harper, 1998). In some instances, the cut banks on opposite sides of a meander neck can migrate into each other, developing an alternative channel across the neck of the meander loop. This is known as a cutoff (Figure 2-4:D), and is not considered an avulsion in this study.

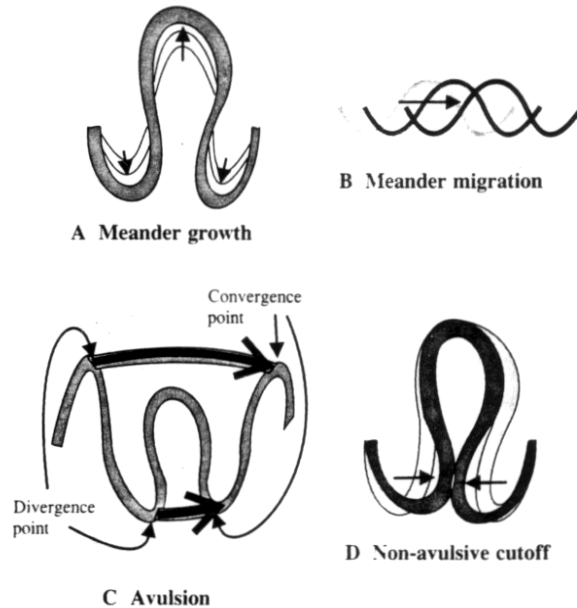


Figure 2-4: Terminology depiction.

2.3.3. Equilibrium versus Stability

This thesis utilizes the concept of channel adjustment in response to variations in inputs as related to a stable, equilibrium state. As a result, the relationship between equilibrium and stability must be explored. From an engineering point of view, stability and equilibrium are not identical concepts (Brice, 1982). One can exist without the other. A river can achieve equilibrium in cross-section and longitudinal profile, but migrates laterally, and therefore be considered unstable to an engineer (Richard, 2001). A river can aggrade or degrade in a state of dynamic equilibrium, and as a result require special design measures to accommodate this “instability” (Brice, 1982). It is also possible to

have a stable river that is not in equilibrium. An example of such a rare occurrence would be if a channels bed and banks were heavily armored, but due to a diversion along a particular reach, there is more water entering the reach than exiting. Another concept proposed by Parker (1979), called the 'stable channel paradox' states that a stable channel width is incompatible with an active bed.

2.3.3.1. Equilibrium

The basic idea of equilibrium is that there exists a balance of inputs to outputs; i.e. the amount of sediment and water passing through a given upstream cross section is the same as that passing through a given downstream cross section. This means that nothing is gained or lost over this reach of finite length. According to Richard (2001), equilibrium refers to a characteristic of open channel systems and their ability for self-regulation. Another way to define the concept of equilibrium is by visualizing how a river will adjust through its cross-sectional form, bed configuration, planform and bed slope to accommodate the water and sediment entering the channel (Brookes, 1992).

Lane's equation (Equation 2-1) (Richardson et al., 2001) summarizes the concept of channel adjustment towards a state of equilibrium.

Equation 2-1: Lane's relationship.

$$Q_s D_{50} \propto QS$$

Where: Q_s = bed material load
 D_{50} = median bed material size
 Q = water discharge
 S = channel slope

The left side of Equation 2-1 ($Q_s D_{50}$) represents the supply, while the right side (QS) represents the capacity. This equation, referred to as Lane's balance, is used to demonstrate how channels will adjust to certain variations in the supply or capacity. The adjustments made are in an effort to return to a state of "balance", or equilibrium. This

geomorphic relation is only an initial step in analyzing long-term channel response. This initial step is important however, because it warns of the possible future difficulties of managing a channel in a state of non-equilibrium when implementing channel modifications and flood protection works (Richardson et al., 2001).

An example of a supply variation and the channel response would be if the sediment supply decreases dramatically (i.e. with the construction of a dam). According to Lane's balance, the tendency of the channel on the downstream side of the dam will be to either coarsen its bed material size through the process of armoring, or decrease its slope through degradation in order to restore the balance that was present prior to dam construction. This is assuming that the water discharge remains constant.

2.3.3.2. Stability

The basic idea of stability is that there is no appreciable change in form or location of the channel from one year to the next. Ideally, a stable channel is one that does not change in size, form, or position through time. However, all alluvial channels change to some degree and, therefore, have some degree of instability (Brice, 1982). It has been argued that in order to achieve stability, which is a very common goal of river restoration projects, stable banks, and continuity of water and sediment must exist. According to Richardson et al. (2001), a stable channel is defined as a condition that exists when a stream has a bed slope and cross section that allows its channel to transport the water and sediment delivered from the upstream watershed without aggradation, degradation, or bank erosion. Over time, there have emerged many definitions of stability. Some of these include:

Mackin (1948):

“A graded stream is one in which, over a period of years, slope is delicately adjusted to provide, with available discharge and with prevailing channel characteristics, just the velocity required for the transportation of the load supplied from the drainage basin. The graded stream is a system in equilibrium.”

Schumm (1977):

“The stable channel is one that shows no progressive change in gradient, dimensions, and shape. Temporary changes occur during floods, but the stable channel, if the classification were not restricted to short segments of the river, would be identical to the graded stream as defined by Mackin (1948).”

Leopold and Bull (1979):

“A graded stream is one in which, over a period of years, slope, velocity, depth, width, roughness, pattern and channel morphology mutually adjust to provide the power and efficiency necessary to transport the load supplied from the drainage basin without aggradation or degradation of the channels.”

Rosgen (1996):

“Stability is the ability of a stream, over time, in the present climate, to transport the flows and sediment from its watershed in such a manner that the stream maintains its dimension, pattern and profile without aggrading or degrading.”

Richardson et al. (2001)

“A condition of a channel when, though it may change slightly at different times of the year as a result of varying conditions of flow and sediment charge, there is no appreciable change from year to year; that is, accretion balances erosion over the years.”

It is interesting to note how the concepts of equilibrium show through in some of these definitions of stability.

It can be seen that there is subjectivity to the way stability and equilibrium are defined. Instability is in the eye of the beholder. To determine whether or not a river is stable, or in a state of equilibrium, depends in part on the definition being used. Because of these many differing viewpoints and definitions that exist, there is no universally accepted set of criteria to date for determining whether all or part of a river system is in equilibrium (Knighton, 1998). Although numerous definitions of stability and equilibrium exist, the underlying concepts are all the same. In order for an alluvial channel to be considered “stable”, it must be in a state of equilibrium.

2.3.4. Causes of Migration

To fully understand a problem, it is important to know the cause of the problem. In this case, migration is the problem, which occurs as a result of channel instability. For this study, instability is defined as movement in the channel bed and/or banks. Bed instability results from channel aggradation or degradation, leading to a vertical adjustment. Bank instability results from the removal of bank material through grain-by-grain detachment or mass wasting, leading to a width adjustment. Bed and bank instabilities are linked because one can cause or be the result of the other. An example of this would be if a channel had stable banks but was incising through bed degradation, increasing the bank heights to a point exceeding the critical height, where bank sloughing or bank collapse occurs.

The focus of this study is on the meander migration of alluvial channels, which results primarily from bank instabilities. In describing the process of meander migration Julien (2002) states that migration in meandering rivers is a result of erosion at the outer bank combined with the equivalent sedimentation near the inner bank. In alluvial river systems, it is the rule rather than the exception that banks will erode (Richardson et al., 2001). The eroded bank material is transported downstream to the next point bar, where outer bank erosion is usually balanced by bar deposition and advance.

There are two main groups of bank erosion processes; these include hydraulic action and mass failure (also known as mass wasting). Hydraulic action is commonly associated with high velocity against the bank, particularly along the outside of a bend. The linkage between these two processes is referred to as basal endpoint control (Schumm et al., 1984). This is where the toe of the slope controls the stability of the bank. There are many causes of bank failures, some of which include:

- **Parallel flow** – stream velocity / shear stress removes granular bank material, causing grain-by-grain detachment of bank particles. This can lead to undercutting of the bank, resulting in a cantilever failure.
- **Concentrated or impinging flow** – flow occurs at an angle to the bank because of obstructions, debris, or bar formations. Turbulence, velocity, shear stress, and 3-D effects such as bursts and plunges remove bank material. This produces a greater effect than that of parallel flow.
- **Fluctuating water levels** – a quick draw down leaves banks saturated where the weight, lubrication of failure planes, piping, or a combination thereof causes failure.
- **Oversteepening of bank** – bank angle greater than cohesive properties of soil.
- **Rilling and gullying** – uncontrolled channelized runoff from overbank areas.
- **Sheet erosion** – unchannelized surface runoff.
- **Freeze / thaw action** – repeated freezing and thawing of water contained in the soil weakens the soil strength, making it more susceptible to erosion.
- **Piping and seepage** – flow through the soil may transport soil particles through the bank surface, leaving a void in the bank material. This leads to cave-ins.
- **Wave induced failure** – erosion generated by vessel forces.
- **Animals and humans** – grazing, disturbance of riparian vegetation, burrowing may lead to piping, etc.

There are many bank stabilization techniques available to try to combat this issue of bank erosion, but that is beyond the scope of this study.

It has been reported by Haap (1948) that significant bank erosion occurred along the Rio Grande between Cochiti and Elephant Butte Reservoir following the floods of 1937 and 1941. Recall that this time was characterized by an aggradational river system, making it prone to flooding, which led to the construction of Cochiti Dam. Since construction of the dam a degradational trend has developed, and Baird (1998) stated that the river has tried to become longer through bank erosion and meandering, which would imply an increasing rate of bank erosion. Localized areas of erosion will always be present along any river, unless it is protected, and there is no way to predict the occurrence of these localized areas (Mussetter Engineering, 2002).

Migration rates are highly variable, and changes can be very slow or rapid. Trying to model/predict these rates is challenging due to the large number of complicated fluvial processes involved from which the variables of importance are

difficult to isolate (Thorne, 1999). Some of the major factors affecting alluvial stream channel forms are: stream discharge (magnitude and duration), temperature, viscosity, sediment load (types and caliber), valley slope, bank and bed resistance to erosion, vegetation, geology (including bedrock outcrops, clay plugs, and changes of valley slope), and human activity.

2.3.5. Studies and Analysis Work

The MMA portion of this study focused primarily on two previous studies. These studies included the bend curvature work of Hickin and Nanson (1984) and the secondary flow work of Rozovskii (1957).

2.3.5.1. Bend Curvature (Hickin and Nanson)

According to Hickin and Nanson (1984), channel migration rates are strongly controlled by bend curvature. To make this conclusion, 189 bends on 21 different rivers (including clay, sand and gravel) in Western Canada were studied. They also performed a detailed study of scroll bars that had developed over 250 years along the Beatton River.

From these studies, a relationship was formed between relative migration rates and the ratio of radius of curvature-to-channel width (R/W). Hickin and Nanson (1984) demonstrated that the rate of relative migration reaches a maximum when $2 < R/W < 3$, decreasing rapidly on either side of this range (see Figure 2-5). The decrease at the lower end of this range (as the bends become sharper) is likely attributable to the large increase in resistance or a decrease in the outer-bank radial force (Knighton, 1998). It was concluded by Baird (1998) that leaving the bends of the MRG at or near an R/W value of 2 to 3 has lessened the need for man-made interventions. This range however, falls into the range of maximum migration, and hence maximum bank erosion according to the Hickin and Nanson (1984).

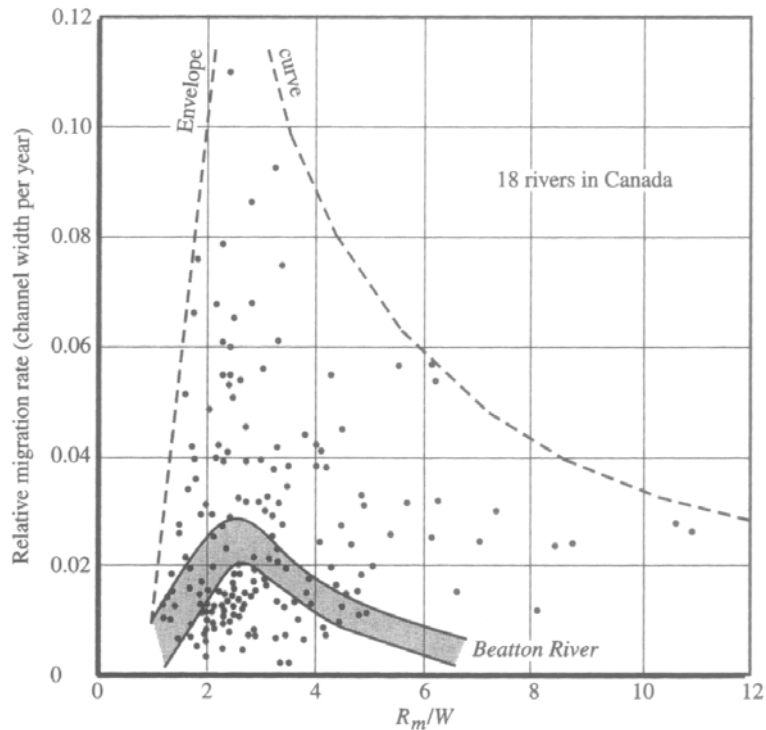


Figure 2-5: Relative migration rates (Hickin and Nanson, 1984).

Nanson and Hickin (1983) remarked on the discontinuous nature of channel bank erosion as a result of seasonal fluctuations in flow. This discontinuous nature, especially when looking at the migration rate of individual bends, could cause enormous errors in prediction. However, if migration rates were taken from a number of different bends along the same reach, an average value could be obtained for the reach that would be more indicative of the erosion to be expected. This average value would only be representative of the flow conditions that occurred during the period of measurement and not necessarily representative of the long term flow record (Nanson and Hickin, 1983).

According to Hooke (1977), too shallow of a curve (large R) gives rise to a shear stress distribution that induces a faster rate of migration in the upstream than in the downstream limb, leading to an increase in curvature. Conversely, with a sharp curve (small R), the downstream limb migrates more rapidly and the bend becomes shallower.

By combining these separate studies of Hickin and Nanson (1984) and Hooke (1977), Knighton (1998) suggests that a natural stream can control both the rate of migration and the pattern of erosion and deposition in meander bends by adjusting channel curvature.

Considerable scatter in the data can be seen in Figure 2-5, suggesting the migration rate of meanders is extremely complex and may be a function of factors other than R/W (Julien, 2002). Nanson and Hickin (1986), further analyzed data from 18 single-thread meandering river reaches (gravel-bed and sand-bed) to explore the relationship between migration and variables other than those relating to the channels curvature characteristics. This analysis was performed utilizing sets of sequential aerial photographs that showed the channel shifting over a period of 21 to 33 years. Multiple regressions on migration rates with discharge (Q), slope (S), and bed material (D_{50}) were performed. The best result from this analysis is shown in Equation 2-2.

Equation 2-2: Migration rate regression.

$$M \cdot h = f(Q, S, D_{50})$$

M·h represents the volume of migration. This regression had an r^2 value of 69.1. Nanson and Hickin (1986) concluded that the river size is the most important variable contributing to channel migration, using either discharge (Q) or width (W) to represent this variable.

By scaling the migration rate to the size (width) of the river, Nanson and Hickin (1986) found no increase in the success of the above regression, but did discover the importance the size of basal sediments plays. When the migration rate was scaled by the river's width, the D_{50} of the basal sediment was seen to be more important than the stream power. It was argued that the erosion of the bed material at the toe of the slope is more important to guard against because undermining of the bank through basal erosion

can cause bank erosion even along well-vegetated banklines. It was further speculated that bank erosion and channel migration are largely determined by bed material transport. This notion is what drove their theory that "...a simple relationship involving stream power and basal sediment size provides such an effective means of expressing the driving and resisting forces in this predictive model of channel migration" (Nanson and Hickin 1986, p. 504). By concluding that bed material transport plays a significant role in channel migration suggests that the presence of a dam may have large impacts on downstream channel movement (Richard, 2001).

2.3.5.2. Secondary Flow (Rozovskii)

Secondary flows in bends are generated through a change in the downstream channel circulation (Julien, 2002). The streamlines near the river surface produce a centrifugal force that is in the direction of the outer bank. The streamlines near the riverbed produce a pressure force that is in the direction of the inner bank. In addition, the velocity near the bed, the tangential bed shear stress, and the drag on the bed particles are also usually directed toward the inner bank (Julien, 2002). Combining these variables yields a shear force that acts towards the outer bank. To achieve a force balance, the pressure force must balance with the centrifugal and shear forces resulting in a helical flow (a.k.a. secondary flow). Similarly, Chow (1959) attributes this phenomenon to (1) friction on the channel walls, causing higher velocities near the center of the channel than near the walls; (2) a centrifugal force, causing particles of water to deviate from a straight line motion as well as causing super-elevation in the flow surface at the outer bank; (3) a vertical velocity distribution existing in the approach channel, thus initiating helical motion in the downstream flow.

Prus-Chacinski (1954) has credited helical flow as the basic mechanism responsible for the initiation and development of meanders. It was showed that by the

introduction of artificial secondary currents at the beginning of a bend, various kinds of secondary currents were produced in the next successive bend, which affects the circulation in the next bend, and so on. It is clear that helical flows play an important role in the processes of erosion and deposition, but it is not yet known what the relationships are between these flows and channel width, curvature and meander length (Leopold et al., 1995).

The strength of secondary flows, which affects particle stability, is influenced by the magnitude of the deviation angle (λ) of streamlines near the bed, which is defined in Equation 2-3 (Julien, 2002).

Equation 2-3: Deviation angle calculation.

$$\tan\lambda = \frac{\tau_{rR}}{\tau_{\theta}} = \left[\frac{a^2}{\Omega_R} \cdot \left(\frac{h}{D_s} \right)^{2m} \right] \cdot \frac{h}{R}$$

In this equation, τ_{rR} represents the radial shear stress, τ_{θ} represents the downstream bed shear stress while a and m are constants that vary with relative submergence that are obtained through the power form of the grain resistance equation. The dimensionless parameter Ω_R denotes the ratio of the centrifugal force (generating secondary motion) to the shear force (abating secondary motion and dissipating energy) (Julien, 2002). Finally, h is the flow depth, D_s the grain size and R the radius of curvature. Rozovskii (1957) found the term in brackets to be approximately equal to 11. It can, therefore, be seen that the deviation angle depends primarily on the ratio of flow depth-to-radius of curvature (h/R). It can therefore further be noted that sharp bends (small R) and high flows (large h) will exhibit stronger secondary flows, with the maximum scour potential near the outer bank.

Changes in cross-sectional geometry depend on the magnitude of the deviation angle λ (Julien, 2002). When $\lambda < 15^\circ$, there is a decrease in particle stability near the

outer bank, coupled with an increase in particle stability near the inner bank. These processes are generally occurring in a state of equilibrium, in which material lost to bank caving equals the material gained by deposition. When $15^\circ < \lambda < 55^\circ$, a larger portion of the channel becomes unstable, and the channel is in or approaching a state of non-equilibrium. For extreme cases where $\lambda > 55^\circ$, the entire channel cross section becomes unstable and widening occurs. This process is always occurring in a state of non-equilibrium.

To reach a state of stability in a graded bed material channel where armoring is possible, coarser grains are generally found near the outer bank and finer grains near the inner bank. This is because under significant secondary flows, stability is maintained through a heavier particle weight to counterbalance the high erosive forces at the outer bank. This leaves the finer particles to deposit and form a point bar near the inner bank. In a channel with uniform erodible bed material, secondary flows will result in scour of the toe at the outer bank, resulting in bank caving, which in turn results in channel migration (Julien, 2002).

2.3.5.3. Additional Analyses

In addition to looking at the studies of Hickin and Nanson (1984) and Rozovskii (1957), additional investigations were performed to try and gain a better understanding of the observed migration patterns and the forces influencing these patterns. These included the analysis of sine-generated curves, a hydrological analysis, stream power analysis, specific stream power analysis and the evaluation of trends between migration rates (M) and relative migration rates (M/W) as compared with depth-to-radius of curvature (h/R) ratios and width-to-depth (W/h) ratios.

Sine-generated curves were developed to see how close (geometrically) each bend followed an idealized meander. Next, a hydrological analysis was performed to see

what effects higher and lower points in the flow regime had on channel migration rates. The goal of this analysis was to link these higher and lower points in the flow regime to an increased and decreased rate of channel migration, respectively. Also, a stream power analysis was executed because Nanson and Hickin (1986) found that migration rate correlated better with stream power than it did with discharge. It has been argued by Yang and Song (1979), that a natural stream moving towards a state of dynamic equilibrium chooses a course in which to minimize the rate of energy expenditure, one manifestation of which is minimum stream power. Stream power (Ω) is defined through Equation 2-4.

Equation 2-4: Stream power calculation.

$$\Omega = \gamma QS$$

In this relationship, γ ($=\rho g$) is the specific weight of water, Q is the discharge and S is the channel slope. This is an expression for the rate of potential energy expenditure (or rate of doing work) per unit length of channel (Knighton, 1998). Although the concept of minimum stream power has been used to explain discontinuities in the process of channel adjustment (Chang, 1985), direct considerations of energy expenditure are rare, and there remains a need to relate fluvial process activities to the physical concept of work (Knighton, 1998).

With the hope of quantifying the state of the channel as with the calculation of deviation angles from the secondary flow analysis, the specific stream power ($\omega=\Omega/W$) was calculated for each bend during the time periods of interest. This characterized the energy level of the floodplain. Nanson and Croke (1992) identified three major types of floodplains according to specific stream power. These floodplain types are as follows: (Knighton, 1998)

- **High-energy:** ($\omega > 300 \text{ W m}^{-2}$) non-cohesive floodplains where confinement by bedrock or boulders inhibits lateral migration, and the vertical accumulation of relatively coarse sands and gravels is the dominant process.
- **Medium-energy:** ($10 < \omega < 300 \text{ W m}^{-2}$) non-cohesive floodplains, typical of meandering and braided rivers, in which the main mechanism is lateral point-bar or braid-channel accretion.
- **Low-energy:** ($\omega < 10 \text{ W m}^{-2}$) cohesive floodplains, usually associated with laterally stable single-thread or anastomosing channels, whose development is governed largely by vertical accretion of fine-grained deposits and infrequent channel avulsions. Abrupt avulsions are an important mechanism in the evolution of larger floodplains whose cohesive bank material severely constrains channel migration.

Finally, to see what affects other factors had on channel migration, trends among migration rates (M) and relative migration rates (M/W) when compared to h/R ratios and W/h ratios were analyzed. The strength of the trend indicated the variables degree of influence on channel migration rates.

2.4 Available Data

State and federal agencies including the USACE, the USBR, the USGS and the Soil Conservation Service (SCS), which is now the Natural Resources Conservation Service (NRCS), began intensive surveys of the Rio Grande in the early 1900's. Cross section surveys were initiated in 1918, bed material sampling began in the 1930's, suspended sediment measurements started in the 1940's and aerial photography/topographic surveys are available from 1918 to 2001 (Richard, 2001). This collection of data results in documentation of the Cochiti Reach for nearly 100 years.

The compilation of this data into a consistent database began in 1997 by Claudia Leon and others at Colorado State University under contract with the USBR Albuquerque office (Richard, 2001). These efforts resulted in a computer database that consists of Microsoft® Excel® spreadsheets displaying cross-section data and plots, water discharge data with corresponding statistical plots, suspended sediment concentration, discharge, and particle size distributions as well as bed material grain size data. This database can be found on CD-ROM (Leon et al., 1999h) and in a seven

volume report (Leon et al., 1999a, 1999b, 1999c, 1999d, 1999e, 1999f, 1999g). Another database mimicking this format was later constructed for the Albuquerque Reach. Together these two databases make up the MRG database, available on CD-ROM.

Aggradation/Degradation (agg/deg) line surveys, collected by the USBR, are available for 1962, 1972 and 1992. These cross sections are photogrammetrically surveyed and spaced approximately every 500 feet apart. The mean bed elevations were estimated by the USBR based on the water surface elevation, slope, channel roughness and discharge at the time of the survey. In addition, field-surveyed cross sections collected by the USBR are also available. These cross sections, which are more coarsely spaced (approximately 5,000 feet), include Cochiti (CO) lines, Bernalillo Island (BI) lines, San Felipe Pueblo (SFP) lines and others. All of these line surveys are included as part of the MRG database.

Reclamation's GIS and Remote Sensing group in Denver, CO digitized the Cochiti Reach aerial photographs and topographic surveys, which are available for 1918, 1935, 1949, 1962, 1972, 1985, 1992 and 2001. Information on the aerial photographs (dates, scales, type, etc.) as well as the estimated mean daily discharges in the channel (according to USGS gaging stations) corresponding to the dates of the photographs, are summarized in Appendix A (Tables A-1 and A-2, respectively). Also included in this appendix is the metadata file for the photograph sets revealing the data's processing technique, accuracy, purpose, projection and additional information.

The MRG database, digitized aerial photographs and the most current data from the USBR and USGS were utilized in this study. A more detailed look into what data specifically was used for the HMA and MMA is discussed in Chapter's 3 and 4, respectively.

2.5 Summary

This literature review revealed some pertinent background information about the MRG including location, climate, history and hydrology. Also discussed were the ideas and processes of the two main analyses (HMA and MMA) that make up this study, both performed on subreaches of the Cochiti Reach. Based on available literature, it is hypothesized that by analyzing historical data and estimating potential conditions of the river channel, prediction of future equilibrium conditions could be made to facilitate the identification of sites that are more conducive to restoration efforts. It is further hypothesized that by analyzing the meander migration patterns and secondary flow characteristics of isolated bends, trends could be exposed, displaying the channels current state of stability and its likelihood for continued and/or future movement.

CHAPTER 3: HYDRAULIC MODELING ANALYSIS (HMA)

3.1 Introduction

The objective of the HMA was to analyze historic data to estimate pre-dam and post-dam characteristics of the reach. Looking at the effects of Cochiti Dam, and trying to predict the future conditions of the channel will facilitate with the identification of sites that are more conducive to restoration efforts. This analysis was performed on the San Felipe Reach.

In order to achieve this objective, the following analyses were performed:

- Identification of spatial and temporal trends in channel geometry through the analysis of cross-section survey data.
- Planform classification through analysis of aerial photographs and channel geometry data.
- Analysis of temporal trends in water and sediment discharge and sediment concentration using USGS gaging station data.
- Identification of temporal trends in bed material through the analysis of gradation curves and histograms.
- Evaluation of the equilibrium state of the river through the application of sediment transport analyses.

3.2 Reach Background

3.2.1. Reach Definition

The San Felipe Reach is included as a part of the Cochiti Reach in the MRG. This reach begins at the mouth of the Arroyo Tonque and ends 6.15 miles downstream of the confluence at the Angostura Diversion Dam (Figure 2-1). It spans from agg/deg line 174 to agg/deg line 236. There are seven Cochiti (CO) range lines (CO-17 to CO-23) located in this reach. CO-17 is located just downstream of the Arroyo Tonque confluence (agg/deg 174). The other CO-lines, 18, 19, 20, 21, 22 and 23 correspond to agg/deg lines 187, 195, 206, 216, 226 and 235, respectively. For a more detailed discussion on agg/deg and CO range lines, refer to Section 2.4. The San Felipe Reach is the next upstream reach from the Santa Ana Restoration Project.

Maps generated utilizing a Geographic Information System (GIS) depicting the locations of the agg/deg lines and CO-lines can be seen in Appendix B (Figures B-1 and B-2, respectively). Also included in this appendix (Figures B-3 to B-5) are aerial photographs of the San Felipe Reach showing the locations of the CO-lines along with pertinent geographic features.

3.2.2. Available Data

The sources of data utilized in the HMA included gaging station data, cross section data and eight sets of digitized aerial photographs. For a more detailed discussion of the aerial photographs, including error, refer to Section 4.2.4. From this data, numerous geomorphic analyses were performed in the pursuit of finding reach trends.

There is a USGS gaging station (San Felipe - #08319000) located at the upstream end of the San Felipe Reach. In addition, there are two gaging stations upstream (Cochiti - #08317400 and Otowi - #08313000) and two gaging stations

downstream (Bernalillo - #08329500 and Albuquerque - #08330000) of the reach (Figure 2-1). The Bernalillo gaging station is located approximately 13 miles downstream of the mouth of the Arroyo Tonque and the Albuquerque gaging station is approximately 28.5 miles downstream of the Angostura Diversion Dam. The three main gages of interest that were utilized in this analysis were the San Felipe, Bernalillo and Albuquerque.

Appendix C summarizes the available data for the San Felipe Reach. Table C-1 summarizes the available water discharge and suspended sediment data from the San Felipe, Bernalillo and Albuquerque gages. Additionally, bed material particle size distribution data were collected at these gaging stations. Table C-2 summarizes the periods of record for this data. Also, bed material samples were collected at the field-surveyed CO-lines and SFP-lines. Table C-3 lists the bed material surveyed dates at these cross sections. The survey dates for the CO-lines that lie within the San Felipe Reach are summarized in Table C-4. CO-line plots representing two surveys pre-Cochiti Dam (1973) and two surveys post-Cochiti Dam are included in Appendix D. A more detailed discussion of these plots as they relate to the closure of Cochiti Dam is discussed later in this chapter.

3.2.3. Channel Forming Discharge

Reclamation's Albuquerque office determined the channel forming discharge from a discharge/frequency analysis of the Santa Ana Reach. The San Felipe Reach is the next upstream reach from the Santa Ana Restoration Project (Figure 2-1). The two year instantaneous peak discharge ($Q_{2Y} = 5,000$ cfs) used as the channel forming discharge in the Santa Ana Geomorphic Analysis (Mosley and Boelman, 1998) was also used in this study. It's important to note that for this study, "channel forming discharge", "dominant discharge" and "bankfull discharge" are used interchangeably.

Figure 3-1 shows the annual maximum discharges recorded by the USGS at the San Felipe gaging station. Since 1967, there haven't been any flows recorded at San Felipe exceeding 10,000 cfs. Because flow regulation began at the Abiquiu Dam on the Rio Chama in 1963 and at the Cochiti Dam on the Rio Grande in 1973, the regulated two-year flow has decreased to 5,650 cfs (Bullard and Lane, 1993). Figure 3-2 shows annual peak flow histograms before and after 1963. Most of the flows are between 3,000 cfs and 7,000 cfs after 1963. Annual peak discharge plots at the Bernalillo and Albuquerque gages are included in Appendix E (Figures E-1 and E-2, respectively).

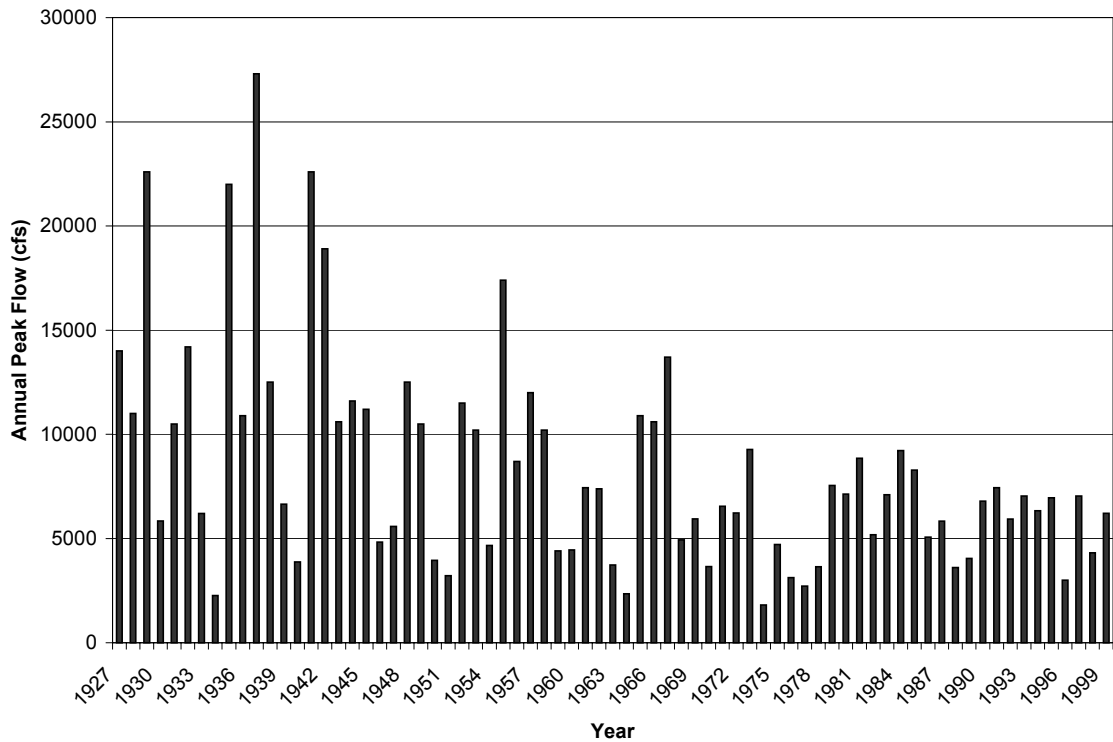


Figure 3-1: Maximum mean daily annual discharge in cfs on the Rio Grande at San Felipe (1927-1999).

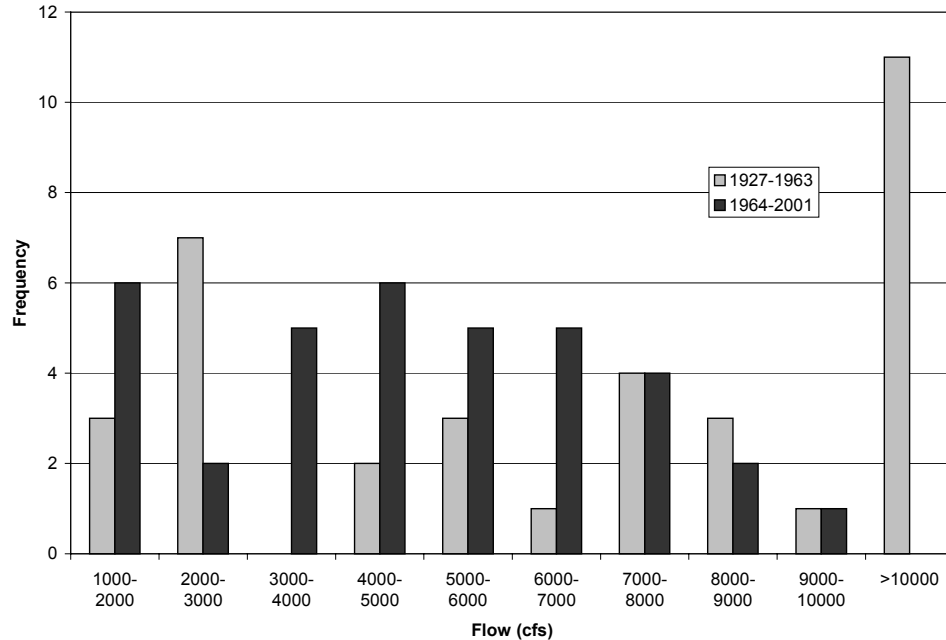


Figure 3-2: Maximum mean daily annual discharge frequency histograms on the Rio Grande at San Felipe (1927 – 2001).

3.3 Geomorphic Characterization

3.3.1. Channel Classification

Current channel pattern was qualitatively described from the 2001 set of aerial photographs. In addition, qualitative descriptions of the non-vegetated channel planform were performed from the GIS coverage's from 1918 to 2001.

Several channel classification methods were applied to the study reach to characterize the spatial and temporal trend of the channel planform. These methods are based on different concepts, such as slope-discharge relationships, channel morphology and unit stream power. Using a dominant discharge of 5,000 cfs along with various parameters from HEC-RAS® and D_{50} values from gradation curves as inputs, the following methods were analyzed for the study reach: Leopold and Wolman (1957), Lane (1957, from Richardson et al., 2001), Henderson (1963, from Henderson, 1966), Ackers

and Charlton (1970, from Ackers, 1982), Schumm and Khan (1972), Rosgen (1996), Parker (1976), van den Berg (1995), Knighton and Nanson (1993) and Chang (1979).

Figure 3-3 was produced from the GIS coverage's of the San Felipe Reach and represents the changes in river planform that occurred in the non-vegetated active channel in 1918, 1935, 1962, 1992 and 2001. It is evident that the study reach planform has not experienced significant changes since 1962. The San Felipe channel has been confined since the 1930's, after the MRG Conservancy District constructed the floodway along the river. Narrowing of the channel is evident as time progresses. The greatest decrease in width for the reach occurred from 1918 to 1935 (196 feet).

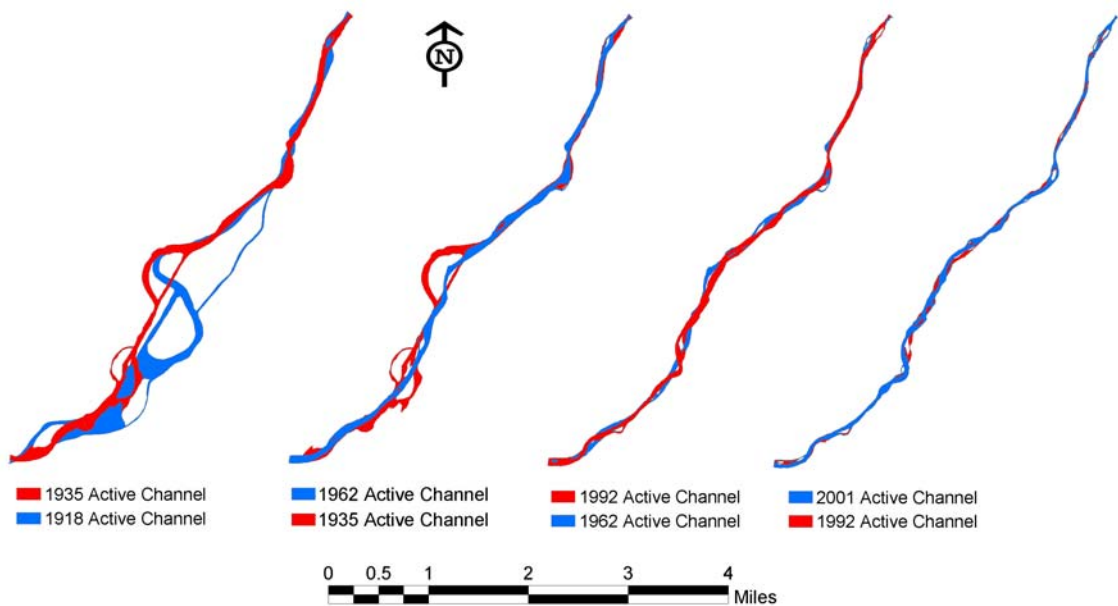


Figure 3-3: Non-vegetated active channel of the San Felipe Reach. 1918 planform from topographic survey. All other planforms from aerial photographs.

The current channel pattern description is based on observation of the 2001 set of aerial photographs, which were taken during the winter season (Figures B-3, B-4 and B-5). At flows below bankfull (<5,000 cfs), the San Felipe Reach exhibits a multi-channel pattern in some short reaches. Vegetated bars lateral to the low flow channels as well as within the channel are present sporadically. Channel width is fairly constant along the

entire reach. According to the HEC-RAS® results from the 1998 cross section data, most of the middle channel bars are not under water at a discharge equal to 5,000 cfs.

These methods produced descriptions of the channel that range from straight to meandering and braided (Table 3-1). The discrepancy among classification methods is likely due to the fact that this stretch of the Rio Grande is not in a state of equilibrium, and the classification methods were designed under the assumption that the river is in state of equilibrium.

Table 3-1: Channel pattern classification for 1962, 1972, 1992 and 1998.

Date	Slope-discharge					Channel Morphology		Stream Power		
	Leopold and Wolman	Lane	Henderson	Ackers & Charlton		Schumm & Khan	Rosgen	Parker	van den Berg	Chang
				Comparing with channel slope	Comparing with valley slope					
1962										
	Straight	Intermediate	Braided	Meandering	Meandering	Straight	D5	Meandering	Low stream power single thread narrow channel	from meandering to steep braided
1972										
	Straight	Intermediate	Braided	Meandering	Meandering	Straight	D5	Meandering	Low stream power single thread narrow channel	from meandering to steep braided
1992										
	Straight	Braided	Braided	Meandering	Meandering	Straight	D4	Meandering	Low stream power single thread narrow channel	from meandering to steep braided
1998										
	Straight	Intermediate	Braided	Meandering	Meandering	Straight	D4	Meandering	Low stream power single thread narrow channel	from meandering to steep braided

3.3.2. Sinuosity

The sinuosity (P) of the study reach was estimated as the ratio of the channel thalweg length to the valley length. Reclamation's GIS and Remote Sensing Group in Denver, CO digitized the channel thalweg and measured valley lengths from aerial photographs and topographic maps. The thalweg length was used as the active channel length in the sinuosity computations. Identification of the channel length is subject to the quality of the photographs and surveys.

The sinuosity of the San Felipe Reach has remained close to 1.05 since 1918 (Figure 3-4). The sinuosity of the reach decreased from 1918 to 1972 from about 1.08 to 1.02. After 1972 it increased to 1.07. These results indicate that the channel is straight and coming back close to its original value of 1.08 in 1918.

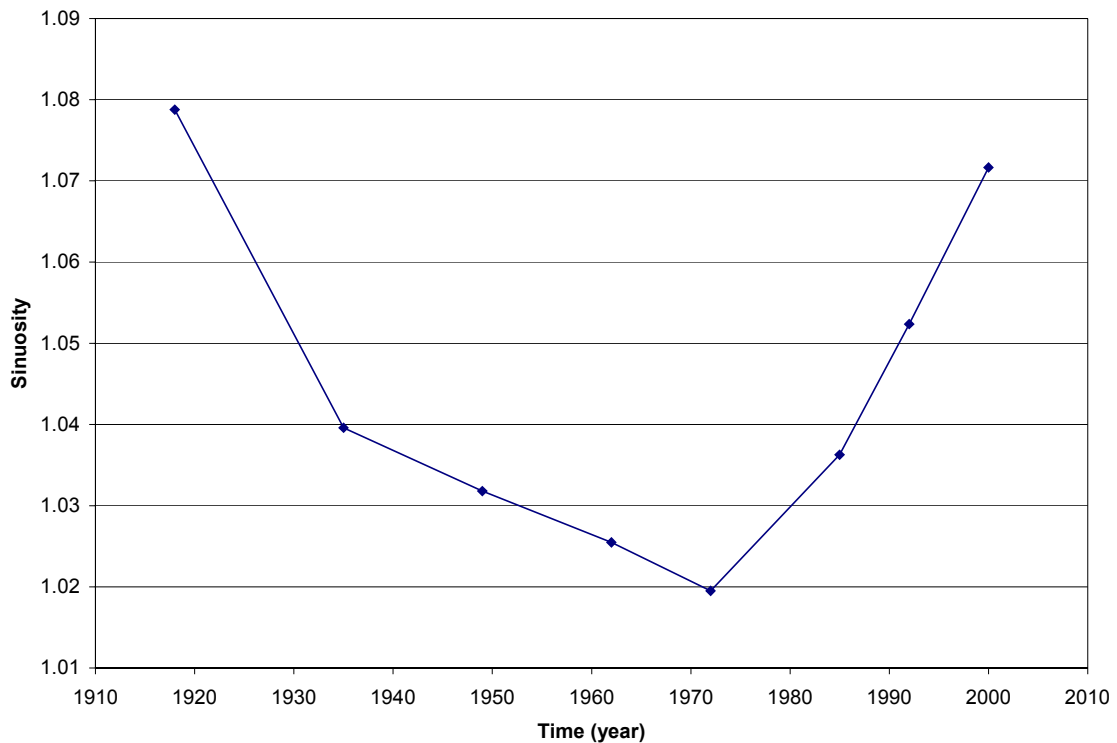


Figure 3-4: Time series of sinuosity of the San Felipe Reach as measured from the digitized aerial photographs.

3.3.3. Longitudinal Profile

Longitudinal profiles were plotted for the study reach for the years of 1962, 1972, 1992 and 1998. The profiles for the first three sets of years were generated from the agg/deg data. The longitudinal profile for 1998 was generated from the CO data and plotted together with the agg/deg line longitudinal profiles. All profiles were generated using the same methodology. Parameters calculated from HEC-RAS® were utilized in this methodology. The HEC-RAS® runs were executed using the channel forming discharge (5,000 cfs). In calculating the mean bed elevation, Equation 3-1 was utilized.

Equation 3-1: Mean bed elevation calculation.

$$MBE = WSE - \frac{A}{Tw} = WSE - H$$

In this equation, MBE represents the mean bed elevation (ft), WSE represents the water surface elevation (ft), A represents the channel area (ft²), Tw represents the channel top width (ft) and H represents the hydraulic depth (ft) which is seen to be equivalent to the area-to-top width (A/Tw) ratio.

Longitudinal profiles of the mean bed elevations for 1962, 1972, 1992, and 1998 are presented in Figure 3-5. It can be seen that the entire reach aggraded an average of 1.2 feet with a maximum of approximately 4 feet between 1962 and 1972 and degraded an average of 3.8 feet with a maximum of approximately 6 feet from 1972 to 1998. 1992 channel elevations are slightly lower than the 1962 elevations, about 1 foot on average. The change from the aggradational trend (1962-1972) to the degradational trend (1972-1998) corresponds to the closure of Cochiti Dam (1973).

Mean Bed Elevation Profile

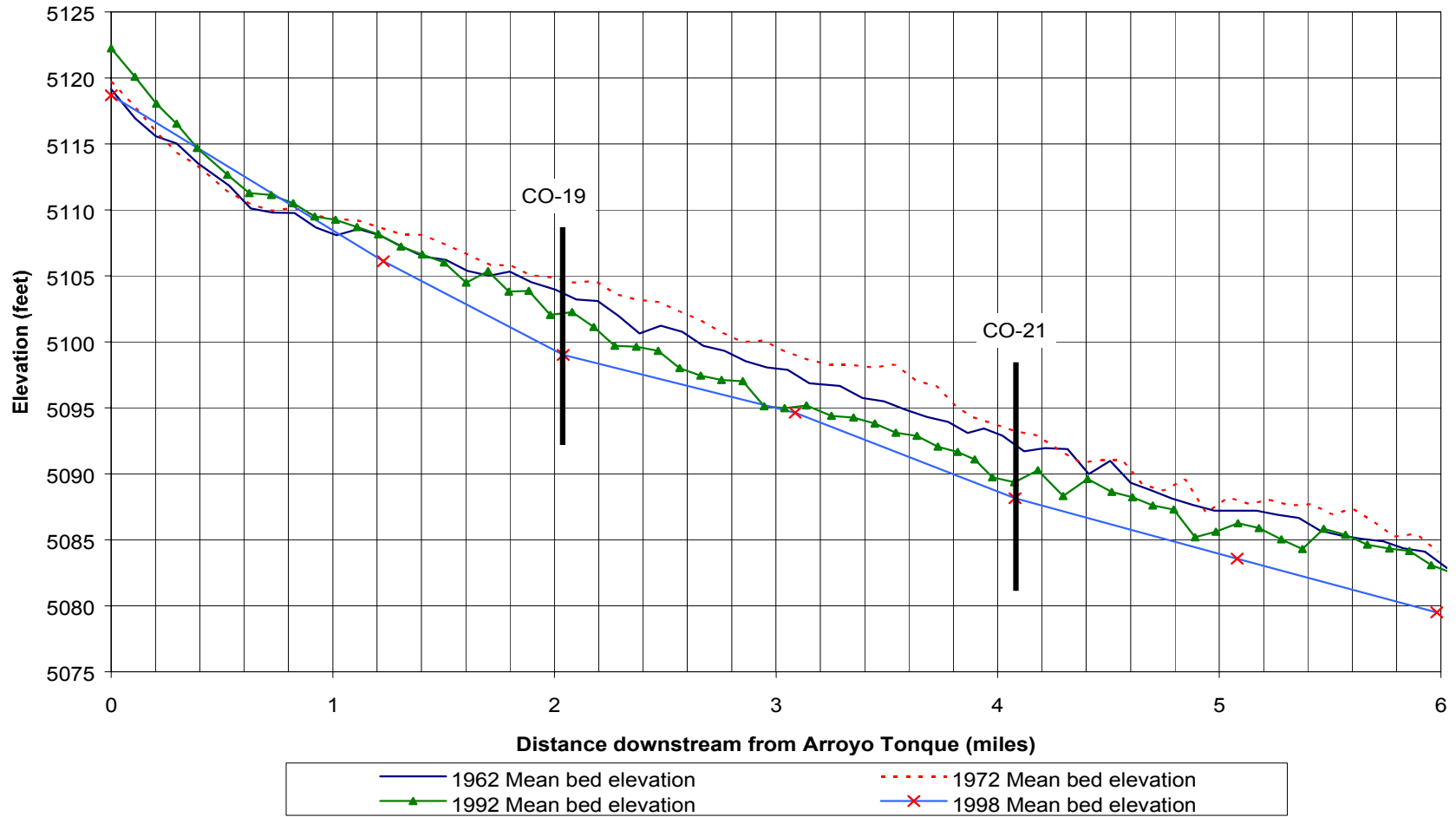


Figure 3-5: Longitudinal mean bed elevation profile to San Felipe Reach for 1962, 1972, 1992 and 1998.

3.3.4. Channel Cross Sections

Each of the seven cross sections from the CO-line surveys was plotted for four different survey dates. These dates were chosen based on the closure of Cochiti Dam (1973). Two of the dates represent pre-dam conditions and two of the dates represent post-dam conditions. These survey dates were chosen to emphasize the impacts of the dam on the channel.

The cross section for CO-22 representing the channel conditions in 1971, 1973, 1995 and 1998 is graphically displayed in Figure 3-6. 1971 and 1973 represent the pre-dam conditions, while 1995 and 1998 represent post-dam conditions. It can be seen that as much as six feet of degradation has occurred since the closure of Cochiti Dam. These results are consistent with those of the longitudinal profiles (Figure 3-5). Similar results can be seen in the other six cross sections, which are attached in Appendix D (Figures D-1 through D-3).

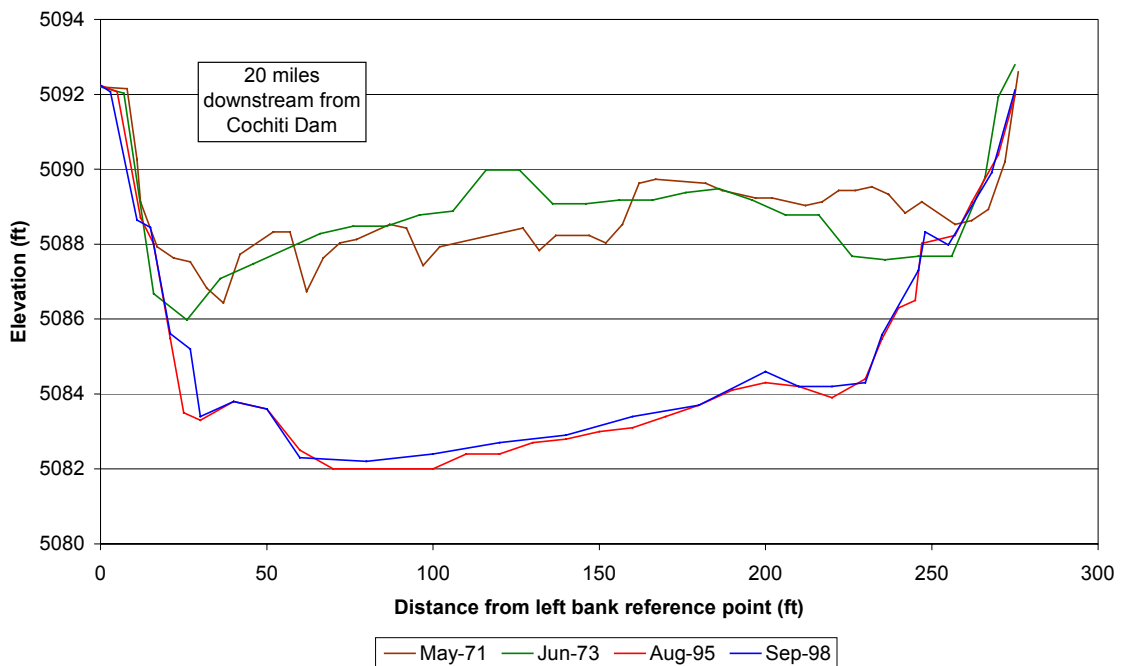


Figure 3-6: Cross section CO-22 (San Felipe Reach) representing pre-dam and post-dam construction.

3.3.5. Channel Geometry

Two methods were used to describe the channel geometry characteristics of the study reach: 1) HEC-RAS® model and 2) digitized aerial photograph interpretation. HEC-RAS® was used to model the channel geometry of the study reach with the available agg/deg line data for 1962, 1972 and 1992 and CO-line data for 1998. A total of 63 agg/deg cross sections spaced approximately 500 feet apart, were modeled. The model for 1998 was performed with seven CO-lines spaced from approximately 4200 feet to 6500 feet apart. A channel-forming discharge of 5,000 cfs was routed through the reach. HEC-RAS® was not calibrated. A Manning's n value of 0.02 was used for the channel and 0.1 for the floodplain for all simulations. All HEC-RAS® results for each of the simulated years are summarized in Appendix F (Table F-1). Digitized aerial photographs were used for active channel delineation as well as to measure the non-vegetated channel width at each agg/deg line. This was executed through the use of GIS. ArcGIS® v. 8.2 was utilized for all digitized aerial photograph analysis.

The resulting channel geometry parameters at each cross section were then averaged over the reach using a weighting factor equal to the sum of one half of the distances to each of the adjacent upstream and downstream cross sections.

The following channel geometry parameters were computed:

Wetted Perimeter = WP
Wetted Cross Section Area = A
Mean Flow Velocity = $V = Q/A$
Where Q = Flow discharge
Top Width = Tw
Hydraulic Depth = $H = A/W$
Width-to-Depth ratio = W/h
Froude Number $Fr = V/(gh)^{0.5}$

The HEC-RAS® results are divided into main channel flow and overbank flow. The main channel results were used for the analyses of this work as this is where the majority of the sediment transport occurs.

The temporal changes in channel geometry as calculated from HEC-RAS® under a dominant discharge of 5,000 cfs are summarized in Figure 3-7. Increasing trends are seen in velocity and depth while decreasing trends are observed in cross sectional area, width-to-depth ratio, and wetted perimeter. The channel has incised since 1962 as evidenced by the increase in flow depth and decrease in width-depth ratio. The increasing trend in velocity is likely the result of channel narrowing. The channel narrowing is evident from the decreasing trend in cross sectional area and wetted perimeter.

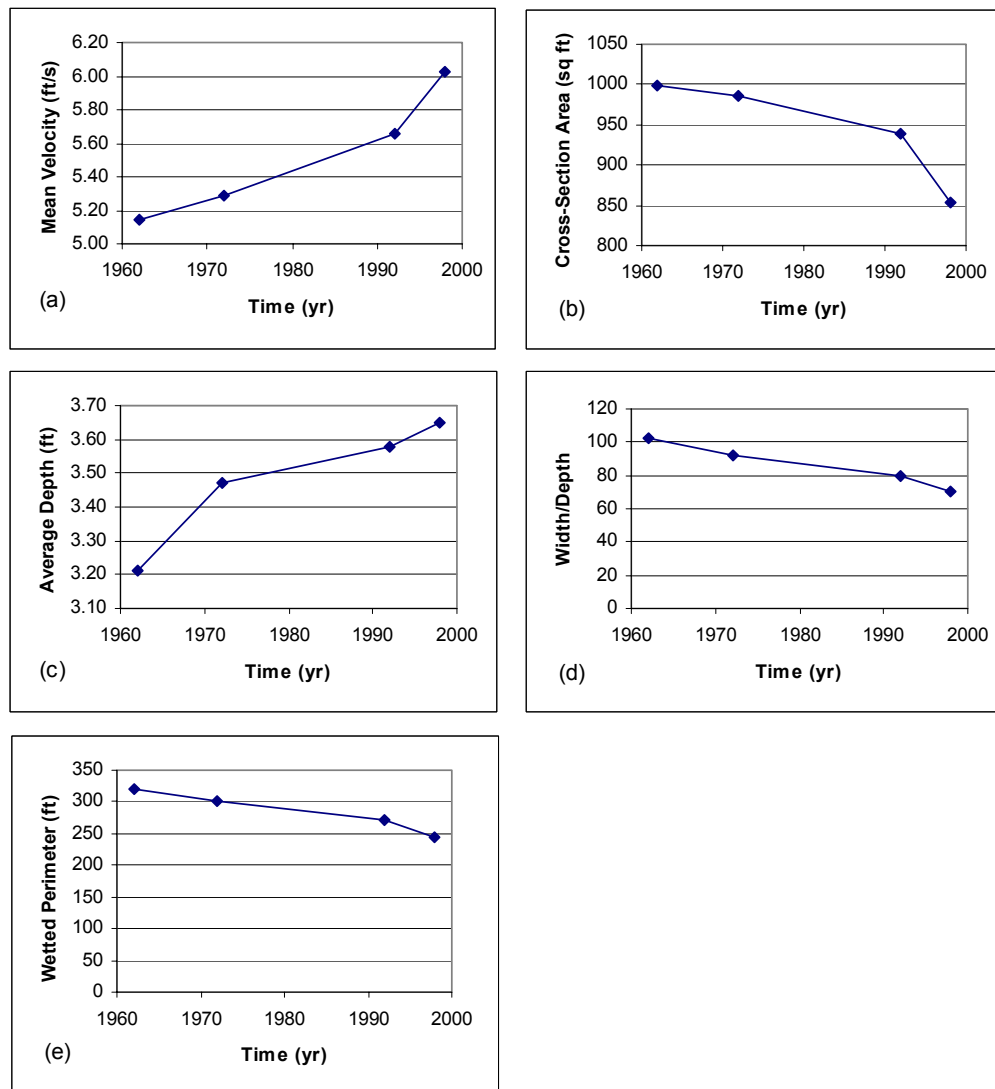


Figure 3-7: Average main channel geometry from HEC-RAS® results for Q = 5,000 cfs. (a) Velocity, (b) Cross-sectional area, (c) Depth, (d) W/h, (e) Wetted perimeter.

Most of the flow occurs in the main channel and not in the overbank region in 1962, 1972, 1992 and 1998 according to the HEC-RAS® results at 5,000 cfs. However, more overbank flow is seen in 1972 which demonstrates the evident aggradational trend during the 1962-1972 period, seen in the mean bed elevation profiles (Figure 3-5).

3.3.5.1. Width

The active channel width time series from the digitized vegetation boundaries are presented in Figure 3-8. The study reach exhibits a general declining trend with time. The largest decrease in width occurs from 1918 to 1935 (approximately 200 feet). From 1935 to 1949 the width leveled off and remained nearly constant during this time period. From 1949 to 1985 the rivers width declined at a rather steady rate. A slight increase in the width occurred between 1985 and 1992 (approximately 30 feet) before returning to a decreasing trend from 1992 to 2001. This slight increase in channel width is seen to be inconsistent with the overall decreasing trend. This could be the result of a time period that was wetter than average, in which higher than normal flows would cause some bank failure resulting in channel widening. The flow discharge data however does not support this notion.

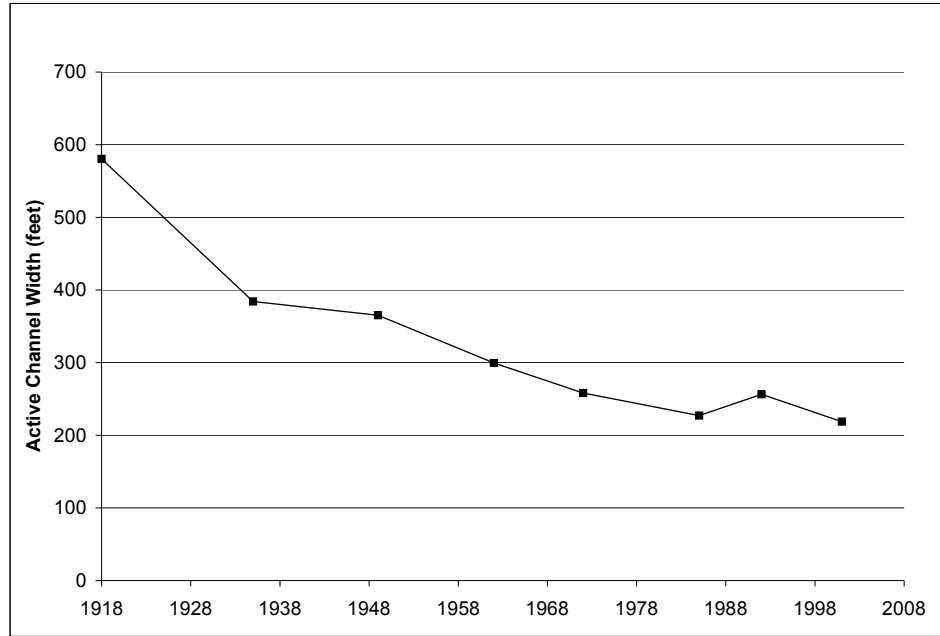


Figure 3-8: Active channel width from digitized aerial photographs.

In addition to the channel widths determined from digitized aerial photographs, the active channel widths were also determined from HEC-RAS® modeling under a dominant discharge of 5,000 cfs. These results can be seen in Appendix F (Figure F-1). It can be seen that there is a decreasing trend in width since 1962. The biggest decrease in width, of approximately 28 feet, occurred in the 6-year time period between 1992 and 1998. This overall decreasing trend in the main channel width is consistent with that of Figure 3-8.

3.3.6. Bed Material

Characterization of the spatial and temporal variability of median bed material size (D_{50}) was performed for the reach. Median grain sizes were computed for 1961, 1972, 1992 and 1998 from USGS gaging stations and CO-line data. Apparent temporal and spatial trends were noted through the generation of bed material gradation curves. In addition, histograms were generated using the D_{50} and D_{84} sizes at each of the seven

cross sections from the CO-line surveys. These histograms were generated using the available data for dates as far back as 1970 (see Table C-4).

Several samples were collected across each cross section. The average of the median bed material sizes (D_{50}) of all the samples collected in the bed of the channel at each station were calculated to characterize the bed material of the reach. These averages were input into the channel classification methods. In addition, different statistics such as minimum, maximum and standard deviation of the median bed material sizes were computed for each year analyzed. These statistics were used to further analyze the bed material trends occurring in the reach.

The bed material for both 1961 and 1972 is classified as fine sand. The data used for the 1961 gradation curve was obtained from the Bernalillo gage, while the data for the 1972 gradation curve was obtained from the San Felipe gage. The bed material for both 1992 and 1998 is classified as medium sand-to-coarse gravel (1992 being coarser than 1998). The data used in the generation of these curves was obtained from the average of CO-20 and CO-22. These gradation curves can be seen in Figure 3-9.

In general, the bed material coarsens with time from 1961 to 1998 (Figure 3-9). This trend is likely due to the high sediment detention by Cochiti Dam (~99% trap efficiency) and tributary sediment detention structures. This sediment detention results in the release of virtually clear water into the reach, causing scour of the fine sand until the bed becomes armored with gravel. Clear water scour does not however account for the fining of the bed material observed from 1992 to 1998. This trend is likely due to the time of year in which the data were collected. The 1998 data were collected in mid-September when low flows are common, which would be less effective transporting finer material off the bed. Conversely, the 1992 data were collected in mid-July when high flows are more likely to be observed (Figure 2-3). These high flows would likely transport smaller bed material sizes downstream, leaving behind coarser materials.

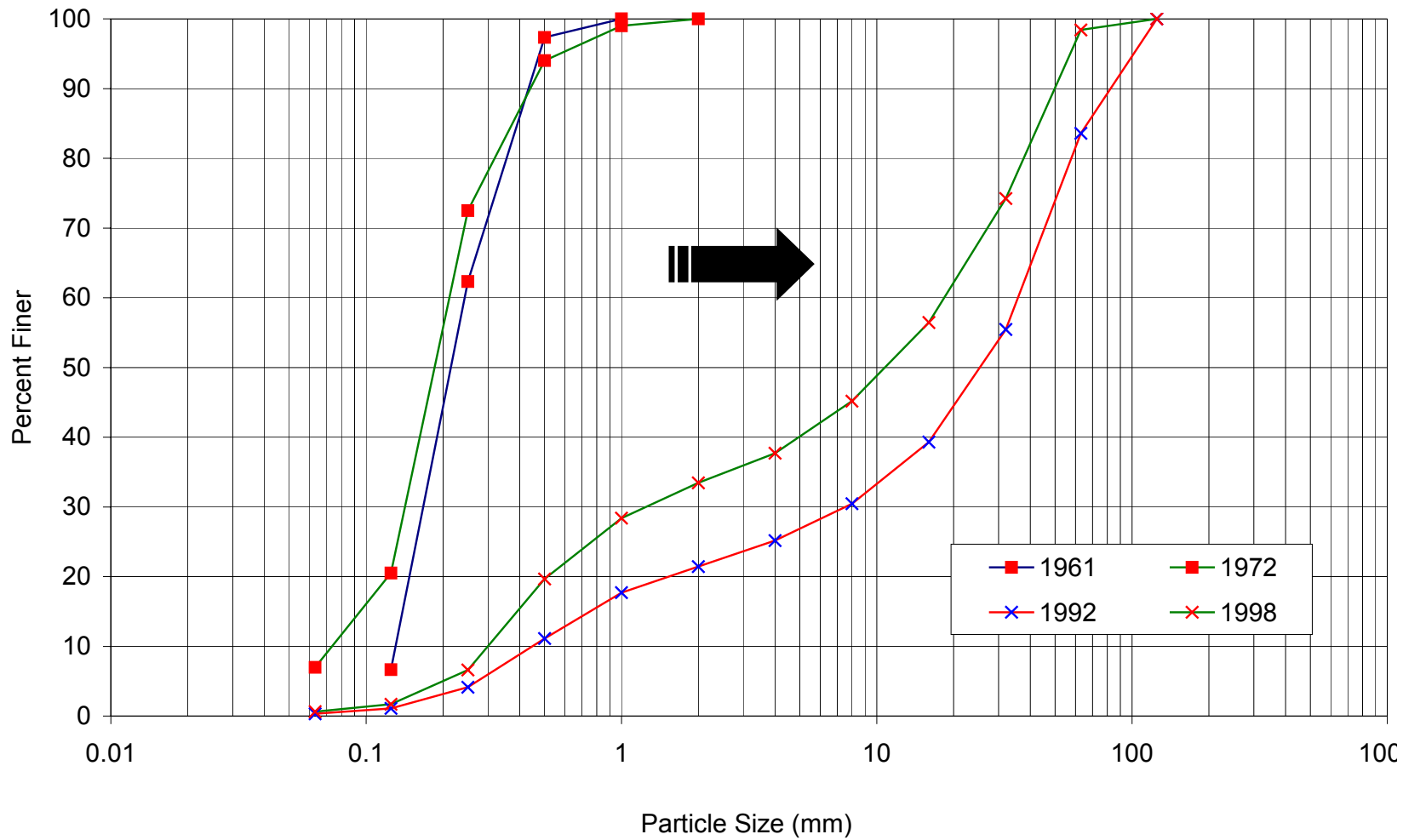


Figure 3-9: Comparison of bed material gradation curves for 1961, 1972, 1992 and 1998.

A histogram showing how the D_{50} and D_{84} sizes change with time is shown in Figure 3-10 for CO-20. It can be seen that both the D_{50} and D_{84} values coarsen after 1975, which roughly corresponds to the closure of Cochiti Dam. It can also be seen how the bed material in 1992 is coarser than the bed material in 1998. Similar trends are seen in the other six cross sections, with the exception of CO-19 in 1970. Although this value seems out of place with respect to the other cross sections, it is possible as Nordin and Culbertson (1961) found coarse material in the upper reaches of the Cochiti project before the dam was built. The remaining six histograms are attached in Appendix G (Figures G-1 through G-3).

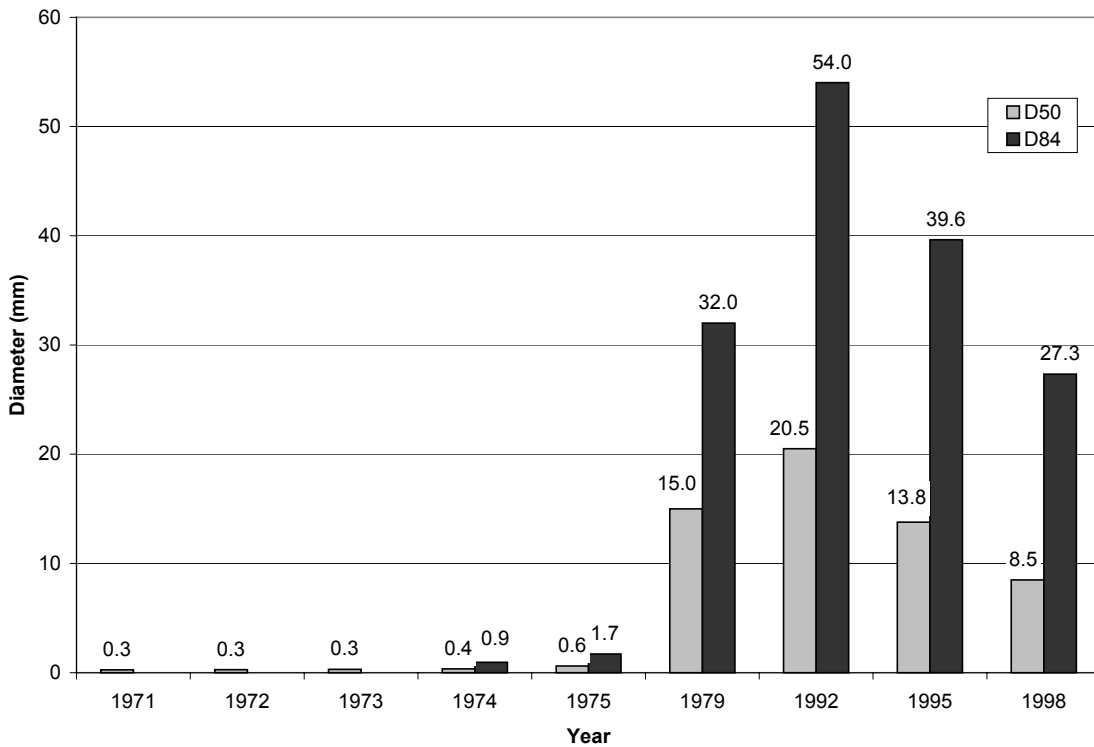


Figure 3-10: Histogram depicting the D_{50} and D_{84} change with time for CO-20.

The average, minimum, maximum and standard deviation statistics of the median bed material sizes at each station were computed for 1962, 1972, 1992, and 1998. These results are summarized in Appendix G (Table G-1). All of the median grain sizes

(D₅₀) are in the sand range for 1961 and 1972. The average (CO-20 and CO-22) median grain sizes are in the gravel range for 1992 and 1998. The majority of the sediment was surveyed at flows near 1,000 cfs with the exception of the 1961 sediment, which was surveyed at flows ranging from 2,140 to 3,850 cfs. These statistics further reveal the coarsening pattern of the bed material since the closure of Cochiti Dam.

3.4 Suspended Sediment and Water History

Water and sediment flow trends in the San Felipe Reach were analyzed through the development of two single-mass curves and one double-mass curve. There was not enough suspended sediment data available to generate difference-mass curves and perform a sediment continuity analysis of the reach.

The following curves were developed for the San Felipe, Bernalillo and Albuquerque gages, for the entire period of record:

- Mass curve of water discharge (acre-feet/year) from 1927 to 2000 (San Felipe gage).
- Mass curve of sediment discharge (tons/year) from 1956 to 1999 (Bernalillo and Albuquerque gages).
- Double mass curve with water and sediment discharge for trends in sediment concentration (mg/l) from 1956 to 1999 (all three gages).

The slopes of each curve and the time periods of breaks in the curves were also estimated.

3.4.1. Single Mass Curves

3.4.1.1. Discharge Mass Curve

The discharge mass curve for the San Felipe gage is presented in Figure 3-11. There are three breaks in slope approximated by eye in the discharge mass curve (1927-1950, 1950-1978 and 1978–2000), with an increase in annual discharge rate from

1978 to 2000 (Figure 3-11). The drier water discharge period (1950-1978) at the San Felipe gage coincides with the drier water period at Cochiti gage, as identified by Richard (2001). These slope breaks in the mass curve represent changes in water regime in the river. These changes may be due to changes in climate and/or flood management or regulation in the Rio Grande basin.

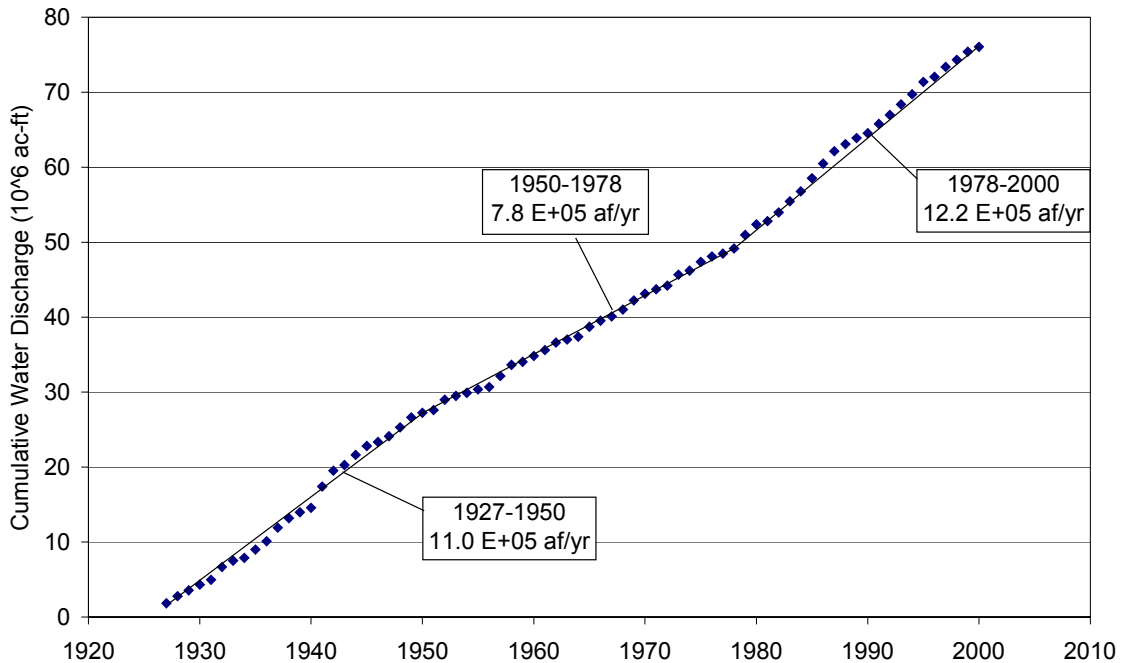


Figure 3-11: Discharge mass curve at the San Felipe gage (1927 – 2000).

3.4.1.2. Suspended Sediment Mass Curve

The suspended sediment mass curve for Bernalillo and Albuquerque gages is shown in Figure 3-12. The Bernalillo gage was decommissioned in 1969 at which time the Albuquerque gage data, located approximately 20 miles downstream was utilized. There were nine slope breaks approximated for this mass curve (Figure 3-12). In general, the slopes are steeper from 1956 to 1973 than after 1973. The slope values range from 2.3 E+06 to 10.8 E+06 tons/year between 1956 and 1973. After 1973, the slope values are between 0.3 E+06 to 2.8 E+06 tons/year. This change in sediment rate in 1973 directly coincides with the closure of Cochiti Dam. There was an increase of

suspended sediment discharge from 1993 to 1995 ($2.8 \text{ E}+06$ tons/year) with respect to the 1978-1993 discharges ($1.1 \text{ E}+06$ and $0.3 \text{ E}+06$ tons/year). However, the 1995-1999 suspended sediment discharge has decreased to $0.8 \text{ E}+06$ tons/year and is comparable to the 1978-1985 sediment discharge ($1.1 \text{ E}+06$ tons/year).

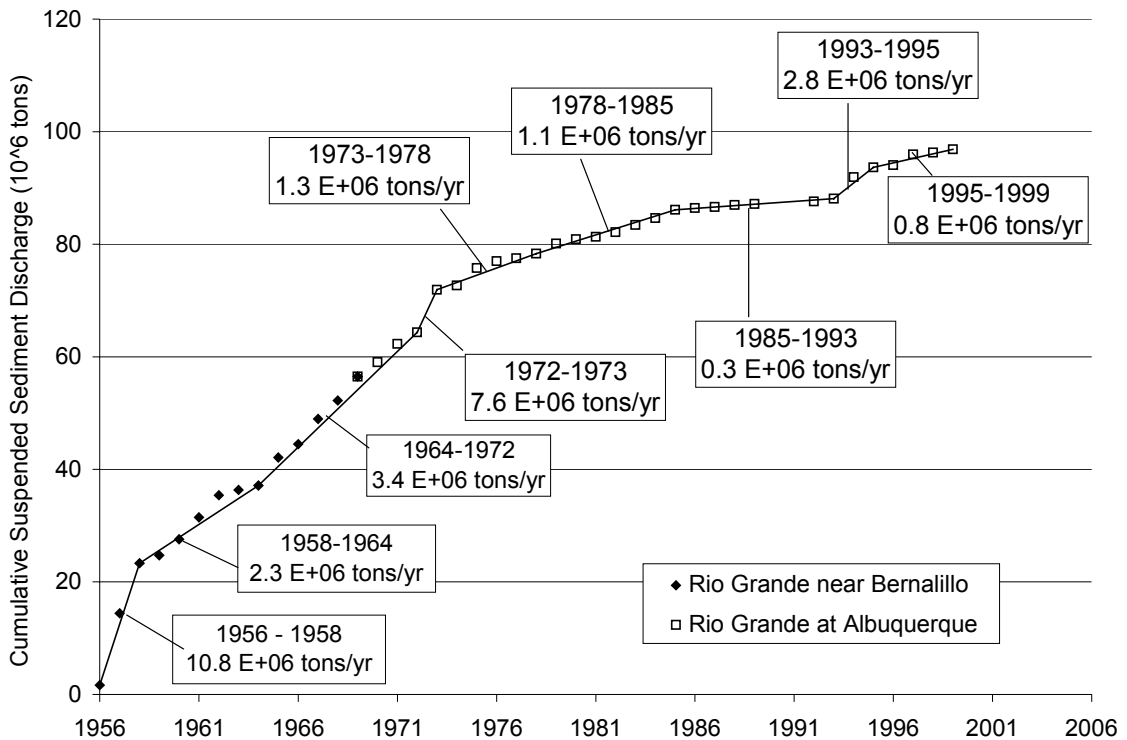


Figure 3-12: Suspended sediment mass curve at Bernalillo and Albuquerque gages (1956 – 1999).

3.4.2. Double Mass Curves

The double mass curve of cumulative water discharge versus cumulative sediment discharge, shown in Figure 3-13, shows the changes of suspended sediment concentration with time. It can be seen that higher concentrations of suspended sediment occur from 1956 to 1973 with the average concentration varying from 3,128 mg/l to 6,439 mg/l. After 1973, the concentration does not exceed 1,357 mg/l. Again, this directly coincides with the closure of Cochiti Dam. In general, the double mass curve shows a similar trend as the suspended sediment single mass curve. An average

concentration of 587 mg/l has persisted from 1995 to 1999 and is comparable to the average concentration from 1978 to 1984 (606 mg/l).

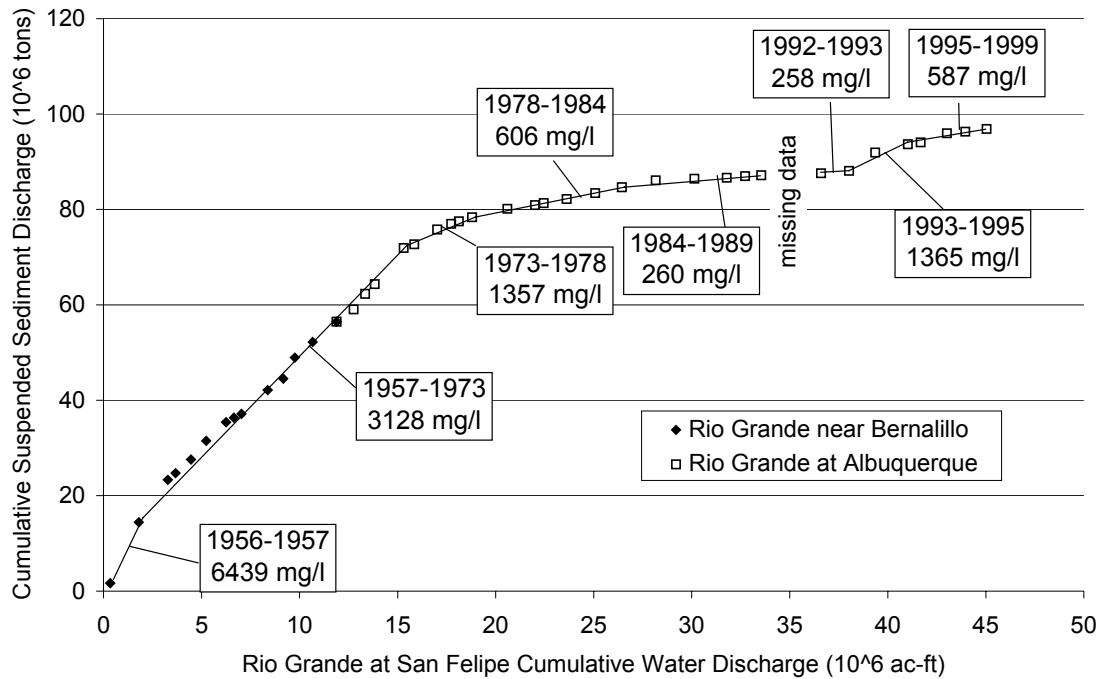


Figure 3-13: Cumulative discharge at San Felipe gage vs. cumulative suspended sediment load at Bernalillo and Albuquerque gages (1956 – 1999).

The Angostura Diversion Dam, which is located between the San Felipe and Bernalillo-Albuquerque gages, does not appear to affect the water and sediment balance between the gages. This is due to the fact that the double mass curve generated using only water and sediment data from the Bernalillo and Albuquerque gages has the same general trend and range of values as that generated with the use of the San Felipe gage (Figure 3-13). This double mass curve utilizing only data from the Bernalillo and Albuquerque gages can be seen in Figure H-1 (Appendix H). By comparing Figure 3-13 and H-1 an expected slight increase in sediment load can be seen between San Felipe and the downstream gage (Albuquerque), which is located approximately 28.5 miles downstream from the diversion dam. This slight increase in sediment load doesn't have an affect on the overall trend of the double mass curve.

3.5 Sediment Transport Analysis

The concept behind sediment transport can be seen graphically in Figure 3-14. This figure displays the sediment transport capacity and supply curves as a function of grain size (D_s). If a river can transport more sediment than what is entering the reach, it is said to be supply limited; that is, the sediment transport is limited by the supply of sediments. This condition is typical of gravel bed rivers where degradation is usually occurring as is the case of Cochiti Reach. Conversely, when a river does not have the transport capacity to pass the incoming supply of sediments it is said to be capacity limited. This condition is typical of rivers having a finer bed material (silt/sand) and that are usually in a state of aggradation. Also shown in Figure 3-14 is the grain size cutoff value (D_{10}) between wash load and bed material load, the sum of which equals the total load. This particular method used in calculating the total load is driven by the source of the sediment.

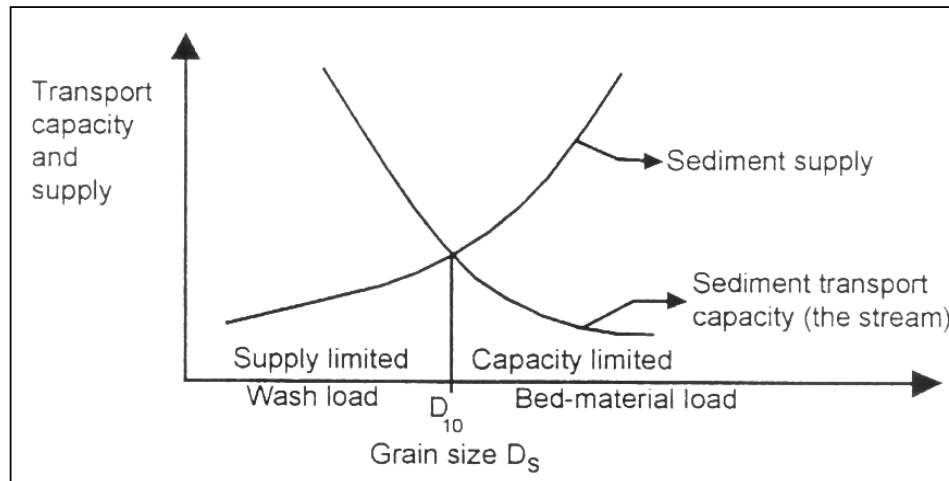


Figure 3-14: Sediment transport capacity and supply curves (Julien, 1998).

A sediment transport analysis was performed to compare the reach transport capacity with: 1) the incoming sand load ($0.0625 \text{ mm} < D_s < 2 \text{ mm}$); and 2) the incoming bed material load ($0.30 \text{ mm} < D_s < 2 \text{ mm}$). Field observations performed by the USBR indicate that sand size particles are mobile at all flows greater than 300 cfs as bedload

material and become suspended at flows greater than 3,000 cfs (Massong, 2001). According to these field observations, it is believed that the bed material load is comparable to the sand load (0.0625 mm and 2 mm) (Massong, 2001).

However, very fine and fine sand size particles (0.0625 mm to 0.25 mm) are not found in large quantities in the bed (D_{10} of bed material = 0.30 mm (Figure 3-9)) at flows close to 5,000 cfs, which suggests that they behave as washload (Table 3-2). In addition, the amount of sand particles in suspension finer than 0.30 mm (D_{10} of the bed material) is approximately 80% or more at flows close to 5,000 cfs (Table 3-2). As a result, the bed material load comprises only the sediment particles coarser than 0.30 mm at flows close to 5,000 cfs. In estimating the bed material load, a methodology was used where the bed material and suspended material gradation data were utilized. The complete set of raw gradation data can be seen in Appendix I (Table I-1) along with the resulting bed material and suspended material curves representing the gradation averages (Figures I-1 through I-4). In addition, a summary of percents of total load behaving as washload and bed material load is attached in Appendix I (Table I-2).

Table 3-2: Percentages of total load that behave as washload and bed material load at flows close to 5,000 cfs; taken from BI-line surveys.

Date	Inst. Discharge (cfs)	D_{10} bed material (mm)	% washload	% bed material load
6/18/1993	4638	0.30	74	26
6/19/1993	4426	0.35	63	37
6/20/1993	4459	0.30	78	22
5/28/1994	4839	0.24	73	27
5/27/1994	4509	0.39	95	5
5/27/1994	4807	0.31	93	7
6/5/1995	4723	0.33	92	8
6/22/1995	5442	0.30	79	21
6/22/1995	5437	0.33	81	19
6/5/1995	4652	0.38	90	10
7/2/1995	5331	0.31	77	23
Average =	4842	0.32	81	19

Total sediment input to the reach was estimated using the Modified Einstein Procedure (MEP) (Colby and Hembree, 1955, US Bureau of Reclamation, 1955). Cross-

section geometry measurements, suspended sediment and bed material samples at Bernalillo Island (BI-lines 286, 291 and 296) surveys from 1992 to 1995 were used for the purposes of estimating the incoming total load and sand load to the reach using the MEP. The BI-lines are located approximately six miles downstream from the study reach. As a result, the total load might be slightly over estimated since sediment is likely mined from the bed and banks between the study reach and the BI-lines. A non-linear regression function was fit to the MEP results to develop a sand load rating curve.

Channel transport capacities were estimated for the reach for 1962, 1972, 1992 and 1998 using different sediment transport equations. The following bed material load equations were used to estimate the transport capacity for 1962 and 1972: Laursen, Engelund and Hansen, Ackers and White (D_{50} and D_{35}), Yang – sand (D_{50} and size fraction), Einstein and Toffaleti (Stevens and Yang, 1989, Julien, 1998). The following bedload equations were used to estimate the transport capacity for 1962 and 1972: Schoklitsch, Kalinske, Meyer-Peter and Müller, Rottner and Einstein. Between 1972 and 1998, the bed material gradation analysis indicated that the reach became coarser with a median grain size of coarse gravel (Figure 3-9). Therefore, usage of the majority of bed-material transport relationships would not be appropriate. The suitability of sediment transport relationships related to sediment size is summarized in Table I-3 (Appendix I). As a result, the 1992 and 1998 transport capacities were computed with four bed material load relationships and five bedload relationships. The bed material load relationships utilized were the following: Ackers and White (D_{50} and D_{35}) and Yang – gravel (D_{50} and size fraction). The bedload relationships utilized were the following: Schoklitsch, Kalinske, Meyer-Peter and Müller, Rottner and Einstein.

Sediment transport capacities were estimated for comparative purposes. Unfortunately, comparisons could only be made between 1962-1972 and 1992-1998 due to the different sets of transport equations used for each set of years. Again, this is a

result of the bed material coarsening from fine sand to coarse gravel. The input data used in the sediment transport equations were the reach-averaged channel geometry values resulting from HEC-RAS® simulations at 5,000 cfs. Table I-4 (Appendix I) summarizes the input data for the reach for each year analyzed.

The total load computed from the MEP comprises mostly sand material. Gravel load occurs with flows close to 5,000 cfs and is not represented in the total MEP load. Figure 3-15 presents the sand load (0.0625 mm – 2 mm) data. A non-linear regression function was fit to the data to obtain the rating curve at the BI-lines. Using a channel-forming discharge of 5,000 cfs, the estimated MEP sand load near the BI-lines is 9,550 tons/day. The variability of the data points is about one order of magnitude around the regression line (Figure 3-15). As a result, the actual sand load could vary considerably from the estimated value.

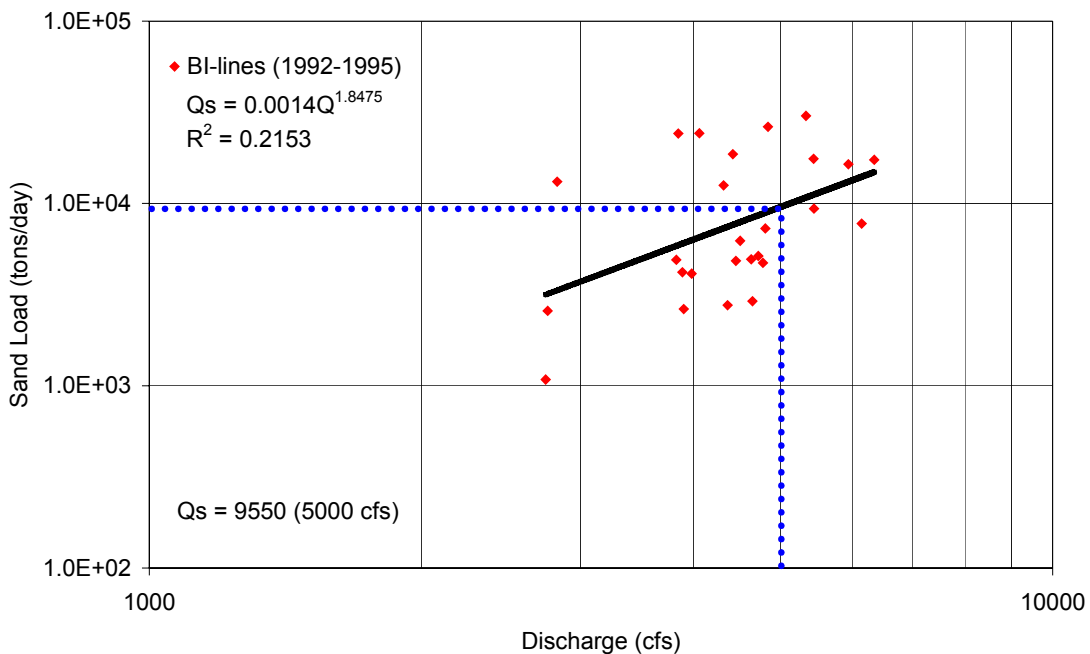


Figure 3-15: Albuquerque gage sand load rating curve for the spring and summer seasons from 1978 to 1999.

Table I-5 (Appendix I) lists the transport capacity calculations for 1962 and 1972 for the San Felipe Reach. The slopes in this table correspond to the water surface slopes. The different types of equations as well as the different applications of these equations (bedload/bed material load) yield varying results. For the 1962 bed material load equations: Engelund and Hansen's, Ackers and White's (D_{50}) and Einstein's equations yield similar results, while Laursen's and Yang's - sand (D_{50} and size fraction) equations results are also comparable to each other. Ackers and White's (D_{35}) and Toffaleti's equations provide somewhat higher values. For the 1962 bedload equations: Kalinske's, Meyer-Peter and Müller's and Einstein's equations yield comparable results. Somewhat higher values were calculated using Schoklitsch's and Rottner's. For the 1972 bed material load equations: Laursen's, Engelund and Hansen's, Ackers and White's (D_{50}) and Einstein's equations yield comparable results, while Yang's – sand (D_{50} and size fraction) equations are comparable as well. Ackers and White's (D_{35}) and Toffaleti's equations calculated somewhat larger values. The 1972 bedload equations produce similar result trends as compared to the 1962 bedload equations. For 1962, no sediment transport capacity exceeds 132,000 tons/day (bed material load) or 14,500 tons/day (bedload). For 1972, no sediment transport capacity exceeds 184,000 tons/day (bed material load) or 15,000 tons/day (bedload).

Table I-6 (Appendix I) lists the transport capacity calculations for 1992 and 1998 for the San Felipe Reach. The slopes indicated in this table correspond to the water surface slopes. The different types of equations and the different applications of these equations (bedload/bed material load) bear varying results. For the 1992 bed material load equations: Ackers and White's (D_{35}) and Yang's – gravel (D_{50} and size fraction) equations have similar results, while Ackers and White's (D_{50}) equation gives a somewhat lower value. For the 1992 bedload equations: Schoklitsch's, Kalinske's and Meyer-Peter and Müller's equations yield comparable results, while Rottner's and

Einstein's equations surrender somewhat lower values. For the 1998 bed material load equations, all equations yield analogous results. For the 1998 bedload equations: Schoklitsch's, Kalinske's and Meyer-Peter and Müller's equations generate comparable results. Rottner's equation yields a somewhat higher value and Einstein's equation produces a somewhat lower value. For 1992, no sediment transport capacity exceeds 4,000 tons/day (bed material load) or 2,000 tons/day (bedload). For 1998, no sediment transport capacity exceeds 4,500 tons/day (bed material load) or 4,000 tons/day (bedload).

The average bed material transport capacity in 1992 is lower than the average transport capacity in 1998 (2,016 tons/day and 3,288 tons/day, respectively), (Table I-6). These values are both lower than the incoming sand load (9,550 tons/day). This would indicate a capacity limited condition along with an aggradational trend, which is not in agreement with the observed degradation of the channel bed that occurred between 1992 and 1998 (Figure 3-5). However, using the incoming bed material load would make a more representative comparison. These low transport capacities are likely a direct result of the coarse material present in the bed.

In general, the washload is comprised of the fine particles not found in large quantities in the bed ($D_s < D_{10}$) (Julien, 1998). The D_{10} of the bed material from the BI-line surveys is on average 0.30 mm (Table I-2). The percent of material in suspension finer than 0.30 mm is about 80% at flows close to 5,000 cfs (Table 3-2), which suggests that very fine and fine sand particles behave as washload. As a result, the incoming bed material load is approximately 1,910 tons/day, representing 20% of the sand load (Appendix I). This methodology for the bed material load estimation is carried out under the assumption that the silt load is small enough to be neglected. Bed material transport capacities for 1992 and 1998 (2,016 tons/day and 3,288 tons/day, respectively), are both higher than the incoming bed material load (1,910 tons/day). This would indicate a

supply limited condition as well as degradation along the reach, which is in agreement with the observed degradation during this period from the elevation profiles (Figure 3-5).

This methodology was undertaken using the BI-line surveys for 1992 – 1995, for which a graphical example is shown in Figure 3-16. This figure shows the bed material together with the suspended material gradation curves at the BI-lines for 1992. It can be seen that the average D_{10} of the bed material (0.30 mm) approximately corresponds to a percent finer value of 80% on the suspended material gradation curves. This indicates that approximately 80% of the sand load is washload while the remaining 20% of the sand load represents the bed material load. All bed material and suspended material gradation curves (Figures I-1 through I-4) used in this methodology complete with the raw data (Table I-1) used in generating the curves in addition to a complete summary (Table I-2) of all values used for the bed material load estimation are attached in Appendix I.

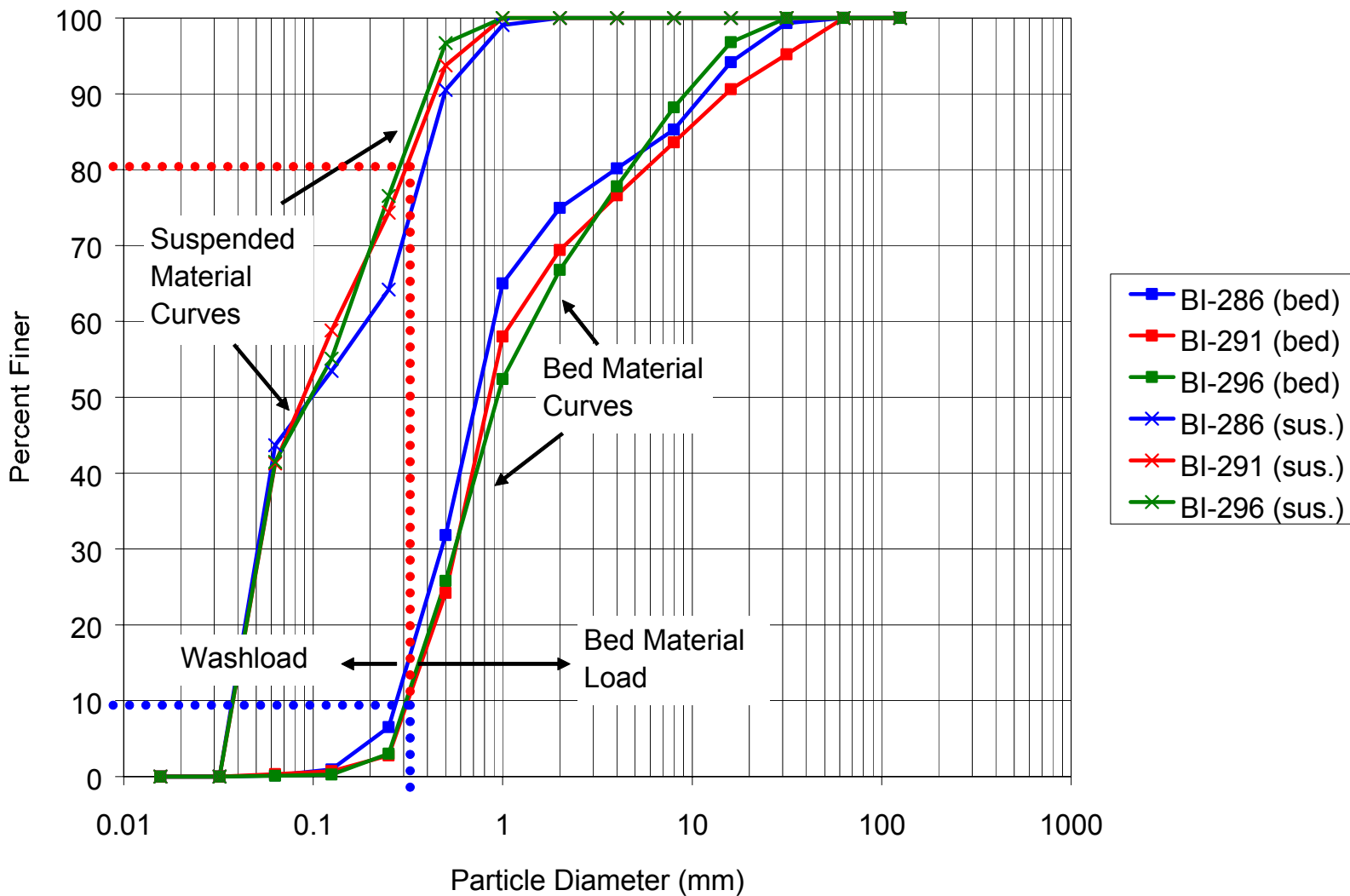


Figure 3-16: Example of bed material load estimation methodology from 1992 BI-line surveys.

3.6 Summary and Conclusions

The hydraulic modeling analysis (HMA) was performed on the San Felipe Reach of the MRG, which spans 6.15 miles from the mouth of the Arroyo Tonque (agg/deg 174) to the Angostura Diversion Dam (agg/deg 236). By analyzing and characterizing the historic conditions of the study reach, an evaluation of the potential future equilibrium conditions can be made. General trends of the study reach include a decrease in width, width-to-depth ratio, wetted perimeter and cross sectional area and an increase in flow velocity and depth during the 1962 to 1998 time period. The main conclusions are:

- The entire reach aggraded approximately 1.2 feet between 1962 and 1972 and degraded approximately 3.8 feet between 1972 and 1998. The bed degraded a maximum of roughly 4 feet from 1992 to 1998. Changing from an aggradational trend to a degradational trend directly corresponds to the closure of Cochiti Dam; likely the result of clear water scour. The dam's trap efficiency is approximately 99%.
- From 1972 to 1998, the bed material of the study reach changed from sand to a bimodal sand-coarse gravel bed material distribution. There exists a depletion of sand within the reach. Pending man-made interventions, the sand supply is expected to continue to decrease throughout the next decade, which will result in a continued trend of bed degradation until the bed is completely armored.
- The reach averaged active channel width of the study reach decreased from 580 feet in 1918 to 219 feet in 2001. The largest decrease in channel width occurred between 1918 and 1935 (approximately 200 feet). After 1949, the channel width declined at a rather steady rate until 1985, at which time a slight increase in width occurred until 1992 before

returning to a decreasing trend (Figure 3-8). This slight increase in width, which is seen to be inconsistent with the overall decreasing trend, could be the result of a time period that was wetter than average. That being, the channel would be conveying higher than normal flows, which could cause bank failure resulting in channel widening. The historical flow data however does not support this notion. Since these widths were measured utilizing aerial photographs, another possible explanation of this channel widening could be the time of year the photograph was taken, or the digitized quality of the photograph. For a more detailed look at photograph error, refer to Section 4.2.4. The overall decreasing channel width trend from 1918-2001 is likely due to decreasing flow rates, controlled flow rates being released from the dam and coarsening of the bed material occurring throughout this time period.

- Planform geometry of the entire reach is a straight single-thread channel with few vegetated islands at bankfull discharge of 5,000 cfs. The channel sinuosity for the entire reach remained nearly constant at 1.07 throughout the entire period analyzed, indicative of a nearly straight channel.
- According to the modeling results from HEC-RAS®, the 1962, 1992 and 1998 channels have greater capacity to convey the modeled discharge (5,000 cfs) without overbank flow than the channel in 1972. The simulated increase in flow velocity from 1992 to 1998 increased the capacity of the reach to transport the bed material load ($0.3 \text{ mm} < D_s < 2 \text{ mm}$) in 1998. This increase in flow velocity is likely due to a decrease in the cross sectional area of the channel for this time period.
- At flows close to 5,000 cfs, very fine and fine sand particles ($0.0625 \text{ mm} < D_s < 0.25 \text{ mm}$) behave as washload. The bed material load is

approximately 20% of the sand load (9,550 tons/day). Therefore, the incoming bed material load is 1,910 tons/day.

- The sediment transport capacity for 1962 and 1972 was calculated with eight different bed material load equations (Laursen, Engelund and Hansen, Ackers and White (D_{50}/D_{35}), Yang-sand ($D_{50}/\text{size fraction}$), Einstein and Toffaleti) and five different bedload equations (Schoklitsch, Kalinske, Meyer-Peter and Müller, Rottner and Einstein) together with the 1962 and 1972 channel geometry. These results are summarized in Table 3-3. The results details can be see in Table I-5 (Appendix I).

Table 3-3: Summarized sediment transport results for 1962 and 1972.

Year	BML average (tons/day)	BL average (tons/day)	Minimum BML (tons/day)	Maximum BML (tons/day)	Minimum BL (tons/day)	Maximum BL (tons/day)
1962	65,164	5,818	33,877	131,301	992	14,443
1972	86,619	6,033	36,581	183,012	658	14,715

- The sediment transport capacity for 1992 and 1998 was calculated with four different bed material load equations (Ackers and White (D_{50}/D_{35}) and Yang-gravel ($D_{50}/\text{size fraction}$)) and five different bedload equations (Schoklitsch, Kalinske, Meyer-Peter and Müller, Rottner and Einstein) together with the 1992 and 1998 channel geometry. These results are summarized in Table 3-4. The results details can be seen in Table I-6 (Appendix I).

Table 3-4: Summarized sediment transport results for 1992 and 1998.

Year	BML average (tons/day)	BL average (tons/day)	Minimum BML (tons/day)	Maximum BML (tons/day)	Minimum BL (tons/day)	Maximum BL (tons/day)
1992	2,016	921	283	3,876	19	1,555
1998	3,288	1,793	2,545	4,174	351	4,000

The increase in channel transport capacity from 1992 to 1998 is likely due to the fining of the bed material during this time period.

The incoming bed material load (1,910 tons/day) is much closer to the average transport capacities than the incoming sand load (9,550 tons/day). According to the results for 1992, the equation that best estimates the bed material load is Yang's – gravel (size fraction) with 1,834 tons/day. According to the results for 1998, the equation that produces the closest result to the bed material load is Schoklitsch's with 2,087 tons/day. The 1992 and 1998 average bed material capacity loads (2,016 tons/day and 3,288 tons/day, respectively) are both slightly higher than the incoming bed material load (1,910 tons/day), resulting in a channel that is supply limited (typical of gravel bed rivers) in a state of degradation. This conclusion is in agreement with the observed degradation in the channel bed that occurred between 1992 and 1998 (Figure 3-5). However, given the uncertainty involved in the estimation of the bed material load (Figure 3-15); it could be said that the average transport capacity is comparable. As a result, the channel slopes in 1992 and 1998 seem appropriate to transport the incoming bed material load of 1,910 tons/day at a discharge of 5,000 cfs.

The bed material gradation curves for the reach in 1992 and 1998 (Figure 3-9) represent a much coarser material than the bed material gradation curves collected at the BI-line surveys that were used for the estimation of the bed material load (see Appendix I). The median grain size (D_{50}) of the bed material at the BI-line surveys is finer than coarse sand for most of the samples (see Appendix I). As a result, the transport capacities computed for the reach do not compare well with the sand load estimated

with the MEP. It is likely that a layer of sand, coming from tributaries and mined from the bed and banks of the channel upstream of the study reach, overlays and moves above a layer of coarser material (armor layer) that the river cannot transport.

CHAPTER 4: MEANDER MIGRATION ANALYSIS (MMA)

4.1 Introduction

The objective of the meander migration analysis (MMA) was to analyze historic photographic data to identify trends among curvature characteristics and migration rates of isolated bends. In achieving this objective, datasets were developed for a number of meanders and an analysis of those datasets was performed. Observed relationships included such variables as migration rates, radii of curvatures, flow depth and channel width. In addition, secondary flow characteristics were analyzed, sine generated curves were developed, a hydrological analysis was performed and stream power/specific stream power analyses were conducted; all to try and aid in the explanation of observed channel trends. This analysis was performed on the Galisteo Reach.

4.2 Reach Background

4.2.1. Reach Definition

The Galisteo Reach is included as part of the Cochiti Reach in the MRG. Beginning at the mouth of Galisteo Creek, this reach spans 8.15 miles downstream to the mouth of the Arroyo Tonque, which marks the beginning of the San Felipe Reach that was utilized in the HMA. The reach encompasses agg/deg survey line 98 to agg/deg survey line 174. There are eight Cochiti (CO) range lines (CO-9 to CO-16) located in this reach. CO-9 is located at the Galisteo Creek confluence (agg/deg 98). CO-lines, 10, 11, 12, 13, 14, 15 and 16 correspond to agg/deg lines 108, 117, 123, 136, 149, 159 and

167, respectively. For a more detailed discussion on agg/deg lines and CO-lines, refer to Section 2.4.

Maps generated utilizing a Geographic Information System (GIS) depicting the locations of the agg/deg lines and CO-lines can be seen in Appendix J (Figures J-1 and J-2, respectively). Also included in this appendix (Figures J-3 to J-6) are aerial photographs of the Galisteo Reach showing locations of the CO-lines along with pertinent geographic features.

4.2.2. Bend Definition

The Galisteo Reach is the most sinuous of the four subreaches making up the Cochiti Reach (Figure 4-1). It is important to note however that all sinuosities are below a value of 1.5, indicative of a straight channel. By observing the Galisteo Reach at a larger scale, some subtle bends become apparent. Seven bends were arbitrarily chosen along the Galisteo Reach for analysis. Each of these bends was isolated at a large scale to facilitate analysis. The locations of these bends are shown graphically in Figure 4-2.

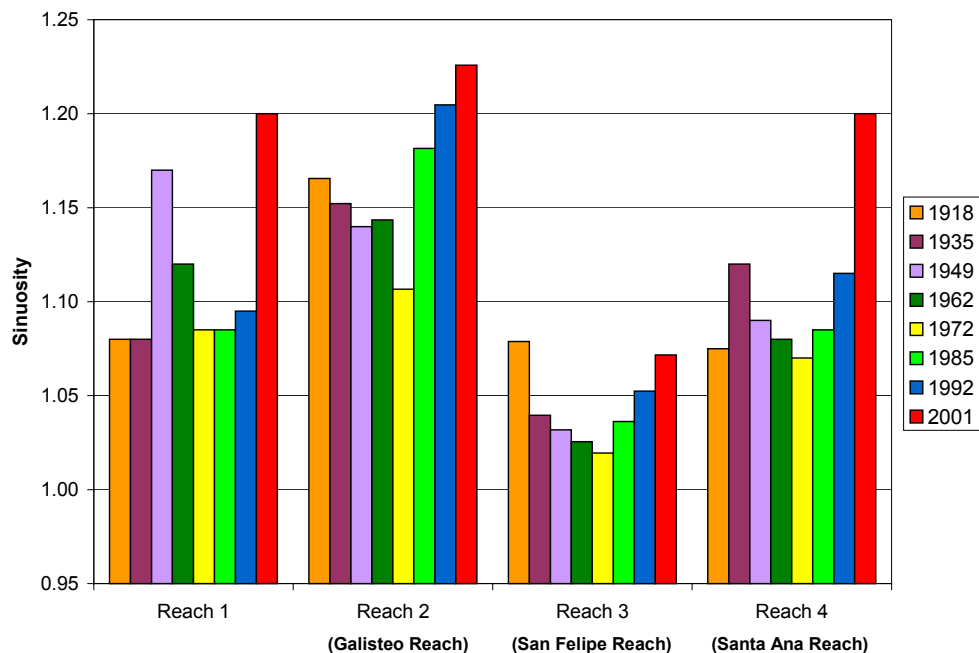


Figure 4-1: Subreach time series of sinuosities along Cochiti Reach.

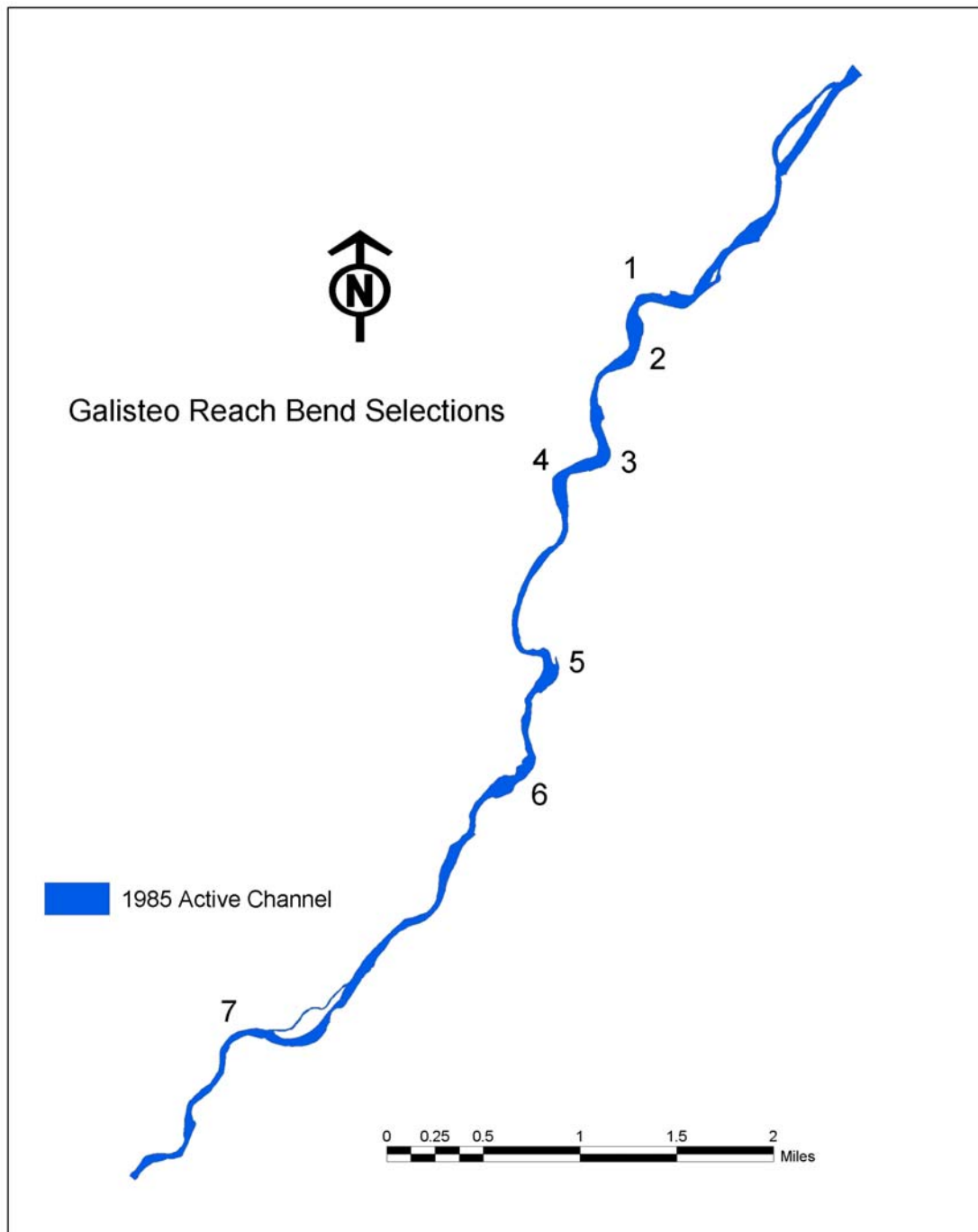


Figure 4-2: Bend selection along Galisteo Reach used in the MMA.

4.2.3. Available Data

The main sources of data utilized for the MMA were sets of aerial photographs. Analysis focused on the 1972 to 1992 time period. Three sets of aerial photographs (1972, 1985 and 1992) exist for this time period; therefore two time periods (1972-1985 and 1985-1992) were analyzed to represent this 20-year span. The digitized format of these photographs displaying only the active channel were used in conjunction with ArcGIS® in the development of a dataset used in the determination of certain bend characteristics, including the coordinates of channel bank features, radii of curvatures, active channel widths, etc. For a more complete discussion of the aerial photographs, refer to Section 4.2.4.

Using aerial photography in measuring and predicting rates of migration is a popular current state of practice. The methodology involves using aerial photography to predict erosion rates by projecting past rates into the future. With this prediction however, comes a big assumption that flow characteristics similar to those of the past will occur into the future. This means that a prediction must be made for the unpredictable behavior of meander patterns. Also, with the potential variables that could evolve with geomorphology such as ox-bows, and geological variables within the zone that the river is migrating through, predictions of real accuracy become increasingly more difficult.

In addition to the GIS analysis, HEC-RAS® analyses were performed on the Galisteo Reach for each bend analyzed in order to determine the approximate flow depth (h) for each bend. The flow depth was utilized in the secondary flow analysis as well as in the relationships analyzed with the relative migration rates (M/W). For obtaining the average flow depth for each bend, agg/deg line surveys were utilized due

to the fine spacing. Recall that agg/deg line surveys are not available for 1985; therefore the 1992 line surveys were substituted for the 1985 HEC-RAS® analysis.

4.2.4. Photograph Error Analysis

A raw aerial photograph is not as accurate as a map. It contains scale distortions resulting from such effects as camera tip and tilt, lens distortion, aircraft flying pattern, terrain relief displacement, earth curvature, topology and atmospheric refraction. Because of these distortions, it is impossible to make accurate, meaningful measurements directly from an aerial photograph. For these photographs to be useful, these errors must be removed. Removal of these scale variations and image displacements is done through processes referred to as differential rectification, orthorectification, or in the case where the underlying relief does not change significantly over the extent of the photograph, advanced digital rectification (ADR). This process involves matching known geographical locations on the ground (control points) with the same positions on the photographic image (Adams, 1998). By applying photogrammetric mathematics, each pixel in the image is repositioned to its correct geographical location. The result is an orthophotograph. An orthophoto is a uniform-scale photograph, or a photographic map that shows image features in their true planimetric positions (Avery and Berlin, 1992). Therefore, orthophotos combine the advantages of both aerial photos and line maps (Wolf and Ghilani, 2002).

The 1985 and 1992 source mapsheets are orthophotos, while the 1972 source mapsheet is a photo-mosaic (Table A-1). It's important to make this distinction because if the mapsheet is not an orthophoto, any claim of accuracy will be ambiguous since the accuracy of the image cannot be reclaimed without photogrammetric methods (Oliver, 2003). However, even if the source data are orthophotos, it's difficult to precisely quantify the error involved with using the digitized aerial images. A definitive statement

of error or accuracy can't be made but only an educated opinion, making sure that opinion is broad enough to span the gap in information (Oliver, 2003).

For use in GIS, the three sets (1972, 1985 and 1992) of aerial photographic mapsheets were digitized. The mapsheets were digitized using an Altek digitizing table with a Hewlett Packard 700 series work station using Arc/Info software. The mapsheets utilized State Plane coordinates, Central Zone, New Mexico with a 1927 North American Datum (NAD27) and map units of feet. The active channel was screen digitized (a.k.a. "heads up" digitizing), where the thalweg placement was "best guess".

An important mapsheet characteristic to ensure accurate digitizing is the contrast, which, if poor, could make the historic channel hard to distinguish from shadows and vegetation. The 1972 contrast was poor for light tones. The contrast for 1985 was poor for very light and very dark features. The light tones included recent changes in the active channel, which is the main focus of this analysis. The 1992 mapsheet contrast was good. A mapsheet mismatch error for this year was determined to be up to 1/16 inches, corresponding to approximately 25 feet. Even though the 1962 mapsheet was not used for this analysis, it's worth noting that this year had the highest Root-Mean-Square (RMS) error of all the mapsheets from the digitizing process. An error as high as 0.018 digitizer inches was noted. This was primarily due to a very dark contrast, making the historic channel difficult to distinguish from shadows.

The RMS error is calculated using a statistical formula. It can be visually represented as the average distance of the points from the best fit line passing through a "cloud" of data (x,y). Therefore the points for 1962, which had the highest RMS error, are within +/- 0.018 inches (0.46 mm) of the best fit line according to the digitizing tablet entries for the position of the tic marks of the mapsheet. So the tic marks don't exactly match the real world coordinates for that point. However, the 0.018 digitizer inches doesn't convert to a direct quantifiable error because it is transformed using a series of

linear equations causing the distortion to be a triangulation over the image according to the error of each tic mark on the mapsheet (Oliver, 2003). Recall that the 1962 set of mapsheets were not used in this study; therefore all utilized mapsheets (1972, 1985 and 1992) had an RMS error less than 0.018 digitizer inches. These RMS errors are not revealed likely because they are small enough to be considered negligible.

According to the metadata (Appendix A), the 1962-1992 mapsheets are within National Map Accuracy Standards (NMAS) at a scale of 1:12,000 and are assumed to be within NMAS at a scale of 1:4,800, which is the scale of the source material for this study (Table A-1). These standards, developed by the United States Bureau of the Budget in 1941 and later revised in 1947, provide specifications governing both the horizontal and vertical accuracy with which features are depicted on maps (Wolf and Ghilani, 2002). NMAS horizontal position specifications require that maps produced at scales larger than 1:20,000 (e.g. 1:4,800) not have more than 10% of well defined points in error by more than 1/30 inches (0.85 mm). Therefore, for a map with scale 1:4,800 (1 inch = 400 feet), NMAS require +/- approximately 13 feet of horizontal accuracy. There are also NMAS for vertical accuracy; this position however was not utilized in this study.

The other factor contributing to horizontal error would be the on-screen digitizing in GIS. This error was minimized through utilizing the snapping feature with a low snapping tolerance setting in the ArcMap® program. An estimated range for this error would be 3-5 feet. Therefore, by combining this error with the NMAS horizontal position error, the total estimated horizontal error on the ground would be less than 20 feet. This value represents approximately 5 percent of the 1992 channel width.

The above error analysis focused on possible sources of errors introduced by converting the aerial mapsheets source data into a digital format for use in GIS. Photogrammetric terminology and methods related to error and this particular study were defined and discussed in the goal of portraying not only informative material, but a high

level of confidence with using the digitized photographic data. According to the error analysis, the 1972, 1985 and 1992 sets of digitized aerial mapsheets appear appropriate for making representative measurements and observations to draw conclusions from. For the complete set of photographic properties, including source data, hydrologic data, metadata and the utilized GIS projection and coordinate system, refer to Appendix A.

4.3 Dataset Development (GIS Methodology)

The MMA hinges on the development of a dataset and method by which the dataset was analyzed. For ease of discussion, the dataset is divided into four sub-datasets that include:

- Radius of curvature dataset (3-point methodology)
- Radius of curvature dataset (Nanson and Hickin methodology)
- Migration dataset
- HEC-RAS® dataset

4.3.1. Radius of Curvature Dataset (3-point Methodology)

Each bend had a number of radii (approximately 20) calculated along the channel centerline using a 3-point methodology. In an ideal bend, the radius of curvature would be large at the entrance, get smaller up to the bend axis, and then continually increase at the bend exit, reaching an infinite value for a straight channel planform. The smallest value represents the apex of the bend, or the point of maximum curvature. In performing this 3-point methodology, ArcGIS® was utilized through digitizing the following features and utilizing the following process for each bend:

- Bounds identifying the limits of analysis were defined.
- The channel centerline located within the bounds was defined.

- The channel centerline was edited by dividing it into equal length segments (approximately 100 feet), making sure that each bend for each successive year had the same number of divisions. This insured constant averaging without having to use weighted averages. It is important to note that the number of centerline divisions was arbitrarily chosen. Choosing more divisions (smaller length segments) would yield more radii of curvatures and likely a more accurate apex length. The chosen segment lengths seemed appropriate for the purposes of this study.
- Centerline points representing the beginning and ending of the centerline segments were defined.
- Active channel widths acting perpendicular to the direction of flow at each centerline point were defined.
- The coordinates of the centerline points and lengths of the active channel widths were obtained through programmed scripts in ArcGIS® and exported to the dataset.

The above features can be seen graphically in Figure 4-3.

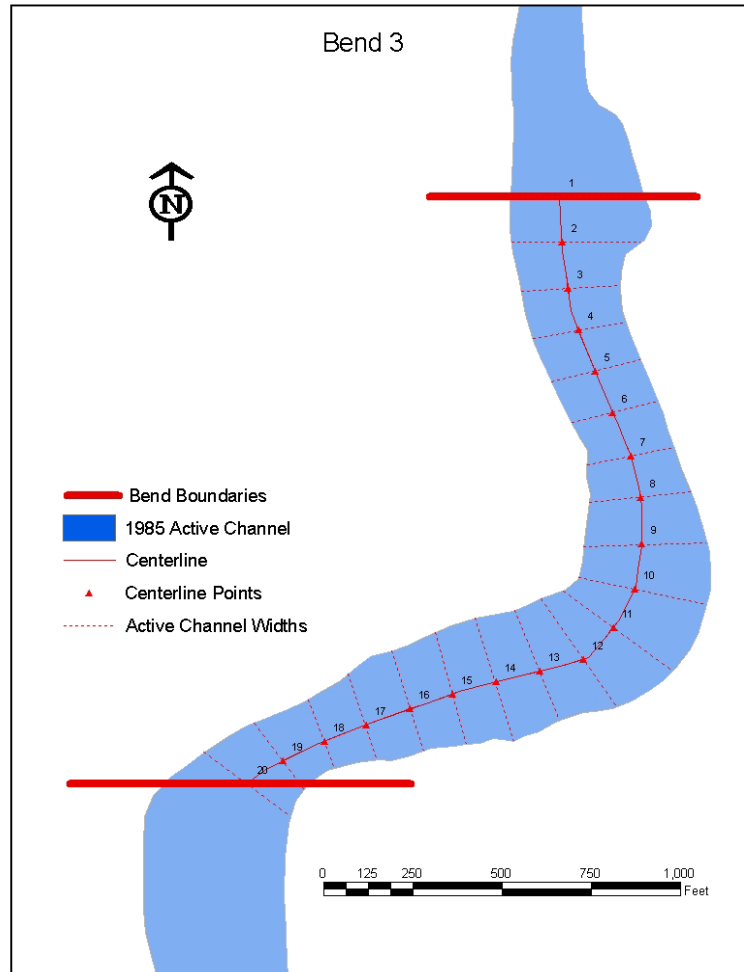


Figure 4-3: Radius of curvature features used in 3-point methodology.

With the inputted centerline coordinates, the dataset was set up to calculate the parameters in Equation 4-1 used in the process of calculating the radius of curvature:

Equation 4-1: Calculations used in 3-point methodology.

- Midpoint coordinates: (x_{mid}, y_{mid})

$$x_{mid} = \left[\frac{x_1 - x_2}{2} \right] + x_2$$

$$y_{mid} = \left[\frac{y_1 - y_2}{2} \right] + y_2$$

- Midpoint line slopes: (m, p)

$$m = \frac{y_2 - y_1}{x_2 - x_1}; p = \frac{y_3 - y_2}{x_3 - x_2}$$

- Tangent line slopes: (a,c)

$$a = m^{-1} ; c = p^{-1}$$

- Tangent line intercepts: (b,d)

$$b = y_{\text{mid1}} - ax_{\text{mid1}} ; d = y_{\text{mid2}} - cx_{\text{mid2}}$$

- Centroid coordinates: (x_c, y_c)

$$x_c = \frac{d-b}{a-c} ; y_c = ax_c + b$$

- Radius of curvature: (R)

$$R = \left[(x_2 - x_c)^2 + (y_2 - y_c)^2 \right]^{1/2}$$

Note that this radius of curvature calculation utilized only the first 3-centerline points in the bend. This methodology repeats throughout the bend, shifting down to the next subsequent set of 3-centerline points, meaning that the last 2-centerline points do not have a corresponding radius of curvature.

The above parameters and 3-point methodology can be seen graphically in Figure 4-4. The complete radius of curvature dataset using this methodology is attached in Appendix K (Tables K-1 through K-20).

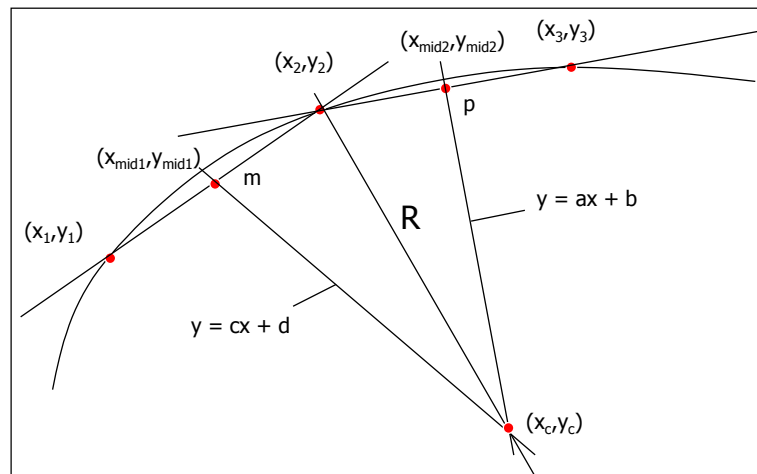


Figure 4-4: Example of 3-point methodology used in radius of curvature calculation.

4.3.2. Radius of Curvature Dataset (Nanson and Hickin Methodology)

Because part of the analysis involved testing the applicability of research by Hickin and Nanson (1984), another methodology was used for determining the mean radius of curvature (r_m) that ensured consistency among methodologies. This methodology was developed to eliminate operator bias, which can significantly alter the results (Nanson and Hickin, 1983).

The definition of the mean radius of curvature according to Nanson and Hickin is $r_m = (r' + r'')/2$. That is, the mean radius of curvature is the average of two circles: one passing through points 1, 0 and 2; the other passing through points 3, 0 and 4 (Figure 4-5). Therefore, it can be seen that the 3-point methodology previously discussed is also utilized in this methodology. Point 0 is located on the bend axis (point of maximum curvature). The spacing between the five points is equal to the mean active channel width measured along straight reaches. It can be seen that this methodology reflects both the strong curvature at the bend axis as well as the broader sweep of the limbs of the bend (Nanson and Hickin, 1983). If the bend had an ideal planform (perfectly circular), the two circles would equal each other ($r_m = r' = r''$). The points used in this calculation are located on the convex bank as this represents a bend curvature intermediate to those defined by the concave bank line.

ArcGIS® was again used in the development of this dataset. A graphical example of this methodology can be seen in Figure 4-5.

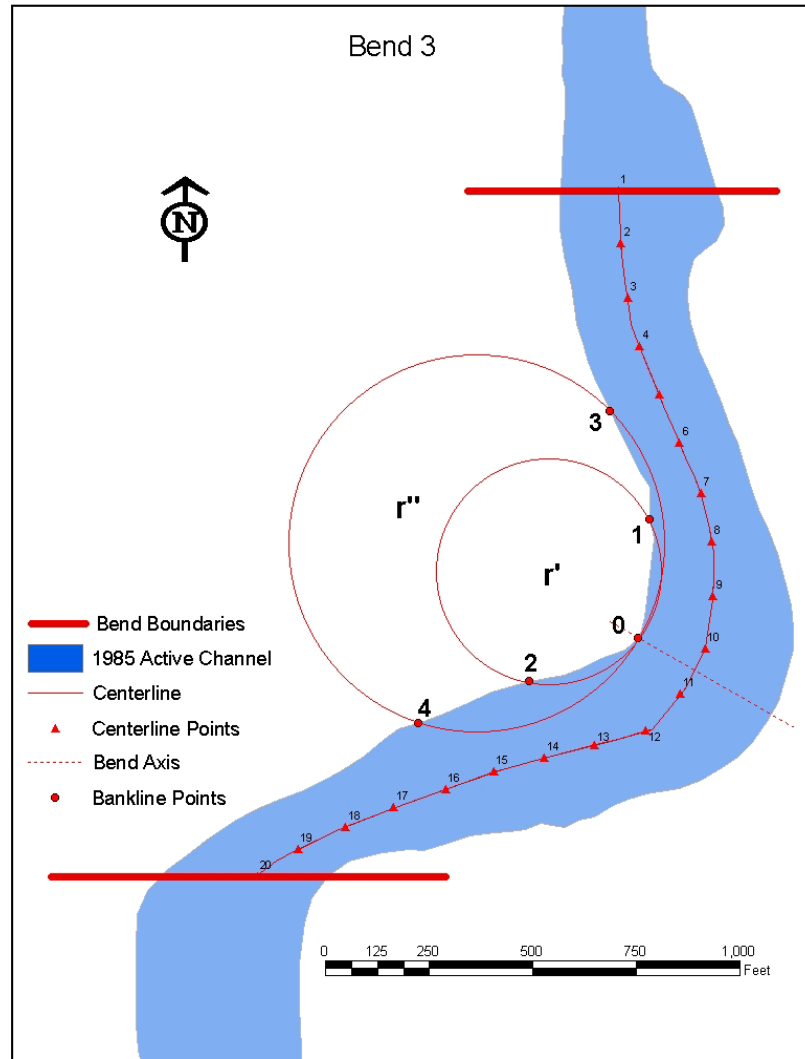


Figure 4-5: Example of mean radius of curvature calculation using the Nanson and Hickin (1983) methodology.

The complete dataset using this methodology is attached in Appendix L (Tables L-1 through L-20).

4.3.3. Migration Dataset

Approximately 20 estimates of migration rate were calculated for each bend at fabricated migration lines (M-lines). To ensure consistency in the measurements, the M-lines were fixed for each set of years analyzed. The migration rates were later averaged to obtain a single average migration rate for each bend during a particular time period. In

calculating the migration rates for each bend, the following features were digitized in ArcGIS® for each bend:

- Bounds identifying the limits of analysis were defined.
- The channel centerline located within the bounds was defined.
- M-lines were defined based on the 1972 active channel widths.
- Active channel widths passing through the M-lines, centerline and located perpendicular to the direction of flow were defined. By basing the M-lines on the 1972 active channel widths, this simplified the step of defining these widths by clipping the M-lines with the active channel.
- Right bank points were defined at each M-line. Right and left banks were defined looking downstream.
- Left bank points were defined at each M-line.
- The coordinates of the right bank and left bank points, and lengths of the active channel widths were obtained through programmed scripts and exported to the dataset.

The above features can be seen graphically in Figure 4-6.

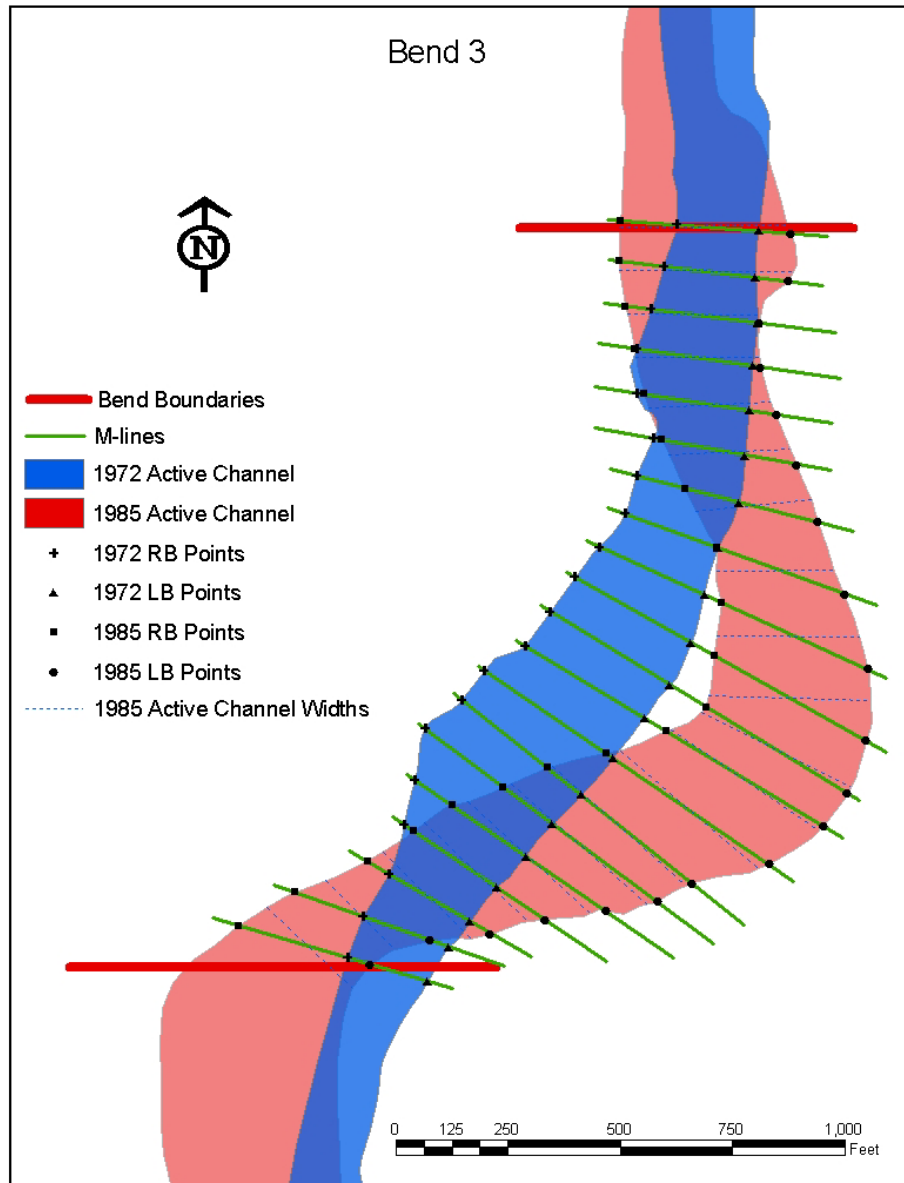


Figure 4-6: Example of migration rate calculation from bend 3 for the 1972-1985 time period.

With the inputted right bank coordinates, left bank coordinates and widths, the dataset was set up to calculate the parameters of Equation 4-2, used in the process of calculating the migration rate. It's important to note that variables with subscript "1" refer to the earlier year in the time period while variables with subscript "2" refer to the later year.

Equation 4-2: Calculations used in migration rate determination.

- Coordinates representing movement of the channel's right bank: (Δr)

$$\Delta r = \left[(x_2 - x_1)^2 + (y_2 - y_1)^2 \right]^{1/2}$$

- Coordinates representing movement of the channel's left bank: (Δl)

$$\Delta l = \left[(x_2 - x_1)^2 + (y_2 - y_1)^2 \right]^{1/2}$$

- Change in active channel width: (ΔW)

$$\Delta W = W_2 - W_1$$

Note that due to the order in which this calculation is set up, a positive (+) value would indicate that the channel has widened during the time period, while a negative (-) value would indicate the channel narrowing.

- Time period span: (Δt)

$$\Delta t = t_2 - t_1$$

Using these calculated parameters, the migration rate was calculated using Equation 4-3.

Equation 4-3: Migration rate calculation.

- Migration rate: (M)

$$M = \frac{\Delta r + \Delta l}{\Delta t} - \frac{\Delta W}{\Delta t}$$

The change in active channel width was subtracted because it is the measure of width between the outermost banks of the channel (Richard, 2001). Attached in Appendix M (Figures M-1 through M-7) are maps graphically displaying the location of each bend at three different times (1972, 1985 and 1992) showing the movement that occurred from 1972 to 1992. Also included in this appendix (Tables M-1 through M-20) is the set of GIS input data used in the determination of the migration rates along with the complete migration dataset (Tables M-21 through M-27) quantifying all the migration

results for each bend during three time periods (1972-1985, 1985-1992 and 1972-1992). An additional feature of the migration dataset is the identification of each bend apex for each year analyzed. This shows the migration of the apex over the studied time period.

4.3.4. HEC-RAS® Dataset

HEC-RAS® modeling was utilized in obtaining the average depth at each bend for each year analyzed (1972, 1985 and 1992). Approximately five agg/deg cross sections, spaced approximately 500 feet apart, were used to represent each bend. As mentioned previously, 1992 agg/deg line surveys were substituted for the 1985 analysis for availability reasons. A channel-forming discharge of 5,000 cfs was routed through each bend. HEC-RAS® was not calibrated. A Manning's n value of 0.02 was used for the channel and 0.1 for the floodplain for all simulations. The average depth results for each bend for each year analyzed are summarized in Table 4-1.

Table 4-1: Average depth (feet) of each bend based on HEC-RAS® analysis.

Year	Bend 1	Bend 2	Bend 3	Bend 4	Bend 5	Bend 6	Bend 7
1972	2.9	3.1	3.1	3.5	2.6	N.A.	3.0
1985	2.8	3.2	2.9	3.1	2.0	2.4	3.5
1992	2.7	3.2	2.9	3.2	2.0	2.4	3.5

4.4 Data Analysis and Results

All of the above datasets were used in the analysis of numerous different parameters, each of which was believed to contribute to the process of meander migration. This section summarizes the pertinent analyses performed using the data from the generated datasets, and the results that came from those analyses.

4.4.1. Curvature Analysis (Hickin and Nanson – 1984)

This analysis work involves relationships between a variable that represents a time period (migration rate (M) – ft/yr) and a variable that represents one point in time (radius of curvature-to-width ratio (R/W) – ft/ft). Because of this, two methodologies can

be used to relate R/W with M. Method 1 involves using R/W from the earlier year in the time period (e.g. 1972 for the 1972-1985 time period), as this is what drives the migration during this time. Method 2 involves averaging R/W from the earlier year and later year in the time period, as this represents both the beginning and ending points in the period. Even though methods 1 and 2 were talked about specifically for these two variables, they can be employed when relating any time period variable with any time instant variable.

Both methodologies were tried and Method 1 was seen to yield better results. This method will therefore be used when relating any time period variable with any time instant variable throughout this thesis.

Relative migration rates (M/W) are shown plotted with mean radius of curvature-to-width ratios (r_m/W) in Figure 4-7. All variables are bend averaged. Recall that the mean radius of curvature was obtained in a consistent fashion as Nanson and Hickin's work (Section 4.3.2).

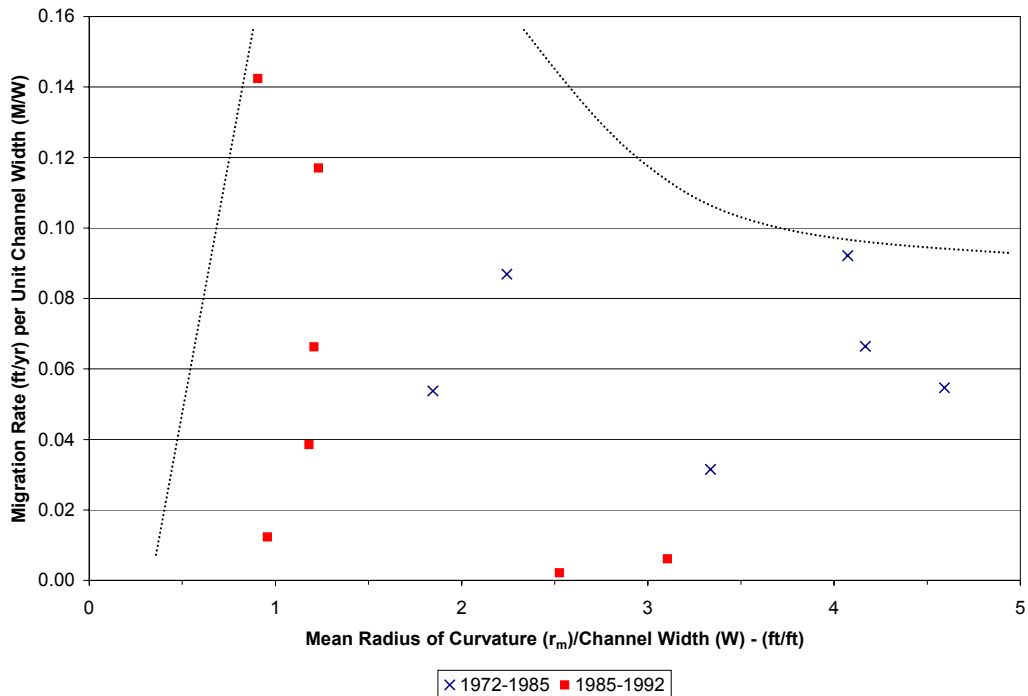


Figure 4-7: Bend averaged relative migration rate versus r_m/W .

The data appear somewhat scattered with no real apparent trend. This is likely due to the fact that this reach does not have traits that are typical of a meandering channel, as was studied by Hickin and Nanson. These non-typical traits include a sinuosity less than 1.5, an armored gravel bed as well as the incised and perched (above the surrounding floodplain) characteristic of the channel.

Regardless, other analyses were performed in the hopes that a pattern similar to Hickin and Nanson's would emerge. These analyses included looking at points around the apex of each bend; specifically, averaging the two points on both the upstream and downstream sides of the apex with the apex. Also, relative migration rates were plotted with the minimum radius of curvature-to-width ratios (R_{\min}/W) for both the bend-averaged case as well as for the apex-area-averaged case. The minimum radius of curvature was calculated through Equation 4-4.

Equation 4-4: Minimum radius of curvature calculation.

$$R_{\min} = \frac{L}{2\pi\theta_m}$$

In this relationship, L represents the channel length (ft) measured along the centerline and θ_m represents the maximum orientation angle (radians), which was obtained from the sine-generated curves that will be discussed in detail later in this chapter. In addition, each of these plots was re-generated using the migration rate (M) as opposed to the relative migration rate (M/W). Unfortunately, a trend similar to that found by Hickin and Nanson (1984) did not appear to emerge in these additional plots. All of these plots can be seen in the attached Appendix N (Figures N-1 through N-7).

4.4.2. Secondary Flow Analysis (Rozovskii – 1957)

Recall that the deviation angle λ , which directly corresponds to the magnitude of the secondary flows, depends primarily on the ratio of flow depth (h) to radius of

curvature (R). To be conservative, the minimum radius of curvature (R_{min}) representing the point of maximum curvature in each bend was used in this analysis. Refer to Section 4.4.1 for the calculation of this parameter. The calculated average deviation angle for each bend for each year analyzed is summarized in Table 4-2. It can be seen that no deviation angle exceeds 15 degrees. These “small” angles are representative of a channel in which equilibrium prevails between outer-bank erosion and inner-bank deposition (Julien, 2002). Therefore, migration of the channel could still occur, but the width is expected to remain nearly constant. Three width regression models, the Williams and Wolman (1984) hyperbolic model and Richard’s (2001) exponential models, were run on the San Felipe Reach (Figure 2-1) as part of a hydraulic modeling analysis (Sixta et al., 2003c). The hyperbolic model predicted the channel width to continue to decrease slightly in the future, while both exponential models predicted that the channel width should not change significantly in the future, which is consistent with the channel being in a state of equilibrium.

Table 4-2: Bend averaged deviation angles.

Bend 1				Bend 2			
Date	R_{min} (apex)	h (avg.)	λ (deg)	Date	R_{min} (apex)	h (avg.)	λ (deg)
1972	445	2.92	4.1	1972	890	3.13	2.2
1985	362	2.75	4.8	1985	536	3.21	3.8
1992	294	2.73	5.8	1992	387	3.21	5.2

Bend 3				Bend 4			
Date	R_{min} (apex)	h (avg.)	λ (deg)	Date	R_{min} (apex)	h (avg.)	λ (deg)
1972	1057	3.12	1.9	1972	979	3.47	2.2
1985	439	2.94	4.2	1985	500	3.14	4.0
1992	508	2.93	3.6	1992	435	3.18	4.6

Bend 5				Bend 6			
Date	R_{min} (apex)	h (avg.)	λ (deg)	Date	R_{min} (apex)	h (avg.)	λ (deg)
1972	409	2.58	4.0	1985	490	2.36	3.0
1985	297	2.01	4.3	1992	482	2.36	3.1
1992	330	2.02	3.8				

Bend 7			
Date	R_{min} (apex)	h (avg.)	λ (deg)
1972	593	3.01	3.2
1985	359	3.54	6.2
1992	350	3.54	6.3

4.4.3. Sine Curve Analysis

Sine curves were generated for each bend for each year of analysis using data from the radius of curvature dataset (3-point methodology). By taking the inverse tangent of the midpoint line slopes (m), the downstream orientation angle (θ) was obtained. By then plotting this orientation angle as a function of the downstream distance (x), a sine curve is produced. This curve is useful for obtaining the maximum orientation angle (θ_m) for use in calculating the minimum radius of curvature (R_{\min} – see Section 4.4.1), to observe how closely each bend follows an ideal meandering planform (sine curve) as well as to quantify each bend's curvature. In addition, a rough estimate of the sinuosity (P) can be calculated by using Equation 4-5.

Equation 4-5: Sinuosity calculation.

$$P \equiv 1 + 0.1\theta_m^5$$

Utilizing this calculation yields similar results to those obtained in Figure 4-1, which were calculated through the quotient of the river length and the valley length, both of which were obtained through GIS measurements. The sine curves for bend 2 are shown in Figure 4-8. It can be seen that each bend has much more curvature in 1985 and 1992 as compared with 1972. This change in curvature corresponds with the closure of Cochiti Dam. It is also seen that the orientation angles follow an idealized meander fairly well. These same observations can be made for the sine curves for the rest of the bends, all of which can be seen in attached Appendix O (Figures O-1 through O-6).

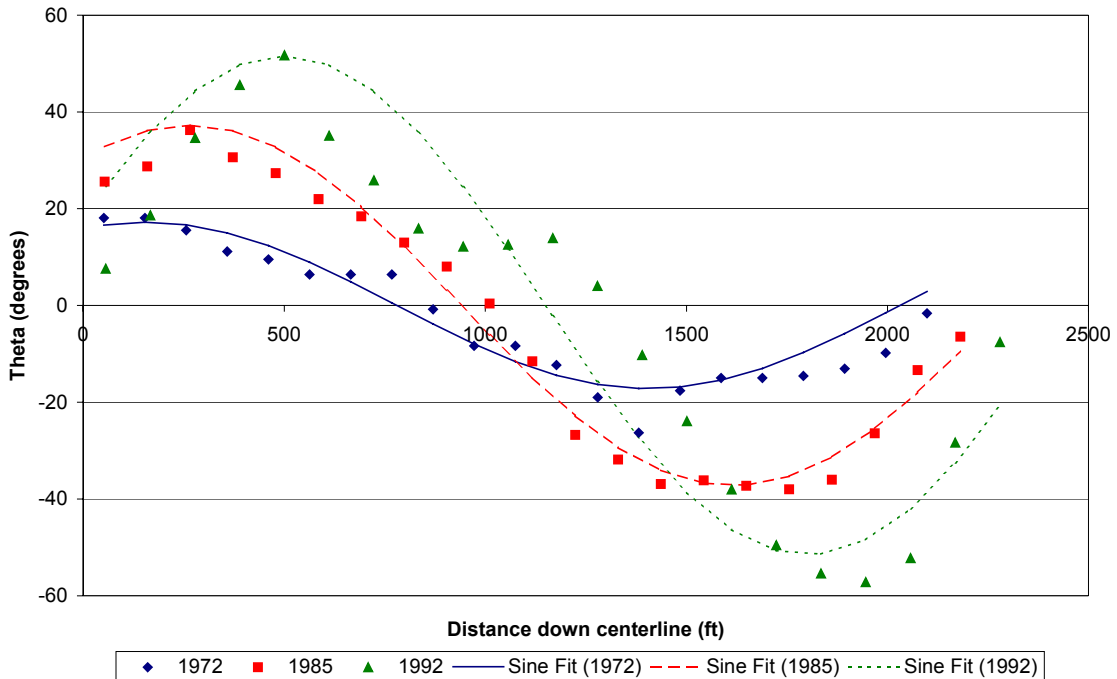


Figure 4-8: Sine-generated curves for bend 2.

4.4.4. Hydrological Analysis

Recall that the migration rates were calculated for two periods (1972-1985 and 1985-1992). Since discharge (Q) is one important factor influencing rates of migration, the flow regime was analyzed for these two periods by looking at the mean daily flow (cfs) at the San Felipe gage. This gage is located just on the downstream end of the Galisteo Reach (Figure 2-1). The resulting flow regime for these two periods is shown graphically in Figure 4-9.

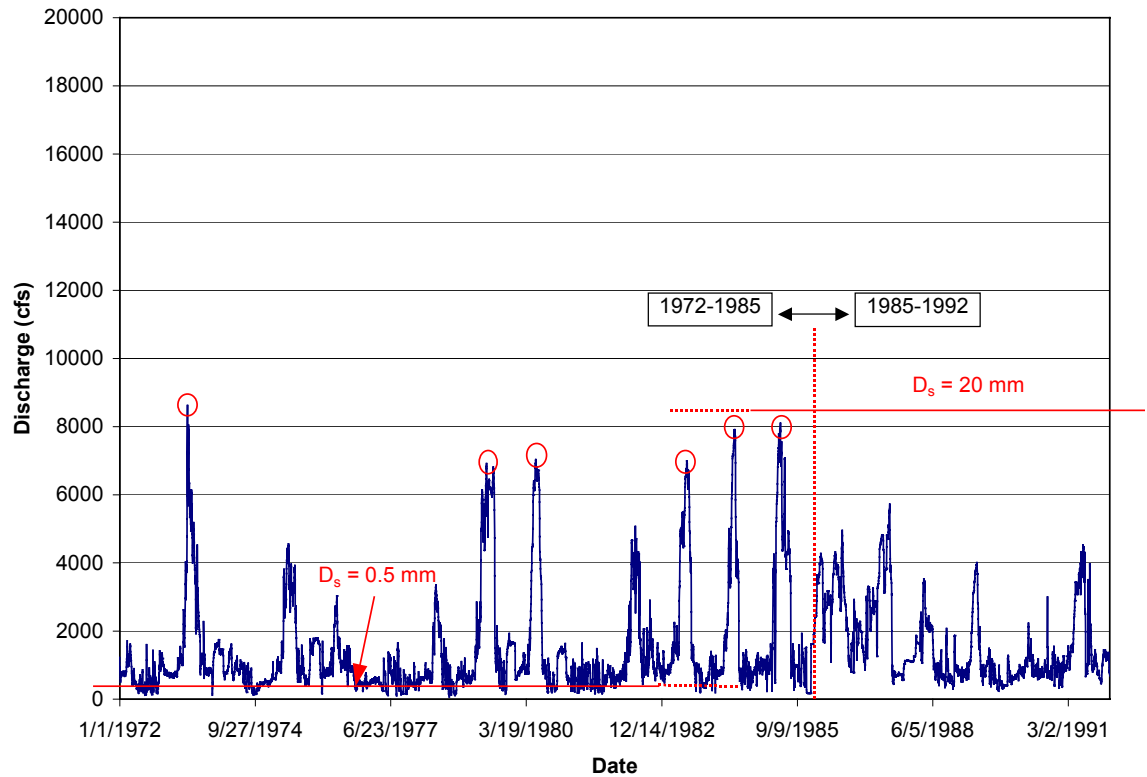


Figure 4-9: Mean daily flow (cfs) at San Felipe (1972-1992).

It is shown that the 1972-1985 time period, in general, exhibits greater, more frequent peak flows than the 1985-1992 period. There are six occurrences during the 1972-1985 time period where the flows exceeded 6,000 cfs as compared with zero occurrences in the 1985-1992 time period. This would likely correspond to a higher rate of migration during the 1972-1985 time period. To verify/refute this hypothesis, a sub-analysis was performed by plotting the migration rate against the peak flows, where a positive upward trend from the second time period to the first would be expected. This trend was not observed, indicating that there are additional dominant forces at work other than discharge causing the channel to migrate.

Another sub-analysis was performed to see how much discharge would be needed to move the average size particle making up the bed during these two time periods. To achieve this, an incipient motion calculation was performed. The equation

used in calculating the critical shear stress (τ_c), that is, the minimum amount of shear stress needed to move a particle of a particular size can be put in terms of discharge (Q) with a substitution for the hydraulic radius (R_h) from the Manning Equation. This results in Equation 4-6.

Equation 4-6: Critical shear stress calculation.

$$\tau_c = \gamma_w R_h S_f = \gamma_w \left[\frac{nQ}{AS_f^{1/2}} \right]^{3/2} S_f$$

Because all the variables in the above equation have known approximate values including the critical shear stress, which is dependent on grain size, the above equation can be rearranged to solve for the critical discharge (Q_c). This result is shown in Equation 4-7.

Equation 4-7: Equation 4-6 rewritten to solve for critical discharge.

$$Q_c = \frac{\tau_c^{2/3} A}{\gamma_w^{2/3} n S_f^{1/6}}$$

Where: τ_c = critical shear stress = 0.006 psf (0.5 mm) = 0.334 psf (20 mm)
 A = channel cross sectional area = 1,185 ft²
 γ_w = specific weight of water = 62.4 pcf (50°F)
 n = Manning's roughness coefficient = 0.02
 S_f = friction slope = 0.001 ft/ft

The average grain size (D_{50}) is 0.5 mm and 20 mm for the 1972-1985 and 1985-1992 time periods, respectively (Figure 3-9). Recall that this was attributed to clear water release from the dam. For a more detailed discussion on the bed material sediment, refer back to Section 3.3.6. These two different grain sizes result in two different values for critical shear stress, while all other variables remain constant. Using the above values, a discharge of approximately 550 cfs and 8,500 cfs was calculated to mobilize the bed material for the 1972-1985 and 1985-1992 time periods, respectively. This large jump in critical discharge is a direct result of the armoring that has occurred since

construction of the dam. Lines corresponding to these critical discharges can be seen in Figure 4-9.

The critical discharge for the 1972-1985 time period is exceeded much more frequently, while the 1985-1992 critical discharge was never exceeded during that time period (Figure 4-9). This indicates that future channel incision causing undercutting and failure of the banks is unlikely due to the infrequency of a large enough event to mobilize the bed material. Therefore, the migration that has occurred between 1985 and 1992 is likely the result of a direct attack on the banks through impinging flow or secondary currents. Recall that this period shows an increase in average channel width also (Figure 3-8).

4.4.5. Stream Power/Specific Stream Power Analysis

A maximum stream power (Ω) (Equation 2-4) was calculated for two time periods of interest using the annual peak flows during those years. Peak flows were utilized to correlate larger stream power values with higher rates of migration. The stream power values for the 1972-1985 and 1985-1992 time periods (2,575 N/s and 2,303 N/s, respectively) were too close to make any kind of generalization about stream power as it relates to channel migration rates.

In estimating the energy level of the floodplain during these two time periods, the average specific stream power ($\omega = \Omega/W$) was calculated for each bend. These values are summarized in Table 4-3. All specific stream power values fall into the 10-300 W m⁻² range, indicating a medium-energy floodplain. Recall that this energy level corresponds to non-cohesive floodplains in which the main mechanism is lateral point-bar accretion. Based on other analyses performed (i.e. width regression and secondary flow analyses), these values for specific stream power are expected to decrease in the future. This could move the floodplain to a low-energy level indicating a laterally stable channel.

Table 4-3: Average specific stream power for each bend during two time periods.

1972-1985		1985-1992	
Bend id	SSP (W/m ²)	Bend id	SSP (W/m ²)
1	19.0	1	16.7
2	24.8	2	17.0
3	21.2	3	16.4
4	26.1	4	17.3
5	18.5	5	18.0
7	19.4	6	17.2
		7	24.3

4.4.6. Additional Analyses

Additional analyses were performed by looking at relationships among migration rates (M) and relative migration rates (M/W) plotted with flow depth-to-radius of curvature (h/R) ratios and width-to-depth (W/h) ratios. Analyses were performed on individual bends as well as on the entire reach.

The only relationship that displayed any kind of trend was that of M and W/h. For this relationship, a positive increasing trend is expected. That is, higher width-to-depth ratios should yield higher migration rates. In general, channels with high width-to-depth ratios tend to be unstable while channels with low width-to-depth ratios tend to have more stability. An anastomosing river is generally agreed to have stable banks with individual channels showing little tendency to migrate (Knighton and Nanson, 1993). According to Smith and Putnam (1980), one distinguishing characteristic of anastomosing, meandering and braided channel patterns is a low, moderate and high width-to-depth ratio, respectively. Further, anastomosing rivers are characterized by low gradients, very small stream powers, and cohesive banks, which produce laterally stable channels of low width-to-depth ratios (Knighton, 1998). The Cochiti Reach, for example, has been historically characterized as a wide, shallow channel (high width-to-depth ratio) due to an aggradational trend with extensive lateral movement. That was the driving

reason for the implementation of the comprehensive plan of improvement that culminated with the construction of Cochiti Dam.

Figure 4-10 shows the relationship and resulting trend between M and W/h for the Galisteo Reach during the 1972-1985 period. It can be seen that the expected positive increasing trend is verified.

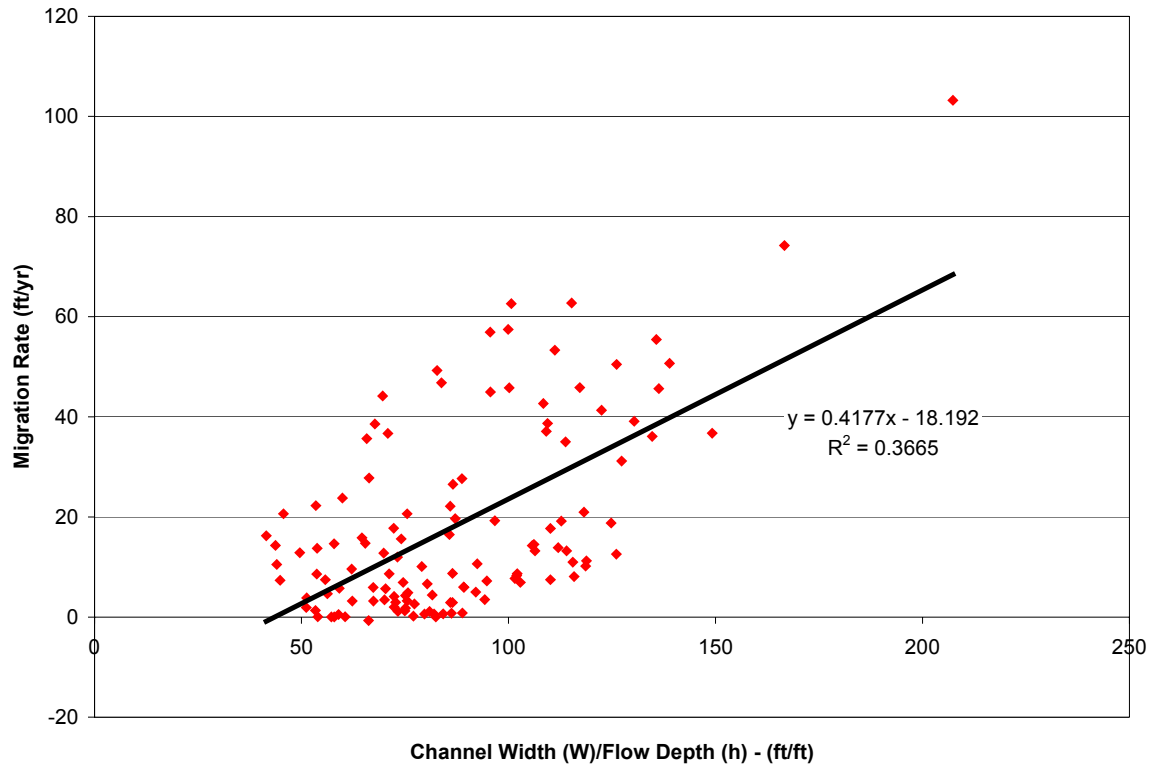


Figure 4-10: M versus W/h for 1972-1985 time period (Galisteo Reach).

Other plots using this relationship (M vs. W/h) are attached in Appendix P. Figure P-1 shows the Galisteo Reach during the 1985-1992 period, which has a subtle positive increasing trend. Next, just the area around the apex of each bend was investigated. Figures P-2 and P-3 (Appendix P) show these results for the 1972-1985 and 1985-1992 periods, respectively. These figures showed the location of outliers more clearly, indicating non-uniform movement among the bends. This could be the result of the bends being composed of different materials that erode at different rates. Finally, one

point representing each bend (average of apex point and one point on each side) was plotted for both time periods, and by eliminating possible outliers, the positive increasing trend proceeded to get stronger. These relationships can be seen in attached Figures P-4 through P-7 (Appendix P).

4.5 Summary and Conclusions

The meander migration analysis (MMA) was performed on the Galisteo Reach of the MRG, which spans 8.15 miles from the mouth of Galisteo Creek (agg/deg 98) to the mouth of the Arroyo Tonque (agg/deg 174). There were many analyses performed through utilizing extensive datasets developed with the use of ArcGIS® and HEC-RAS®. The datasets focused on curvature characteristics and migration patterns of arbitrarily selected bends along the reach. The analyses included a curvature analysis based on the work of Hickin and Nanson (1984), a secondary flow analysis based on the work of Rozovskii (1957), a sine curve analysis, a hydrological analysis and additional analyses.

The curvature analysis was performed using the same methodology used by Nanson and Hickin (1983) to ensure consistency. Unfortunately, the data appeared somewhat scattered with no real apparent trend like that found by Hickin and Nanson (1984). This is likely due to the fact that the Galisteo Reach does not have the traits of a typical meandering channel. These non-typical traits that summarize the Galisteo Reach include a sinuosity less than 1.5, a gravel bed (armored), an incised and perched geometry.

The secondary flow analysis yielded deviation angles less than 15 degrees, indicating that the channel is in a state where equilibrium prevails between outer-bank erosion and inner-bank deposition (Julien, 2002). This observation was found to be consistent with the results of two width regression models performed on the downstream

reach (San Felipe Reach), which predicted that the channel width would not change significantly in the future.

The sine curve analysis showed that the bends in 1985 and 1992 have more curvature than the bends in 1972, which directly corresponds to the closure of Cochiti Dam. That is, as the channel was in a state of degradation (see HMA), the width started to decrease and form more distinct meanders. The formation of these meanders could be due to the channel trying to minimize its slope for given input conditions such as water and/or sediment. However, there is as yet no completely satisfactory explanation of how or why meanders develop (Knighton, 1998). Additionally, the orientation angles follow an idealized meander fairly well.

The hydrological analysis showed a flow regime for the 1972-1985 period with higher overall and more frequent peak flows than the 1985-1992 period. The migration rates however were not consistently higher during 1972-1985, indicating there are additional forces affecting the migration rate. A minimum calculated flow discharge of approximately 8,500 cfs appeared necessary to move the armored bed that existed between 1985 and 1992. A flow of 8,500 cfs is uncommon; suggesting the likelihood of future channel incision leading to geotechnical failure of the banks is low due to the infrequency of a large enough event to mobilize the bed. Hence, channel incision driven bank failure is ruled out as one mechanism of bank failure. Therefore, the migration that has occurred between 1985 and 1992 is likely the result of a direct attack on the banks such as impinging flow or secondary currents.

The stream power analysis did not yield a distinct relationship among stream power and migration rates. Calculated specific stream power values ranged from 17-to-26 $W m^{-2}$. These values indicate a floodplain at a medium-energy level, corresponding to floodplains that are non-cohesive with the main mechanism being lateral point-bar

accretion. The values for specific stream power as well as the floodplain energy level are expected to decrease in the future.

Additional analyses on both the individual bends and the entire reach were performed between such variables as M and M/W plotted with h/R and W/h . The relationship that yielded the best trend was that of migration rates (M) plotted with width-to-depth (W/h) ratios, which yielded the expected positive increasing trend. By looking at points just around the apex and eliminating suspected outliers, the trend improved.

Trying to model and understand such a complex process as channel migration has proven to be challenging. According to Nanson and Hickin (1983), to successfully model migration trends, many factors such as stream power, resistance of bank materials to erosion, height of the convex bank, degree of incision, sediment supply rate and bend planform influence should all be evaluated, and preferably simultaneously. With these features known, a multiple linear regression could be performed to identify a relationship between them. The methods needed to obtain these factors and perform this analysis are extremely data intensive and beyond the scope of this study. Also, according to Nanson and Hickin (1983), “the discontinuous nature of channel migration means that predictions of migration rates for individual bends based on short term measurements (such as from time lapsed aerial photography over 20 or 30 years) are highly suspect, but should be possible.”

In summary, there were numerous analyses performed using an extensive set of developed datasets with few distinct migration trends being found. According to width regression models performed on the reach just downstream (San Felipe Reach), the channel width is expected to remain fairly constant in the future with a possible continued slight decrease. Also, continued future degradation is not expected due to the infrequency of large flow events required to move the armored bed. Further, according to calculated deviation angles, the channel should be in a state of equilibrium. Therefore,

the migration rates are expected to decrease in the future, reaching a state of stability. It's important to note that this prediction assumes future hydrological patterns to be similar with the patterns of the past.

CHAPTER 5: SUMMARY AND CONCLUSIONS

5.1 Introduction

This thesis focused on two analyses performed on two subreaches of the Cochiti Reach located along the Middle Rio Grande (MRG). A hydraulic modeling analysis (HMA) was performed on the San Felipe Reach, while a meander migration analysis (MMA) was performed on the Galisteo Reach. The purpose of these analyses was to evaluate historic data in addition to developing new data to estimate the potential trends of the reaches, and ultimately forecast future changes. These analyses will aid in the overall goal of helping facilitate restoration and management issues of the river channel.

5.2 HMA

General trends of the San Felipe Reach include a decrease in width, width-to-depth ratio, wetted perimeter and cross sectional area and an increase in flow velocity and depth during the period of study (1962-1998). Some of the more detailed conclusions include the following:

- An average of 1.2 feet of aggradation between 1962 and 1972 and 3.8 feet of degradation between 1972 and 1998 occurred, while degradation upwards of 4 feet maximum occurred from 1992 to 1998.
- Coarsening of the bed material from sand to gravel occurred from 1972 to 1998. This armoring effect of the channel bed will likely cause the degradational pattern to stop in the near future.

- Active channel widths decreased from 580 feet in 1918 to 219 feet in 2001, of which the largest decrease (approximately 200 feet) occurred between 1918 and 1935.
- The sand load was approximated to be 9,550 tons/day. The bed material load estimated to be 20% of the sand load (1,910 tons/day).
- From the sediment transport analyses conducted on the San Felipe Reach, the average bedload and bed material load values from 1972 exceeded those from 1962 (Table 3-3). Results from 1992 and 1998 show an increase in channel transport capacity (Table 3-4), as a result of fining of the bed material during this period. The average bed material load for 1992 and 1998 are both slightly higher than the incoming bed material load, indicating degradation, which is in agreement with observed degradational patterns during this time period. Given the uncertainty involved with the MEP methodology, the channel slopes in 1992 and 1998 seem appropriate to transport the incoming bed material load of 1,910 tons/day at a channel forming discharge of 5,000 cfs.

5.3 MMA

The order in which these analyses were performed proved to be important because many of the observations made in the HMA were used to help clarify and explain trends found in the MMA. For the MMA, many analyses were performed through using extensive datasets that were tailored specifically for use in this analysis. In general, the datasets focused on curvature characteristics and migration patterns of arbitrarily selected bends along the Galisteo Reach.

From a curvature analysis, no real trends are readily apparent, likely the result of traits not conforming to those of a typical meandering channel. From a secondary flow

analysis, deviation angles less than 15 degrees were calculated, indicating a channel that is in a state of equilibrium. According to a sine curve analysis, the bends in 1985 and 1992 have more curvature as compared with the bends of 1972, coinciding with the closure of Cochiti Dam. In addition, the sine curves showed the orientation angles to follow the pattern of an idealized meander fairly well.

A hydrological analysis showed the flow regime for the 1972-1985 period with higher and more frequent peak flows than the 1985-1992 period. This did not indicate greater amounts of migration for the 1972-1985 period however, leading to the belief that there are additional forces affecting migration rates than just discharge. Further, future channel incision is unlikely due to the infrequency of the calculated 8,500 cfs flow needed to mobilize the bed material.

A stream power analysis yielded no distinct trend with migration rates. Specific stream power calculations resulted in a floodplain at a medium-energy level. This type of floodplain is characteristic as being non-cohesive with lateral point-bar accretion as the main mechanism. Finally, the expected positively increasing trend of migration rate versus width-to-depth ratios yields stronger trends through apex isolation and outlier elimination.

5.4 Conclusions

According to the HMA, the overall planform geometry of the MRG from 1918 to the present has changed from braided to meandering. This change resulted in a decreasing trend in active channel width. The rate of this decreasing trend is expected to slow in the future as the channel approaches a state of equilibrium. The other significant trend that has occurred since the closure of Cochiti Dam (1973) has been channel bed degradation, resulting in significant bed armoring. Currently, the channel bed is armored with a gravel material, representing supply limited sediment transport conditions. This

bed armoring is expected to cease the degradational pattern in the next 5-10 years. Although the rates of the channel narrowing and degradational trends are expected to slow and eventually halt, a reversal of these trends is not expected without a significant increase in sediment supply such as from the removal of tributary dams.

The MMA showed migration rates along the Galisteo Reach that varied largely among not only the bends, but also among the two time periods studied. The low migration rates shown for some of the bends (i.e. bends 6 and 7 during the 1972-1985 time period) are likely linked to the residual braided morphology. All MMA results indicated a channel in a state of near equilibrium that is moving as a result of bank erosion as opposed to basal erosion. The majority of this reach is located between a system of levees and riverside drains, inhibiting much of its lateral movement. In addition, some of the observed bends have been locked into place through riprap placement in the mid-1990's, allowing no more lateral movement. Riprap was placed because the bends movements were threatening the integrity of the levees and drains.

In summary, migration rates depend on so many chaotic and unpredictable factors that it is difficult to forecast future rates of lateral migration on the Rio Grande with any degree of certainty. In fact, it would be impossible to make a definitive statement regarding future channel movement and location. However, according to results from both analyses, migration rates are expected to decrease in the future while the channel approaches a state of near stability. This prediction assumes future hydrologic and sediment regimes to be similar to those of the past 30 years.

REFERENCES

- Ackers, P. (1982). Meandering Channels and the Influence of Bed Material. In: Gravel Bed Rivers. Fluvial Processes, Engineering and Management. Hey, R. D., Bathurst, J. C., and Thorne, C. R. (eds). John Wiley and Sons Ltd, pp. 389-414.
- Adams, J. (1998). (Support Officer). A Guide to Aerial Photography. <http://cebe.cf.ac.uk/learning/habitat/HABITAT5/areal.html>.
- Avery, T.E. and Berlin, G.L. (1992). Fundamentals of Remote Sensing and Airphoto Interpretation (5th ed.). Prentice-Hall, Inc., Upper Saddle River, NJ. 472 pp.
- Baird, D. C. (1998). Bank Stabilization Experience on the Middle Rio Grande. Water Resources Engineering 98, ASCE, New York, NY. pp. 387-392.
- Baird, D. C. (2003). Personal Communication. Senior Hydraulic Engineer. Representing U.S. Bureau of Reclamation. Technical Services Division. River Analysis Team. Albuquerque, NM. Colorado State University, Fort Collins, CO.
- Bauer, T. R. (2000). Morphology of the Middle Rio Grande from Bernalillo Bridge to the San Acacia Diversion Dam, New Mexico. M.S. Thesis. Colorado State University, Fort Collins, CO. 308 pp.
- Brice, J. C. (1982). Stream Channel Stability Assessment, January 1982, Final Report. U.S. Department of Transportation, FHA, Washington, D.C.
- Brookes, A. (1992). River Channel Change. In: The Rivers Handbook, Hydrological and Ecological Principles. P. Calow and G. Petts (eds.). Blackwell Scientific Publications, Oxford. pp. 55-75.
- Bullard, K. L. and Lane, W. L. (1993). Middle Rio Grande Peak Flow Frequency Study. U.S. Department of Interior, Bureau of Reclamation, Albuquerque, NM.
- Chang, H. H. (1979). Minimum Stream Power and River Channel Patterns. *Journal of Hydrology*. 41:303-327.

- Chang, H. H. (1985). River Morphology and Thresholds. *Journal of Hydraulic Engineering*. 111:503-519.
- Chow, V. T. (1959). Open Channel Hydraulics. McGraw-Hill Book Company, Inc., New York, NY. Reissued 1988.
- Colby, B. R. and Hembree, C. H. (1955). Computations of Total Sediment Discharge Niobrara River near Cody, Nebraska. Geological Survey Water-Supply Paper 1357. pp. 187.
- Darby, S. (director). (2001). Numerical Simulation of Bank Erosion and Channel Migration in Meandering Rivers. Engineering and Physical Sciences Research Council (EPSRC). <http://www.geog.soton.ac.uk/users/darbyse/epsrc>.
- Graf, W. L. (1994). Plutonium and the Rio Grande. Environmental Change and Contamination in the Nuclear Age. Oxford University Press, New York.
- Haap, S. C. (1948). Sedimentation in the Middle Rio Grande Valley, New Mexico. *Geological Society of America Bulletin*. 59:12:1191-1216.
- Henderson, F. M. (1966). Open Channel Flow. Macmillan Publishing Co., Inc., New York, NY. 522 pp.
- Hickin, E. J. and Nanson, G. C. (1984). Lateral Migration Rates of River Bends. *Journal of Hydraulic Engineering*. 110:1557-1567.
- Hooke, J. M. (1977). The Distribution and Nature of Changes in River Channel Patterns: The Example of Devon. In: River Channel Changes. Gragory, K. J. (ed.). John Wiley & Sons, Ltd., Chichester. pp. 265-280.
- Jones, L. S. and Harper, J. T. (1998). Channel Avulsions and Related Processes, and Large Scale Sedimentation Pattern Since 1875, Rio Grande, San Luis Valley, Colorado. *Geological Society of America Bulletin*. 110:411-421.
- Julien, P. Y. (1998). Erosion and Sedimentation. Cambridge University Press, Cambridge, U.K.
- Julien, P. Y. (2002). River Mechanics. Cambridge University Press, Cambridge, U.K.

- Knighton, A. D. and Nanson, G. C. (1993). Anastomosis and the Continuum of Channel Pattern. *Earth Surface Processes and Landforms*. 18:613-625.
- Knighton, D. (1998). Fluvial Forms and Processes - A New Perspective. John Wiley & Sons, Inc., New York, NY.
- Lagasse, P. F. (1980). An Assessment of the Response of the Rio Grande to Dam Construction - Cochiti to Isleta Reach. U.S. Army Corps of Engineers. Albuquerque, NM.
- Lagasse, P. F. (1994). Variable Response of the Rio Grande to Dam Construction. In: The Variability of Large Alluvial Rivers. ASCE Press, New York, NY.
- Leon, C. (1998). Morphology of the Middle Rio Grande from Cochiti Dam to Bernalillo Bridge, New Mexico. M.S. Thesis. Colorado State University, Fort Collins, CO. 210 pp.
- Leon, C. and Julien, P. (2001a). Bernalillo Bridge Reach. Highway 44 Bridge to Corrales Flood Channel Outfall. Hydraulic Modeling Analysis. 1962 - 1992. Middle Rio Grande, New Mexico. Prepared for U.S. Bureau of Reclamation. Albuquerque, New Mexico. Colorado State University, Fort Collins, CO. 85 pp.
- Leon, C. and Julien, P. (2001b). Hydraulic Modeling on the Middle Rio Grande, NM. Corrales Reach. Corrales Flood Channel to Montano Bridge. Prepared for U.S. Bureau of Reclamation. Albuquerque, New Mexico. Colorado State University, Fort Collins, CO. 83 pp.
- Leon, C., Richard, G., Bauer, T., and Julien, P. (1999a). Middle Rio Grande, Cochiti to Bernalillo Bridge, Hydraulic Geometry, Discharge and Sediment Data Base and Report. Volume I - Cross section geometry data and plots. Prepared for U.S. Bureau of Reclamation, Albuquerque Office. Colorado State University, Fort Collins, CO. 242 pp.
- Leon, C., Richard, G., Bauer, T., and Julien, P. (1999b). Middle Rio Grande, Cochiti to Bernalillo Bridge, Hydraulic Geometry, Discharge and Sediment Data Base and Report. Volume IA - Cross section geometry data and plots - Agg/deg and SCS Lines. Prepared for U.S. Bureau of Reclamation, Albuquerque Office. Colorado State University, Fort Collins, CO. 17 pp.

- Leon, C., Richard, G., Bauer, T., and Julien, P. (1999c). Middle Rio Grande, Cochiti to Bernalillo Bridge, Hydraulic Geometry, Discharge and Sediment Data Base and Report. Volume II - Daily mean discharge plots. Prepared for U.S. Bureau of Reclamation, Albuquerque Office. Colorado State University, Fort Collins, CO. 39 pp.
- Leon, C., Richard, G., Bauer, T., and Julien, P. (1999d). Middle Rio Grande, Cochiti to Bernalillo Bridge, Hydraulic Geometry, Discharge and Sediment Data Base and Report. Volume IIIA - Bed material data. Prepared for U.S. Bureau of Reclamation, Albuquerque Office. Colorado State University, Fort Collins, CO. 120 pp.
- Leon, C., Richard, G., Bauer, T., and Julien, P. (1999e). Middle Rio Grande, Cochiti to Bernalillo Bridge, Hydraulic Geometry, Discharge and Sediment Data Base and Report. Volume IIIB - Suspended sediment concentration data and plots. Prepared for U.S. Bureau of Reclamation, Albuquerque Office. Colorado State University, Fort Collins, CO. 206 pp.
- Leon, C., Richard, G., Bauer, T., and Julien, P. (1999f). Middle Rio Grande, Cochiti to Bernalillo Bridge, Hydraulic Geometry, Discharge and Sediment Data Base and Report. Volume IIIC - Suspended sediment discharge data and plots. Prepared for U.S. Bureau of Reclamation, Albuquerque Office. Colorado State University, Fort Collins, CO. 193 pp.
- Leon, C., Richard, G., Bauer, T., and Julien, P. (1999g). Middle Rio Grande, Cochiti to Bernalillo Bridge, Hydraulic Geometry, Discharge and Sediment Data Base and Report. Volume IIID - Suspended sediment particle size data and plots. Prepared for U.S. Bureau of Reclamation, Albuquerque Office. Colorado State University, Fort Collins, CO. 124 pp.
- Leon, C., Richard, G., Bauer, T., and Julien, P. (1999h). Middle Rio Grande, Cochiti to Bernalillo Bridge, Hydraulic Geometry, Discharge and Sediment Data Base CD-Rom. Prepared for U.S. Bureau of Reclamation, Albuquerque Office. Colorado State University, Fort Collins, CO.
- Leopold, L. B. and Bull, W. B. (1979). Base Level, Aggradation, and Grade. *Proceedings of the American Philosophical Society*. pp. 168-202.
- Leopold, L. B. and Wolman, M. G. (1957). River Channel Patterns: Braided, Meandering and Straight. USGS Professional Paper 282-B. 85 pp.
- Leopold, L. B. and Wolman, M. G. (1960). River Meanders. *Geological Society of America Bulletin*. 71:769-794.

- Leopold, L. B., Wolman, M. G., and Miller, J. P. (1995). Fluvial Processes in Geomorphology. Dover Publications, Inc., Mineola, NY.
- Mackin, J. H. (1948). Concept of the Graded River. *Bulletin of the Geological Society of America*. 59:463-512.
- Massong, T. (2001). Personal Communication. Geomorphologist. Representing U.S. Bureau of Reclamation. Environmental and Lands Division. Albuquerque, NM.
- Molnár, P. (2001). Precipitation and Erosion Dynamics in the Rio Puerco Basin. Ph.D. Dissertation. Colorado State University, Fort Collins, CO. 258 pp.
- Mosley, H. and Boelman, S. (1998). Santa Ana Reach. Geomorphic Report - DRAFT. U.S. Bureau of Reclamation, Albuquerque, NM.
- Mussetter Engineering, Inc. (2002). Geomorphic and Sedimentologic Investigations of the Middle Rio Grande Between Cochiti Dam and Elephant Butte Reservoir. Prepared for New Mexico Interstate Stream Commission. Albuquerque, New Mexico. Mussetter Engineering, Inc., Fort Collins, CO.
- Nanson, G. C. and Croke, J. C. (1992). A Genetic Classification of Floodplains. *Geomorphology*. 4:459-486.
- Nanson, G. C. and Hickin, E. J. (1983). Channel Migration and Incision on the Beatton River. *Journal of Hydraulic Engineering*. 109:327-337.
- Nanson, G. C. and Hickin, E. J. (1986). A Statistical Analysis of Bank Erosion and Channel Migration in Western Canada. *Geological Society of America Bulletin*. 97:497-504.
- Nordin, C. and Culbertson, J. K. (1961). Particle-Size Distribution of Stream Bed Material in the Middle Rio Grande Basin. New Mexico. *Short Papers in the Geologic and Hydrologic Sciences*. Article 147-292:C323-C326.
- Oliver, J. (2003). Personal Communication. Physical Scientist. U.S. Bureau of Reclamation. Remote Sensing and Geographic Information Group. Denver, CO.
- Parker, G. (1976). On the Cause and Characteristic Scales of Meandering and Braiding in Rivers. *Journal of Fluid Mechanics*. 76:part 3:457-480.

- Parker, G. (1979). Hydraulic Geometry of Active Gravel Rivers. *Journal of the Hydraulics Division*. 105:1185-1201.
- Pemberton, E. L. (1964). Sediment Investigations - Middle Rio Grande. In: Proceedings of the American Society of Civil Engineers. *Journal of the Hydraulic Division*. 90:HY2:pp. 163-185.
- Prus-Chacinski, T. M. (1954). Patterns of Motion in Open-Channel Bends. *Association International d'Hydrologie*. 3:38:311-318.
- Richard, G. (2001). Quantification and Prediction of Lateral Channel Adjustments Downstream from Cochiti Dam, Rio Grande, NM. Ph.D. Dissertation. Colorado State University, Fort Collins, CO. 229 pp.
- Richard, G., Leon, C., and Julien, P. (2001). Hydraulic Modeling on the Middle Rio Grande, New Mexico. Rio Puerco Reach. Prepared for U.S. Bureau of Reclamation. Albuquerque, New Mexico. Colorado State University, Fort Collins, CO. 76 pp.
- Richardson, E. V., Simons, D. B., and Lagasse, P. F. (2001). River Engineering for Highway Encroachments: Highways in the River Environment. DRAFT. U.S. Department of Transportation, FHA, Washington, D.C.
- Rittenhouse, G. (1944). Sources of Modern Sands in the Middle Rio Grande Valley, New Mexico. *Journal of Geology*. 52:145-183.
- Rosgen, D. (1996). Applied River Morphology. Wildland Hydrology, Pagosa Springs, CO.
- Rozovskii, I. L. (1957). Flow of Water in Bends of Open Channels. Academy of Sciences of the Ukrainian SSR., Institute of Hydrology and Hydraulic Engineering, Kiev. Translation by Y. Prushansky, 1961 Israel Program for Scientific Translations, S. Monson, Jerusalem, PST Catalog No. 363.
- Sanchez, V. and Baird, D. (1997). River Channel Changes Downstream of Cochiti Dam. Middle Rio Grande, New Mexico. In: Proceedings of the Conference of Management of Landscapes Disturbed by Channel Incision. University of Mississippi, Oxford, MS.
- Schumm, S. A. (1977). The Fluvial System. John Wiley & Sons, Inc., New York, NY.

- Schumm, S. A., Harvey, M., and Watson, C. (1984). Incised Channels, Morphology, Dynamics and Control. Water Resources Publications, Littleton, CO.
- Schumm, S. A. and Khan, H. R. (1972). Experimental Study of Channel Patterns. *Geological Society of America Bulletin*. 83:1755-1770.
- Scurlock, D. (1998). From the Rio to the Sierra. An Environmental History of the Middle Rio Grande Basin. General Technical Report RMRS-GTR5. USDA, Forest Service, Rocky Mountain Research Station, Fort Collins. 440 pp.
- Sixta, M., Albert, J., Leon, C., and Julien, P. (2003a). Bernalillo Bridge Reach. Highway 44 Bridge to Corrales Flood Channel Outfall. Hydraulic Modeling Analysis. 1962 - 2001. Middle Rio Grande, New Mexico. Prepared for U.S. Bureau of Reclamation. Albuquerque, New Mexico. Colorado State University, Fort Collins, CO. 87 pp.
- Sixta, M., Albert, J., Leon, C., and Julien, P. (2003b). Corrales Reach. Corrales Flood Channel to Montano Bridge. Hydraulic Modeling Analysis. 1962 - 2001. Middle Rio Grande, New Mexico. Prepared for U.S. Bureau of Reclamation. Albuquerque, New Mexico. Colorado State University, Fort Collins, CO.
- Sixta, M., Albert, J., Leon, C., and Julien, P. (2003c). San Felipe Reach. Arroyo Tonque to Angostura Diversion Dam. Hydraulic Modeling Analysis. 1962 - 1998. Middle Rio Grande, New Mexico. Prepared for U.S. Bureau of Reclamation. Albuquerque, New Mexico. Colorado State University, Fort Collins, CO. 85 pp.
- Smith, D. G. and Putnam, P. E. (1980). Anastomosed River Deposits: Modern and Ancient Examples in Alberta, Canada. *Canadian Journal of Earth Sciences*. 17:1396-1406.
- Stevens, H. H. and Yang, C. T. (1989). Summary and Use of Selected Fluvial Sediment-Discharge Formulas. USGS Water Resources Investigations Report 80-4026. 62 pp.
- Thorne, C. R. (1999). Meander Migration Prediction. <http://www.geog.nottingham.ac.uk/newgeog/research/projects/fluvialgroup/meander.htm>.
- US Bureau of Reclamation (1955). Step Method for Computing Total Sediment Load by the Modified Einstein Procedure. Prepared by the Sedimentation Section, Hydrology Branch. pp. 18.

- van den Berg, J. H. (1995). Prediction of Alluvial Channel Pattern of Perennial Rivers. *Geomorphology*. 12:259-279.
- Williams, G. and Wolman, G. (1984). Downstream Effects of Dams on Alluvial Rivers. Geological Survey Professional Paper 1286, 83 pp.
- Wolf, P.R. and Ghilani, C.D. (2002). Elementary Surveying: An Introduction to Geomatics (10th ed.). Prentice-Hall, Inc., Upper Saddle River, NJ. 472 pp.
- Woodson, R. C. (1961). Stabilization of the Middle Rio Grande in New Mexico. In: Proceedings of the American Society of Civil Engineers. Journal of the Waterways and Harbor Division. 87:No. WW4:pp. 1-15.
- Woodson, R. C. and Martin, J. T. (1962). The Rio Grande comprehensive plan in New Mexico and its effects on the river regime through the middle valley. In: Control of Alluvial Rivers by Steel Jetties, American Society of Civil Engineers Proceedings. Carlson, E. J. and Dodge E. A. eds. *Journal of the Waterways and Harbor Division*. American Society of Civil Engineers, NY, NY, 88:pp. 53-81.
- Yang, C. T. and Song, C. S. S. (1979). Theory of Minimum Rate of Energy Dissipation. *Journal of the Hydraulics Division*. American Society of Civil Engineers. 105:HY7:769-784.

**APPENDIX A:
Aerial Photograph Data**

Table A-1: Aerial Photograph Data (Source: Richard et al. 2001).

Aerial Photographs digitized in the Rio Grande Geomorphology Study, v. 1 by the

USBR, Remote Sensing and Geographic Information Group, Denver, CO:

- 1) 1918 – Scale: 1:12,000, Hand drafted linens (39 sheets), USBR Albuquerque Area Office. Surveyed in 1918, published in 1922.
- 2) 1935 – Scale: 1:8,000. Black and white photography, USBR Albuquerque Area Office. Flown in 1935, published 1936.
- 3) 1949 – Scale 1:5,000. Photo-mosaic. J. Ammann Photogrammetric Engineers, San Antonio, TX. USBR Albuquerque Area Office.
- 4) March 15, 1962 – Scale: 1:4,800. Photo-mosaic. Abram Aerial Survey Corp. Lansing, MI. USBR Albuquerque Area Office.
- 5) April 1972 – Scale: 1:4,800. Photo-mosaic. Limbaugh Engineers, Inc., Albuquerque, NM. USBR Albuquerque Area Office.
- 6) March 31, 1985 – Scale: 1:4,800. Orthophoto. M&I Consulting Engineers, Fort Collins, CO. Aero-Metric Engineering, Sheboygan, MN. USBR Albuquerque Area Office.
- 7) February 24, 1992 – Scale: 1:4,800. Orthophoto. Koogle and Poules Engineering, Albuquerque, NM. USBR Albuquerque Area Office.
- 8) Winter 2001 – Scale: 1:4,800. Ratio-rectified photo-mosaic. Pacific Western Technologies, Ltd. USBR Albuquerque Area Office.

Table A-2: Aerial photograph dates and mean daily discharge on those days.

Aerial Photograph Dates	Mean Daily Discharge at San Felipe (cfs)	Mean Daily Discharge at Bernalillo (cfs)	Mean Daily Discharge at Albuquerque (cfs)
February 24, 1992	314	No data	159
March 31, 1985	570	No data	109
April 1972	Mean = 564 Max = 894 Min = 400	No data	Mean = 705 Max = 2540 Min = 116
March 15, 1962	722	493	No data
1949 (unknown date)	Mean = 1806 Max = 10500 Min = 316	Extreme low flow (from meta-data file)	No data
1935 (unknown date)	Mean = 1555 Max = 8000 Min = 310	Annual data from Otowi: Mean = 1,520 Max = 7,490 Min = 350	No data
1918 (unknown date)	No data	No data	No data

METADATA

Report Date: 02-Oct-1998

Metadata Data Set Name:

Rio Grande Geomorphology Study (1918-1992)

1 Identification Information

1.1 Citation:

8 Citation Information:

8.1 Originator:

US Bureau of Reclamation

8.2 Publication Date:

19980925

8.4 Title:

Rio Grande Geomorphology Study

8.5 Edition:

Version 1

99.8.6 Data Presentation Form:

Map

8.8.1 Publication Place:

Denver Federal Center, Mail Code D-8260, POB
25007, Denver, CO 80225

8.8.2 Publisher:

Remote Sensing and Geographic Information Group

1.2 Description

1.2.1 Abstract:

The GIS database was created for the Middle Rio Grande Project as a component of the Floodway and Low Flow Channel Operations and Maintenance Study for the US Bureau of Reclamation Albuquerque Projects office. The main objective of the study is to understand the geomorphic behavior of the Rio Grande over the past 80 years and use this information to project future geomorphic characteristics. The study area extends from Velarde, New Mexico to Otowi, New Mexico and from Cochiti Dam to the Narrows of Elephant Butte of New Mexico. The study area is broken into five reaches which were determined by the Albuquerque Area Office. The focus for the interpretation of fluvial features is in support of modeling and analysis of sediment, river sinuosity, and river morphology.

1.2.2 Purpose:

The purpose of the Rio Grande Geomorphology Study is to investigate the geomorphic changes of the Middle Rio Grande using existing historic source data. The GIS database was created to show the fluvial activity and man-made changes to the river channel for the United States Bureau of Reclamation Albuquerque Projects Office at

Albuquerque, New Mexico.

1.2.3 Supplemental Information:

ABBREVIATIONS FOR REACHES (ALL IN THE STATE OF NEW MEXICO) USED IN THE NAMING CONVENTION: al -Hwy 44

bridge at Bernalillo to the San Acacia Diversion Dam // cd - Cochiti Dam to the Hwy 44 Bridge at Bernalillo // eb - San Antonio Hwy380 Bridge to the Narrows of Elephant Butte Reservoir // sa - San Acacia Diversion Dam to the Hwy 380 Bridge at San Antonio // sb - San Acacia Diversion Dam to the Narrows of Elephant Butte Reservoir // sm - San Acacia Diversion Dam to the San Marcial Railroad Bridge // vo - Velarde to Hwy 4 Bridge at Otowi

*****NAMING CONVENTION AND CONTENTS

(prefixes + year + reach abbreviation)***** Flood prone: (flood) * Geomorphology coverages: (geom)

* Linear features such as hydrology, bridges, railroads, dams, etc. This coverage contains annotations (except for the San Acacia and Elephant Butte reaches which have annotations in the coverages titled "marker"): (hyd) *

Mapsheet/plot boundaries and photo coverage: (map foto) * Markers or locations of irrigation

control features, bridges, station guages, etc. for reference points current to 1992: (mark) *

Aggradation/degradation lines, River miles, and

Elephant Butte Reservoir : (range lines aggdeglin rivmile ebrnglin) * Scanned

linens of the 1918/1922 data (georeferenced):

(mgr18) * Valley length - arc visually centered within the historic channels: (valley) * Cross

sections digitized in feet for various years from bluelines of historic data The xsecdxdir is a sub-directory of *.dxf files.: (xsec)

1.3 Time Period Of Content

9.2 Multiple Date/Times

9.1.1 Calendar Date:

1908, 1918,1935,1949,1962,1972,1985,1992

1.3.1 Currentness Reference:

Ground Condition

1.4 Status

1.4.1 Progress:

In Work

1.4.2 Maintenance and Update Frequency:

None Planned

99.1.5 Geographic Extent

99.1.5.1 Description of Geographic Extent:

Middle Rio Grande, New Mexico; from Velarde to the Narrows of Elephant Butte Reservoir (excluding Otowi to Cochiti Dam). The interpretation along the river was governed by the width of the flood

plane, features that would obstruct channel change, such as levees, steep elevations, or upland conditions. The Flood Prone coverages were taken from 1935 photography for the reaches north of San Acacia Diversion Dam. Reaches start/end at Velarde, Hwy 4 bridge at Otowi, Cochiti Dam, Hwy 44 bridge at Bernalillo, San Acacia Diversion Dam, Hwy 380 bridge at San Antonio, The Narrows of Elephant Butte Reservoir; all are within the state of New Mexico.

99.1.5.2 Bounding Rectangle Coordinates

1.5.2.1 West Bounding Coordinate:

-107.25

1.5.2.2 East Bounding Coordinate:

-105.875

1.5.2.3 North Bounding Coordinate:

36.25

1.5.2.4 South Bounding Coordinate:

32.34167

1.6 Keywords

1.6.1 Theme

1.6.1.1 Theme Keyword Thesaurus:

None

1.6.1.2 Theme Keyword:

Bureau of Reclamation

1.6.1.2 Theme Keyword:

Middle Rio Grande Project

1.6.1.2 Theme Keyword:

Geomorphology

1.6.1.2 Theme Keyword:

river morphology

1.6.1.2 Theme Keyword:

active channel

1.6.1.2 Theme Keyword:

historic channel

1.6.1.2 Theme Keyword:

diversion dam

1.6.2 Place

1.6.2.1 Place Keyword Thesaurus:

None

1.6.2.2 Place Keyword:

Middle Rio Grande Project, New Mexico

1.6.2.2 Place Keyword:

New Mexico

1.6.2.2 Place Keyword:

Rio Grande

1.6.2.2 Place Keyword:

Rio Grande

1.6.2.2 Place Keyword:

Middle Rio Grande Project

1.6.2.2 Place Keyword:

- New Mexico
- 1.6.2.2 Place Keyword:
 - Bosque del Apache Wildlife Refuge
- 1.6.2.2 Place Keyword:
 - The Narrows of Elephant Butte Reservoir
- 1.6.2.2 Place Keyword:
 - Velarde, New Mexico
- 1.6.2.2 Place Keyword:
 - Cochiti Dam
- 1.6.2.2 Place Keyword:
 - San Acacia, New Mexico
- 1.6.2.2 Place Keyword:
 - San Antonio, New Mexico
- 1.6.2.2 Place Keyword:
 - San Marcial, New Mexico
- 1.6.2.2 Place Keyword:
 - Albuquerque, New Mexico
- 1.8 Access Constraints:
 - Contact Drew Baird at the USBR Albuquerque Area Office. Data archived at University of New Mexico, Albuquerque, New Mexico
- 1.9 Use Constraints:
 - Acknowledgment of the USBR/RS&GIS Group would be appreciated in products derived from this data. Any person using the information presented here should fully understand the data collection and compilation procedures, as described in the metadata, before beginning analysis. Use is intended for the analysis of geomorphology and sedimentation modeling (sedimentation data not included). The interpretation of the data sources does NOT show backwaters, natural habitats for plants or animals, open water, wetlands, land ownership, etc. The burden for determining fitness for use lies entirely with the user.
- 1.10 Point of Contact
 - 10.1 Contact Person Primary
 - 10.1.1 Contact Person:
 - Drew Baird
 - 10.1.2 Contact Organization:
 - USBR Albuquerque Area Office
 - 10.3 Contact Position:
 - Sr. Hyd. Engineer
 - 10.4 Contact Address
 - 10.4.1 Address Type:
 - Mailing Address
 - 10.4.2 Address:
 - 505 Marquette Ave. N W , Suite 1313
 - 10.4.2 Address:
 - Mail Code ALB-240
 - 10.4.3 City:

Albuquerque
10.4.4 State or Province:
New Mexico
10.4.5 Postal Code:
87102
10.4.6 Country:
USA
10.5 Contact Voice Telephone:
(505)248-5335
1.12 Data Set Credit:
(Karri) Jan Oliver, Physical Scientist, Remote
Sensing and Geographic Information Group as
contracted by Albuq. Area Office and Sedimentation
and River Hydraulics Group, Denver, CO
1.14 Native Data Set Environment:
UNIX-ARC/INFO
99.1.16 Analytical Tool
99.1.16.1 Analytical Tool Description:
AML's for Channel Comparisons, Channel Widths and
Average Width, Sinuosity, and Plotting.
99.1.16.2 Tool Access Information
99.1.16.2.2 Tool Access Instruction:
call for applications
99.1.16.3 Tool Contact:
10.2 Contact Organization Primary
10.1.2 Contact Organization:
US Bureau of Reclamation Remote Sensing and
Geographic Information Group
10.1.1 Contact Person:
Jan Oliver
10.3 Contact Position:
Physical Scientist
10.4 Contact Address
10.4.1 Address Type:
Mailing Address
10.4.2 Address:
POB 25007
10.4.2 Address:
Mail code D-8260
10.4.3 City:
Denver
10.4.4 State or Province:
Colorado
10.4.5 Postal Code:
80225-0007
10.4.6 Country:
USA
10.5 Contact Voice Telephone:
(303)445-2281
99.10.8 Internet Address:
joliver@do.usbr.gov

- 99.1.16.4 Tool Citation:
 - 8.1 Originator:
 - US Bureau of Reclamation
 - 8.2 Publication Date:
 - 19980925
 - 8.4 Title:
 - Rio Grande Geomorphology Study
 - 8.5 Edition:
 - Version 1
 - 99.8.6 Data Presentation Form:
 - Map
 - 8.8.1 Publication Place:
 - Denver Federal Center, Mail Code D-8260, POB
25007, Denver, CO 80225
 - 8.8.2 Publisher:
 - Remote Sensing and Geographic Information Group
- 99.1.16.1 Analytical Tool Description:
 - Arc/Info AML programs
- 99.1.16.2 Tool Access Information
 - 99.1.16.2.3 Tool Computer and Operating System:
 - UNIX Arc/Info
- 99.1.16.3 Tool Contact:
- 99.1.16.4 Tool Citation:
- 2 Data Quality Information
 - 2.1 Attribute Accuracy
 - 2.1.1 Attribute Accuracy Report:
 - Has not been assessed by field work. QA/QC was performed by comparing plots to the photography and perceived errors corrected. Attributes have been added to the project over time and the definitions refined. Definitions are consistent through out the project once established.
 - 2.2 Logical Consistency Report:
 - no report at this time
 - 2.3 Completeness Report:
 - San Acacia and Elephant Butte reaches 99%, Cochiti Reach 90%, Velarde reach 90%, Albuquerque reach 60% finished.
 - 2.4 Positional Accuracy
 - 2.4.1 Horizontal Positional Accuracy
 - 2.4.1.1 Horizontal Positional Accuracy Report:
 - Dependent upon the source data mapsheet. 1962 - 1992 are within National Map Accuracy Standards at 1:12,000 and assumed to be within NMAS at 1:4,800, the scale of source materials. Years prior to 1962 may or may not be within NMAS. See Entity Overview for discussion of data quality and Source data notations concerning accuracy. // 1918 Rubber-sheeting was performed by overlaying the 1:12000 hand-drafted 1918 maps on to a 1:24000 2X enlargement of a 7.5 minute USGS quad and creating

a link point coverage for transformation using Arc/info. For a best visual fit of the mapsheet to the base map, the hard copy mapsheet was warped to fit the general area on the base map and four to six link points were digitized onto the Polyconic Quad and a link point assigned to the corresponding location on the continuous mosaic coverage for rubber-sheeting. The control point coverage created from the link points assigned to USGS 7.5 minute quads was re-projected from Polyconic to State Plane coordinate system NAD27 and joined to form a continuous coverage. The 1918 continuous mosaics were rubber sheeted to the State Plane control point coverage using Arc/info. ****FYI**** error of the 1918 control points was up to a radius of 700 feet from the USGS basemap control points at a scale of 1:12000. While georeferencing the 1918 data should improve the accuracy of the information provided by the linens, error is inherent to rubber sheeting. Transformation to a non-grid set of control points does not rubber sheet the Data uniformly which may cause greater distortion of the data. The further from the control point the data are the greater amount of distortion can occur. This distortion may be greater than 700 feet. This error should be taken into account when measuring distances, area or volume. This database is recommended for visual comparison only. Better control points are needed to reduce Error within this database. Control points for this data were not extended to the edges of the data. The main feature used for control placement was the railroad. The next feature was the few roads that may have occupied a similar location in both years. The side of the river having less remarkable features to use for control was adjusted using the elevations on the base map and a general fit of the 1918 mapsheet contours. According to the surveyor's instruction to the survey crews, the elevations were taken as time permitted and were not a major function of the survey, therefore, it is probable the contours were extrapolated during drafting of the mapsheets and are not reliable control. Survey notes are archived at the Army Corps of Engineers Albuquerque Office. Roads and irrigation features did not appear in the same location as the features on later photography or the USGS quads. Survey boundaries of the township and range lines, county lines, Land Grant and Reservation

boundaries have been resurveyed since 1918 as represented on the USGS quad. The Township & Range line numbers are not the same as in 1918. The active channel coverage was screen digitized. Active channel and vegetated islands were the only features delineated. The active channel was defined as the open water and the sandbars sharing contact with the open water. The approximate thalweg of the 1918 active channel was determined by comparing the open water area, the approximate thalweg of 1935, best guess from the elevations.// 1908 Rio Grande river channel was digitized from plane table sheets (24Pt503) numbered 12 thru 17. The plane table sheets were reproduced from aperture cards archived at USBR in Salt Lake City, Utah. The scale is approximately 1:12000. The control points used for georeferencing were the end points of the Elephant Butte Reservoir Rangelines. From looking at the monuments named on the 1908 map and the 1925 Silt Survey report by Brown which showed several Range Lines terminating on the monument marks, it was determined that some of the endpoints were the same as the monuments. At some later date (one note is dated 1935) the sheets had most of the rangeline endpoint monuments added to the originals before they were photographed for the aperture cards. The primary monuments used for registration were those named on the 1908 blue-line continuous map of the PT sheets included in a report titled "Silt Survey - Elephant Butte Dam". The report contains several other technical memos including one titled "The Triangulation System for the Silt Survey of the Elephant Butte Reservoir New Mexico". These were the original monuments on the PT sheets. Most of the other Rangeline monuments were added to the PT sheets at a later date. The addition appears to be quite accurate considering the RMS errors and that the PT sheets are reproductions. The exception being sheet 15 where few of either set of monuments were useful in obtaining a low RMS error. It is impossible to determine if the drafting is incorrect or if the reproduction was distorted at some point in the archiving/reconstruction process. The latter would be more suspect. The RMS errors for the PT sheets were: (FEET + SHEET) * (27' #12) (13' #13) (13' #14) (61' #15) (14' #16) (23' #17)

2.5 Lineage

99.2.5.1 Methodology

99.2.5.1.1 Methodology Type:

Lab

99.2.5.1.2.1 Methodology Keyword Thesaurus:

None

99.2.5.1.2.2 Methodology Keyword:

Arc/info

99.2.5.1.2.2 Methodology Keyword:

river morphology photo interpretation

99.2.5.1.2.2 Methodology Keyword:

digitized

99.2.5.1.3 Methodology Description:

The mapsheets for 1949 - 1992 were digitized on an Altek digitizing table, Hewlett Packard 700 series work station using Arc/Info software. The mapsheets use State Plane coordinates, Central Zone, New Mexico. // 1935 photography was enlarged to the scale of the 1949 mapsheets which were used as basemaps. Enlargement was accomplished using a Saltzman transfer projector and the image was drafted onto mylar overlays registered to the 1949 mapsheets (Plot numbering corresponds to 1949 numbers). The drafted mylar overlays were digitized as above. // The 1918 hand-drafted linens were scanned using an Anatech 4080ET scanner at 400 dpi and vectorized using Provec software to create a *.tiff file. The *.tiff file was used to generate a line coverage in Arc/info. Scans were transformed, "rubber-sheeted", and the active channel was screen digitized using Arc/Info software. The base maps used for control of rubbersheeting were 2X enlarged 1:24000 USGS 7.5 minute Quadrangle maps having a Polyconic projection. See Horizontal Positional Accuracy Report. The active channel was screen digitized, thalweg placement was "best guess". // 1908 data from BOR Surveying Plane Table sheets, digitized as above. Control points used for georeferencing were the end points of the Elephant Butte Reservoir Rangelines. The final GIS database was projected to UTM, zone 13, NAD27. February 24, 1992 photography contrast was good. The mapsheet mismatch error was up to 1/16" (25'). Low Flow Conveyance Channel centerline corrected using 1985 data. March 31, 1985 photography contrast is poor for very light and very dark features. Light tones include thalweg, floodway clearing, and recent changes of the active channel which are the main focus of interpretation. April 1972 contrast is poor for light tones. Mapsheets 101 and 103 were out of the study area. March 15, 1962 contrast is very dark making the historic channel

difficult to distinguish from shadows. 1962 had the highest Root-Mean-Square (RMS) Error of all the mapsheets when digitizing (as high as .018 digitizer inches, greatest error on mapsheets 89-100). Tics contributing the greatest error were not used. The aggradation/degradation lines on the mapsheets do not match the agg/deg line coverage generated from surveyed coordinates. Documentation indicates problems with the contractor and the poor quality of the photo-mosaic product. 1949 photography contrast was acceptable to poor for very light and very dark. San Marcial Lake was present at this time (feature 11). Flooding distributed the water flow through riparian areas and out of the active channel in many places creating a secondary channel (feature 5). Sedimentation Group decided that the thalweg be digitized in the flow path of prior years although there is no water in this channel during 1949 low flow. The flood event is not considered a recent change from the active channel. 1935/1936 photography contrast was good. 1935 plots correspond to the numbers on the 1949 mapsheets which were used for a base map. Flood-prone area was determined from 1935 stereo pair photographs. The historic channel areas show more variation in vegetative growth than do the years following 1936. Height, density, and fullness of riparian vegetation may be affected by agricultural clearing or by hydrologic dynamics. The river itself is more braided than in later years so the thalweg is a representation of greatest flow through the braided area. 1918 hand-drafted linens compiled by the Bureau of Reclamation published June 1922. The original field work was performed under the direction of the New Mexico State Engineer's Office dated 1917-1918.

99.2.5.1.4 Methodology Citation:

8.1 Originator:

US Bureau of Reclamation

8.2 Publication Date:

19980925

8.4 Title:

Rio Grande Geomorphology Study

8.5 Edition:

Version 1

99.8.6 Data Presentation Form:

Map

8.8.1 Publication Place:

Denver Federal Center, Mail Code D-8260, POB
25007, Denver, CO 80225

- 8.8.2 Publisher:
 - Remote Sensing and Geographic Information Group
- 2.5.2 Source Information
 - 2.5.2.1 Source Citation:
 - 2.5.2.2 Source Scale Denominator:
 - 12000
 - 2.5.2.3 Type Of Source Media:
 - hand drafted linens (39 sheets)
 - 2.5.2.4 Source Time Period Of Content:
 - 2.5.2.4.1 Source Currentness Reference:
 - data 1918 but published 1922
 - 2.5.2.6 Source Contribution:
 - Albuq. Area Office
- 2.5.2 Source Information
 - 2.5.2.1 Source Citation:
 - 2.5.2.2 Source Scale Denominator:
 - 8000
 - 2.5.2.3 Type Of Source Media:
 - black and white photography
 - 2.5.2.4 Source Time Period Of Content:
 - 2.5.2.4.1 Source Currentness Reference:
 - flown 1935 but published 1936
 - 2.5.2.6 Source Contribution:
 - Albuq. Area Office
- 2.5.2 Source Information
 - 2.5.2.1 Source Citation:
 - 2.5.2.2 Source Scale Denominator:
 - 5000
 - 2.5.2.3 Type Of Source Media:
 - photo-mosaic
 - 2.5.2.4 Source Time Period Of Content:
 - 2.5.2.4.1 Source Currentness Reference:
 - 1949
 - 2.5.2.5 Source Citation Abbreviation:
 - J. Ammann Photogrammetric Engineers, San Antonio,
TX
 - 2.5.2.6 Source Contribution:
 - Albuq. Area Office
- 2.5.2 Source Information
 - 2.5.2.1 Source Citation:
 - 2.5.2.2 Source Scale Denominator:
 - 4800
 - 2.5.2.3 Type Of Source Media:
 - photo-mosaic
 - 2.5.2.4 Source Time Period Of Content:
 - 2.5.2.4.1 Source Currentness Reference:
 - 1962
 - 2.5.2.5 Source Citation Abbreviation:
 - Abram Aerial Survey Corp. Lansing, MI
 - 2.5.2.6 Source Contribution:
 - Albuq. Qrea Office

- 2.5.2 Source Information
 - 2.5.2.1 Source Citation:
 - 2.5.2.2 Source Scale Denominator:
4800
 - 2.5.2.3 Type Of Source Media:
photo-mosaic
 - 2.5.2.4 Source Time Period Of Content:
 - 2.5.2.4.1 Source Currentness Reference:
1972
 - 2.5.2.5 Source Citation Abbreviation:
Limbaugh Engineers, Inc., Albuquerque, NM
 - 2.5.2.6 Source Contribution:
Albuq. Area Office
- 2.5.2 Source Information
 - 2.5.2.1 Source Citation:
 - 2.5.2.2 Source Scale Denominator:
4800
 - 2.5.2.3 Type Of Source Media:
orthophoto
 - 2.5.2.4 Source Time Period Of Content:
 - 2.5.2.4.1 Source Currentness Reference:
1984/1985
 - 2.5.2.5 Source Citation Abbreviation:
M&I Consulting Engineers, Ft. Collins, CO /
Aero-Metric Engineering, Sheboygan, MN
 - 2.5.2.6 Source Contribution:
Albuq. Area Office
- 2.5.2 Source Information
 - 2.5.2.1 Source Citation:
 - 2.5.2.2 Source Scale Denominator:
4800
 - 2.5.2.3 Type Of Source Media:
orthophoto
 - 2.5.2.4 Source Time Period Of Content:
 - 2.5.2.4.1 Source Currentness Reference:
1992
 - 2.5.2.5 Source Citation Abbreviation:
Koogle and Poules Engineering, Albuquerque, NM
 - 2.5.2.6 Source Contribution:
Albuq. Area Office
- 2.5.2 Source Information
 - 2.5.2.1 Source Citation:
 - 2.5.2.2 Source Scale Denominator:
12000
 - 2.5.2.3 Type Of Source Media:
Aperture Card reproductions
 - 2.5.2.4 Source Time Period Of Content:
 - 2.5.2.4.1 Source Currentness Reference:
1908 but published 1909
 - 2.5.2.6 Source Contribution:
USBR Records and Archives, Salt Lake City, UT

2.5.3 Process Step

2.5.3.1 Process Description:

Source materials having State Plane coordinates were registered to a tic coverage of State Plane Coordinates, New Mexico Central Zone, NAD27 Datum, for digitizing (except for the Velarde Reach where USGS 7.5' Quads were used. All coverages were reprojected to UTM, zone 13, NAD27 Datum, for archiving at University of New Mexico, Albuquerque, NM.

2.5.3.3 Process Date:

Not Complete

2.5.3.6 Process Contact

10 Contact Information

10.2 Contact Organization Primary

10.1.2 Contact Organization:

US Bureau of Reclamation Remote Sensing and Geographic Information Group

10.1.1 Contact Person:

Jan Oliver

10.3 Contact Position:

Physical Scientist

10.4 Contact Address

10.4.1 Address Type:

Mailing Address

10.4.2 Address:

POB 25007

10.4.2 Address:

Mail code D-8260

10.4.3 City:

Denver

10.4.4 State or Province:

Colorado

10.4.5 Postal Code:

80225-0007

10.4.6 Country:

USA

10.5 Contact Voice Telephone:

(303)445-2281

99.10.8 Internet Address:

joliver@do.usbr.gov

3 Spatial Data Organization Information

3.2 Direct Spatial Reference Method:

Vector

4 Spatial Reference Information

4.1 Horizontal Coordinate System Definition

4.1.2 Planar

4.1.2.2 Grid Coordinate System

4.1.2.2.1 Grid Coordinate System Name:

Universal Transverse Mercator

4.1.2.2.1 UTM Zone Number:

13

4.1.2.1.2.2 Longitude Of Central Meridian:

-105

4.1.2.1.2.3 Latitude Of Projection Origin:

0

4.1.2.1.2.4 False Easting:

0

4.1.2.1.2.5 False Northing:

0

4.1.2.1.2.17 Scale Factor at Central Meridian:

.9996

4.1.4 Geodetic Model

4.1.4.1 Horizontal Datum Name:

North American Datum of 1927

4.1.4.2 Ellipsoid Name:

Clarke 1866

4.1.4.3 Semi-Major Axis:

6378137

4.1.4.4 Denominator of Flattening Ratio:

298.257

5 Entity and Attribute Information

5.1 Detailed Description

5.1.1 Entity Type

5.1.1.1 Entity Type Label:

POLYGON FEATURES

5.1.1.2 Entity Type Definition:

1=ACTIVE RIVER CHANNEL - channel of the current river flow is clear of vegetation or is actively clearing vegetation. Active channel may have a seasonal growth at low flow. (See the 1935 and 1949 photography south of San Marcial where the active channel has noticeable vegetation but is the active channel). Boundaries of the active channel may be vegetative or either natural or man-made levees// 2=RECENT CHANGE FROM ACTIVE CHANNEL - the current river flow is no longer clearing vegetation from the channel and vegetation is beginning to grow; or the current channel flow has not yet cleared all vegetation from the channel. The vegetation is a different density than the historic channel vegetation and may or may not be as mature as the historic channel vegetation. Vegetation may not be present at all if the floodway has been altered by human activity, causing the river to abandon the active river channel// 3=HISTORIC ABANDONED RIVER CHANNEL - The historic floodplain that is recognizable as being created by once active river channel; such as meanders and oxbows that are currently filled by mature riparian vegetation, marshes, or fluvial deposits. Agriculture and other human activity

that has destroyed clear evidence of the historic channel is not included as historic channel. The riparian vegetation may partially recover in formerly agricultural areas causing the historic channel delineation to be vague; a best estimate is made given the appearance on the orthophoto or topographic quad sheet. (See UPLAND)//

4=VEGETATED ISLAND - Isolated vegetation within the active channel (or recent change to the active channel which surrounds an island). The vegetation of interest was of several seasons growth but may become inundated during high flows. Historic channel that has been dissected by a man made channel for the purpose of changing the channel was not called a vegetated island until the river channel caused it to remain isolated vegetation within the channel//

5=UPLAND - Non-riparian vegetation or human activity such as agriculture that has cleared the riparian vegetation from the historic channel//

6=THE CONVEYANCE CHANNEL LEVEE - A classification to represent the area created between the toe of the levee line (vegetation) and the centerline of the conveyance channel//

6=LEVEE - Areas north of the San Acacia Diversion Dam, this represents the levees created by irrigation features//

7=FLOODWAY CLEARING - Evidence of human activity in the active channel for the purpose of flood/channel control//

8=OUT OF THE STUDY AREA//

9=RESERVIOR - Water ponded behind a dam//

10=ARROYO//

11=FLOOD PRONE - Recent historic flood plain. The boundary was determined by 1935 aerial photography. The scale of the stereo pairs used was 1:31000 and the transfer to the base map was by finding as many recognizable features as possible. Some areas are "best guess" where stereo pairs were not available or the terrain has been altered such that fluvial evidence could not be established during field checking. (Sept. 1995)

Much of this classification was active agriculture in 1935//

12=VEGETATION CHANGE IN THE JEMEZ RIVER DELTA (1935 and 1949) The vegetation growth between 1935 and 1949 makes the river delta appear to be quite small. This feature class was created to retain the information for this area//

19=PONDED WATER OR LAKE LAKE//

20=COCHITI DAM//

21=RESERVIOR//

22=TRIBUTARY//

23=AVULSION

5.1.1.3 Entity Type Definition Source:

Drew Baird, Sr. Hyd. Engineer, USBR Albuquerque Area Office; Bob Strand and Paula Makar, Hyd. Engineers, USBR Sedimentation and River Hydraulics

Group, Denver, CO

5.1.1 Entity Type

5.1.1.1 Entity Type Label:

LINE FEATURE

5.1.1.2 Entity Type Definition:

1=APPROXIMATE THALWEG - visual center of flow, not necessarily the deepest water. Where braided river channel is predominant, the thalweg represents the greatest flow// 2=CENTERLINE OF THE CONVEYANCE CHANNEL// 3=TOE (VEGETATION LINE) OF THE CONVEYANCE CHANNEL LEVEE - The toe of the levee is often vegetated such that the actual toe is not visible. The vegetation line is considered the toe of the levee for this study// 4=RAILROAD// 5=TIFFANY CHANNEL OR RIVERSIDE DRAIN - 1992 or 1949 delineations// 5=IRRIGATION FEATURES - North of San Acacia Reach// 6=STUDY AREA BOUNDARY LINE AND RANGELINES// 7=LEVEE ROAD 1949// 8=RIVER MILE MARKER// 9=BRIDGE// 10=HIGHWAY// 11=DIVERSION DAM// 12=COCHITI DAM -- centerline of the road across the top of the structure// 13=ANGOSTURA DIVERSION DAM LOCATION (silted over)// 14=AT & SF RAILROAD BRIDGE// \$ID=OUTLINES OF THE MAP SHEETS ARE LABELED THE SAME NUMBER AS THE MAP SHEET// 15=RESERVOIR RANGE LINES// 16=FUTURE SITE OF HIGHWAY 380 (1935-36)// 17=SECONDARY CHANNEL flood event or temporary diversion of the active channel// 18=POWERLINE// 19=ELEPHANT BUTTE RESERVOIR GRANT BOUNDARY// 20=JETTY JACK LINES// 21=PIPELINE

5.1.1.3 Entity Type Definition Source:

Drew Baird, Sr. Hyd. Engineer, USBR Albuquerque Area Office; Bob Strand and Paula Makar, Hyd. Engineers, USBR Sedimentation and River Hydraulics Group, Denver, CO

5.1.1 Entity Type

5.1.1.1 Entity Type Label:

POINT FEATURES

5.1.1.2 Entity Type Definition:

21=BRIDGE// 22=CULVERT// 23=CHECK STRUCTURE// 24=WASTEWAY// 26=ARROYO OUTSIDE OF THE STUDY AREA// 27=GAGING STATION// 28=CMP

5.1.1.3 Entity Type Definition Source:

Drew Baird, Sr. Hyd. Engineer, USBR Albuquerque Area Office; Bob Strand and Paula Makar, Hyd. Engineers, USBR Sedimentation and River Hydraulics Group, Denver, CO

5.2 Overview Description

5.2.1 Entity and Attribute Overview:

The study area addresses five reaches: Velarde to the Highway 4 Bridge at Otowi, Cochiti Dam to

Highway 44 bridge at Bernalillo, Bernalillo to the San Acacia Diversion Dam, San Acacia Diversion Dam to Highway 380 bridge at San Antonio, and Highway 380 bridge at San Antonio to the "Narrows" of Elephant Butte Reservoir. The study areas north of San Accia Diversion Dam was bounded by "flood-prone" areas in 1935. From 1949 to 1992 the study area is bounded by constructions along the river which limit channel movement. The 1918 coverage consists of only the active channel. The study area south of the San Acacia Diversion Dam is bounded on the west side of the Rio Grande by the Low Flow Conveyance Channel (CC) for the years of 1962, 1972, 1985, and 1992. For 1935 and 1949, the western boundary is the upland edge of the historic channel, railroad levee, or San Antonio Drain, which ever had the closest proximity to the river. The eastern boundary of the study area is upland vegetation or uses. All aerial photography is black and white. The orthophotos and photo-mosaics are printed on mylar except 1949 (acetate film), and 1935 (photograph paper). The alignment discrepancies between years are inherent to the accuracy of the source data. Be aware of this when data are analyzed and plots are viewed.

5.2.2 Entity and Attribute Detail Citation:

This project and attributes were determined by USBR : Drew Baird, Sr. Hyd. Engineer, Albuquerque Area Office, and Paula Makar and Bob Strand, Hyd. Engineers, Sedimentation and River Hydraulics Group, Denver CO

6 Distribution Information

6.1 Distributor

10.1 Contact Person Primary

10.1.1 Contact Person:

Drew Baird

10.1.2 Contact Organization:

USBR Albuquerque Area Office

10.3 Contact Position:

Sr. Hyd. Engineer

10.4 Contact Address

10.4.1 Address Type:

Mailing Address

10.4.2 Address:

505 Marquette Ave. N W , Suite 1313

10.4.2 Address:

Mail Code ALB-240

10.4.3 City:

Albuquerque

10.4.4 State or Province:

New Mexico

10.4.5 Postal Code:

87102

10.4.6 Country:

USA

10.5 Contact Voice Telephone:

(505)248-5335

6.3 Distribution Liability:

Although these data have been processed successfully on a computer system at the Bureau of Reclamation - Remote Sensing and Geographic Information Group, no warranty expressed or implied is made regarding the accuracy or utility of the data on any other system or for general or scientific purposes, nor shall the act of distribution constitute any such warranty. This disclaimer applies both to individual use of the data and aggregate use with other data. It is strongly recommended that these data are directly acquired from a Bureau of Reclamation server, and not indirectly through other sources which may have changed the data in some way. It is also strongly recommended that careful attention be paid to the contents of the metadata file associated with these data. The Bureau of Reclamation shall not be held liable for improper or incorrect use of the data described and/or contained herein.

7 Metadata Reference Information

7.1 Metadata Date:

19980925

7.4 Metadata Contact:

10.2 Contact Organization Primary

10.1.2 Contact Organization:

US Bureau of Reclamation Remote Sensing and Geographic Information Group

10.1.1 Contact Person:

Jan Oliver

10.3 Contact Position:

Physical Scientist

10.4 Contact Address

10.4.1 Address Type:

Mailing Address

10.4.2 Address:

POB 25007

10.4.2 Address:

Mail code D-8260

10.4.3 City:

Denver

10.4.4 State or Province:

Colorado

10.4.5 Postal Code:

80225-0007

10.4.6 Country:

USA

10.5 Contact Voice Telephone:

(303)445-2281

99.10.8 Internet Address:

joliver@do.usbr.gov

7.5 Metadata Standard Name:

FGDC Content Standards For Digital Geospatial data

7.6 Metadata Standard Version:

NBII Draft of December 1995, Based FGDC of June 8,
1994

GIS PROJECTION AND COORDINATE SYSTEM

NAD 1983 StatePlane New Mexico Central FIPS 3002 Feet

Projection: Transverse Mercator

Parameters:

False Easting: 1640416.67

False Northing: 0.00

Central Meridian: -106.25

Scale Factor: 0.99

Latitude of Origin: 31.00

Linear Unit: Foot U.S. (0.3048)

Geographic Coordinate System:

Name: GCS North American 1983

Angular Unit: Degree (0.017453292519943295)

Prime Meridian: Greenwich

Datum: North American 1983

Spheroid: GRS 1980

Semimajor Axis: 6378137.00

Semiminor Axis: 6356752.31

Inverse Flattening: 298.26

APPENDIX B:
Location Maps (San Felipe Reach)

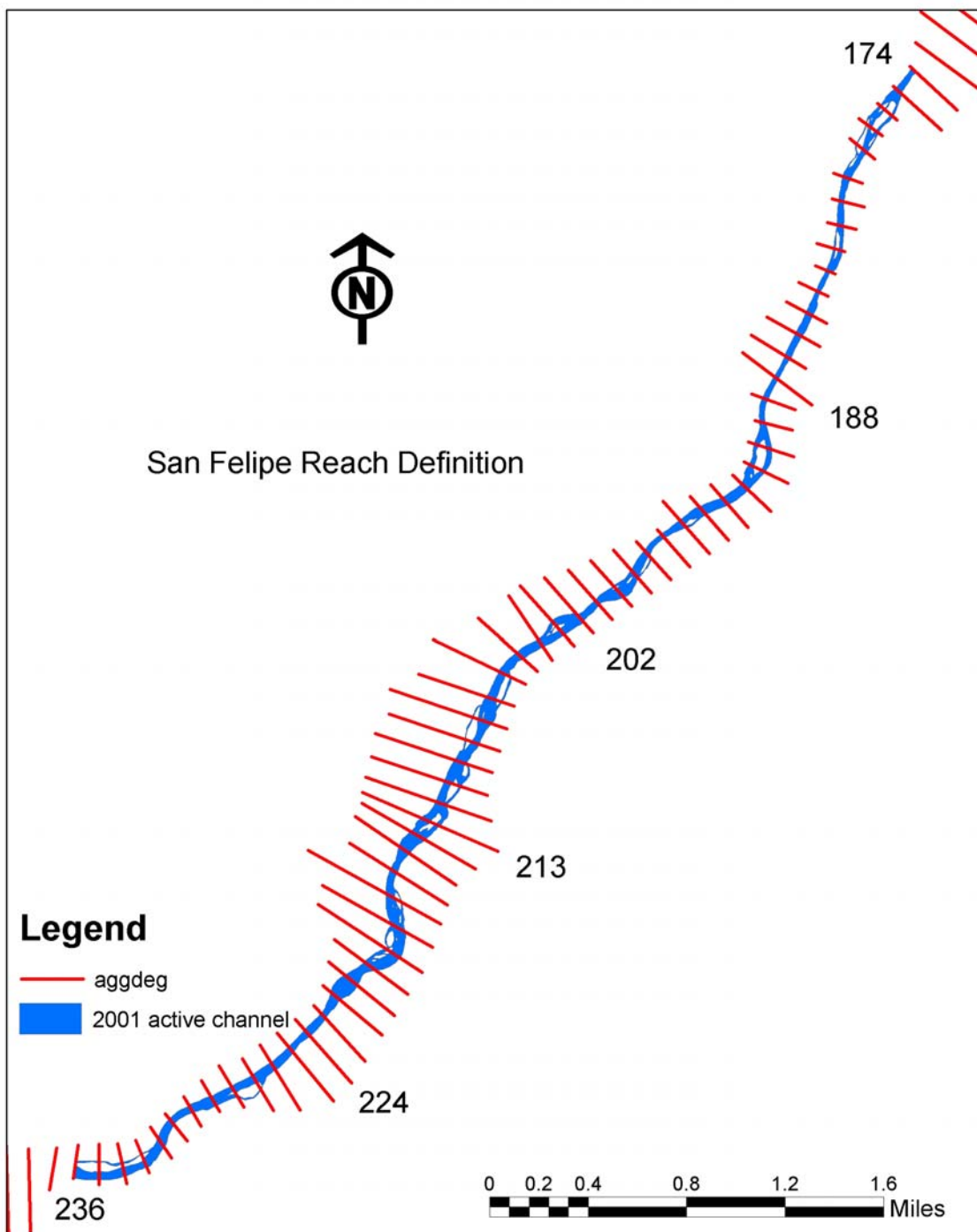


Figure B-1: 2001 river planform of the San Felipe Reach displaying locations of the agg/deg lines.

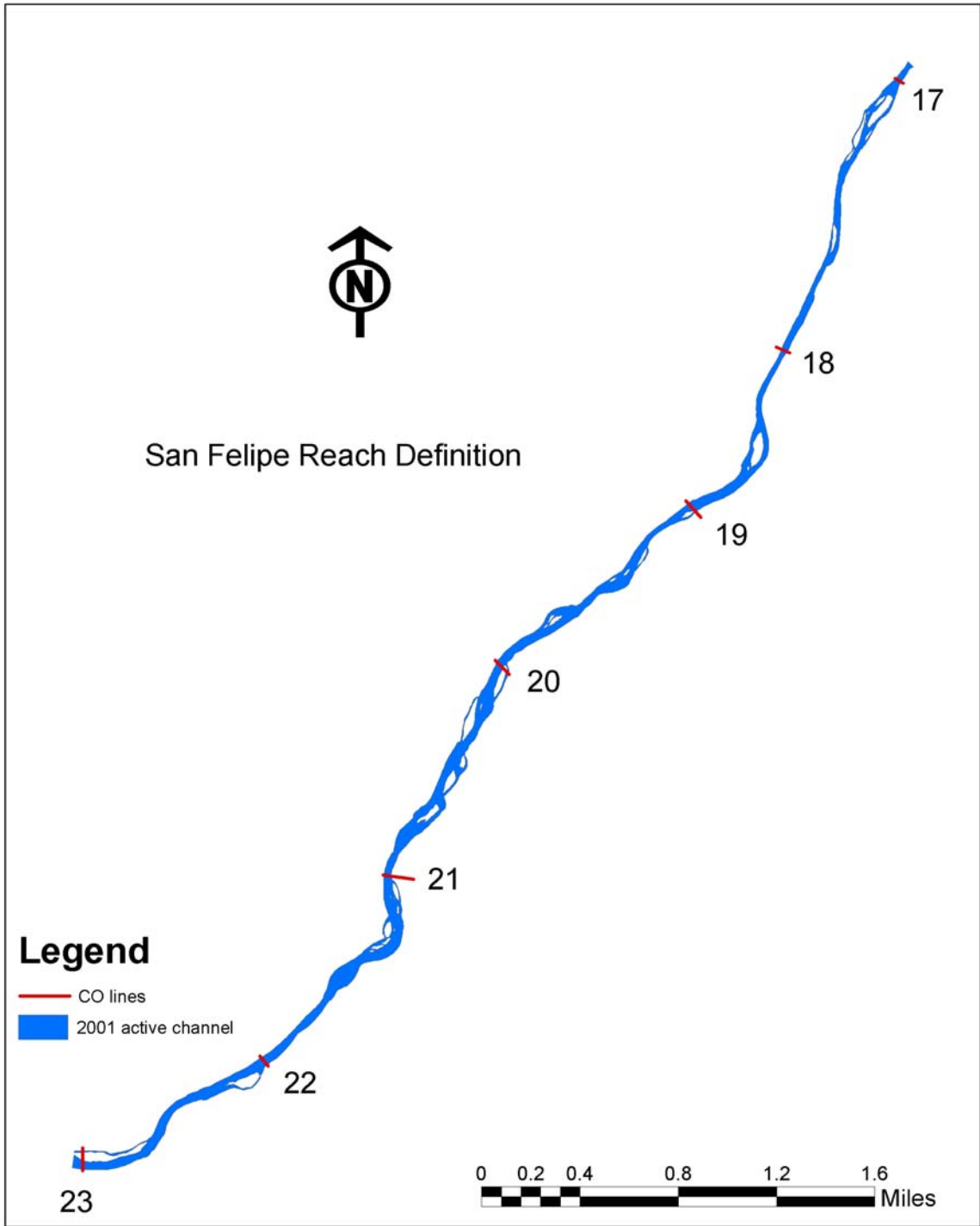


Figure B-2: 2001 river planform of the San Felipe Reach displaying locations of the CO-lines.

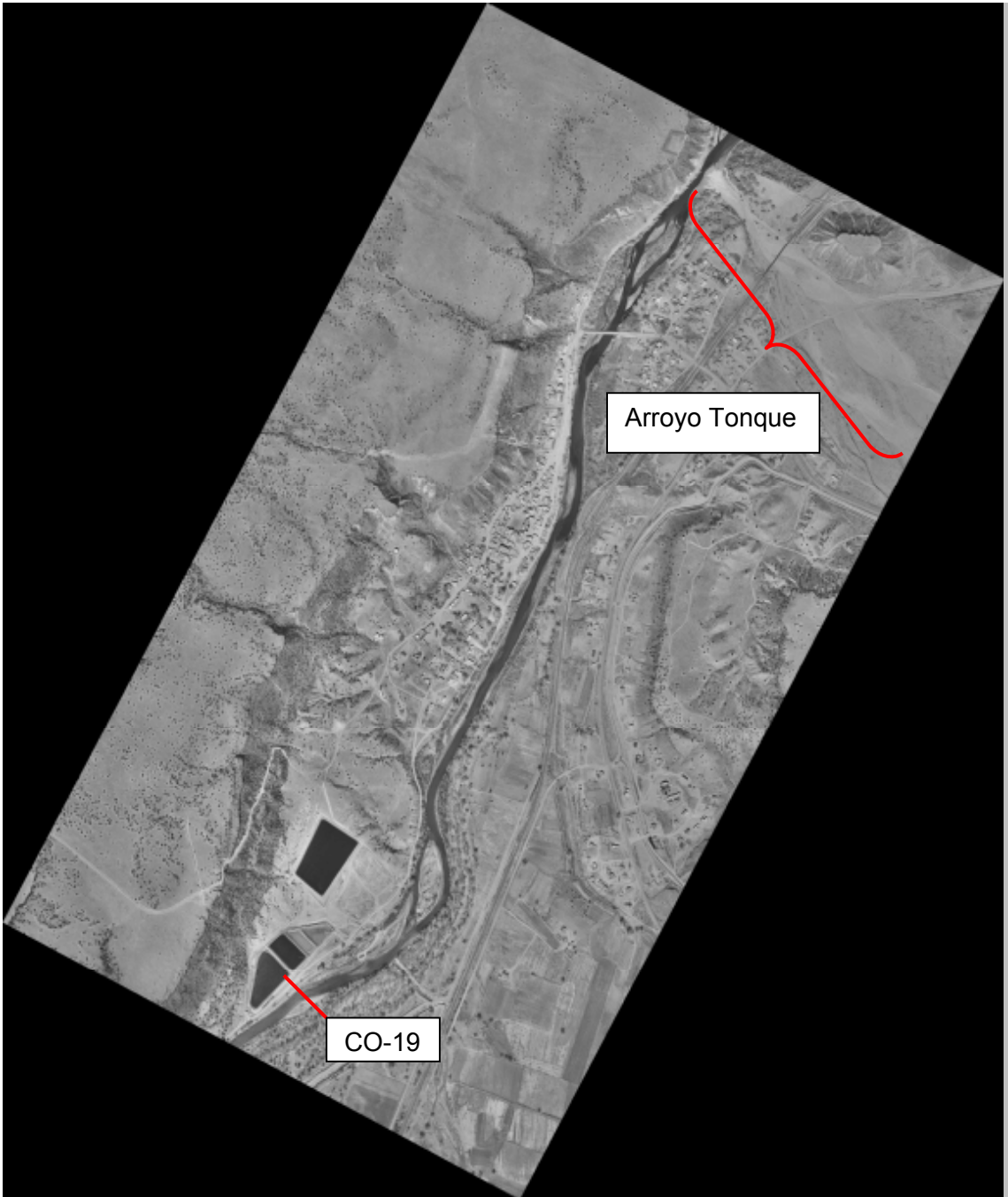


Figure B-3: Aerial photograph of San Felipe Reach (photo 1 of 3).

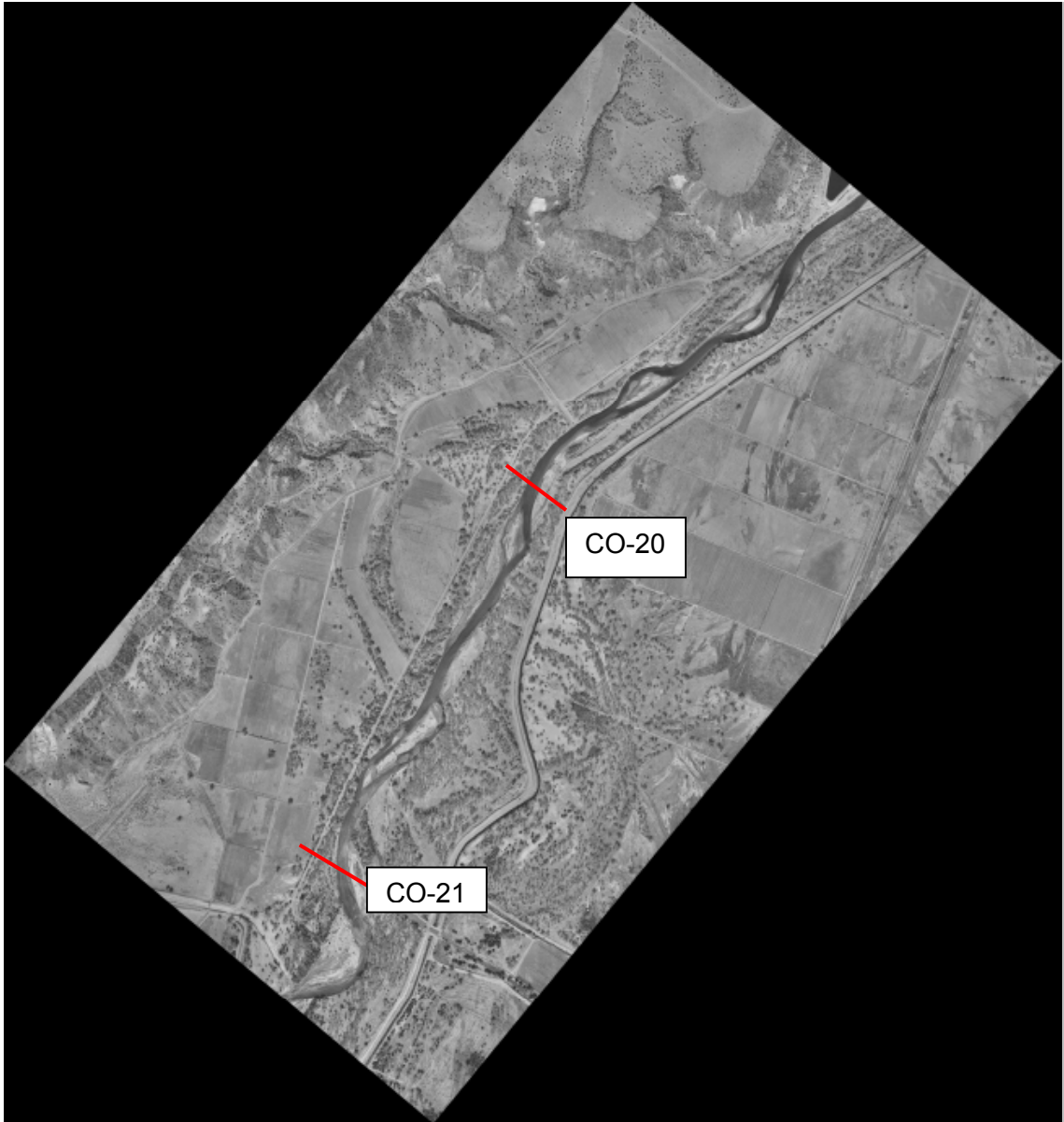


Figure B-4: Aerial photograph of San Felipe Reach (photo 2 of 3).

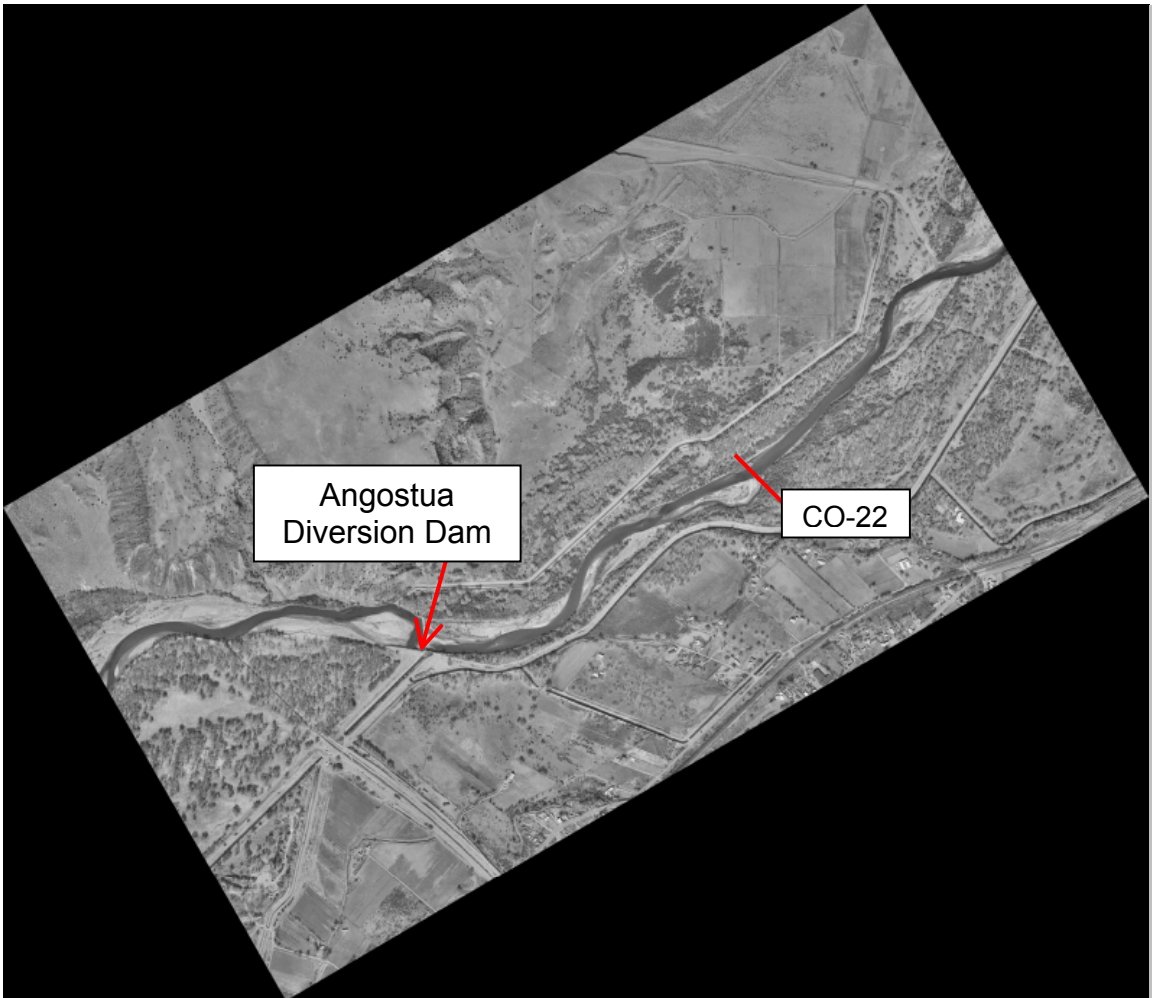


Figure B-5: Aerial photograph of San Felipe Reach (photo 3 of 3).

APPENDIX C:
Available Data (San Felipe Reach)

Table C-1: Periods of record for discharge and continuous suspended sediment data collected by the USGS.

Stations	Mean Daily Discharge	Continuous Suspended Sediment Discharge
	Period of Record	Period of Record
Rio Grande at San Felipe	1927-2001	----
Rio Grande near Bernalillo	1942-1968	1956-1969
Rio Grande at Albuquerque	1942-2001	1969-1989 1992-1999

Table C-2: Periods of record for bed material particle size distribution data collected by the USGS.

Stations	Bed Material Particle Size Distributions
	Period of Record
Rio Grande at San Felipe	1970 - 1974
Rio Grande near Bernalillo	1961, 1966 - 1969
Rio Grande at Albuquerque	1969 - 2001

Table C-3: Surveyed dates for bed material particle size distribution data at CO-lines and SFP-lines collected by the USBR.

Stations	Bed Material Particle Size Distributions
	Surveyed Date
CO-17	1971 - 1974
CO-18	1971 - 1975
CO-19	1970 - 1975
CO-20	1971 - 1979, 1992, 1995, 1998
CO-21	1970 - 1980
CO-22	1971 - 1980, 1992, 1995, 1998
CO-23	1970-1982
SFP-178	1989
SFP-194	1989
SFP-195	1989
SFP-196	1989
SFP-199	1989
SFP-200	1989

Table C-4: Surveyed dates for the Cochiti range lines collected by the USBR.

Date	Cross Section Number						
	CO-17	CO-18	CO-19	CO-20	CO-21	CO-22	CO-23
May-70			X				X
May-71	X	X	X	X	X	X	X
Sep-71	X	X	X	X	X	X	X
Mar-72	X	X	X	X	X	X	
Nov-72	X	X	X	X	X	X	X
May-73		X					
Jun-73		X	X	X	X	X	X
Jan-74	X	X	X	X	X	X	X
May-74	X	X	X	X	X	X	
Sep-74	X	X	X	X	X	X	X
Nov-74				X		X	X
May-75	X	X	X	X	X	X	X
Jul-75		X	X	X	X	X	X
Nov-75	X	X	X	X	X	X	X
Apr-79	X	X	X	X	X	X	X
Jul-79	X	X	X	X	X	X	X
Jan-80	X	X	X	X	X	X	X
Oct-82		X	X	X	X	X	X
Nov-83	X	X	X	X	X	X	X
Nov-86	X	X	X	X	X	X	X
Jul-92	X	X	X	X	X	X	X
Aug-95	X	X	X	X	X	X	X
Sep-98	X	X	X	X	X	X	X

APPENDIX D:
Cross Sections (San Felipe Reach)

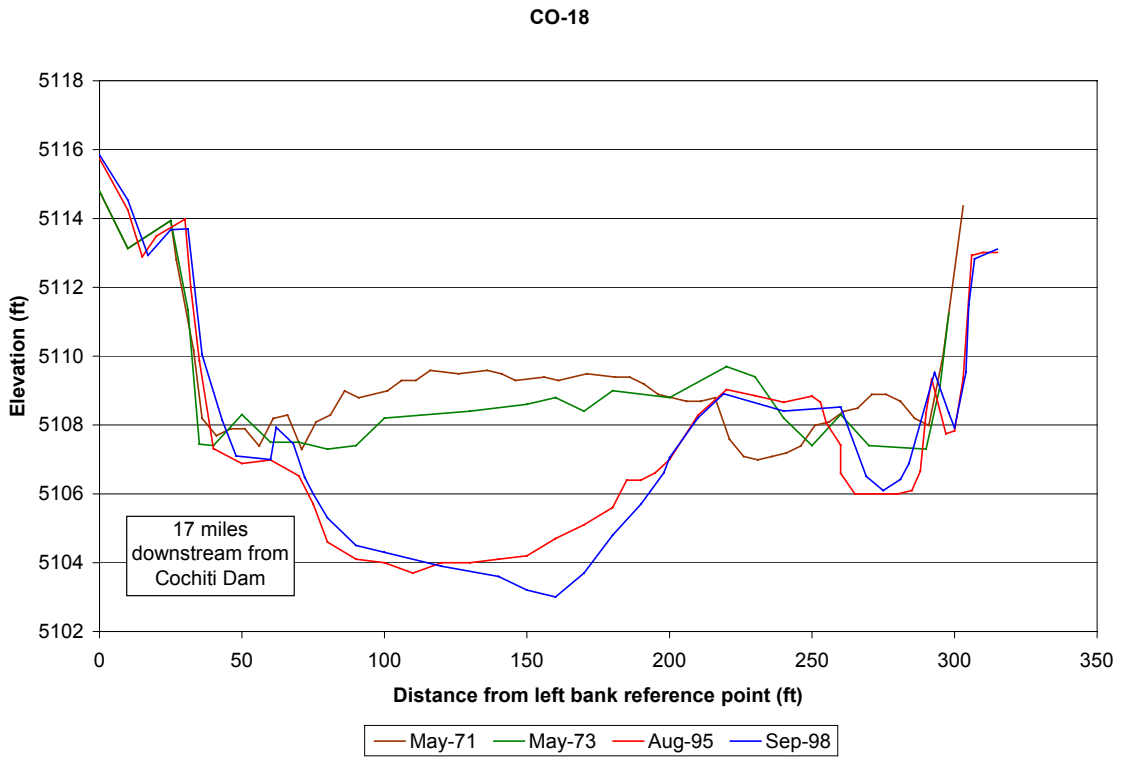
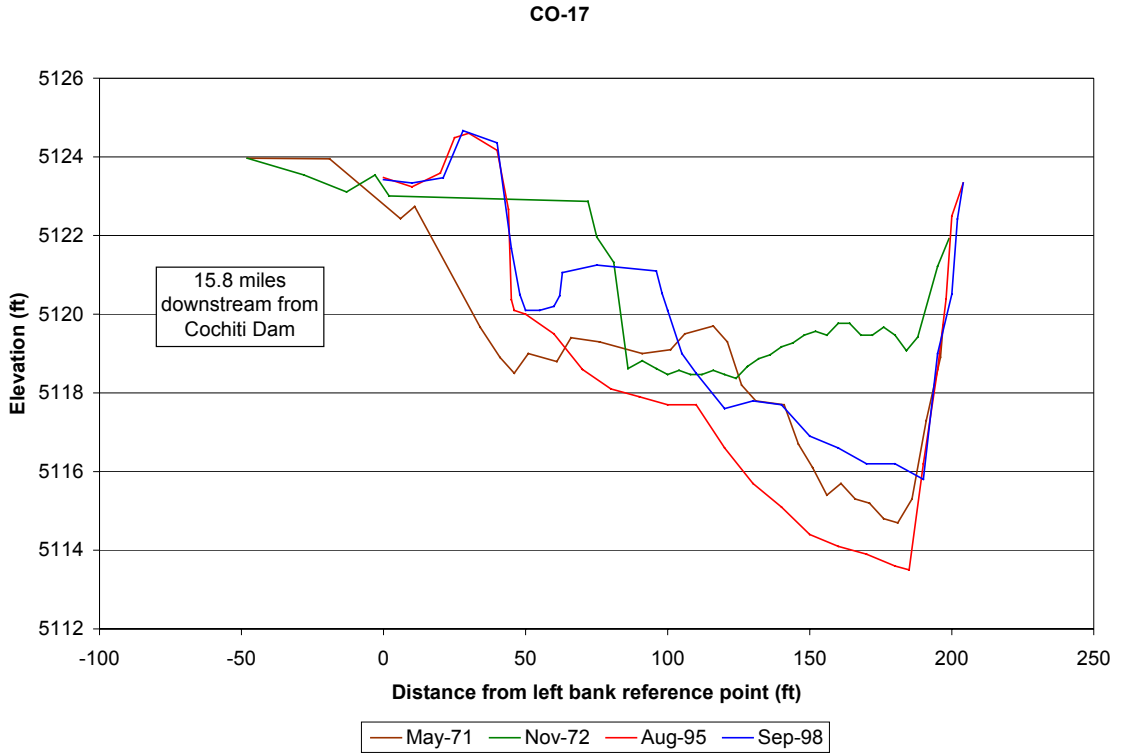


Figure D-1: Cross sections CO-17 and CO-18 (San Felipe Reach) representing pre-dam and post-dam construction.

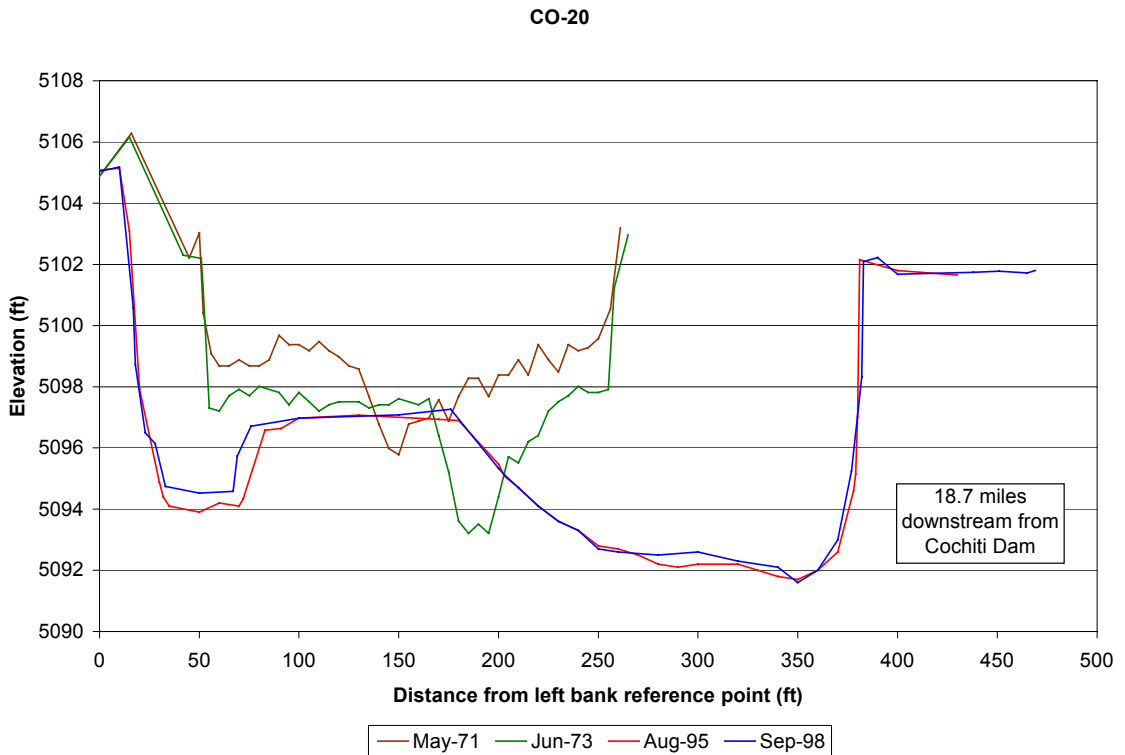
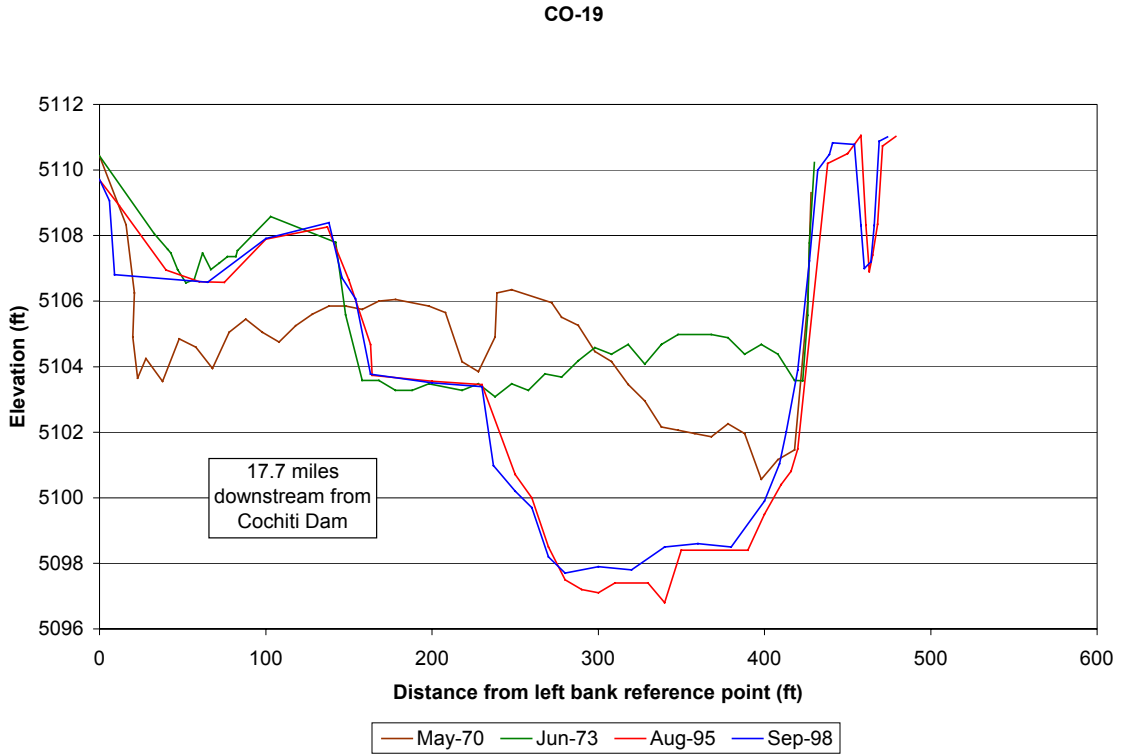
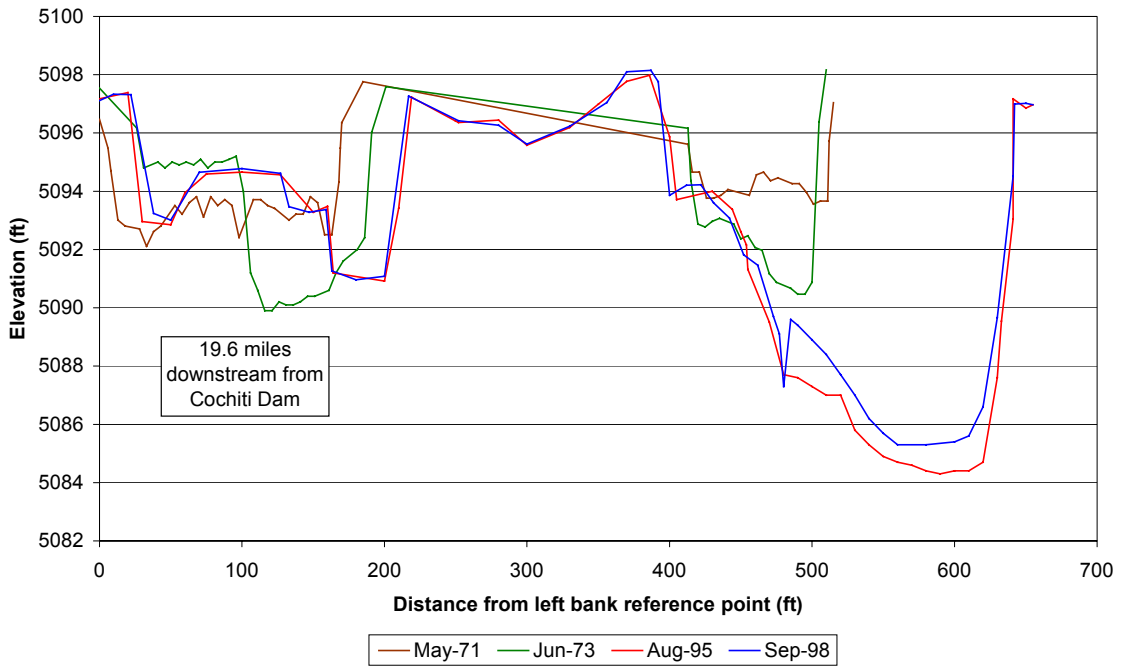


Figure D-2: Cross sections CO-19 and CO-20 (San Felipe Reach) representing pre-dam and post-dam construction.

CO-21



CO-23

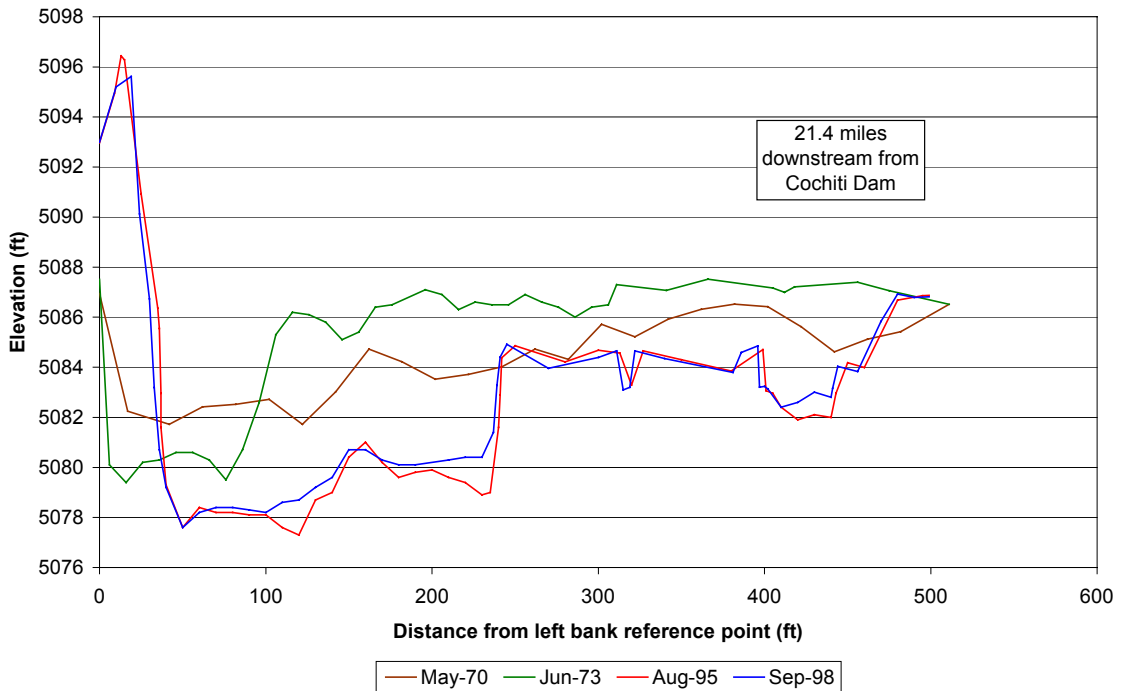


Figure D-3: Cross sections CO-21 and CO-23 (San Felipe Reach) representing pre-dam and post-dam construction.

APPENDIX E:
Annual Peak Mean Discharges
(Bernalillo and Albuquerque Gages)

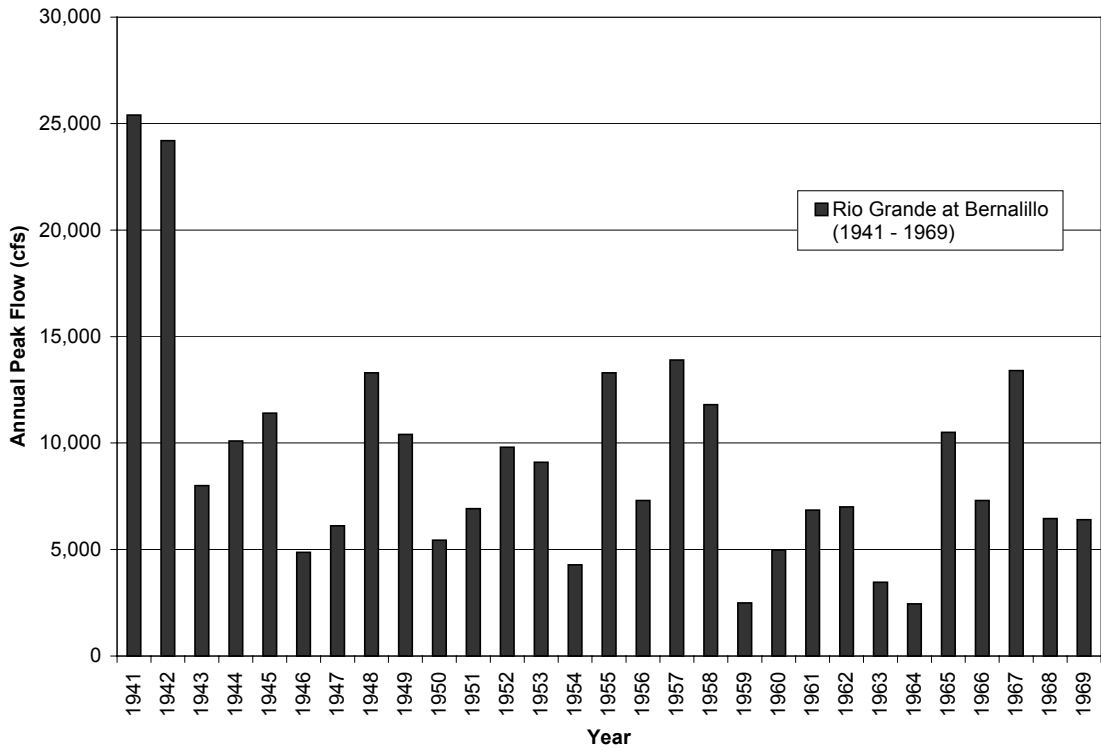


Figure E-1: Annual peak discharge in cfs at Bernalillo (1941-1969).

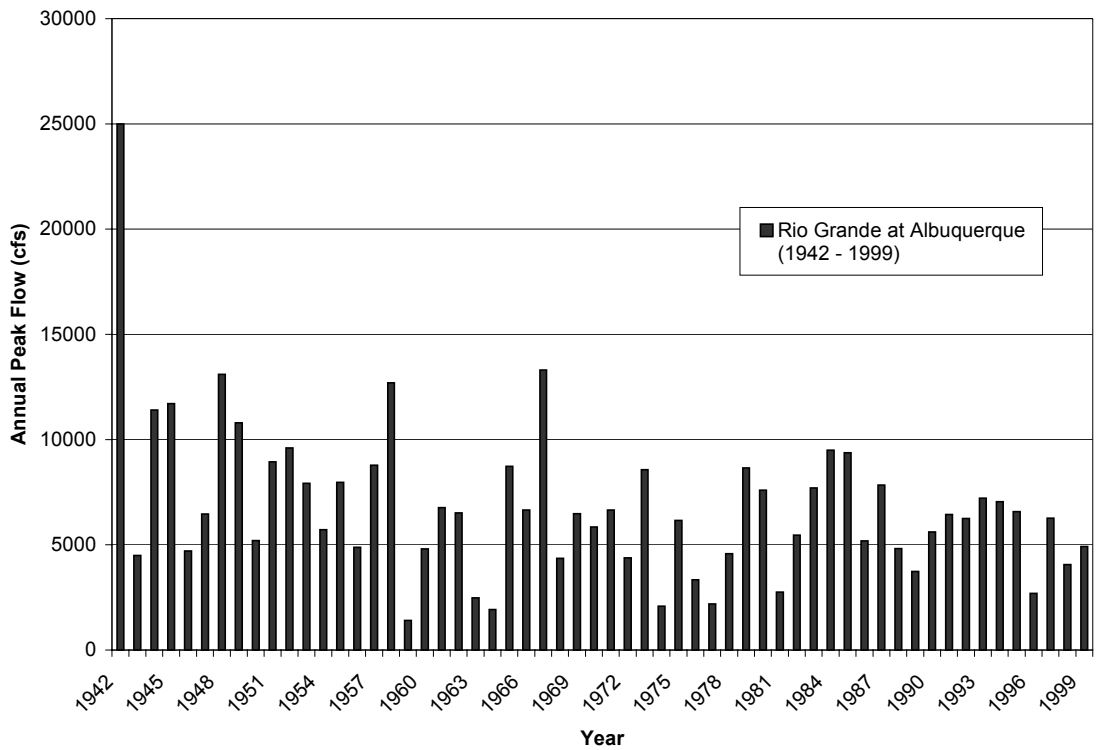


Figure E-2: Annual peak discharge in cfs at Albuquerque (1942-1999).

**APPENDIX F:
HEC-RAS® Modeling Results
(San Felipe Reach)**

Table F-1: HEC-RAS® results.

Figure F-1: Active channel widths from HEC-RAS® modeling.

(See landscaped pgs.doc)

APPENDIX G:
Bed Material Histograms and Statistics
(San Felipe Reach)

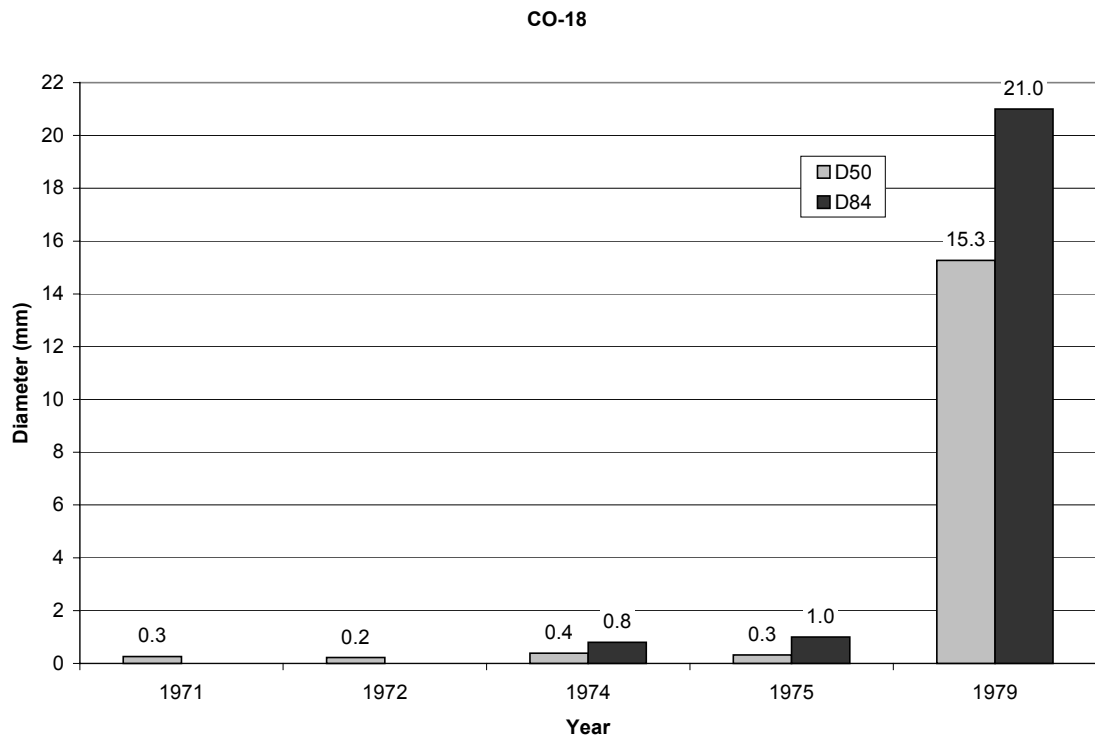
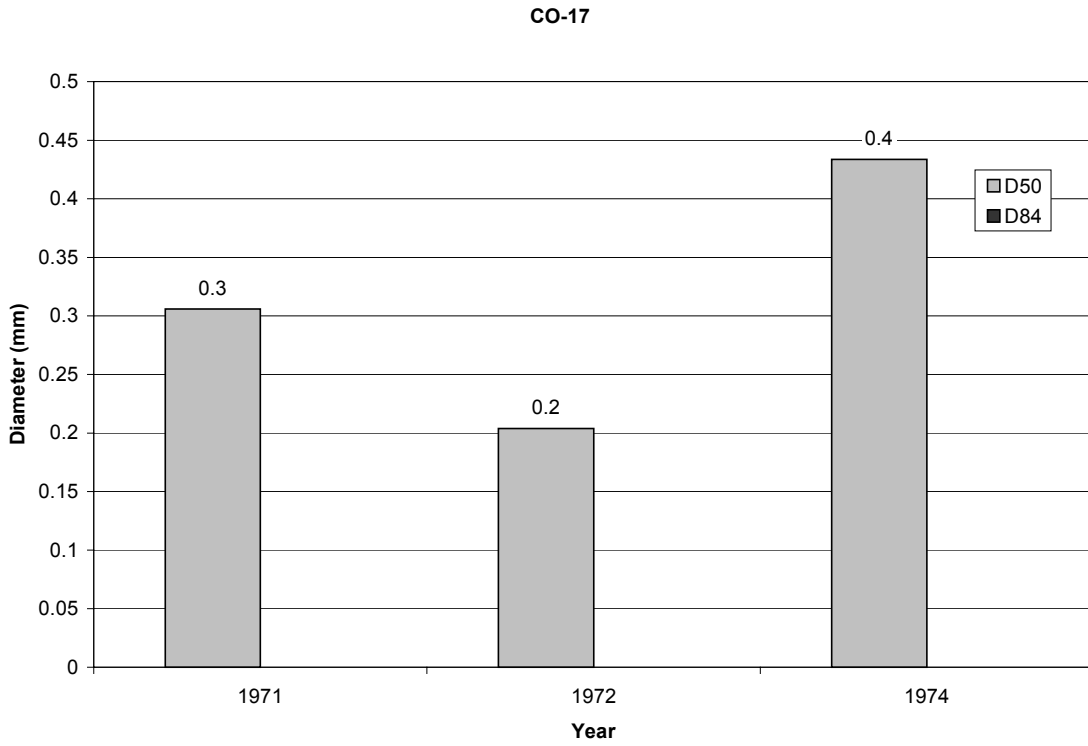
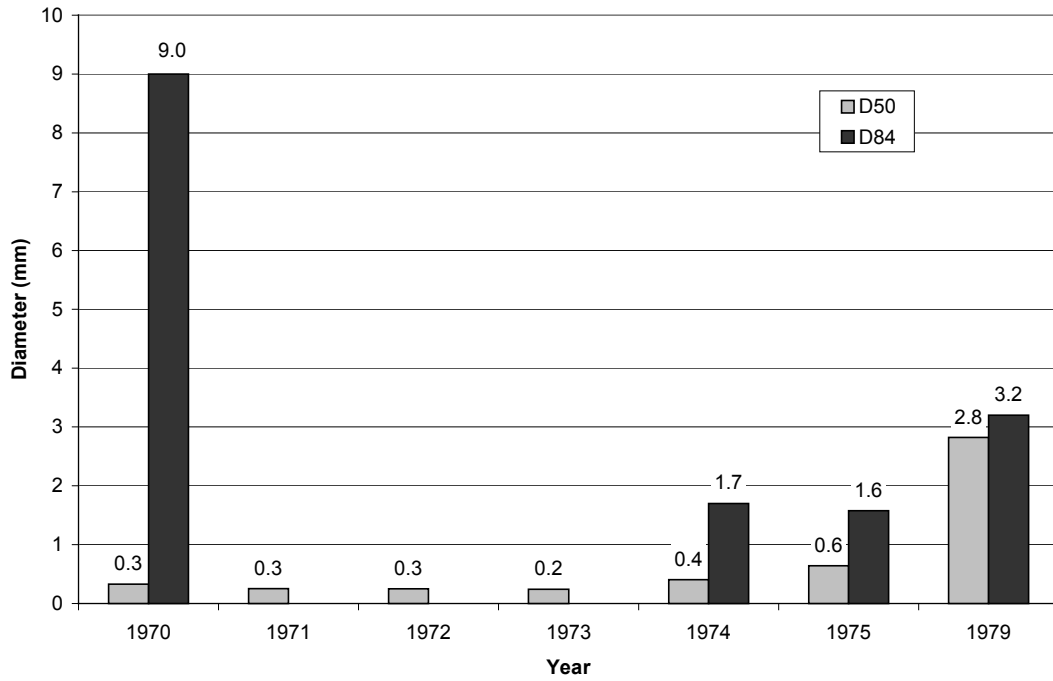


Figure G-1: Histograms depicting the D_{50} and D_{84} change with time for CO-17 and CO-18 (San Felipe Reach).

CO-19



CO-21

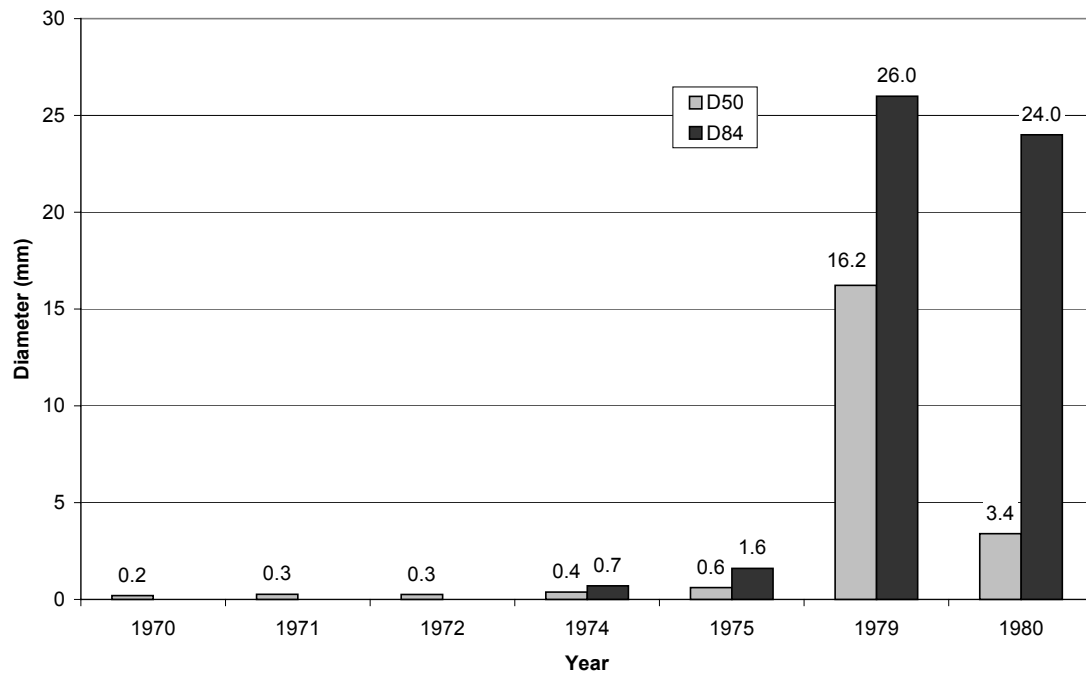


Figure G-2: Histograms depicting the D_{50} and D_{84} change with time for CO-19 and CO-21 (San Felipe Reach).

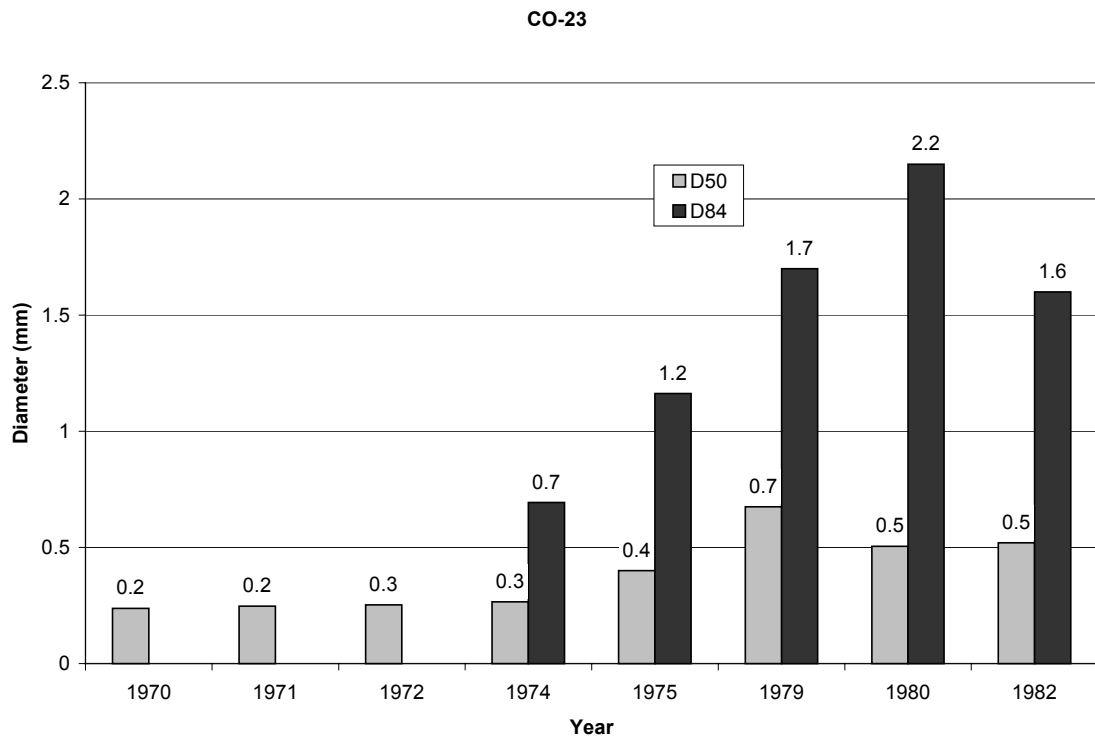
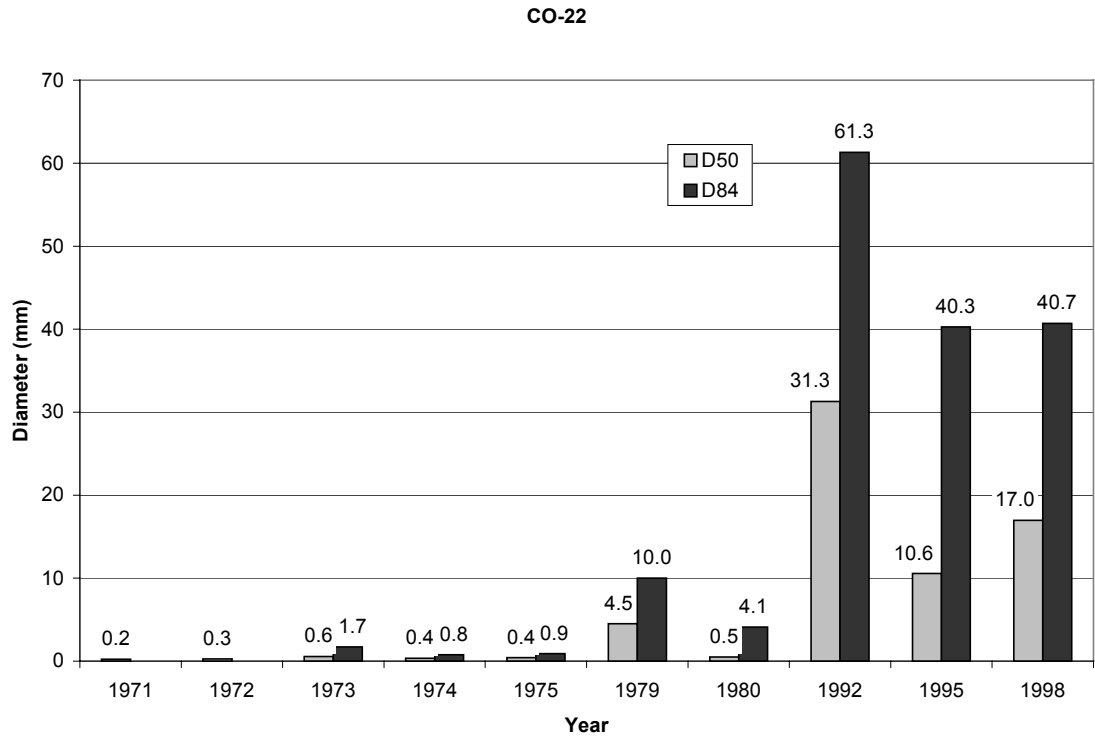


Figure G-3: Histograms depicting the D_{50} and D_{84} change with time for CO-22 and CO-23 (San Felipe Reach).

Table G-1: Median grain size statistics from material samples at Bernalillo gage, San Felipe gage, and CO-lines.

APPENDIX H:
Double Mass Curve (1956-1999)
(Rio Grande at Bernalillo and Albuquerque)

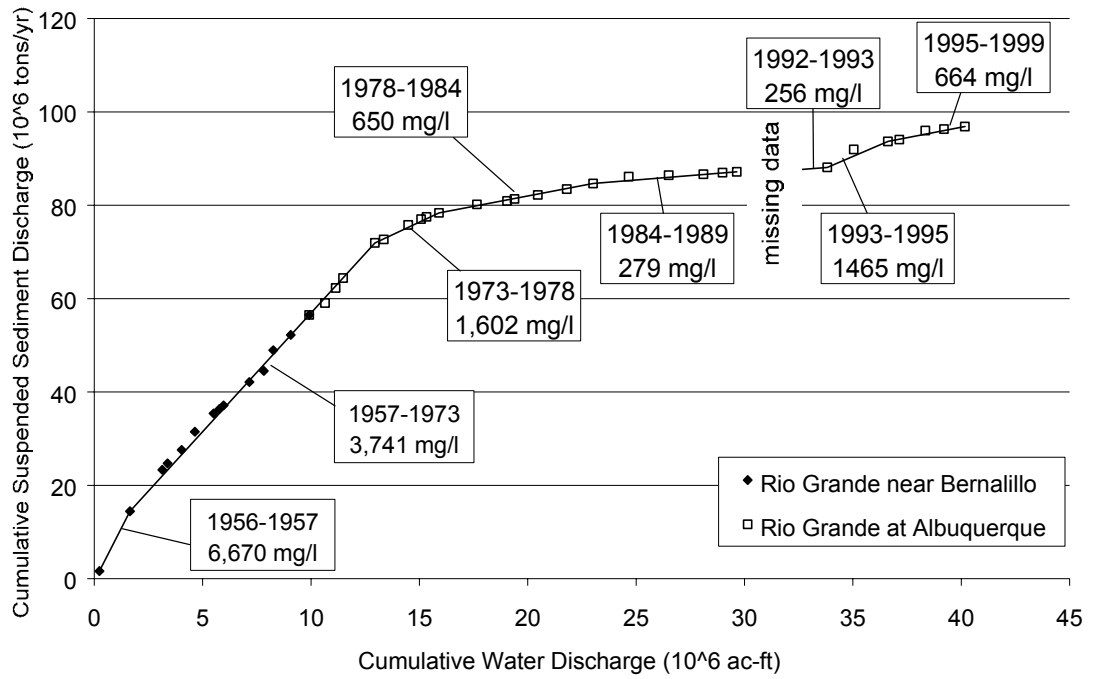


Figure H-1: Double mass curve from Rio Grande at Bernalillo and Rio Grande at Albuquerque (1956 – 1999).

**APPENDIX I:
Sediment Transport Work**

**Bed Material Load Methodology Summary
Sediment Transport Equation Suitability
Sediment Transport HEC-RAS® Input
Sediment Transport Results for 1962, 1972, 1992 and 1998**

Table I-1: Bed material and suspended material gradation data for BI-286, BI-291 and BI-296 (1992-1995).

**BI-286
5/28/1992**

D _s (mm)	Bed Material (Percent Finer)						Average
0.0156	0	0	0	0	0	0	0
0.032	0	0	0	0	0	0	0
0.063	0.1	0.1	0.5	0.05	0.03	0.2	0.2
0.125	0.3	0.2	4.6	0.2	0.1	0.2	0.9
0.25	2	1	30	2	2	2	6.5
0.5	17	20	81	36	7	30	31.8
1	57	75	99.1	87	9	63	65.0
2	75	92	99.7	95	10	78	75.0
4	85	98	100	98	13	87	80.2
8	96	99.4	100	99.3	24	93	85.3
16	100	100	100	100	67	98	94.2
31.5	100	100	100	100	96	100	99.3
63	100	100	100	100	100	100	100
125	100	100	100	100	100	100	100
D _s (mm)	Suspended Material (Percent Finer)						Average
0.0156	0	0	0	0	0	0	0
0.032	0	0	0	0	0	0	0
0.063	71.2	1.3	69.4	63.8	41.9	14.4	43.7
0.125	85	1.6	95.1	73.3	50.6	15.2	53.5
0.25	99.1	3.85	98.4	82	75.3	26.6	64.2
0.5	100	55.1	100	100	96.6	91.3	90.5
1	100	96.1	100	100	100	98.3	99.1
2	100	100	100	100	100	100	100
4	100	100	100	100	100	100	100
8	100	100	100	100	100	100	100
16	100	100	100	100	100	100	100
31.5	100	100	100	100	100	100	100
63	100	100	100	100	100	100	100
125	100	100	100	100	100	100	100

**BI-291
5/29/1992**

D _s (mm)	Bed Material (Percent Finer)					Average
0.0156	0	0	0	0	0	0
0.032	0	0	0	0	0	0
0.063	0.2	0.1	0.04	1.1	0.1	0.3
0.125	0.3	0.3	0.1	2.5	0.4	0.7
0.25	2	3	2	5	2	2.8
0.5	28	25	14	34	20	24.2
1	74	73	35	74	34	58.0
2	87	94	39	85	42	69.4
4	94	99	43	92	55	76.6
8	99.1	99.9	50	96	73	83.6
16	100	100	60	100	93	90.6
31.5	100	100	76	100	100	95.2
63	100	100	100	100	100	100
125	100	100	100	100	100	100

D _s (mm)	Suspended Material (Percent Finer)					Average
0.0156	0	0	0	0	0	0
0.032	0	0	0	0	0	0
0.063	69.2	47.4	46.2	15.9	27.7	41.3
0.125	75.2	57.8	65.1	51.8	44.1	58.8
0.25	84.4	73.9	92.9	39.8	80.6	74.3
0.5	94.7	89.1	97.3	91.9	95.8	93.8
1	100	100	100	100	100	100
2	100	100	100	100	100	100
4	100	100	100	100	100	100
8	100	100	100	100	100	100
16	100	100	100	100	100	100
31.5	100	100	100	100	100	100
63	100	100	100	100	100	100
125	100	100	100	100	100	100

BI-296
5/28/1992

D _s (mm)	Bed Material (Percent Finer)					Average
0.0156	0	0	0	0	0	0
0.032	0	0	0	0	0	0
0.063	0.1	0.01	0.1	0.2	0.1	0.1
0.125	0.6	0.1	0.2	0.2	0.2	0.3
0.25	4	2	4	3	2	3.0
0.5	26	15	54	22	12	25.8
1	49	29	94	52	38	52.4
2	61	42	98	74	59	66.8
4	70	57	100	88	74	77.8
8	83	74	100	96	88	88.2
16	96	92	100	100	96	96.8
31.5	100	100	100	100	100	100
63	100	100	100	100	100	100
125	100	100	100	100	100	100
D _s (mm)	Suspended Material (Percent Finer)					Average
0.0156	0	0	0	0	0	0
0.032	0	0	0	0	0	0
0.063	57	37.5	24.6	32.2	56.1	41.5
0.125	74.3	52.5	29.7	48.5	70.4	55.1
0.25	88.9	78	50.5	77.7	87.6	76.5
0.5	100	95.3	88.2	100	100	96.7
1	100	100	100	100	100	100
2	100	100	100	100	100	100
4	100	100	100	100	100	100
8	100	100	100	100	100	100
16	100	100	100	100	100	100
31.5	100	100	100	100	100	100
63	100	100	100	100	100	100
125	100	100	100	100	100	100

BI-286
4/8/1993

D _s (mm)	Bed Material (Percent Finer)					Average	
0.0156	0	0	0	0	0	0	0
0.032	0	0	0	0	0	0	0
0.063	0.1	0.1	0.1	0.1	0.1	0.1	0.1
0.125	0.2	0.2	0.4	0.2	0.1	0.2	0.2
0.25	0.8	2.4	3	0.7	0.6	1.5	1.5
0.5	13	59	15	10	4.1	20.2	20.2
1	53	60	23	43	23.1	40.4	40.4
2	76	79	28	72	48	60.6	60.6
4	91	90	37	92	70.6	76.1	76.1
8	98.2	97	68	94	87.5	88.9	88.9
16	100	100	68	97	96.9	92.4	92.4
31.5	100	100	83	100	100	96.6	96.6
63	100	100	100	100	100	100	100
125	100	100	100	100	100	100	100
D _s (mm)	Suspended Material (Percent Finer)					Average	
0.0156	0	0	0	0	0	0	0
0.032	0	0	0	0	0	0	0
0.063	68	46.9	49.1	17.3	38.5	44.0	44.0
0.125	84	60.2	69.4	19.8	47.7	56.2	56.2
0.25	99.8	88.8	89.8	50.4	78.5	81.5	81.5
0.5	100	100	100	100	100	100	100
1	100	100	100	100	100	100	100
2	100	100	100	100	100	100	100
4	100	100	100	100	100	100	100
8	100	100	100	100	100	100	100
16	100	100	100	100	100	100	100
31.5	100	100	100	100	100	100	100
63	100	100	100	100	100	100	100
125	100	100	100	100	100	100	100

BI-286
5/31/1993

D _s (mm)	Bed Material (Percent Finer)						Average
0.0156	0	0	0	0	0	0	0
0.032	0	0	0	0	0	0	0
0.063	0.1	0.1	0.1	0.1	0.1	0.2	0.1
0.125	0.5	0.5	0.5	0.4	0.1	0.3	0.4
0.25	1.6	8.8	6.4	5.1	0.5	0.5	3.8
0.5	4.1	61.9	36.2	56.8	7.5	1.8	28.1
1	23.1	90.2	82.8	78.1	54	22.4	58.4
2	48	95.7	95	79.8	66.9	53.4	73.1
4	70.6	98.6	100	80.7	74.7	74.5	83.2
8	87.5	99	100	83.3	97.7	87.3	92.5
16	96.9	100	100	88.6	100	97.7	97.2
31.5	100	100	100	100	100	100	100
63	100	100	100	100	100	100	100
125	100	100	100	100	100	100	100

D _s (mm)	Suspended Material (Percent Finer)						Average
0.0156	0	0	0	0	0	0	0
0.032	0	0	0	0	0	0	0
0.063	61.5	43	41.2	21.7	17.3	54	39.8
0.125	83.4	66.4	60.8	33.3	72.4	72.3	64.8
0.25	95.5	90.4	84.7	58.2	83.8	89.1	83.6
0.5	100	99.4	97	91.5	95.6	93.9	96.2
1	100	100	100	96.2	100	100	99.4
2	100	100	100	100	100	100	100
4	100	100	100	100	100	100	100
8	100	100	100	100	100	100	100
16	100	100	100	100	100	100	100
31.5	100	100	100	100	100	100	100
63	100	100	100	100	100	100	100
125	100	100	100	100	100	100	100

BI-286
6/18/1993

D _s (mm)	Bed Material (Percent Finer)						Average
0.0156	0	0	0	0	0	0	0
0.032	0	0	0	0	0	0	0
0.063	0.3	0.1	0.2	0.1	0.1	0.1	0.2
0.125	0.3	0.3	0.3	0.1	0.2	0.2	0.2
0.25	1.3	3.5	1.6	2	1	1.9	1.9
0.5	30.4	45	45	51	12.6	36.8	36.8
1	73.2	94.7	88	81	41.7	75.7	75.7
2	86	98.4	96	88	61.9	86.1	86.1
4	92.3	99.3	98.3	92	76.4	91.7	91.7
8	97.6	99.6	99.4	94	87	95.5	95.5
16	100	100	100	97	95.1	98.4	98.4
31.5	100	100	100	100	100	100	100
63	100	100	100	100	100	100	100
125	100	100	100	100	100	100	100
D _s (mm)	Suspended Material (Percent Finer)						Average
0.0156	0	0	0	0	0	0	0
0.032	0	0	0	0	0	0	0
0.063	48.1	54.3	51.9	14.9	15.6	37.0	37.0
0.125	67.7	71.1	70.1	20.4	22.6	50.4	50.4
0.25	84.4	82.7	91.9	39.3	40.8	67.8	67.8
0.5	94.9	96.3	97.1	90.5	75.2	90.8	90.8
1	100	100	100	100	100	100	100
2	100	100	100	100	100	100	100
4	100	100	100	100	100	100	100
8	100	100	100	100	100	100	100
16	100	100	100	100	100	100	100
31.5	100	100	100	100	100	100	100
63	100	100	100	100	100	100	100
125	100	100	100	100	100	100	100

BI-291
4/8/1993

D _s (mm)	Bed Material (Percent Finer)					Average
0.0156	0	0	0	0	0	0
0.032	0	0	0	0	0	0
0.063	0.2	0.2	0.1	0.1	0.1	0.1
0.125	0.3	2	0.2	0.2	0.6	0.7
0.25	4	10	1.4	1.2	4.1	4.1
0.5	21	55	21	19	29	29.0
1	66	90	63	66	44	65.8
2	90	98.7	81	80	68	83.5
4	98	100	90	87	81	91.2
8	99.8	100	95	98.6	91	96.9
16	100	100	98.2	98.6	97	98.8
31.5	100	100	100	100	100	100
63	100	100	100	100	100	100
125	100	100	100	100	100	100
D _s (mm)	Suspended Material (Percent Finer)					Average
0.0156	0	0	0	0	0	0
0.032	0	0	0	0	0	0
0.063	55.8	68.4	2	4	45.6	35.2
0.125	65.5	92.4	2	4	46.1	42.0
0.25	71.7	100	5	5	56.5	47.6
0.5	100	100	64	25	98.9	77.6
1	100	100	99	98	100	99.4
2	100	100	100	100	100	100
4	100	100	100	100	100	100
8	100	100	100	100	100	100
16	100	100	100	100	100	100
31.5	100	100	100	100	100	100
63	100	100	100	100	100	100
125	100	100	100	100	100	100

BI-291
5/31/1993

D _s (mm)	Bed Material (Percent Finer)					Average
0.0156	0	0	0	0	0	0
0.032	0	0	0	0	0	0
0.063	0.1	0.1	0.3	0.1	0.1	0.1
0.125	0.3	1.8	0.4	0.2	0.1	0.6
0.25	1.6	15.7	3.6	2.4	0.3	4.7
0.5	24.8	50	27.3	43	3.1	29.6
1	84.1	86.6	79.2	80.6	30.3	72.2
2	98.7	97.7	94.3	84	61.7	87.3
4	99.7	99.7	96.9	86.3	79.7	92.5
8	100	100	98.4	89.2	89.5	95.4
16	100	100	100	95.1	97	98.4
31.5	100	100	100	100	100	100
63	100	100	100	100	100	100
125	100	100	100	100	100	100

D _s (mm)	Suspended Material (Percent Finer)					Average
0.0156	0	0	0	0	0	0
0.032	0	0	0	0	0	0
0.063	35.4	2.3	32.2	21.3	51.1	28.5
0.125	41.6	4	52.3	32.1	64.3	38.9
0.25	48.2	16.5	81.4	58.3	79.7	56.8
0.5	85.3	39.4	96.2	99.1	96.4	83.3
1	100	72.3	100	100	100	94.5
2	100	93.1	100	100	100	98.6
4	100	100	100	100	100	100
8	100	100	100	100	100	100
16	100	100	100	100	100	100
31.5	100	100	100	100	100	100
63	100	100	100	100	100	100
125	100	100	100	100	100	100

BI-291
6/19/1993

D _s (mm)	Bed Material (Percent Finer)					Average
0.0156	0	0	0	0	0	0
0.032	0	0	0	0	0	0
0.063	0.1	0.2	0.1	0.1	0.1	0.1
0.125	1	0.2	0.2	0.2	0.4	0.4
0.25	7.7	0.4	2.8	0.7	2.9	2.9
0.5	26.4	1.4	33.7	9.9	17.8	17.8
1	74.1	18	74	34.7	50.2	50.2
2	95.2	96	86.2	52.6	82.5	82.5
4	100	100	90.9	70	90.2	90.2
8	100	100	94.1	83	94.2	94.3
16	100	100	97.2	96.2	95.7	97.8
31.5	100	100	100	100	100	100
63	100	100	100	100	100	100
125	100	100	100	100	100	100
D _s (mm)	Suspended Material (Percent Finer)					Average
0.0156	0	0	0	0	0	0
0.032	0	0	0	0	0	0
0.063	44.1	30.5	4.1	50.1	5.3	26.8
0.125	59.7	45.3	8.1	67.3	7.6	37.6
0.25	84.1	65.7	14.9	83	11.6	51.9
0.5	100	93.4	48.5	94.9	21.1	71.6
1	100	96.7	86.2	100	91.7	94.9
2	100	100	100	100	100	100
4	100	100	100	100	100	100
8	100	100	100	100	100	100
16	100	100	100	100	100	100
31.5	100	100	100	100	100	100
63	100	100	100	100	100	100
125	100	100	100	100	100	100

BI-296
4/7/1993

D _s (mm)	Bed Material (Percent Finer)						Average
0.0156	0	0	0	0	0	0	0
0.032	0	0	0	0	0	0	0
0.063	0.2	0.1	0.1	0.1	0.1	0.1	0.1
0.125	1	0.3	0.3	1.1	0.2	0.6	0.6
0.25	13	11	9	7	0.8	8.2	8.2
0.5	30	69	60	23	7	37.8	37.8
1	40	98	97	32	45	62.4	62.4
2	52	99.4	99.2	37	76	72.7	72.7
4	77	99.7	100	47	89	82.5	82.5
8	84	100	100	64	95	88.6	88.6
16	97.4	100	100	94	100	98.3	98.3
31.5	100	100	100	100	100	100	100
63	100	100	100	100	100	100	100
125	100	100	100	100	100	100	100
D _s (mm)	Suspended Material (Percent Finer)						Average
0.0156	0	0	0	0	0	0	0
0.032	0	0	0	0	0	0	0
0.063	40.7	18.1	29.7	54.7	66.5	41.9	41.9
0.125	56.7	29.6	44.5	76.9	74.5	56.4	56.4
0.25	95.3	89.4	93.7	99.5	83.9	92.4	92.4
0.5	100	100	100	100	100	100	100
1	100	100	100	100	100	100	100
2	100	100	100	100	100	100	100
4	100	100	100	100	100	100	100
8	100	100	100	100	100	100	100
16	100	100	100	100	100	100	100
31.5	100	100	100	100	100	100	100
63	100	100	100	100	100	100	100
125	100	100	100	100	100	100	100

BI-296
6/1/1993

D _s (mm)	Bed Material (Percent Finer)						Average
0.0156	0	0	0	0	0	0	0
0.032	0	0	0	0	0	0	0
0.063	0.1	0.8	0.1	0.1	0.1	13.1	2.4
0.125	0.3	1.3	0.4	0.3	0.1	14	2.7
0.25	3	5.4	4.1	5	1.9	14	5.6
0.5	33.5	23.2	36.1	45.9	9.5	21	28.2
1	87.8	57.2	81.1	73.2	33.8	59	65.4
2	96.4	93.5	92.5	82.5	44.3	76	80.9
4	98.7	97.6	100	89.3	56.4	84	87.7
8	99.7	99.4	100	94.9	71.5	90	92.6
16	100	100	100	97.8	89.2	97	97.3
31.5	100	100	100	100	100	100	100
63	100	100	100	100	100	100	100
125	100	100	100	100	100	100	100

D _s (mm)	Suspended Material (Percent Finer)						Average
0.0156	0	0	0	0	0	0	0
0.032	0	0	0	0	0	0	0
0.063	5.3	40.2	26.5	24.9	44.7	5.1	24.5
0.125	7.6	59.7	41.5	36.8	65	7.2	36.3
0.25	11.6	79.8	66.3	71	89.4	11.1	54.9
0.5	21.1	96.6	97.2	99.6	97.4	26.9	73.1
1	91.7	100	100	100	100	73.1	94.1
2	100	100	100	100	100	100	100
4	100	100	100	100	100	100	100
8	100	100	100	100	100	100	100
16	100	100	100	100	100	100	100
31.5	100	100	100	100	100	100	100
63	100	100	100	100	100	100	100
125	100	100	100	100	100	100	100

**BI-296
6/20/1993**

D _s (mm)	Bed Material (Percent Finer)						Average
0.0156	0	0	0	0	0	0	0
0.032	0	0	0	0	0	0	0
0.063	0.1	0	0.1	0.3	0.1	0.1	0.1
0.125	0.2	0.1	1.1	0.3	0.2	0.4	0.4
0.25	2	1.5	14.9	0.8	0.5	3.9	3.9
0.5	23	21.2	96.7	11.5	5	31.5	31.5
1	74	54	100	45.7	36	61.9	61.9
2	89	72	100	62.7	55	75.7	75.7
4	95	83.6	100	77	70	85.1	85.1
8	99	93.5	100	88.9	83	92.9	92.9
16	100	100	100	100	98	99.6	99.6
31.5	100	100	100	100	100	100	100
63	100	100	100	100	100	100	100
125	100	100	100	100	100	100	100
D _s (mm)	Suspended Material (Percent Finer)						Average
0.0156	0	0	0	0	0	0	0
0.032	0	0	0	0	0	0	0
0.063	49.7	45.3	18.4	30.9	43.7	37.6	37.6
0.125	61.1	65.4	32.2	47.8	61	53.5	53.5
0.25	82.1	77.9	51.5	73.1	75.1	71.9	71.9
0.5	96.9	91.6	94.1	94.7	88	93.1	93.1
1	100	100	100	100	100	100	100
2	100	100	100	100	100	100	100
4	100	100	100	100	100	100	100
8	100	100	100	100	100	100	100
16	100	100	100	100	100	100	100
31.5	100	100	100	100	100	100	100
63	100	100	100	100	100	100	100
125	100	100	100	100	100	100	100

BI-286
5/28/1994

D _s (mm)	Bed Material (Percent Finer)							Average
0.0156	0	0	0	0	0	0	0	0
0.032	0	0	0	0	0	0	0	0
0.063	0.13	0.2	0.21	0.1	0.02	0.1	1.1	0.3
0.125	1.01	0.7	0.24	0.1	0.2	0.2	7.8	1.5
0.25	7.53	10.5	2.22	0.9	1.6	0.66	52.5	10.8
0.5	13	42.1	17.9	9.7	22.3	13.1	88.3	29.5
1	34.16	73.6	49.77	42.9	36.2	49.2	98.7	54.9
2	65.59	85.7	75.99	61.4	44.1	61.9	99.6	70.6
4	90.01	93.6	85.1	73.6	63.1	70.9	100	82.3
8	98.54	98.6	91.46	85.1	71.5	78.8	100	89.1
16	100	100	95.01	95.1	91.4	85.9	100	95.3
31.5	100	100	100	100	100	100	100	100
63	100	100	100	100	100	100	100	100
125	100	100	100	100	100	100	100	100
D _s (mm)	Suspended Material (Percent Finer)							Average
0.0156	0	0	0	0	0	0	0	0
0.032	0	0	0	0	0	0	0	0
0.063	47.6	63.7	57.7	43.8	2.9	42.8	83.1	48.8
0.125	57.9	78.6	77	58.1	4	56.6	100	61.7
0.25	61	88.3	100	71	12	72.9	100	72.2
0.5	100	100	100	100	100	100	100	100
1	100	100	100	100	100	100	100	100
2	100	100	100	100	100	100	100	100
4	100	100	100	100	100	100	100	100
8	100	100	100	100	100	100	100	100
16	100	100	100	100	100	100	100	100
31.5	100	100	100	100	100	100	100	100
63	100	100	100	100	100	100	100	100
125	100	100	100	100	100	100	100	100

BI-286
5/9/1994

D _s (mm)	Bed Material (Percent Finer)					Average
0.0156	0	0	0	0	0	0
0.032	0	0	0	0	0	0
0.063	0.1	0.1	0.1	0.1	0.1	0.1
0.125	0.2	0.5	0.1	0.1	0.2	0.2
0.25	1.2	14	1.1	3.9	0.7	4.2
0.5	14.4	76	15.8	47	17.6	34.2
1	71.9	88.9	36.9	64.1	65.9	65.5
2	94.9	91.7	44.5	69.4	79.1	75.9
4	99.3	92	52.5	74.6	86.4	81.0
8	100	92.7	64.1	81.4	91.8	86.0
16	100	94.9	83	89.6	95.1	92.5
31.5	100	100	100	100	100	100
63	100	100	100	100	100	100
125	100	100	100	100	100	100

D _s (mm)	Suspended Material (Percent Finer)					Average
0.0156	0	0	0	0	0	0
0.032	0	0	0	0	0	0
0.063	21.6	27.5	36.2	22.3	8.7	23.3
0.125	26.5	45	50.2	32.5	24.2	35.7
0.25	100	85.8	69.5	52.7	43.3	70.3
0.5	100	100	100	100	100	100
1	100	100	100	100	100	100
2	100	100	100	100	100	100
4	100	100	100	100	100	100
8	100	100	100	100	100	100
16	100	100	100	100	100	100
31.5	100	100	100	100	100	100
63	100	100	100	100	100	100
125	100	100	100	100	100	100

BI-291
5/27/1994

D _s (mm)	Bed Material (Percent Finer)					Average
0.0156	0	0	0	0	0	0
0.032	0	0	0	0	0	0
0.063	0.02	0.07	0.06	0.06	0.1	0.1
0.125	0.4	0.1	0.08	0.09	0.3	0.2
0.25	2.7	1.53	0.9	1.7	2.4	1.8
0.5	16.9	12.14	12.8	25.9	6.2	14.8
1	46.6	61.37	65.2	71.4	7.5	50.4
2	71.8	87.02	89.2	81.9	9.5	67.9
4	88.5	94.58	93.7	88.9	11.05	75.3
8	99.94	97.02	97.2	95.9	15.4	81.1
16	100	100	97.6	100	35.6	86.6
31.5	100	100	100	100	83.1	96.6
63	100	100	100	100	100	100
125	100	100	100	100	100	100
D _s (mm)	Suspended Material (Percent Finer)					Average
0.0156	0	0	0	0	0	0
0.032	0	0	0	0	0	0
0.063	89.1	85.1	69	52.7	78	74.8
0.125	96.4	93.6	77.7	61	88.3	83.4
0.25	100	100	82.9	74.8	93.3	90.2
0.5	100	100	92.8	100	100	98.6
1	100	100	100	100	100	100
2	100	100	100	100	100	100
4	100	100	100	100	100	100
8	100	100	100	100	100	100
16	100	100	100	100	100	100
31.5	100	100	100	100	100	100
63	100	100	100	100	100	100
125	100	100	100	100	100	100

BI-291
5/9/1994

D _s (mm)	Bed Material (Percent Finer)					Average
0.0156	0	0	0	0	0	0
0.032	0	0	0	0	0	0
0.063	0.3	0.1	0.1	0.1	0.1	0.1
0.125	2.4	0.2	0.2	0.2	0.2	0.6
0.25	15.4	1.5	1.3	3	0.2	4.3
0.5	30.9	18.3	18.3	40	2.6	22.0
1	59.3	41.4	44.6	62.3	32	47.9
2	77.7	77.6	64.4	76.6	64.6	72.2
4	86.8	93.7	81.4	91	79.3	86.4
8	96	99.1	91.2	97.1	82.4	93.2
16	100	100	97.6	100	84.8	96.5
31.5	100	100	100	100	100	100
63	100	100	100	100	100	100
125	100	100	100	100	100	100
D _s (mm)	Suspended Material (Percent Finer)					Average
0.0156	0	0	0	0	0	0
0.032	0	0	0	0	0	0
0.063	30.1	27.3	25.9	16	1.9	20.2
0.125	42.4	40	36.5	24.9	2.7	29.3
0.25	44.7	53.3	56	48.9	3.6	41.3
0.5	54.6	100	88.6	94.4	7.4	69.0
1	88.5	100	100	100	42	86.1
2	100	100	100	100	74.1	94.8
4	100	100	100	100	100	100
8	100	100	100	100	100	100
16	100	100	100	100	100	100
31.5	100	100	100	100	100	100
63	100	100	100	100	100	100
125	100	100	100	100	100	100

BI-296
5/27/1994

D _s (mm)	Bed Material (Percent Finer)					Average
0.0156	0	0	0	0	0	0
0.032	0	0	0	0	0	0
0.063	0.02	0.06	0.17	0.3	0.1	0.1
0.125	0.9	0.1	0.35	0.8	0.2	0.5
0.25	2.6	1.6	2.09	4.1	0.75	2.2
0.5	35.07	16	35.03	25.3	13.1	24.9
1	88.67	59.3	71.71	39.9	59.5	63.8
2	96.62	80.8	79.13	45.6	83.8	77.2
4	97.76	88.5	83.22	52.4	92.5	82.9
8	98.83	92.7	88.72	63	95.1	87.7
16	100	94.9	96.79	81.9	98.7	94.5
31.5	100	100	100	100	100	100
63	100	100	100	100	100	100
125	100	100	100	100	100	100

D _s (mm)	Suspended Material (Percent Finer)					Average
0.0156	0	0	0	0	0	0
0.032	0	0	0	0	0	0
0.063	84.3	79.2	44.8	70.5	82.8	72.3
0.125	92.2	88.9	52	80.3	91.2	80.9
0.25	100	95	69	88.1	96.5	89.7
0.5	100	100	100	100	100	100
1	100	100	100	100	100	100
2	100	100	100	100	100	100
4	100	100	100	100	100	100
8	100	100	100	100	100	100
16	100	100	100	100	100	100
31.5	100	100	100	100	100	100
63	100	100	100	100	100	100
125	100	100	100	100	100	100

BI-296
5/8/1994

D _s (mm)	Bed Material (Percent Finer)					Average
0.0156	0	0	0	0	0	0
0.032	0	0	0	0	0	0
0.063	0.1	0.1	0.1	0.2	0.1	0.1
0.125	0.3	0.2	0.2	0.9	0.2	0.4
0.25	5.6	5.6	5.7	4.7	1	4.5
0.5	44.4	62.8	46.2	14	20.6	37.6
1	86.7	87.4	71.7	22	47.8	63.1
2	93.9	90.4	90.8	26.2	63.6	73.0
4	96.4	92	96	34.1	77.8	79.3
8	97.6	93.6	98	46.6	89.3	85.0
16	100	97.3	100	70.6	97.4	93.1
31.5	100	100	100	90.1	100	98.0
63	100	100	100	100	100	100
125	100	100	100	100	100	100
D _s (mm)	Suspended Material (Percent Finer)					Average
0.0156	0	0	0	0	0	0
0.032	0	0	0	0	0	0
0.063	45.4	34.1	20.2	41.8	21.8	32.7
0.125	66.4	47.3	31.6	66.7	31.3	48.7
0.25	100	71.7	56.9	91	44.1	72.7
0.5	100	100	100	100	93.6	98.7
1	100	100	100	100	100	100
2	100	100	100	100	100	100
4	100	100	100	100	100	100
8	100	100	100	100	100	100
16	100	100	100	100	100	100
31.5	100	100	100	100	100	100
63	100	100	100	100	100	100
125	100	100	100	100	100	100

BI-286
5/14/1995

D _s (mm)	Bed Material (Percent Finer)					Average
0.0156	0	0	0	0	0	0
0.032	0	0	0	0	0	0
0.063	1.1	0.1	0.1	0	1.2	0.5
0.125	6	1.1	0.2	0.1	1.6	1.8
0.25	27	3	1.1	1.2	21.4	10.7
0.5	50	15	15.6	3.1	73.3	31.4
1	73	62	44.6	21.5	84	57.0
2	91	92	56.7	34.9	73.4	69.6
4	99	99	67.2	46.9	99.5	82.3
8	100	99.8	76.2	58.7	100	86.9
16	100	100	88.2	72.9	100	92.2
31.5	100	100	98.4	87.4	100	97.2
63	100	100	100	100	100	100
125	100	100	100	100	100	100
D _s (mm)	Suspended Material (Percent Finer)					Average
0.0156	0	0	0	0	0	0
0.032	0	0	0	0	0	0
0.063	96.6	67.1	1.1	47.9	76.6	57.9
0.125	99.2	100	49.4	60.8	90.1	79.9
0.25	100	100	100	79.6	100	95.9
0.5	100	100	100	100	100	100
1	100	100	100	100	100	100
2	100	100	100	100	100	100
4	100	100	100	100	100	100
8	100	100	100	100	100	100
16	100	100	100	100	100	100
31.5	100	100	100	100	100	100
63	100	100	100	100	100	100
125	100	100	100	100	100	100

BI-286
6/22/1995

D _s (mm)	Bed Material (Percent Finer)					Average	
0.0156	0	0	0	0	0	0	
0.032	0	0	0	0	0	0	
0.063	0.1	0.8	0.1	0	0.3	0.4	0.3
0.125	1.6	4.2	0.2	0.1	0.4	6.4	2.2
0.25	14.4	17.9	2.6	0.8	0.8	6.6	7.2
0.5	32.6	28.1	12.5	19	11.8	14.4	19.7
1	40.9	44.5	26	87.3	54.3	32.9	47.7
2	56.2	62.6	42.4	93.9	65.1	52.7	62.2
4	79.9	81.3	60.5	95.7	71.9	70.4	76.6
8	97.5	98.5	72.4	97.5	77.9	84.1	88.0
16	100	100	93.2	97.6	88	98.1	96.2
31.5	100	100	100	100	100	100	100
63	100	100	100	100	100	100	100
125	100	100	100	100	100	100	100

D _s (mm)	Suspended Material (Percent Finer)						Average
0.0156	0	0	0	0	0	0	0
0.032	0	0	0	0	0	0	0
0.063	83.8	2.2	57.3	40	38.5	52.8	45.8
0.125	95.2	3.1	70.7	51	50.8	68.9	56.6
0.25	97.8	20.8	100	70.7	73.3	82.9	74.3
0.5	100	55.8	100	100	100	100	92.6
1	100	71.6	100	100	100	100	95.3
2	100	100	100	100	100	100	100
4	100	100	100	100	100	100	100
8	100	100	100	100	100	100	100
16	100	100	100	100	100	100	100
31.5	100	100	100	100	100	100	100
63	100	100	100	100	100	100	100
125	100	100	100	100	100	100	100

**BI-286
6/5/1995**

D _s (mm)	Bed Material (Percent Finer)						Average
0.0156	0	0	0	0	0	0	0
0.032	0	0	0	0	0	0	0
0.063	0.3	0.1	0.1	0.1	0.3	0.1	0.2
0.125	2.2	1.2	0.3	0.1	0.4	0.5	0.8
0.25	9.2	2.5	3.1	0.9	1	3	3.3
0.5	20.3	29.2	9.9	24.5	14.7	14.9	18.9
1	39.1	64.4	19.1	68.7	39.2	45	45.9
2	65.2	88.8	28	81.3	54.7	63.3	63.6
4	98.9	97.2	39.6	88.9	65.9	73.1	77.3
8	99.5	100	52.5	94.5	87.6	80.8	85.8
16	100	100	75.2	100	100	90.2	94.2
31.5	100	100	100	100	100	100	100
63	100	100	100	100	100	100	100
125	100	100	100	100	100	100	100

D _s (mm)	Suspended Material (Percent Finer)						Average
0.0156	0	0	0	0	0	0	0
0.032	0	0	0	0	0	0	0
0.063	74.1	54	72.1	20.6	33.7	57.1	51.9
0.125	100	72.3	100	25.8	43.3	76.9	69.7
0.25	100	100	100	40	66.1	100	84.4
0.5	100	100	100	100	100	100	100
1	100	100	100	100	100	100	100
2	100	100	100	100	100	100	100
4	100	100	100	100	100	100	100
8	100	100	100	100	100	100	100
16	100	100	100	100	100	100	100
31.5	100	100	100	100	100	100	100
63	100	100	100	100	100	100	100
125	100	100	100	100	100	100	100

BI-291
5/14/1995

D _s (mm)	Bed Material (Percent Finer)					Average
0.0156	0	0	0	0	0	0
0.032	0	0	0	0	0	0
0.063	0.1	0.1	0	0.1	0	0.1
0.125	0.6	0.4	0.1	0.1	0	0.2
0.25	4	5	0.2	1.6	0.3	2.2
0.5	25	24	1.1	24.3	1.6	15.2
1	39	75	2.6	56.9	12.6	37.2
2	47	98	4	77.1	23.6	49.9
4	61	99.9	6.6	89.7	30.7	57.6
8	87	100	13	95.1	40.3	67.1
16	100	100	21.9	99.3	53.3	74.9
31.5	100	100	49.6	100	67.9	83.5
63	100	100	100	100	100	100
125	100	100	100	100	100	100
D _s (mm)	Suspended Material (Percent Finer)					Average
0.0156	0	0	0	0	0	0
0.032	0	0	0	0	0	0
0.063	75.6	59.7	58.8	19.4	58.4	54.4
0.125	88.7	78.6	74.9	26.4	74.3	68.6
0.25	96.7	92.4	94.6	46.6	90.2	84.1
0.5	100	100	99	100	100	99.8
1	100	100	99.9	100	100	100.0
2	100	100	100	100	100	100
4	100	100	100	100	100	100
8	100	100	100	100	100	100
16	100	100	100	100	100	100
31.5	100	100	100	100	100	100
63	100	100	100	100	100	100
125	100	100	100	100	100	100

BI-291
6/22/1995

D _s (mm)	Bed Material (Percent Finer)					Average
0.0156	0	0	0	0	0	0
0.032	0	0	0	0	0	0
0.063	0.1	0	0.1	0	0	0.0
0.125	0.1	0	0.1	0.1	0.1	0.1
0.25	0.6	0	1.3	3	0.8	1.1
0.5	9.5	0	14.7	63.7	40.4	22.2
1	15.7	45.9	54.9	94.4	97.4	55.1
2	44.3	76.6	80.4	95.5	99	71.6
4	63.2	89.8	93	96.4	99.6	80.7
8	82	95	98.2	97.8	100	88.0
16	97.1	98.6	100	99.2	100	94.9
31.5	100	100	100	100	100	100
63	100	100	100	100	100	100
125	100	100	100	100	100	100

D _s (mm)	Suspended Material (Percent Finer)						Average
0.0156	0	0	0	0	0	0	0
0.032	0	0	0	0	0	0	0
0.063	76.9	1.1	41.1	20	51.6	67.7	43.1
0.125	100	1.5	54.9	27.4	100	100	64.0
0.25	100	3.4	100	48.6	100	100	75.3
0.5	100	31.6	100	100	100	100	88.6
1	100	75.8	100	100	100	100	96.0
2	100	92.8	100	100	100	100	98.8
4	100	99	100	100	100	100	99.8
8	100	100	100	100	100	100	100
16	100	100	100	100	100	100	100
31.5	100	100	100	100	100	100	100
63	100	100	100	100	100	100	100
125	100	100	100	100	100	100	100

**BI-291
6/5/1995**

D _s (mm)	Bed Material (Percent Finer)						Average
0.0156	0	0	0	0	0	0	0
0.032	0	0	0	0	0	0	0
0.063	0.2	0.1	0.2	0.2	0.1	0.2	0.2
0.125	0.3	0.3	0.3	0.2	0.1	0.2	0.2
0.25	1.2	0.7	0.9	1.5	0.4	1	1.0
0.5	8.6	6.1	10.5	33.8	8.7	14.3	13.7
1	28.4	34.6	42.4	66.7	18.2	37	37.9
2	45.7	66.9	63.7	79.5	20.1	53.1	54.8
4	61.9	85.5	73.2	89.5	22.3	64.8	66.2
8	80.6	96.7	77.6	96.5	26.7	75.1	75.5
16	100	100	82.3	100	49.6	87.4	86.6
31.5	100	100	85.9	100	91	97.8	95.8
63	100	100	100	100	100	100	100
125	100	100	100	100	100	100	100
D _s (mm)	Suspended Material (Percent Finer)						Average
0.0156	0	0	0	0	0	0	0
0.032	0	0	0	0	0	0	0
0.063	80	79.8	7.7	24.2	36.3	51.1	46.5
0.125	100	94.2	9.2	32	45.2	70.6	58.5
0.25	100	100	11.1	58.6	61.8	83.6	69.2
0.5	100	100	27	100	99	100	87.7
1	100	100	73.9	100	99.9	100	95.6
2	100	100	100	100	100	100	100
4	100	100	100	100	100	100	100
8	100	100	100	100	100	100	100
16	100	100	100	100	100	100	100
31.5	100	100	100	100	100	100	100
63	100	100	100	100	100	100	100
125	100	100	100	100	100	100	100

BI-296
5/13/1995

D _s (mm)	Bed Material (Percent Finer)					Average
0.0156	0	0	0	0	0	0
0.032	0	0	0	0	0	0
0.063	0	0	0.1	0.1	0	0.0
0.125	0	0.1	0.4	0.4	0	0.2
0.25	1.2	4	4	3.5	0.9	2.7
0.5	17.2	35	14	15	7.6	17.8
1	53.2	67	31	30	34.6	43.2
2	74.4	76	35	40	52.2	55.5
4	87.3	84	42	60	71.7	69.0
8	95	90	55	88	88.3	83.3
16	100	91	82	99	100	94.4
31.5	100	98	98	100	100	99.2
63	100	100	100	100	100	100
125	100	100	100	100	100	100
D _s (mm)	Suspended Material (Percent Finer)					Average
0.0156	0	0	0	0	0	0
0.032	0	0	0	0	0	0
0.063	53.3	19.6	64.2	84.6	72.8	58.9
0.125	67.2	27.3	84.2	97.5	89.7	73.2
0.25	82	55.1	100	99	100	87.2
0.5	100	100	100	99.9	100	100.0
1	100	100	100	100	100	100
2	100	100	100	100	100	100
4	100	100	100	100	100	100
8	100	100	100	100	100	100
16	100	100	100	100	100	100
31.5	100	100	100	100	100	100
63	100	100	100	100	100	100
125	100	100	100	100	100	100

BI-296
6/5/1995

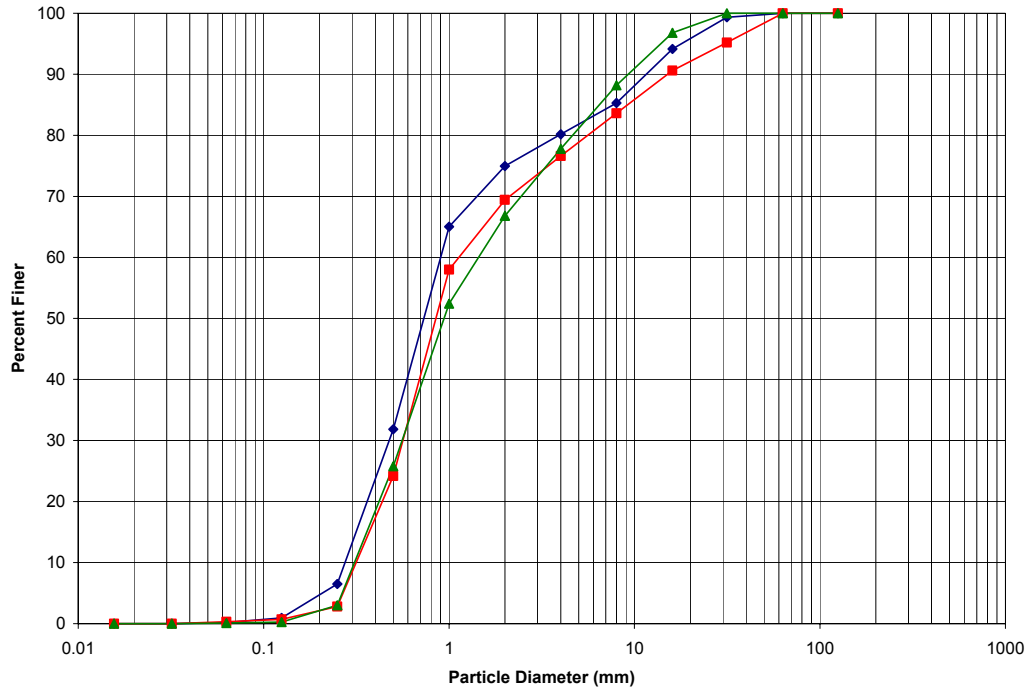
D _s (mm)	Bed Material (Percent Finer)					Average
0.0156	0	0	0	0	0	0
0.032	0	0	0	0	0	0
0.063	0.2	0.1	0.1	0.3	0.1	0.2
0.125	0.2	0.1	0.1	1.4	0.2	0.4
0.25	0.5	2.6	1.4	4.6	1.4	2.1
0.5	5.5	46.7	13.1	8.3	4.9	15.7
1	34.4	89.3	30.4	24	18.4	39.3
2	71.4	95.3	33.8	42.1	30.7	54.7
4	90.6	97.1	39.6	60.8	42.1	66.0
8	97.2	98.1	52.5	81.2	59.7	77.7
16	100	100	72.7	98.8	76.1	89.5
31.5	100	100	100	100	100	100
63	100	100	100	100	100	100
125	100	100	100	100	100	100

D _s (mm)	Suspended Material (Percent Finer)					Average
0.0156	0	0	0	0	0	0
0.032	0	0	0	0	0	0
0.063	46.7	26.8	34.3	81.3	74.2	52.7
0.125	57.6	33.4	44.1	96.3	89.5	64.2
0.25	73.6	55.8	61.8	100	97.6	77.8
0.5	100	100	99	100	100	99.8
1	100	100	100	100	100	100
2	100	100	100	100	100	100
4	100	100	100	100	100	100
8	100	100	100	100	100	100
16	100	100	100	100	100	100
31.5	100	100	100	100	100	100
63	100	100	100	100	100	100
125	100	100	100	100	100	100

**BI-296
7/2/1995**

D _s (mm)	Bed Material (Percent Finer)					Average
0.0156	0	0	0	0	0	0
0.032	0	0	0	0	0	0
0.063	0.3	0.1	0.3	0.1	0.1	0.2
0.125	0.3	0.1	1.8	0.4	0.3	0.6
0.25	1.2	2.4	9.1	1.9	3.2	3.6
0.5	13.5	27.8	51.4	10.5	13.9	23.4
1	41.9	58.4	98	31.8	26.9	51.4
2	63	69.2	99.9	39.5	31.5	60.6
4	80.8	80.9	100	46.3	32.9	68.2
8	93.9	89.3	100	57.5	46.1	77.4
16	98.1	92.9	100	79.2	78.7	89.8
31.5	100	92.9	100	100	100	98.6
63	100	100	100	100	100	100
125	100	100	100	100	100	100
D _s (mm)	Suspended Material (Percent Finer)					Average
0.0156	0	0	0	0	0	0
0.032	0	0	0	0	0	0
0.063	24.3	1.7	88.3	54.5	60.1	45.8
0.125	33	2.5	100	100	100	67.1
0.25	42.6	6.8	100	100	100	69.9
0.5	100	31.6	100	100	100	86.3
1	100	100	100	100	100	100
2	100	100	100	100	100	100
4	100	100	100	100	100	100
8	100	100	100	100	100	100
16	100	100	100	100	100	100
31.5	100	100	100	100	100	100
63	100	100	100	100	100	100
125	100	100	100	100	100	100

1992 Bed Material Distributions



1992 Suspended Material Distributions

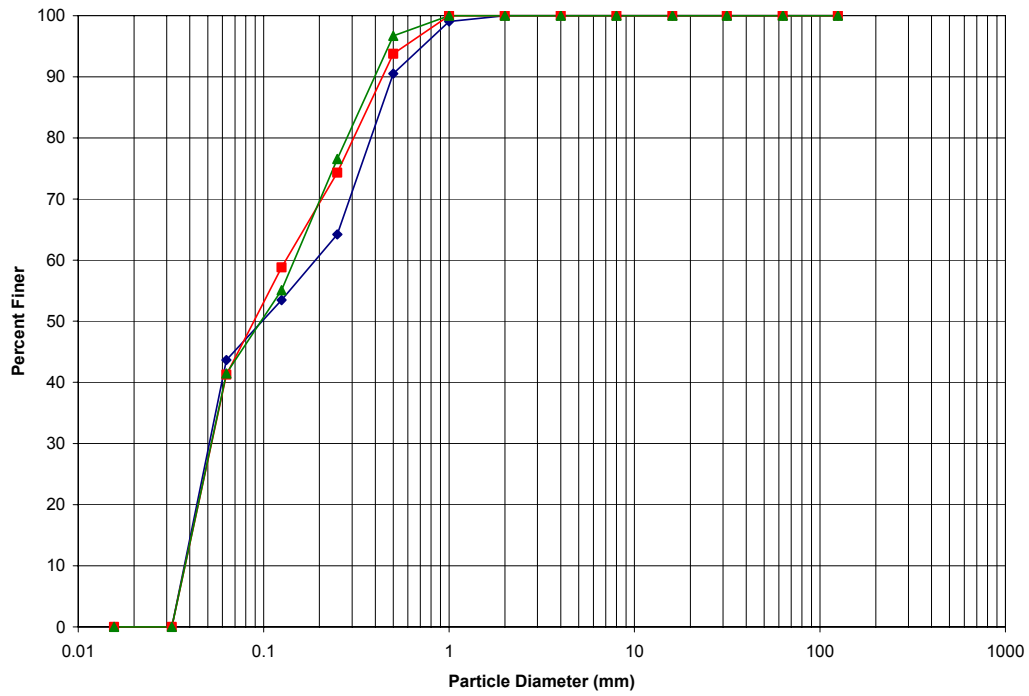
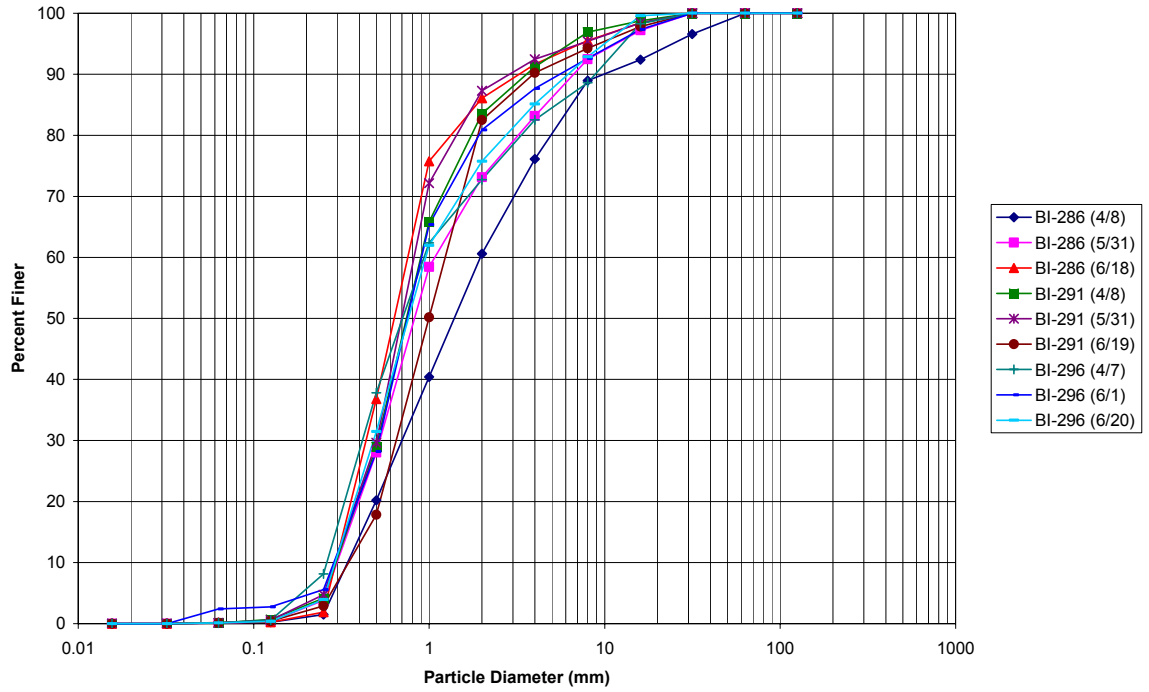


Figure I-1: Bed material and suspended material gradation curves from BI-survey lines for 1992.

1993 Bed Material Distributions



1993 Suspended Material Distributions

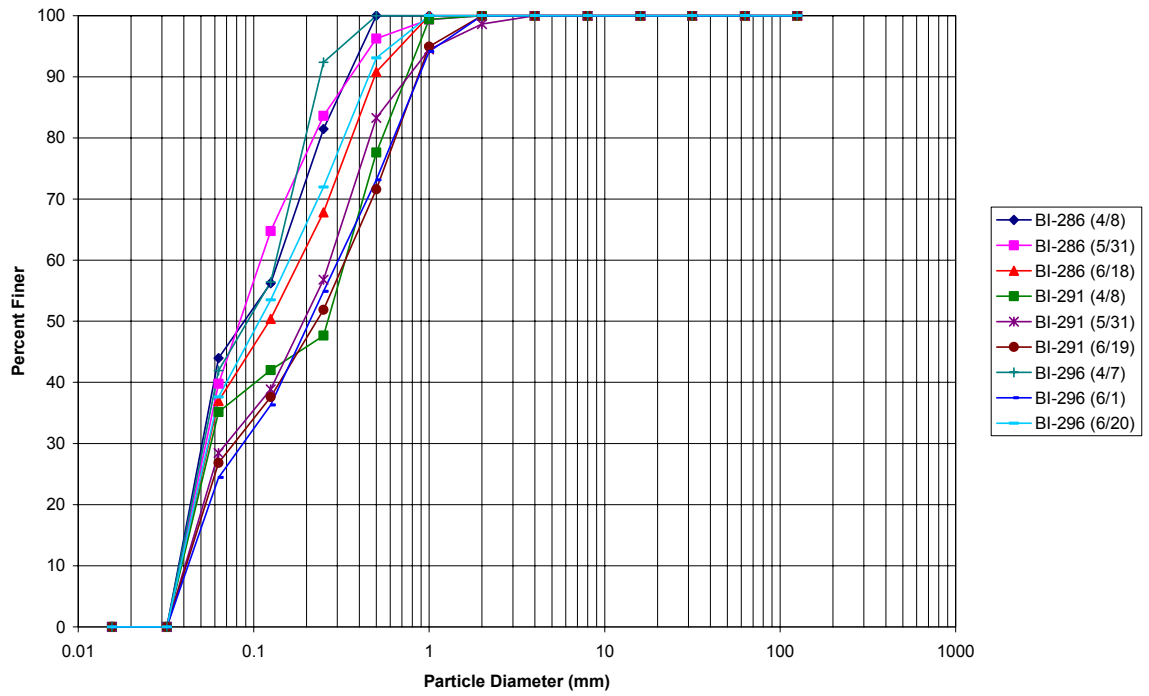
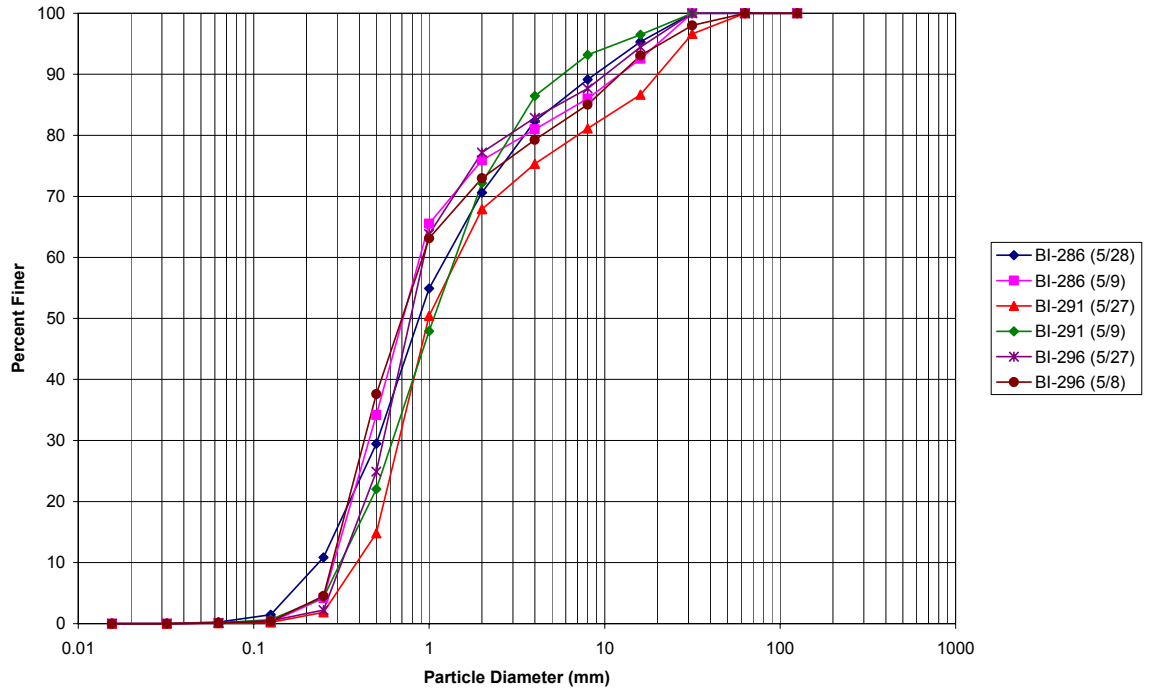


Figure I-2: Bed material and suspended material gradation curves from BI-survey lines for 1993.

1994 Bed Material Distributions



1994 Suspended Material Distributions

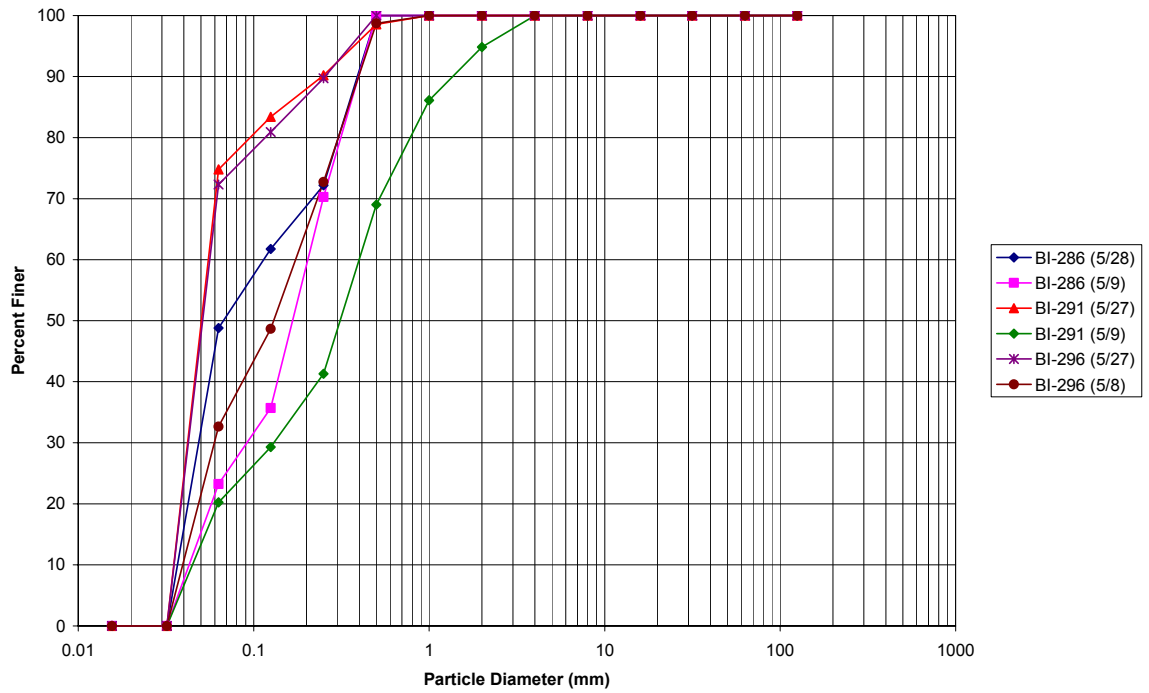
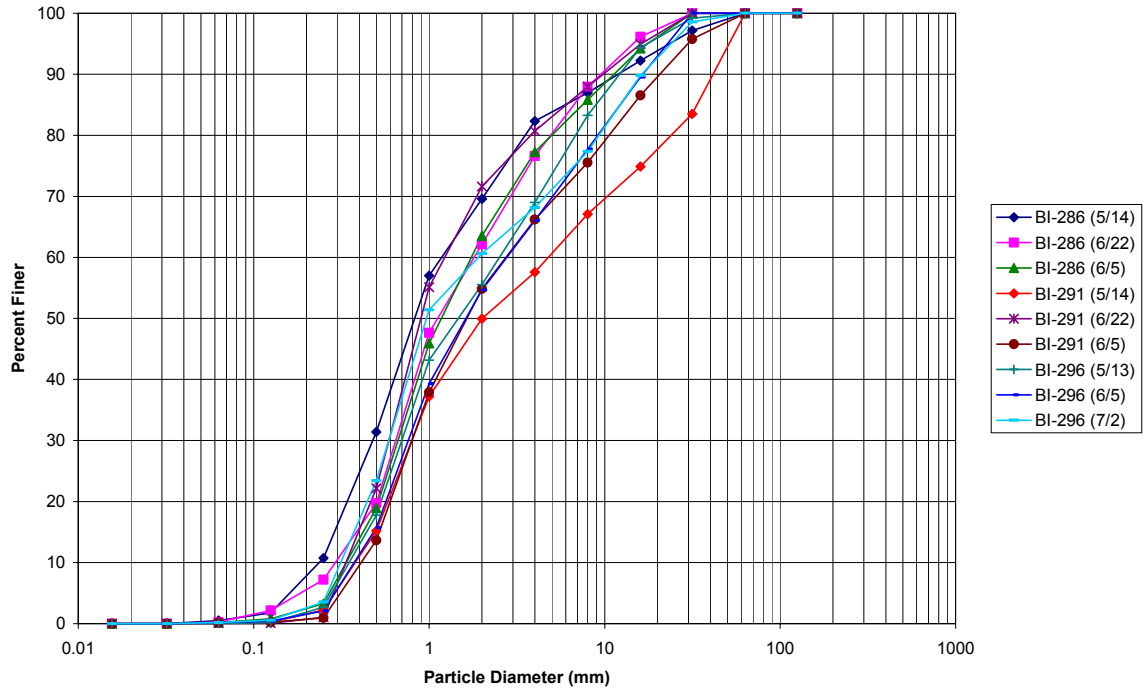


Figure I-3: Bed material and suspended material gradation curves from BI-survey lines for 1994.

1995 Bed Material Distributions



1995 Suspended Material Distributions

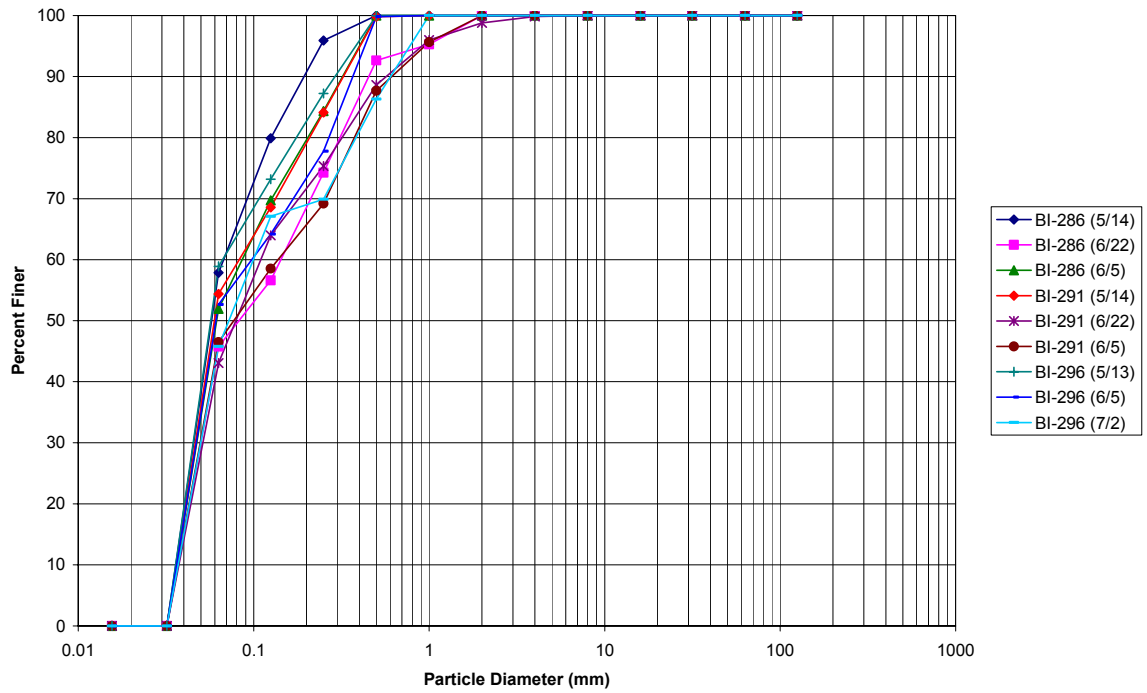


Figure I-4: Bed material and suspended material gradation curves from BI-survey lines for 1995.

Table I-2: Bed material load analysis summary utilizing results from the Modified Einstein Procedure (MEP).

Bl-line	Date	Inst. Discharge (cfs)	D ₁₀ bed material (mm)	% washload	% bed material load	MEP Results			B.M.L. (T/day)
						T.L. (T/day)	S.L. (T/day)	W.L. (T/day)	
286	5/28/1992	3851	0.28	68	32	26480	24202	2278	8473.6
291	5/29/1992	3985	0.30	80	20	5269	4120	1149	1053.8
296	5/28/1992	3905	0.30	82	18	3249	2631	618	584.8
286	4/8/1993	2760	0.35	90	10	2975	2573	402	297.5
286	5/31/1993	6147	0.30	87	13	10014	7748	2266	1301.8
286	6/18/1993	4638	0.30	74	26	5785	4937	847	1504.1
291	4/8/1993	2828	0.30	57	43	13603	13143	460	5849.3
291	5/31/1993	6345	0.30	64	36	19304	17342	1962	6949.4
291	6/19/1993	4426	0.35	63	37	19457	18630	826	7199.1
296	4/7/1993	2747	0.28	93	7	1455	1081	373	101.9
296	6/1/1993	5940	0.30	60	40	18115	16382	1733	7246.0
296	6/20/1993	4459	0.30	78	22	6101	4846	1255	1342.2
286	5/9/1994	4322	0.28	75	25	13510	12563	947	3377.5
286	5/28/1994	4839	0.24	73	27	27852	26284	1867	7520.0
291	5/9/1994	4064	0.31	52	48	25637	24239	1398	12305.8
291	5/27/1994	4509	0.39	95	5	10117	6239	3878	505.9
296	5/8/1994	3831	0.28	76	24	5930	4897	1033	1423.2
296	5/27/1994	4807	0.31	93	7	11911	7293	4618	833.8
286	5/14/1995	3581	0.23	94	6	78944	78336	609	4736.6
286	6/5/1995	4723	0.33	92	8	5952	5150	802	476.2
286	6/22/1995	5442	0.30	79	21	10478	9373	1106	2200.4
291	5/14/1995	3891	0.38	93	7	4906	4197	709	343.4
291	6/5/1995	4779	0.41	83	17	5382	4722	661	914.9
291	6/22/1995	5437	0.33	81	19	18445	17562	883	3504.6
296	5/13/1995	4367	0.35	94	6	3432	2762	669	205.9
296	6/5/1995	4652	0.38	90	10	3598	2910	688	359.8
296	7/2/1995	5331	0.31	77	23	31089	30181	908	7150.5
Average =		4501	0.32	79	21	11925	10616	1321	3193

outlier

Table I-3: Suitability of bedload and bed material load transport equations (Stevens and Yang, 1989).

<i>Author of Formula</i>	<i>Date</i>	<i>Bedload (BL) or Bed-material Load (BML)</i>	<i>Type of Formula (DP)</i>	<i>Sediment Type (SMO)</i>	<i>Sediment Size (SG)</i>
<i>Ackers & White</i>	1973	BML	D	S	S,G
<i>Einstein (BL)</i>	1950	BL	P	M	S,G
<i>Einstein (BML)</i>	1950	BML	P	M	S
<i>Engelund & Hansen</i>	1967	BML	D	S	S
<i>Laursen</i>	1958	BML	D	M	S
<i>Meyer-Peter and Muller</i>	1948	BL	D	S	S,G
<i>Schoklitsch</i>	1934	BL	D	M	S,G
<i>Toffaletti</i>	1968	BML	D	M	S
<i>Yang (sand)</i>	1973	BML	D	O	S
<i>Yang (gravel)</i>	1984	BML	D	O	G

DP - Deterministic/Probabilistic

SMO - Single Size Fraction/Mixture/Optional

SG - Sand/Gravel

Table I-4: Hydraulic input data for sediment transport capacity computations from 1962, 1972, 1992 and 1998 HEC-RAS® runs at 5,000 cfs.

1962
Data

Width (ft)	Depth (ft)	Velocity (ft/s)	WS slope (ft/ft)
317	3.20	5.15	0.0011

1972
Data

Width (ft)	Depth (ft)	Velocity (ft/s)	WS slope (ft/ft)
297	3.47	5.29	0.0011

1992
Data

Width (ft)	Depth (ft)	Velocity (ft/s)	WS slope (ft/ft)
269	3.58	5.66	0.0012

1998
Data

Width (ft)	Depth (ft)	Velocity (ft/s)	WS slope (ft/ft)
241	3.65	6.02	0.0011

Table I-5: Bed material load and bedload transport capacity for 1962 and 1972.

BML Transport Equations	1962 S = 0.0011 ft/ft	1972 S = 0.0011 ft/ft
	BML/BL (tons/day)	BML/BL (tons/day)
Laursen	37,200	62,431
Engelund & Hansen	59,089	65,958
Ackers & White (D ₅₀)	67,636	73,111
Ackers & White (D ₃₅)	131,301	183,012
Yang Sand (D ₅₀)	33,877	36,581
Yang Sand (size fraction)	41,015	50,849
Einstein	55,539	88,522
Toffaleti	95,656	132,486
Average =	65,164	86,619
BL Transport Equations	1962	1972
Schoklitsch	7,604	9,267
Kalinske	992	658
Meyer-Peter & Muller	2,628	2,611
Rottner	14,443	14,715
Einstein	3,425	2,916
Average =	5,818	6,033

Table I-6: Bed material load and bedload transport capacity for 1992 and 1998.

BML Transport Equations	1992 S = 0.0012 ft/ft	1998 S = 0.0011 ft/ft
	BML/BL (tons/day)	BML/BL (tons/day)
Ackers & White (D ₅₀)	283	3,013
Ackers & White (D ₃₅)	2,074	4,174
Yang Gravel (D ₅₀)	3,876	3,419
Yang Gravel (size fraction)	1,834	2,545
Average =	2,016	3,288
BL Transport Equations	1992	1998
Schoklitsch	1,555	2,087
Kalinske	1,418	1,144
Meyer-Peter & Muller	1,233	1,383
Rottner	381	4,000
Einstein	19	351
Average =	921	1,793

APPENDIX J:
Location Maps (Galisteo Reach)

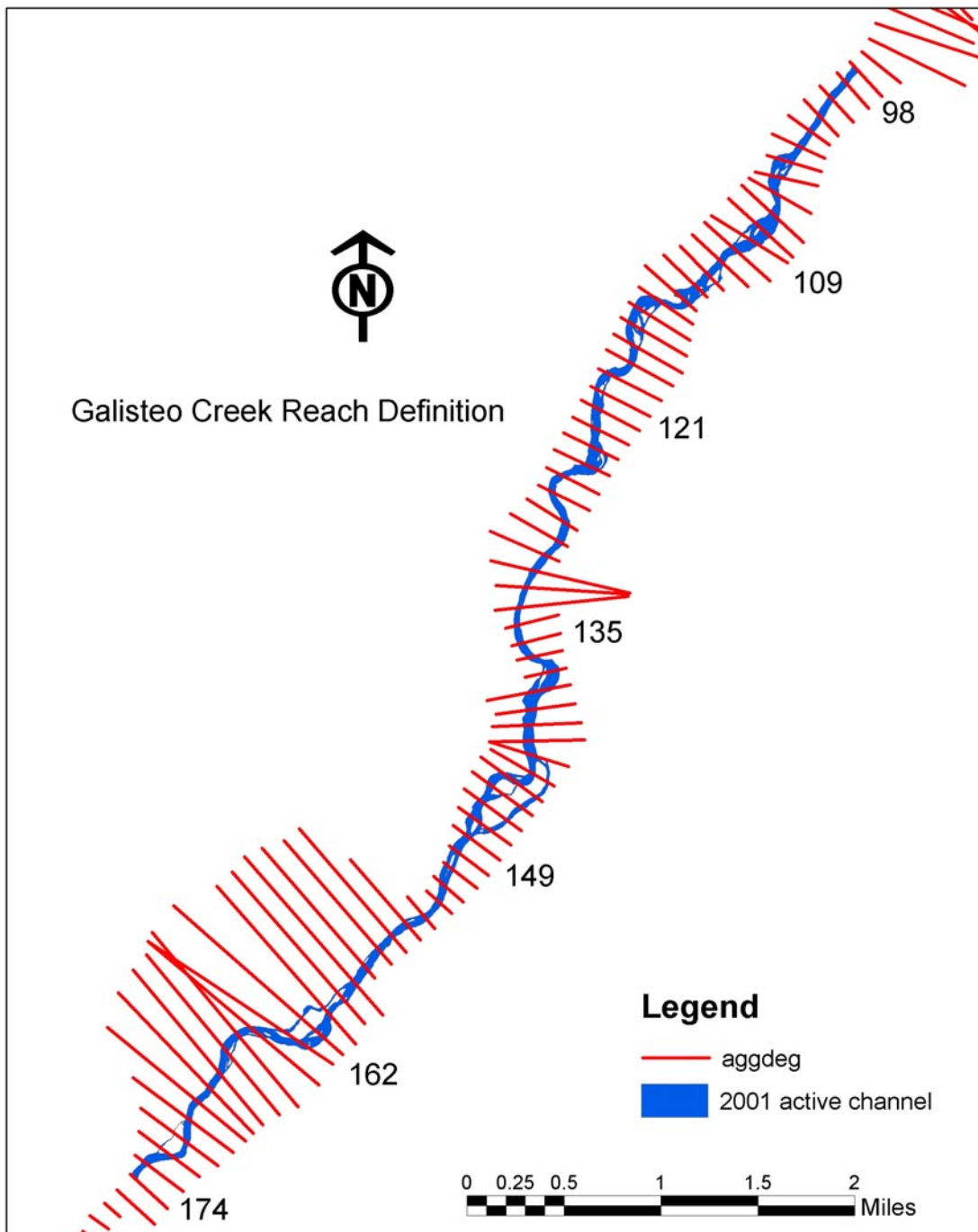


Figure J-1: 2001 river planform of the Galisteo Reach displaying locations of the agg/deg lines.

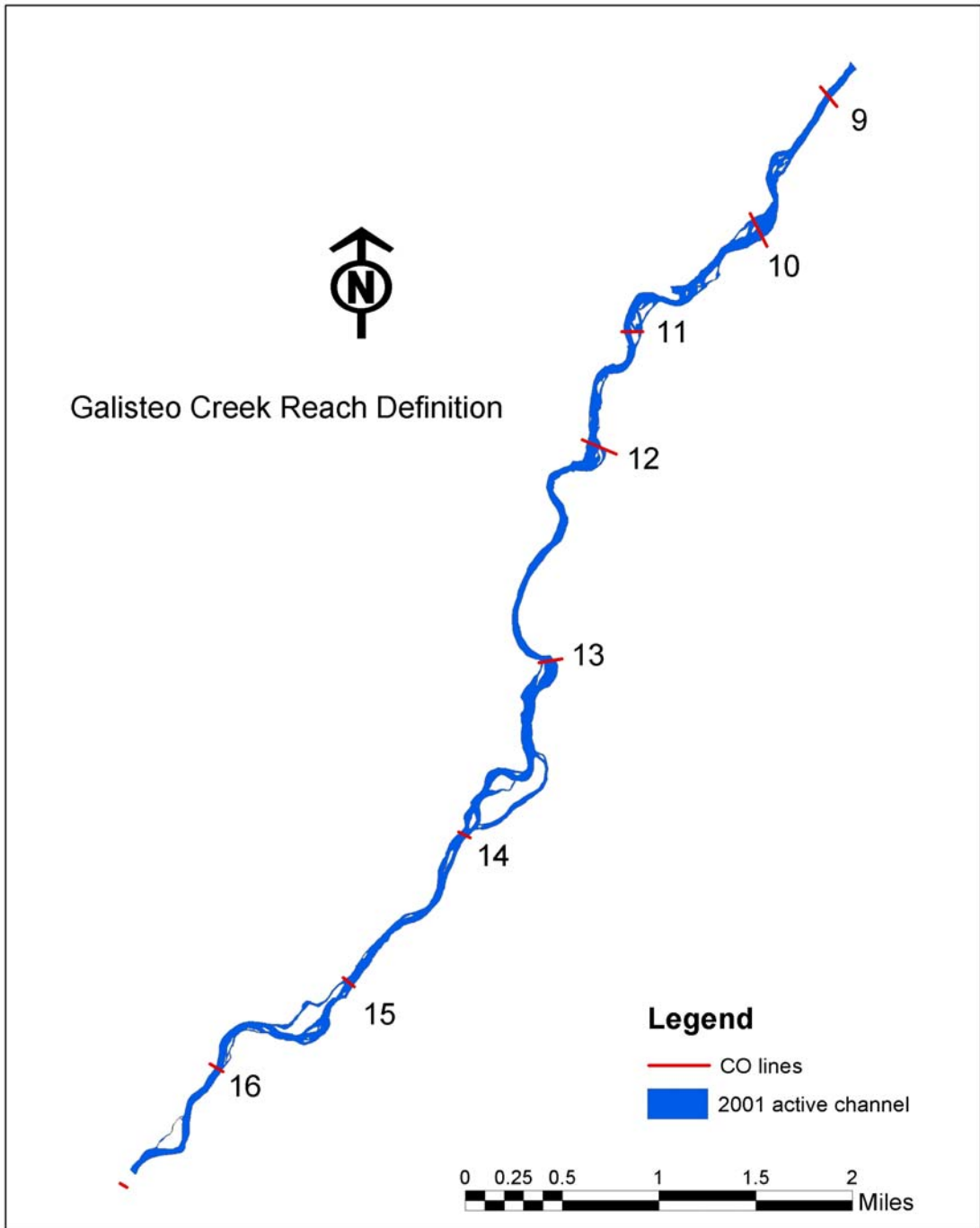


Figure J-2: 2001 river planform of the Galisteo Reach displaying locations of the CO-lines.

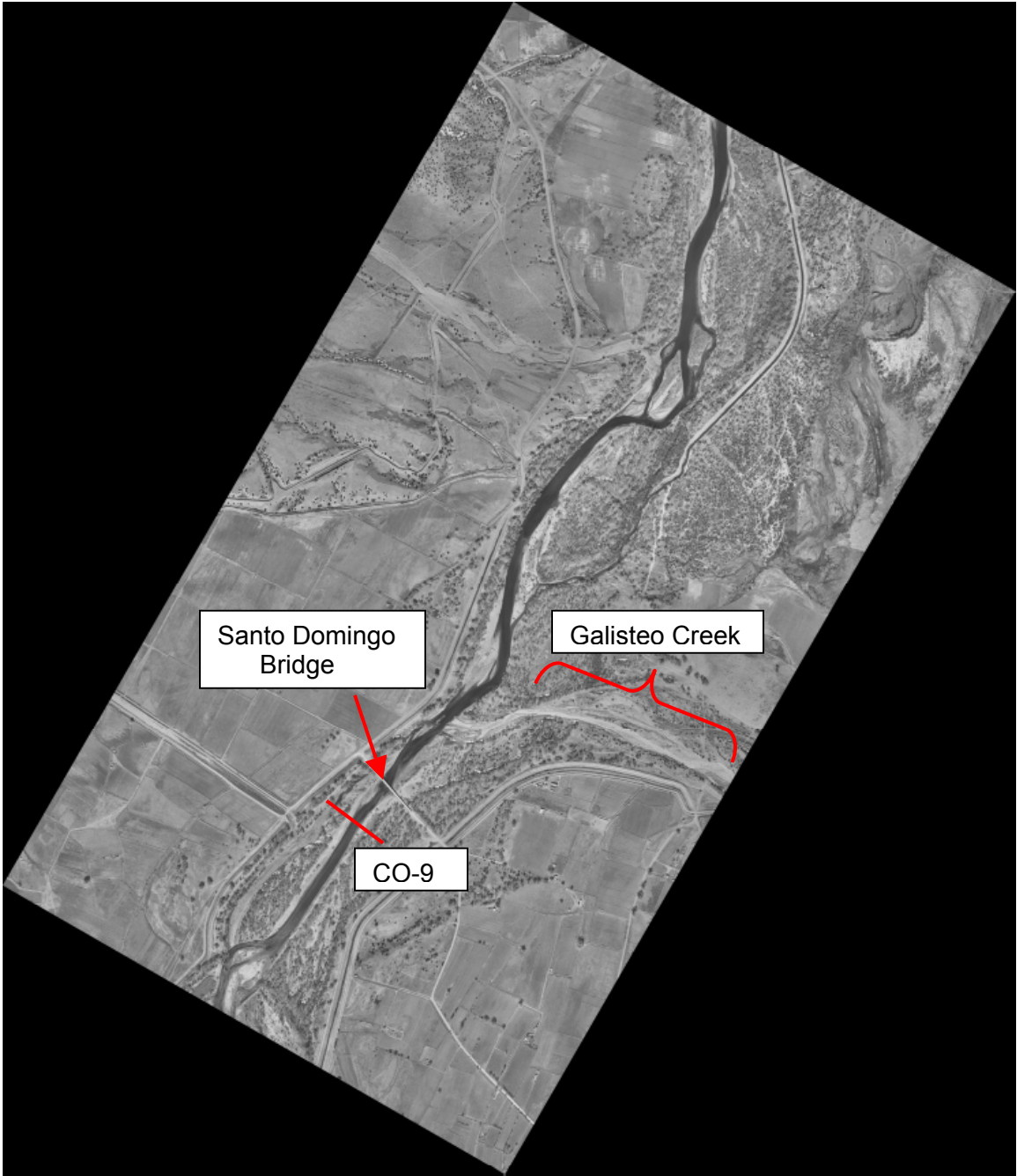


Figure J-3: Aerial photograph of Galisteo Reach (photo 1 of 4).

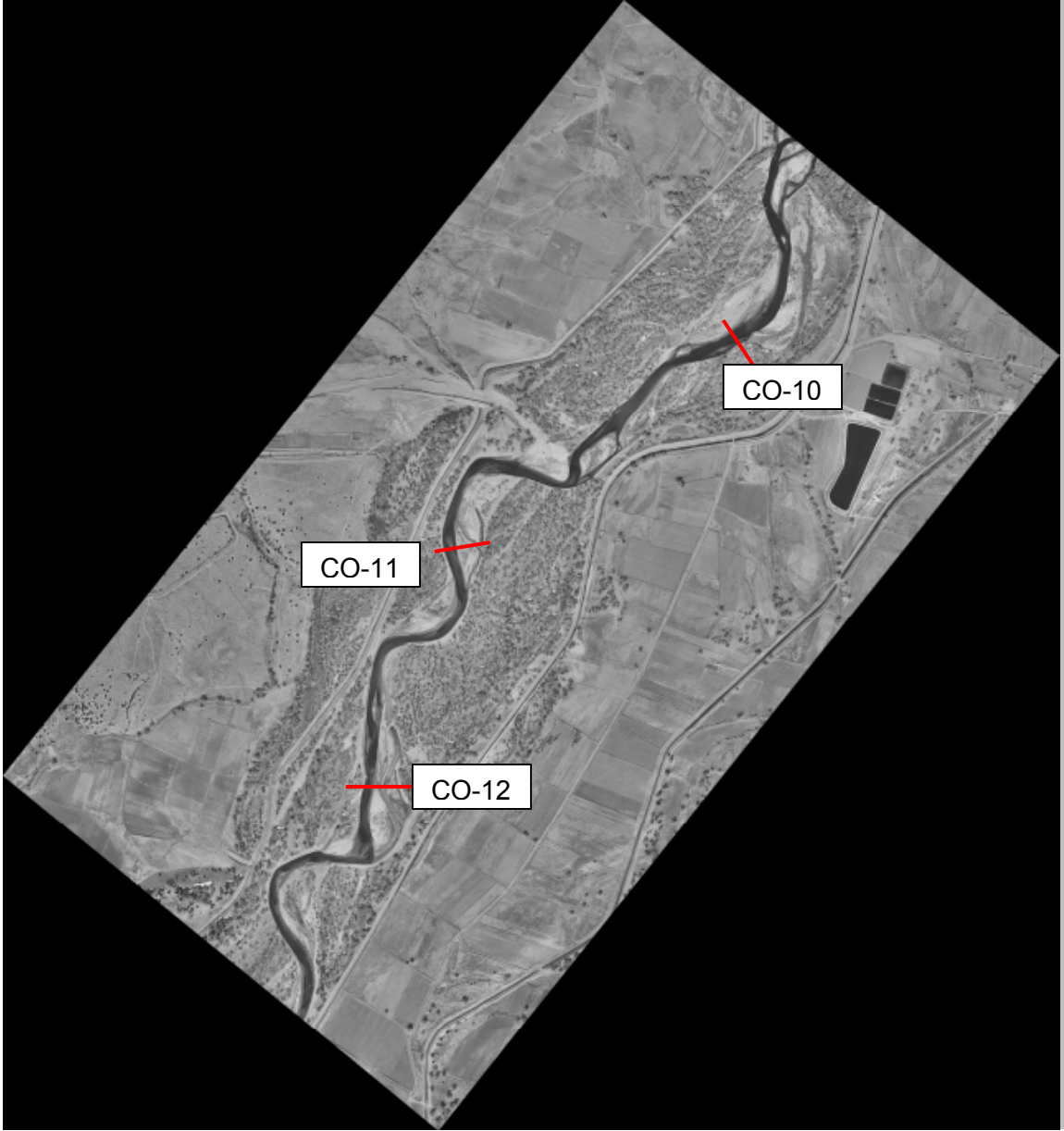


Figure J-4: Aerial photograph of Galisteo Reach (photo 2 of 4).

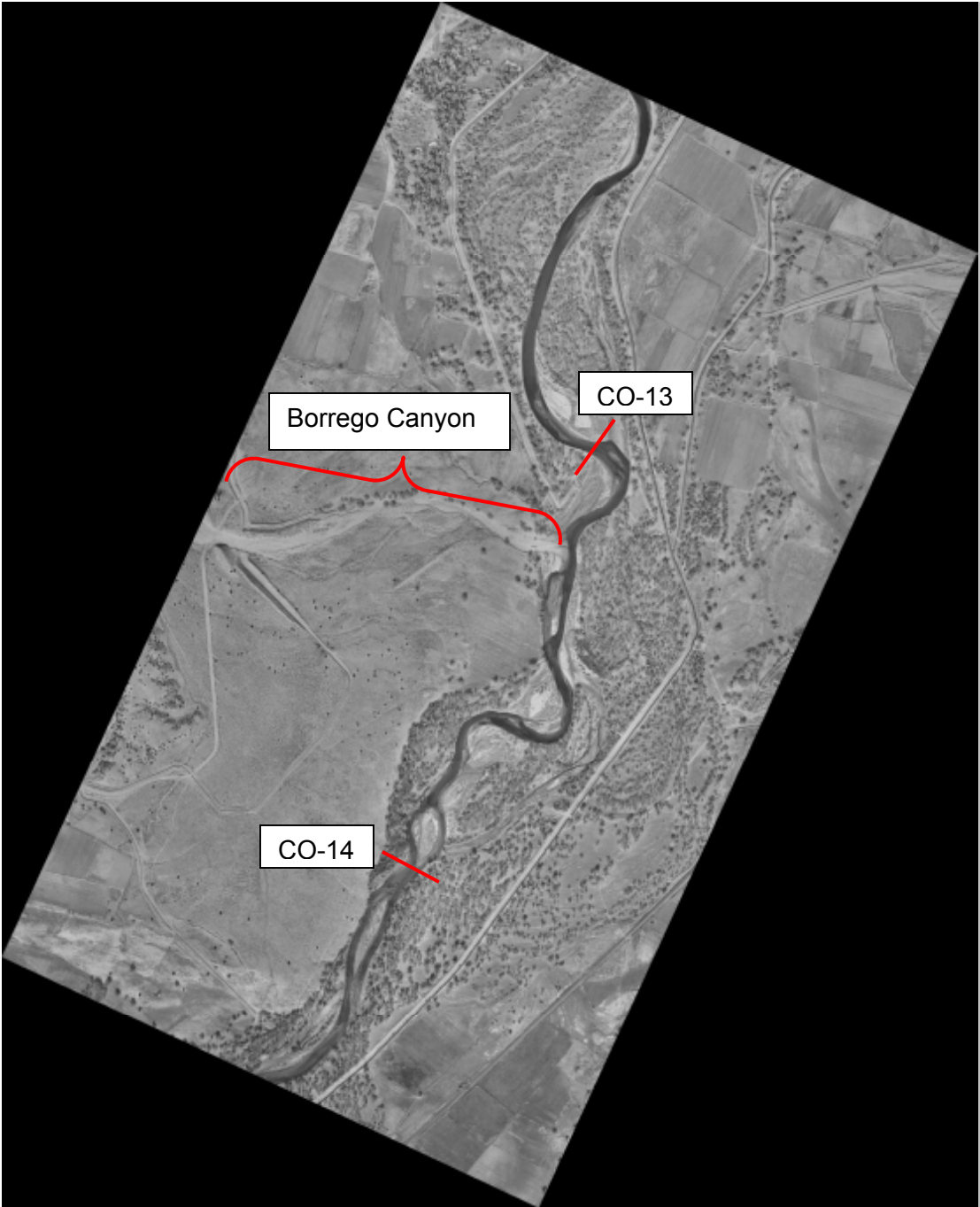


Figure J-5: Aerial photograph of Galisteo Reach (photo 3 of 4).

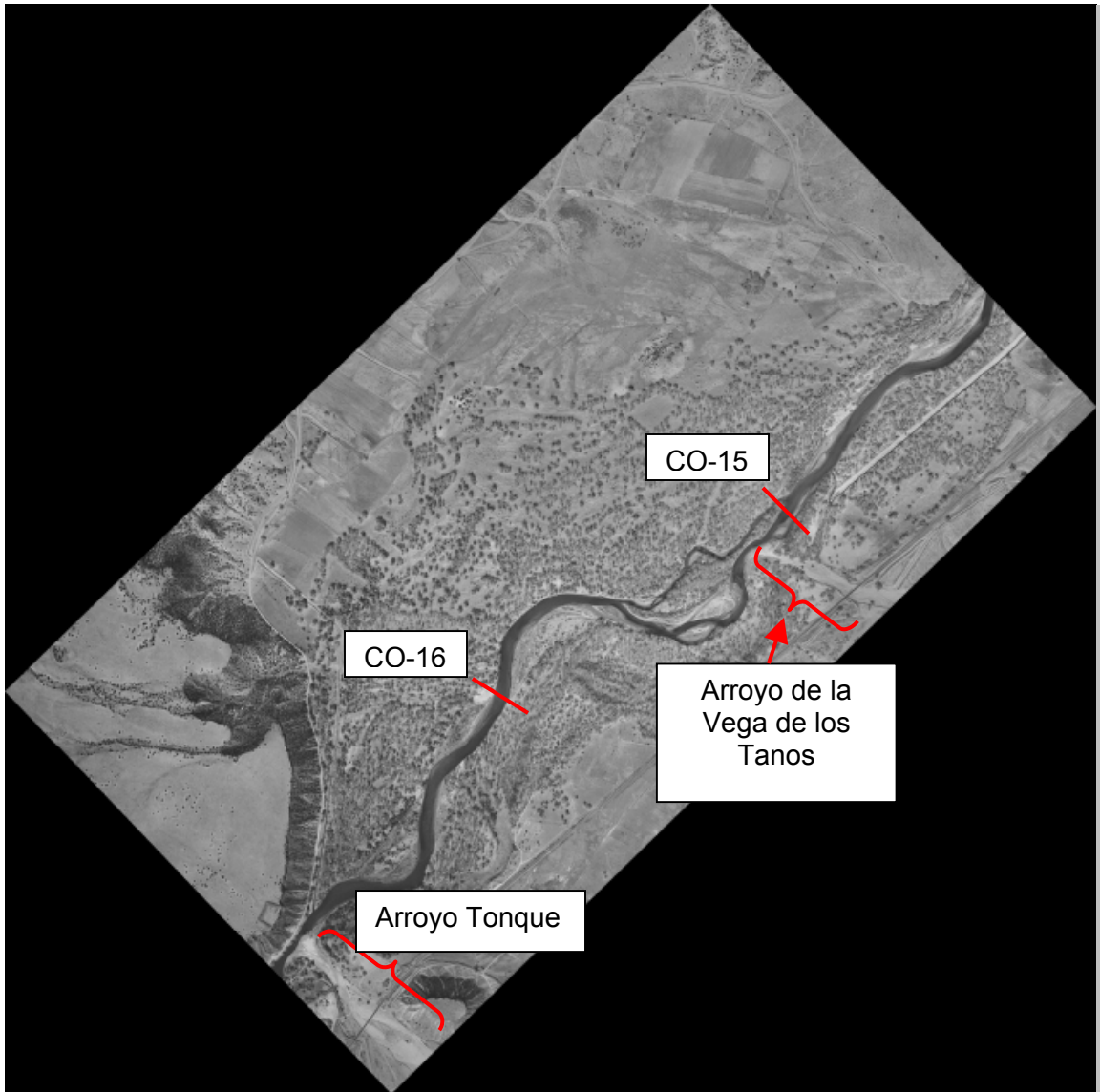


Figure J-6: Aerial photograph of Galisteo Reach (photo 4 of 4).

APPENDIX K:
Radius of Curvature Dataset (3-Point Methodology)

Table K-1: Radius of curvature calculations for bend 1 (1972).

Bend	1
Year	1972
Depth (ft)	2.92 (avg.)

Bend id	Point id	GIS Coordinates (ft)		GIS Coordinates (ft)		Midpoint Slopes (ft/ft)	
		X _{CL}	Y _{CL}	X _{mid}	Y _{mid}	m	p
1_72	1 (u/s)	458460.3	1641444.0	458410.5	1641441.1	0.060	0.234
1_72	2	458360.7	1641438.1	458309.4	1641426.1	0.234	0.300
1_72	3	458258.0	1641414.1	458212.9	1641400.6	0.300	1.035
1_72	4	458167.7	1641387.0	458134.1	1641352.2	1.035	1.033
1_72	5	458100.5	1641317.4	458065.7	1641281.5	1.033	1.283
1_72	6	458031.0	1641245.6	457999.7	1641205.5	1.283	1.809
1_72	7	457968.5	1641165.5	457944.8	1641122.6	1.809	2.000
1_72	8	457921.1	1641079.8	457898.8	1641035.0	2.000	3.729
1_72	9	457876.4	1640990.3	457863.5	1640942.2	3.729	4.374
1_72	10	457850.6	1640894.1	457838.9	1640843.0	4.374	4.375
1_72	11	457827.2	1640791.8	457816.2	1640743.6	4.375	3.764
1_72	12	457805.2	1640695.4	457792.3	1640646.9	3.764	3.000
1_72	13	457779.4	1640598.3	457763.9	1640551.9	3.000	2.568
1_72	14	457748.4	1640505.4	457730.7	1640459.9	2.568	2.286
1_72	15	457713.0	1640414.4	457691.8	1640366.0	2.286	2.286
1_72	16	457670.6	1640317.6	457651.7	1640274.4	2.286	2.286
1_72	17	457632.8	1640231.2	457612.8	1640185.4	2.286	1.972
1_72	18	457592.7	1640139.6	457569.5	1640093.8		
1_72	19 (d/s)	457546.3	1640047.9				

input (GIS)

Tangent Slopes (ft/ft)		Tangent Intercepts (ft)		Centroid Coordinates (ft)		R (ft)	width (ft)
a	c	b	d	x _c	y _c		
-16.745	-4.282	9317313.4	3604052.8	458446.5	1640838.9	605	166
-4.282	-3.332	3604052.8	3168382.2	458674.8	1639861.1	1608	272
-3.332	-0.966	3168382.2	2083890.5	458265.5	1641225.3	189	322
-0.966	-0.968	2083890.5	2084733.5	394134.6	1703173.0	88982	345
-0.968	-0.779	2084733.5	1998208.7	458741.1	1640627.7	941	380
-0.779	-0.553	1998208.7	1894325.3	458499.8	1640815.8	636	398
-0.553	-0.500	1894325.3	1870035.6	460039.7	1639964.3	2394	406
-0.500	-0.268	1870035.6	1763711.7	458339.7	1640814.5	496	396
-0.268	-0.229	1763711.7	1745509.8	460516.7	1640230.8	2747	368
-0.229	-0.229	1745509.8	1745381.9	2509109.1	1171901.0	2104190	319
-0.229	-0.266	1745381.9	1762275.2	455039.0	1641378.4	2849	250
-0.266	-0.333	1762275.2	1793123.4	456247.6	1641057.3	1599	218
-0.333	-0.389	1793123.4	1818695.3	455893.8	1641175.2	1972	226
-0.389	-0.438	1818695.3	1840606.2	455424.8	1641357.8	2475	240
-0.438	-0.437	1840606.2	1840480.5	3476478.6	319646.8	3295053	275
-0.437	-0.438	1840480.5	1840394.1	-2010044.8	2719802.4	2693493	253
-0.438	-0.507	1840394.1	1872174.7	455983.4	1640898.2	1779	233
							220
							223

Apex (est.)

189 290
(Minimum) (Average)

Table K-2: Radius of curvature calculations for bend 1 (1985).

Bend	1
Year	1985
Depth (ft)	2.75 (avg.)

Bend id	Point id	GIS Coordinates (ft)		GIS Coordinates (ft)		Midpoint Slopes (ft/ft)	
		X _{CL}	Y _{CL}	X _{mid}	Y _{mid}	m	p
1_85	1 (u/s)	458430.5	1641368.9	458378.5	1641380.3	-0.219	-0.128
1_85	2	458326.4	1641391.7	458270.7	1641398.8	-0.128	-0.123
1_85	3	458215.0	1641406.0	458159.3	1641412.8	-0.123	0.006
1_85	4	458103.6	1641419.6	458047.8	1641419.3	0.006	0.209
1_85	5	457991.9	1641418.9	457937.1	1641407.5	0.209	0.510
1_85	6	457882.2	1641396.0	457833.3	1641371.0	0.510	1.335
1_85	7	457784.3	1641346.1	457750.7	1641301.2	1.335	2.023
1_85	8	457717.1	1641256.3	457692.3	1641206.0	2.023	3.012
1_85	9	457667.4	1641155.8	457649.2	1641101.0	3.012	17.666
1_85	10	457631.0	1641046.3	457628.0	1640991.8	17.666	-138.580
1_85	11	457624.9	1640937.4	457625.3	1640881.3	-138.580	-17.215
1_85	12	457625.7	1640825.2	457628.9	1640769.2	-17.215	-5.373
1_85	13	457632.2	1640713.3	457642.5	1640658.1	-5.373	-10.385
1_85	14	457652.7	1640602.9	457658.1	1640547.1	-10.385	-42.328
1_85	15	457663.5	1640491.3	457664.8	1640435.2	-42.328	17.698
1_85	16	457666.1	1640379.1	457663.0	1640323.1	17.698	10.715
1_85	17	457659.8	1640267.1	457654.6	1640211.3	10.715	3.783
1_85	18	457649.4	1640155.5	457635.0	1640101.3		
1_85	19 (d/s)	457620.7	1640047.0				

input (GIS)

Tangent Slopes (ft/ft)		Tangent Intercepts (ft)		Centroid Coordinates (ft)		R (ft)	width (ft)
a	c	b	d	x _c	y _c		
4.573	7.800	-454639.3	-1932984.4	458112.3	1640163.2	1247	242
7.800	8.142	-1932984.4	-2088834.7	455579.0	1620404.2	21167	265
8.142	-157.380	-2088834.7	73729106.3	458053.3	1640549.5	872	256
-157.380	-4.783	73729106.3	3831836.4	458051.3	1640860.9	561	244
-4.783	-1.961	3831836.4	2539333.4	458022.1	1641000.7	419	238
-1.961	-0.749	2539333.4	1984104.3	457941.9	1641158.1	245	292
-0.749	-0.494	1984104.3	1867503.4	458238.3	1640936.1	612	280
-0.494	-0.332	1867503.4	1793051.7	458427.0	1640842.8	822	220
-0.332	-0.057	1793051.7	1666896.9	458049.9	1640968.0	426	206
-0.057	0.007	1666896.9	1637579.1	459359.5	1640893.8	1735	251
0.007	0.058	1637579.1	1614186.7	459832.5	1640897.2	2208	328
0.058	0.186	1614186.7	1555482.5	458516.6	1640820.8	891	417
0.186	0.096	1555482.5	1596478.4	456390.0	1640425.0	1275	474
0.096	0.024	1596478.4	1629622.9	456115.9	1640398.6	1550	470
0.024	-0.057	1629622.9	1666182.3	456264.5	1640402.1	1402	446
-0.057	-0.093	1666182.3	1682924.1	454606.3	1640495.8	3062	387
-0.093	-0.264	1682924.1	1761088.6	456981.1	1640274.2	679	336
							289
							298

Apex (est.)

245 **313**
(Minimum) (Average)

Table K-3: Radius of curvature calculations for bend 1 (1992).

Bend	1
Year	1992
Depth (ft)	2.73 (avg.)

Bend id	Point id	GIS Coordinates (ft)		GIS Coordinates (ft)		Midpoint Slopes (ft/ft)	
		X _{CL}	Y _{CL}	X _{mid}	Y _{mid}	m	p
1_92	1 (u/s)	458469.6	1641313.8	458411.5	1641325.9	-0.207	-0.256
1_92	2	458353.3	1641337.9	458298.3	1641352.0	-0.256	-0.209
1_92	3	458243.3	1641366.1	458183.6	1641378.5	-0.209	-0.016
1_92	4	458124.0	1641391.0	458068.8	1641391.9	-0.016	0.054
1_92	5	458013.7	1641392.8	457955.8	1641389.6	0.054	0.403
1_92	6	457898.0	1641386.5	457841.4	1641363.7	0.403	1.145
1_92	7	457784.7	1641340.8	457749.3	1641300.3	1.145	1.977
1_92	8	457713.8	1641259.7	457687.7	1641208.0	1.977	2.409
1_92	9	457661.5	1641156.3	457639.2	1641102.6	2.409	2.345
1_92	10	457617.0	1641049.0	457594.5	1640996.3	2.345	2.444
1_92	11	457572.1	1640943.7	457549.2	1640887.8	2.444	8.989
1_92	12	457526.4	1640832.0	457520.0	1640774.2	8.989	-7.332
1_92	13	457513.5	1640716.5	457521.1	1640660.9	-7.332	-2.727
1_92	14	457528.7	1640605.4	457549.6	1640548.3	-2.727	-2.093
1_92	15	457570.5	1640491.3	457594.4	1640441.4	-2.093	-5.493
1_92	16	457618.2	1640391.5	457628.8	1640333.4	-5.493	942.750
1_92	17	457639.4	1640275.3	457639.3	1640218.7	942.750	5.828
1_92	18	457639.2	1640162.1	457629.4	1640104.9		
1_92	19 (d/s)	457619.6	1640047.6				

input (GIS)

Tangent Slopes (ft/ft)		Tangent Intercepts (ft)		Centroid Coordinates (ft)		R (ft)	width (ft)
a	c	b	d	x _c	y _c		
4.830	3.906	-572679.7	-148891.0	458918.5	1643774.6	2501	164
3.906	4.781	-148891.0	-549128.3	457641.0	1638784.4	2651	170
4.781	63.746	-549128.3	-27558508.9	458059.3	1640784.1	610	215
63.746	-18.537	-27558508.9	10130452.4	458043.3	1639767.7	1625	230
-18.537	-2.479	10130452.4	2776449.5	457975.1	1641032.0	363	228
-2.479	-0.874	2776449.5	2041203.0	457930.9	1641141.5	247	240
-0.874	-0.506	2041203.0	1872750.9	458084.9	1641007.0	449	217
-0.506	-0.415	1872750.9	1831050.0	459069.0	1640509.2	1549	193
-0.415	-0.426	1831050.0	1836102.2	446559.8	1645701.2	11996	192
-0.426	-0.409	1836102.2	1828076.4	464953.4	1637858.7	8000	193
-0.409	-0.111	1828076.4	1691671.4	457941.6	1640727.3	428	193
-0.111	0.136	1691671.4	1578260.4	457978.1	1640723.2	465	188
0.136	0.367	1578260.4	1472748.1	458055.2	1640733.7	542	216
0.367	0.478	1472748.1	1421823.2	458705.4	1640972.2	1233	277
0.478	0.182	1421823.2	1557027.9	457207.9	1640256.8	432	347
0.182	-0.001	1557027.9	1640704.1	457002.5	1640219.4	639	414
-0.001	-0.172	1640704.1	1718627.6	456961.8	1640219.4	680	378
							289
							267

Apex (est.)

247 **243**
(Minimum) (Average)

Table K-4: Radius of curvature calculations for bend 2 (1972).

Bend	2
Year	1972
Depth (ft)	3.13 (avg.)

Bend id	Point id	GIS Coordinates (ft)		GIS Coordinates (ft)		Midpoint Slopes (ft/ft)	
		X _{CL}	Y _{CL}	X _{mid}	Y _{mid}	m	p
2_72	1 (u/s)	457857.1	1640923.2	457846.5	1640873.1	4.730	4.730
2_72	2	457835.9	1640823.0	457825.4	1640773.0	4.730	3.877
2_72	3	457814.8	1640722.9	457802.0	1640673.4	3.877	2.927
2_72	4	457789.3	1640623.9	457772.7	1640575.5	2.927	2.676
2_72	5	457756.2	1640527.1	457738.3	1640479.2	2.676	2.285
2_72	6	457720.4	1640431.3	457699.8	1640384.4	2.285	2.286
2_72	7	457679.3	1640337.5	457658.8	1640290.6	2.286	2.286
2_72	8	457638.3	1640243.7	457617.8	1640196.9	2.286	1.677
2_72	9	457597.3	1640150.0	457571.2	1640106.2	1.677	1.264
2_72	10	457545.1	1640062.4	457513.3	1640022.3	1.264	1.264
2_72	11	457481.6	1639982.2	457449.8	1639942.0	1.264	1.098
2_72	12	457418.1	1639901.9	457383.7	1639864.1	1.098	0.870
2_72	13	457349.3	1639826.3	457310.9	1639792.9	0.870	0.667
2_72	14	457272.4	1639759.5	457229.8	1639731.1	0.667	0.913
2_72	15	457187.3	1639702.7	457149.6	1639668.3	0.913	1.000
2_72	16	457111.9	1639633.9	457075.7	1639597.7	1.000	1.000
2_72	17	457039.5	1639561.5	457003.4	1639525.4	1.000	1.015
2_72	18	456967.2	1639489.2	456931.3	1639452.7	1.015	1.069
2_72	19	456895.4	1639416.3	456860.4	1639378.9	1.069	1.199
2_72	20	456825.4	1639341.5	456792.8	1639302.3	1.199	1.623
2_72	21	456760.2	1639263.2	456733.3	1639219.6		
2_72	22 (d/s)	456706.5	1639176.1				

input (GIS)

Tangent Slopes (ft/ft)		Tangent Intercepts (ft)		Centroid Coordinates (ft)		R (ft)	width (ft)
a	c	b	d	x _c	y _c		
-0.211	-0.211	1737663.7	1737559.1	#####	#####	#####	338
-0.211	-0.258	1737559.1	1758756.2	455556.7	1641252.6	2319	269
-0.258	-0.342	1758756.2	1796963.1	456512.6	1641006.0	1333	223
-0.342	-0.374	1796963.1	1811533.8	454367.4	1641738.9	3599	227
-0.374	-0.438	1811533.8	1840655.5	455990.9	1641132.2	1866	229
-0.438	-0.437	1840655.5	1840495.0	1505265.7	1182011.5	1143460	271
-0.437	-0.438	1840495.0	1840410.7	-1404849.0	2455050.9	2032921	253
-0.438	-0.596	1840410.7	1912934.3	456871.6	1640523.3	816	235
-0.596	-0.791	1912934.3	2001952.0	456905.7	1640503.0	777	219
-0.791	-0.791	2001952.0	2001776.4	1781870.6	592349.6	1688650	222
-0.791	-0.910	2001776.4	2056267.3	456293.1	1640857.0	1476	197
-0.910	-1.150	2056267.3	2165628.6	456736.5	1640453.3	877	179
-1.150	-1.500	2165628.6	2325495.3	456787.0	1640395.3	800	181
-1.500	-1.096	2325495.3	2140637.7	457602.9	1639171.5	674	189
-1.096	-1.000	2140637.7	2096610.3	458654.0	1638019.7	2232	227
-1.000	-1.000	2096610.3	2096591.9	-66774.5	2163375.6	740785	236
-1.000	-0.985	2096591.9	2089428.5	466354.9	1630172.5	13226	237
-0.985	-0.935	2089428.5	2066600.8	459752.9	1636674.0	3961	228
-0.935	-0.834	2066600.8	2020138.0	458170.8	1638153.5	1795	219
-0.834	-0.616	2020138.0	1920713.7	457341.9	1638844.5	717	203
							167
							161

Apex (est.)

674 223
(Minimum) (Average)

Table K-5: Radius of curvature calculations for bend 2 (1985).

Bend	2
Year	1985
Depth (ft)	3.21 (avg.)

Bend id	Point id	GIS Coordinates (ft)		GIS Coordinates (ft)		Midpoint Slopes (ft/ft)	
		X _{CL}	Y _{CL}	X _{mid}	Y _{mid}	m	p
2_85	1 (u/s)	457623.8	1640921.2	457624.4	1640866.6	-99.218	-15.348
2_85	2	457624.9	1640812.0	457628.4	1640759.4	-15.348	-5.025
2_85	3	457631.8	1640706.7	457642.4	1640653.6	-5.025	-10.183
2_85	4	457652.9	1640600.4	457657.8	1640550.5	-10.183	-24.204
2_85	5	457662.7	1640500.6	457665.0	1640445.3	-24.204	18.964
2_85	6	457667.3	1640390.0	457664.5	1640336.6	18.964	8.640
2_85	7	457661.7	1640283.2	457655.5	1640230.0	8.640	4.694
2_85	8	457649.4	1640176.7	457638.5	1640125.8	4.694	3.274
2_85	9	457627.7	1640074.9	457611.6	1640022.3	3.274	2.181
2_85	10	457595.5	1639969.6	457573.6	1639921.9	2.181	1.347
2_85	11	457551.7	1639874.1	457520.9	1639832.6	1.347	0.788
2_85	12	457490.1	1639791.1	457448.0	1639757.9	0.788	0.653
2_85	13	457405.8	1639724.7	457361.6	1639695.8	0.653	0.534
2_85	14	457317.3	1639666.9	457269.9	1639641.5	0.534	0.551
2_85	15	457222.5	1639616.2	457176.4	1639590.8	0.551	0.525
2_85	16	457130.3	1639565.4	457083.0	1639540.6	0.525	0.509
2_85	17	457035.7	1639515.7	456989.0	1639491.9	0.509	0.554
2_85	18	456942.3	1639468.1	456894.7	1639441.8	0.554	0.798
2_85	19	456847.1	1639415.4	456806.0	1639382.6	0.798	1.263
2_85	20	456764.8	1639349.7	456732.2	1639308.5	1.263	1.635
2_85	21	456699.5	1639267.3	456671.5	1639221.5		
2_85	22 (d/s)	456643.5	1639175.7				

input (GIS)

Tangent Slopes (ft/ft)		Tangent Intercepts (ft)		Centroid Coordinates (ft)		R (ft)	width (ft)
a	c	b	d	x _c	y _c		
0.010	0.065	1636254.3	1610943.3	459575.8	1640886.3	1952	338
0.065	0.199	1610943.3	1549572.8	458439.5	1640812.2	815	425
0.199	0.098	1549572.8	1595605.7	456605.1	1640447.1	1059	474
0.098	0.041	1595605.7	1621536.3	455803.4	1640368.4	1864	469
0.041	-0.053	1621536.3	1664469.4	456509.0	1640397.6	1158	451
-0.053	-0.116	1664469.4	1693200.0	455955.5	1640426.7	1712	395
-0.116	-0.213	1693200.0	1737622.9	456547.7	1640358.2	1117	343
-0.213	-0.305	1737622.9	1779779.2	456428.5	1640383.6	1238	292
-0.305	-0.459	1779779.2	1849738.9	456842.3	1640257.2	806	286
-0.459	-0.742	1849738.9	1979376.1	457121.0	1640129.4	501	291
-0.742	-1.269	1979376.1	2220211.3	457203.4	1640068.3	399	334
-1.269	-1.531	2220211.3	2339692.2	456705.0	1640700.7	1202	371
-1.531	-1.872	2339692.2	2495668.1	456700.3	1640707.9	1210	384
-1.872	-1.816	2495668.1	2469601.4	461170.5	1632339.4	8279	354
-1.816	-1.904	2469601.4	2509754.5	454593.8	1644279.6	5353	323
-1.904	-1.963	2509754.5	2536466.1	453127.8	1647070.5	8506	279
-1.963	-1.805	2536466.1	2464279.8	458387.9	1636746.2	3082	239
-1.805	-1.253	2464279.8	2211884.9	457203.4	1638884.5	639	185
-1.253	-0.792	2211884.9	2000994.3	457093.2	1639022.6	464	150
-0.792	-0.612	2000994.3	1918550.6	457420.8	1638763.2	880	148
							140
							124

Apex (est.)

399 **309**
(Minimum) (Average)

Table K-6: Radius of curvature calculations for bend 2 (1992).

Bend	2
Year	1992
Depth (ft)	3.21 (avg.)

Bend id	Point id	GIS Coordinates (ft)		GIS Coordinates (ft)		Midpoint Slopes (ft/ft)	
		X _{CL}	Y _{CL}	X _{mid}	Y _{mid}	m	p
2_92	1 (u/s)	457557.9	1640921.2	457541.3	1640868.3	3.190	8.934
2_92	2	457524.7	1640815.3	457518.4	1640759.0	8.934	-5.895
2_92	3	457512.1	1640702.7	457521.4	1640647.8	-5.895	-2.670
2_92	4	457530.7	1640592.9	457549.3	1640543.3	-2.670	-1.990
2_92	5	457567.9	1640493.7	457593.8	1640442.1	-1.990	-5.638
2_92	6	457619.8	1640390.4	457629.1	1640338.0	-5.638	-68.503
2_92	7	457638.4	1640285.5	457639.2	1640229.0	-68.503	6.242
2_92	8	457640.0	1640172.5	457631.2	1640117.1	6.242	4.378
2_92	9	457622.3	1640061.8	457610.2	1640008.8	4.378	4.540
2_92	10	457598.1	1639955.9	457585.9	1639900.6	4.540	5.108
2_92	11	457573.8	1639845.3	457563.4	1639792.3	5.108	2.606
2_92	12	457553.0	1639739.4	457533.2	1639687.8	2.606	1.414
2_92	13	457513.4	1639636.1	457480.6	1639589.8	1.414	0.872
2_92	14	457447.9	1639543.5	457404.9	1639506.1	0.872	0.509
2_92	15	457361.9	1639468.6	457313.3	1639443.8	0.509	0.276
2_92	16	457264.7	1639419.1	457212.0	1639404.5	0.276	0.169
2_92	17	457159.3	1639390.0	457104.1	1639380.6	0.169	0.137
2_92	18	457048.9	1639371.3	456992.8	1639363.6	0.137	0.227
2_92	19	456936.7	1639356.0	456884.4	1639344.1	0.227	0.744
2_92	20	456832.0	1639332.2	456788.2	1639299.6	0.744	1.564
2_92	21	456744.4	1639267.0	456715.2	1639221.4		
2_92	22 (d/s)	456686.0	1639175.7				

input (GIS)

Tangent Slopes (ft/ft)		Tangent Intercepts (ft)		Centroid Coordinates (ft)		R (ft)	width (ft)
a	c	b	d	x _c	y _c		
-0.313	-0.112	1784287.7	1691968.9	458096.1	1640694.4	584	195
-0.112	0.170	1691968.9	1563040.3	457915.3	1640714.6	403	188
0.170	0.375	1563040.3	1469169.9	458082.3	1640742.9	572	222
0.375	0.503	1469169.9	1410470.9	458514.7	1640904.9	1032	284
0.503	0.177	1410470.9	1559166.8	457254.5	1640271.5	384	339
0.177	0.015	1559166.8	1633548.4	456958.7	1640219.1	683	413
0.015	-0.160	1633548.4	1713432.4	456992.0	1640219.5	650	386
-0.160	-0.228	1713432.4	1744527.7	455973.0	1640382.8	1680	295
-0.228	-0.220	1744527.7	1740694.5	471585.6	1636816.9	14335	257
-0.220	-0.196	1740694.5	1729378.5	462188.0	1638886.9	4713	255
-0.196	-0.384	1729378.5	1815290.4	456945.5	1639913.3	632	237
-0.384	-0.707	1815290.4	1963185.8	457115.7	1639848.0	451	211
-0.707	-1.147	1963185.8	2164328.9	457092.7	1639864.2	479	189
-1.147	-1.964	2164328.9	2537711.4	457108.4	1639846.2	455	184
-1.964	-3.618	2537711.4	3293403.8	457067.9	1639925.8	544	219
-3.618	-5.920	3293403.8	4345240.8	456924.2	1640445.7	1082	222
-5.920	-7.307	4345240.8	4978537.2	456505.7	1642922.7	3593	209
-7.307	-4.410	4978537.2	3654331.3	457164.7	1638108.0	1269	191
-4.410	-1.344	3654331.3	2253371.5	456941.1	1639094.1	262	219
-1.344	-0.639	2253371.5	1931177.0	456965.4	1639061.4	302	223
							198
							191

Apex (est.)

262 **242**
(Minimum) **(Average)**

Table K-7: Radius of curvature calculations for bend 3 (1972).

Bend	3
Year	1972
Depth (ft)	3.12 (avg.)

Bend id	Point id	GIS Coordinates (ft)		GIS Coordinates (ft)		Midpoint Slopes (ft/ft)	
		X _{CL}	Y _{CL}	X _{mid}	Y _{mid}	m	p
3 72	1 (u/s)	456639.9	1638228.3	456638.1	1638178.0	27.618	31.803
3 72	2	456636.3	1638127.8	456634.7	1638078.6	31.803	32.973
3 72	3	456633.2	1638029.5	456631.7	1637981.5	32.973	17.982
3 72	4	456630.3	1637933.6	456627.6	1637884.5	17.982	3.429
3 72	5	456624.8	1637835.4	456611.0	1637788.0	3.429	3.411
3 72	6	456597.2	1637740.5	456583.5	1637693.9	3.411	2.414
3 72	7	456569.8	1637647.3	456551.0	1637601.8	2.414	2.414
3 72	8	456532.1	1637556.2	456513.4	1637511.1	2.414	1.524
3 72	9	456494.7	1637466.0	456468.4	1637425.8	1.524	1.432
3 72	10	456442.0	1637385.7	456413.5	1637344.8	1.432	1.516
3 72	11	456385.0	1637304.0	456359.5	1637265.3	1.516	1.516
3 72	12	456334.0	1637226.6	456305.4	1637183.4	1.516	1.435
3 72	13	456276.9	1637140.1	456249.1	1637100.2	1.435	1.407
3 72	14	456221.3	1637060.3	456193.6	1637021.3	1.407	1.393
3 72	15	456165.9	1636982.3	456137.7	1636943.1	1.393	1.420
3 72	16	456109.6	1636903.9	456081.8	1636864.4	1.420	1.563
3 72	17	456054.0	1636825.0	456026.3	1636781.7	1.563	1.588
3 72	18	455998.6	1636738.4	455973.7	1636698.9	1.588	1.727
3 72	19	455948.9	1636659.4	455924.6	1636617.5		
3 72	20 (d/s)	455900.4	1636575.6				

input (GIS)

Tangent Slopes (ft/ft)		Tangent Intercepts (ft)		Centroid Coordinates (ft)		R (ft)	width (ft)
a	c	b	d	x _c	y _c		
-0.036	-0.031	1654712.0	1652437.0	477524.6	1637421.8	20900	185
-0.031	-0.030	1652437.0	1651830.4	543757.0	1635339.2	87165	208
-0.030	-0.056	1651830.4	1663278.5	452783.5	1638098.2	3850	241
-0.056	-0.292	1663278.5	1770958.1	456198.2	1637908.3	433	267
-0.292	-0.293	1770958.1	1771539.5	388406.2	1657679.8	71046	246
-0.293	-0.414	1771539.5	1826720.0	455711.3	1637949.6	910	212
-0.414	-0.414	1826720.0	1826612.1	29546806.4	-10412523.8	31487275	236
-0.414	-0.656	1826612.1	1936871.4	456038.4	1637707.9	516	224
-0.656	-0.698	1936871.4	1956101.8	453654.0	1639272.1	3366	262
-0.698	-0.660	1956101.8	1938262.1	459378.7	1635274.0	3617	300
-0.660	-0.660	1938262.1	1938169.9	-1660984.9	3033782.5	2536416	322
-0.660	-0.697	1938169.9	1954970.7	453005.1	1639360.3	3954	314
-0.697	-0.711	1954970.7	1961303.5	447877.2	1642932.9	10204	350
-0.711	-0.718	1961303.5	1964501.2	439913.5	1648593.9	19974	344
-0.718	-0.704	1964501.2	1958046.3	464634.9	1630841.1	10461	355
-0.704	-0.640	1958046.3	1928516.4	457915.8	1635572.9	2244	301
-0.640	-0.630	1928516.4	1923769.9	467435.8	1629482.6	13545	251
-0.630	-0.579	1923769.9	1900588.2	458143.6	1635332.8	2565	211
							197
							187

Apex (est.)

433 **261**
(Minimum) **(Average)**

Table K-8: Radius of curvature calculations for bend 3 (1985).

Bend	3
Year	1985
Depth (ft)	2.94 (avg.)

Bend id	Point id	GIS Coordinates (ft)		GIS Coordinates (ft)		Midpoint Slopes (ft/ft)	
		X _{CL}	Y _{CL}	X _{mid}	Y _{mid}	m	p
3_85	1 (u/s)	456570.8	1638229.3	456573.6	1638165.5	-22.680	-7.944
3_85	2	456576.4	1638101.6	456584.6	1638036.6	-7.944	-4.023
3_85	3	456592.8	1637971.5	456607.4	1637912.8	-4.023	-2.467
3_85	4	456622.0	1637854.2	456645.2	1637796.8	-2.467	-2.392
3_85	5	456668.5	1637739.4	456693.1	1637680.5	-2.392	-2.335
3_85	6	456717.8	1637621.6	456743.7	1637561.1	-2.335	-4.466
3_85	7	456769.6	1637500.6	456782.6	1637442.4	-4.466	-46.888
3_85	8	456795.6	1637384.2	456797.0	1637319.2	-46.888	6.806
3_85	9	456798.4	1637254.3	456789.0	1637190.0	6.806	1.832
3_85	10	456779.5	1637125.8	456750.0	1637071.8	1.832	1.071
3_85	11	456720.5	1637017.7	456679.1	1636973.3	1.071	0.271
3_85	12	456637.6	1636928.9	456575.7	1636912.1	0.271	0.254
3_85	13	456513.8	1636895.3	456452.7	1636879.7	0.254	0.278
3_85	14	456391.5	1636864.2	456330.5	1636847.2	0.278	0.354
3_85	15	456269.4	1636830.2	456211.0	1636809.5	0.354	0.361
3_85	16	456152.6	1636788.8	456090.6	1636766.5	0.361	0.393
3_85	17	456028.6	1636744.1	455970.3	1636721.2	0.393	0.477
3_85	18	455912.1	1636698.4	455854.3	1636670.8	0.477	0.667
3_85	19	455796.6	1636643.3	455747.3	1636610.5		
3_85	20 (d/s)	455698.1	1636577.6				

input (GIS)

Tangent Slopes (ft/ft)		Tangent Intercepts (ft)		Centroid Coordinates (ft)		R (ft)	width (ft)
a	c	b	d	x _c	y _c		
0.044	0.126	1618034.6	1580564.4	458166.8	1638235.7	1596	376
0.126	0.249	1580564.4	1524403.3	457638.9	1638169.3	1065	372
0.249	0.405	1524403.3	1452697.2	457445.7	1638121.2	866	278
0.405	0.418	1452697.2	1446729.3	467321.7	1642124.4	11520	268
0.418	0.428	1446729.3	1441981.0	470671.2	1643524.9	15151	259
0.428	0.224	1441981.0	1535163.6	456120.0	1637294.0	682	250
0.224	0.021	1535163.6	1627576.9	456173.2	1637305.9	627	245
0.021	-0.147	1627576.9	1704309.5	456022.2	1637302.7	778	283
-0.147	-0.546	1704309.5	1886365.6	456439.1	1637241.4	360	342
-0.546	-0.933	1886365.6	2063262.0	456325.3	1637303.6	488	375
-0.933	-3.683	2063262.0	3318625.8	456518.3	1637123.4	228	401
-3.683	-3.931	3318625.8	3431418.4	454496.0	1644572.4	7938	378
-3.931	-3.598	3431418.4	3278830.4	457869.6	1631309.0	5748	334
-3.598	-2.821	3278830.4	2923877.9	456812.7	1635112.0	1802	361
-2.821	-2.773	2923877.9	2901645.5	464080.4	1614608.3	23555	328
-2.773	-2.546	2901645.5	2797835.3	457639.9	1632469.8	4568	296
-2.546	-2.098	2797835.3	2592988.3	456625.1	1635053.8	1793	257
-2.098	-1.499	2592988.3	2319953.9	456223.3	1635896.7	860	208
							237
							309

Apex (est.)

228 **308**
(Minimum) **(Average)**

Table K-9: Radius of curvature calculations for bend 3 (1992).

Bend	3
Year	1992
Depth (ft)	2.93 (avg.)

Bend id	Point id	GIS Coordinates (ft)		GIS Coordinates (ft)		Midpoint Slopes (ft/ft)	
		X _{CL}	Y _{CL}	X _{mid}	Y _{mid}	m	p
3_92	1 (u/s)	456628.6	1638229.3	456640.5	1638163.0	-5.576	-15.278
3_92	2	456652.4	1638096.7	456656.4	1638034.5	-15.278	4.423
3_92	3	456660.5	1637972.3	456646.6	1637911.0	4.423	4.759
3_92	4	456632.8	1637849.7	456621.0	1637793.7	4.759	-8.124
3_92	5	456609.2	1637737.6	456617.3	1637671.9	-8.124	-10.227
3_92	6	456625.4	1637606.1	456631.5	1637544.0	-10.227	-56.704
3_92	7	456637.6	1637481.9	456638.7	1637417.9	-56.704	22.283
3_92	8	456639.8	1637353.8	456636.9	1637290.0	22.283	7.612
3_92	9	456634.1	1637226.1	456625.3	1637159.6	7.612	2.471
3_92	10	456616.6	1637093.1	456593.1	1637035.0	2.471	1.246
3_92	11	456569.6	1636977.0	456530.6	1636928.4	1.246	0.537
3_92	12	456491.7	1636879.8	456434.1	1636848.9	0.537	0.279
3_92	13	456376.5	1636818.0	456316.2	1636801.1	0.279	0.197
3_92	14	456256.0	1636784.3	456191.9	1636771.7	0.197	0.190
3_92	15	456127.8	1636759.1	456067.1	1636747.6	0.190	0.181
3_92	16	456006.5	1636736.1	455940.0	1636724.0	0.181	0.318
3_92	17	455873.4	1636712.0	455813.0	1636692.8	0.318	0.371
3_92	18	455752.6	1636673.6	455694.0	1636651.8	0.371	0.449
3_92	19	455635.4	1636630.1	455576.9	1636603.9		
3_92	20 (d/s)	455518.4	1636577.6				

input (GIS)

Tangent Slopes (ft/ft)		Tangent Intercepts (ft)		Centroid Coordinates (ft)		R (ft)	width (ft)
a	c	b	d	x _c	y _c		
0.179	0.065	1556267.2	1608144.0	455502.9	1637959.0	1158	354
0.065	-0.226	1608144.0	1741150.9	456225.3	1638006.3	437	422
-0.226	-0.210	1741150.9	1733737.8	464334.2	1636173.0	7882	448
-0.210	0.123	1733737.8	1581462.6	456985.2	1637717.1	377	391
0.123	0.098	1581462.6	1592892.3	451512.7	1637043.5	5144	335
0.098	0.018	1592892.3	1629364.8	455056.0	1637390.0	1584	347
0.018	-0.045	1629364.8	1657782.8	454591.2	1637381.8	2049	386
-0.045	-0.131	1657782.8	1697146.1	455112.0	1637358.4	1528	451
-0.131	-0.405	1697146.1	1821820.3	456121.9	1637225.7	512	525
-0.405	-0.802	1821820.3	2003223.9	456198.9	1637194.6	430	569
-0.802	-1.862	2003223.9	2486620.6	456285.9	1637124.8	320	580
-1.862	-3.582	2486620.6	3271267.6	456160.9	1637357.4	581	566
-3.582	-5.084	3271267.6	3955897.7	455875.6	1638379.3	1640	524
-5.084	-5.264	3955897.7	4037684.6	452426.2	1655915.0	19510	444
-5.264	-5.532	4037684.6	4158985.5	453349.9	1651052.5	14561	298
-5.532	-3.145	4158985.5	3070349.9	456120.4	1635726.1	1016	214
-3.145	-2.696	3070349.9	2865285.9	456618.7	1634158.6	2660	134
-2.696	-2.229	2865285.9	2652102.8	456355.5	1634868.3	1903	142
							131
							130

Apex (est.)

320 **370**
(Minimum) **(Average)**

Table K-10: Radius of curvature calculations for bend 4 (1972).

Bend	4
Year	1972
Depth (ft)	3.47 (avg.)

Bend id	Point id	GIS Coordinates (ft)		GIS Coordinates (ft)		Midpoint Slopes (ft/ft)	
		X _{CL}	Y _{CL}	X _{mid}	Y _{mid}	m	p
4_72	1 (u/s)	456215.3	1637057.4	456189.2	1637017.3	1.537	1.368
4_72	2	456163.0	1636977.1	456134.8	1636938.4	1.368	1.409
4_72	3	456106.6	1636899.8	456078.4	1636860.2	1.409	1.588
4_72	4	456050.3	1636820.6	456024.9	1636780.2	1.588	1.588
4_72	5	455999.5	1636739.9	455974.0	1636699.4	1.588	1.739
4_72	6	455948.5	1636658.9	455924.4	1636616.9	1.739	2.501
4_72	7	455900.2	1636574.9	455882.8	1636531.4	2.501	3.186
4_72	8	455865.4	1636487.9	455850.8	1636441.3	3.186	3.729
4_72	9	455836.2	1636394.7	455823.6	1636347.6	3.729	5.366
4_72	10	455810.9	1636300.6	455802.2	1636253.9	5.366	8.667
4_72	11	455793.6	1636207.3	455788.0	1636159.0	8.667	10.510
4_72	12	455782.4	1636110.6	455777.8	1636062.7	10.510	21.811
4_72	13	455773.3	1636014.7	455771.1	1635966.8	21.811	26.621
4_72	14	455768.9	1635918.9	455767.1	1635872.6	26.621	17.607
4_72	15	455765.4	1635826.3	455762.6	1635776.8	17.607	12.131
4_72	16	455759.8	1635727.3	455755.9	1635679.8	12.131	12.615
4_72	17	455751.9	1635632.2	455748.2	1635584.4	12.615	13.604
4_72	18	455744.4	1635536.6	455740.8	1635488.7	13.604	13.116
4_72	19	455737.3	1635440.8	455733.8	1635395.0		
4_72	20 (d/s)	455730.3	1635349.2				

input (GIS)

Tangent Slopes (ft/ft)		Tangent Intercepts (ft)		Centroid Coordinates (ft)		R (ft)	width (ft)
a	c	b	d	x _c	y _c		
-0.650	-0.731	1933764.4	1970304.0	454713.7	1637977.1	1761	409
-0.731	-0.710	1970304.0	1960549.2	461731.0	1632848.4	6932	347
-0.710	-0.630	1960549.2	1923907.0	457497.6	1635853.0	1741	301
-0.630	-0.630	1923907.0	1923773.3	2925108.0	82172.3	2917735	254
-0.630	-0.575	1923773.3	1898844.0	458013.8	1635415.1	2411	216
-0.575	-0.400	1898844.0	1818821.7	456506.9	1636281.9	674	201
-0.400	-0.314	1818821.7	1779536.8	457048.1	1636065.5	1256	185
-0.314	-0.268	1779536.8	1758598.1	458059.3	1635748.0	2315	158
-0.268	-0.186	1758598.1	1721200.9	457017.3	1636027.5	1237	144
-0.186	-0.115	1721200.9	1688746.3	457163.3	1636000.3	1385	152
-0.115	-0.095	1688746.3	1679427.1	460595.2	1635604.3	4839	153
-0.095	-0.046	1679427.1	1656863.3	457728.6	1635877.1	1960	156
-0.046	-0.038	1656863.3	1652993.4	467159.9	1635444.6	11401	186
-0.038	-0.057	1652993.4	1661662.5	450772.6	1636060.2	4998	194
-0.057	-0.082	1661662.5	1673248.1	451955.8	1635993.0	3813	178
-0.082	-0.079	1673248.1	1671712.5	486140.1	1633175.2	30487	178
-0.079	-0.074	1671712.5	1668990.0	472447.4	1634260.6	16752	185
-0.074	-0.076	1668990.0	1670141.7	421264.0	1638023.1	34570	187
							206
							257

Apex (est.)

674 **212**
(Minimum) **(Average)**

Table K-11: Radius of curvature calculations for bend 4 (1985).

Bend	4
Year	1985
Depth (ft)	3.14 (avg.)

Bend id	Point id	GIS Coordinates (ft)		GIS Coordinates (ft)		Midpoint Slopes (ft/ft)	
		X _{CL}	Y _{CL}	X _{mid}	Y _{mid}	m	p
4_85	1 (u/s)	456741.8	1637057.4	456702.9	1637003.2	1.394	0.391
4_85	2	456664.0	1636949.0	456607.2	1636926.8	0.391	0.254
4_85	3	456550.3	1636904.6	456486.9	1636888.4	0.254	0.258
4_85	4	456423.5	1636872.3	456360.0	1636856.0	0.258	0.350
4_85	5	456296.4	1636839.6	456235.0	1636818.1	0.350	0.361
4_85	6	456173.6	1636796.6	456111.8	1636774.3	0.361	0.388
4_85	7	456050.0	1636751.9	455989.2	1636728.3	0.388	0.462
4_85	8	455928.3	1636704.8	455869.7	1636677.7	0.462	0.628
4_85	9	455811.0	1636650.6	455756.8	1636616.5	0.628	1.164
4_85	10	455702.6	1636582.5	455660.3	1636533.2	1.164	3.086
4_85	11	455617.9	1636483.9	455598.8	1636424.9	3.086	52.441
4_85	12	455579.6	1636365.8	455578.4	1636298.7	52.441	-5.309
4_85	13	455577.1	1636231.5	455589.0	1636168.2	-5.309	-4.287
4_85	14	455600.9	1636104.9	455615.7	1636041.6	-4.287	-4.283
4_85	15	455630.5	1635978.2	455645.4	1635914.2	-4.283	-3.645
4_85	16	455660.4	1635850.1	455676.7	1635790.6	-3.645	-3.545
4_85	17	455693.1	1635731.1	455711.1	1635667.2	-3.545	-7.720
4_85	18	455729.1	1635603.3	455737.4	1635539.3	-7.720	-18.077
4_85	19	455745.7	1635475.3	455749.2	1635412.3		
4_85	20 (d/s)	455752.7	1635349.2				

input (GIS)

Tangent Slopes (ft/ft)		Tangent Intercepts (ft)		Centroid Coordinates (ft)		R (ft)	width (ft)
a	c	b	d	x _c	y _c		
-0.717	-2.557	1964670.0	2804427.9	456528.3	1637128.5	225	402
-2.557	-3.931	2804427.9	3431412.8	456235.3	1637877.5	1023	401
-3.931	-3.883	3431412.8	3409033.0	467462.0	1593743.7	44519	346
-3.883	-2.854	3409033.0	2939028.7	456743.3	1635367.2	1539	361
-2.854	-2.771	2939028.7	2900662.8	460863.3	1623607.7	13998	337
-2.771	-2.577	2900662.8	2812018.9	457982.3	1631591.2	5511	297
-2.577	-2.166	2812018.9	2624170.9	456741.6	1634788.9	2081	273
-2.166	-1.592	2624170.9	2362146.6	456289.0	1635769.3	1003	214
-1.592	-0.859	2362146.6	2028036.8	455983.8	1636255.2	431	229
-0.859	-0.324	2028036.8	1784035.5	455899.9	1636327.3	323	300
-0.324	-0.019	1784035.5	1644986.0	456013.9	1636290.4	441	392
-0.019	0.188	1644986.0	1550354.0	456216.8	1636286.5	642	396
0.188	0.233	1550354.0	1529762.4	458548.0	1636725.6	3012	396
0.233	0.233	1529762.4	1529525.8	1053863.3	1775591.8	614308	380
0.233	0.274	1529525.8	1510770.4	458878.8	1636669.1	3321	357
0.274	0.282	1510770.4	1507124.1	472944.7	1640528.3	17906	331
0.282	0.130	1507124.1	1576505.8	454850.4	1635424.4	897	289
0.130	0.055	1576505.8	1610201.2	454016.7	1635316.4	1736	225
							172
							155

Apex (est.)

225 **313**
(Minimum) **(Average)**

Table K-12: Radius of curvature calculations for bend 4 (1992).

Bend	4
Year	1992
Depth (ft)	3.18 (avg.)

Bend id	Point id	GIS Coordinates (ft)		GIS Coordinates (ft)		Midpoint Slopes (ft/ft)	
		X _{CL}	Y _{CL}	X _{mid}	Y _{mid}	m	p
4_92	1 (u/s)	456607.8	1637057.4	456574.7	1636995.8	1.867	0.792
4_92	2	456541.7	1636934.1	456489.7	1636892.9	0.792	0.422
4_92	3	456437.8	1636851.7	456372.3	1636824.1	0.422	0.236
4_92	4	456306.8	1636796.5	456241.4	1636781.0	0.236	0.163
4_92	5	456175.9	1636765.6	456109.2	1636754.7	0.163	0.189
4_92	6	456042.6	1636743.9	455972.5	1636730.6	0.189	0.287
4_92	7	455902.4	1636717.4	455837.8	1636698.9	0.287	0.367
4_92	8	455773.2	1636680.3	455709.0	1636656.8	0.367	0.469
4_92	9	455644.9	1636633.2	455579.9	1636602.7	0.469	0.780
4_92	10	455515.0	1636572.2	455461.4	1636530.5	0.780	2.407
4_92	11	455407.9	1636488.8	455381.2	1636424.4	2.407	10.153
4_92	12	455354.4	1636360.0	455347.4	1636289.2	10.153	-5.578
4_92	13	455340.5	1636218.3	455352.6	1636150.8	-5.578	-1.956
4_92	14	455364.7	1636083.4	455395.2	1636023.6	-1.956	-1.764
4_92	15	455425.8	1635963.8	455460.7	1635902.2	-1.764	-1.838
4_92	16	455495.5	1635840.7	455528.6	1635780.0	-1.838	-1.819
4_92	17	455561.6	1635719.2	455595.0	1635658.5	-1.819	-2.419
4_92	18	455628.4	1635597.8	455654.3	1635535.0	-2.419	-3.040
4_92	19	455680.3	1635472.3	455700.5	1635410.7		
4_92	20 (d/s)	455720.8	1635349.2				

input (GIS)

Tangent Slopes (ft/ft)		Tangent Intercepts (ft)		Centroid Coordinates (ft)		R (ft)	width (ft)
a	c	b	d	x _c	y _c		
-0.536	-1.262	1881533.9	2213047.7	456285.5	1637150.7	335	572
-1.262	-2.368	2213047.7	2717705.8	456176.1	1637288.8	509	596
-2.368	-4.243	2717705.8	3572516.3	456053.0	1637580.4	824	565
-4.243	-6.138	3572516.3	4436169.8	455799.5	1638655.8	1927	493
-6.138	-5.292	4436169.8	4049527.7	456993.0	1631330.7	5496	343
-5.292	-3.487	4049527.7	3225984.4	456250.3	1635260.7	1498	240
-3.487	-2.724	3225984.4	2878021.0	456352.9	1634902.8	1870	146
-2.724	-2.130	2878021.0	2606968.6	456262.9	1635148.1	1609	142
-2.130	-1.283	2606968.6	2220813.7	455844.7	1636038.9	627	132
-1.283	-0.415	2220813.7	1825633.3	455622.3	1636324.2	270	131
-0.415	-0.098	1825633.3	1681139.1	455818.2	1636242.8	478	145
-0.098	0.179	1681139.1	1554518.6	455848.7	1636239.8	509	152
0.179	0.511	1554518.6	1403223.7	455801.8	1636231.4	461	156
0.511	0.567	1403223.7	1377775.8	458247.4	1637481.6	3204	147
0.567	0.544	1377775.8	1387940.3	448436.4	1631921.4	8074	179
0.544	0.550	1387940.3	1385205.0	483455.9	1650974.4	31793	177
0.550	0.413	1385205.0	1447186.3	454509.9	1635062.0	1240	165
0.413	0.329	1447186.3	1485496.6	454001.2	1634851.7	1790	139
							104
							146

Apex (est.)

270 **244**
(Minimum) **(Average)**

Table K-13: Radius of curvature calculations for bend 5 (1972).

Bend	5
Year	1972
Depth (ft)	2.58 (avg.)

Bend id	Point id	GIS Coordinates (ft)		GIS Coordinates (ft)		Midpoint Slopes (ft/ft)	
		X _{CL}	Y _{CL}	X _{mid}	Y _{mid}	m	p
5 72	1 (u/s)	455017.1	1631942.6	455051.7	1631907.1	-1.027	-1.189
5 72	2	455086.3	1631871.6	455115.6	1631836.8	-1.189	-1.450
5 72	3	455144.9	1631801.9	455171.0	1631764.0	-1.450	-2.167
5 72	4	455197.1	1631726.1	455216.5	1631684.2	-2.167	-4.538
5 72	5	455235.8	1631642.3	455246.0	1631596.1	-4.538	-12.112
5 72	6	455256.2	1631549.9	455260.0	1631504.0	-12.112	-49.852
5 72	7	455263.8	1631458.1	455264.6	1631414.2	-49.852	2.989
5 72	8	455265.5	1631370.4	455250.4	1631325.1	2.989	2.461
5 72	9	455235.3	1631279.9	455218.1	1631237.7	2.461	1.876
5 72	10	455201.0	1631195.5	455180.4	1631156.9	1.876	1.551
5 72	11	455159.8	1631118.3	455133.3	1631077.2	1.551	1.585
5 72	12	455106.8	1631036.0	455083.7	1630999.4	1.585	1.433
5 72	13	455060.6	1630962.8	455033.4	1630923.9	1.433	1.461
5 72	14	455006.3	1630885.0	454981.3	1630848.5	1.461	1.548
5 72	15	454956.4	1630812.0	454929.8	1630770.9	1.548	1.522
5 72	16	454903.2	1630729.8	454878.6	1630692.4	1.522	1.890
5 72	17	454854.0	1630654.9	454832.5	1630614.2	1.890	2.831
5 72	18	454810.9	1630573.4	454795.5	1630529.9	2.831	4.867
5 72	19	454780.2	1630486.4	454771.6	1630444.7		
5 72	20 (d/s)	454763.0	1630403.0				

input (GIS)

Tangent Slopes (ft/ft)		Tangent Intercepts (ft)		Centroid Coordinates (ft)		R (ft)	width (ft)
a	c	b	d	x _c	y _c		
0.974	0.841	1188838.9	1249155.6	454117.8	1630997.8	1304	535
0.841	0.690	1249155.6	1317906.8	454382.3	1631220.2	959	430
0.690	0.462	1317906.8	1421588.5	454728.9	1631459.2	539	385
0.462	0.220	1421588.5	1531273.5	454824.1	1631503.1	435	322
0.220	0.083	1531273.5	1593916.9	454569.3	1631447.0	695	306
0.083	0.020	1593916.9	1622281.9	453822.1	1631385.3	1443	229
0.020	-0.335	1622281.9	1783629.1	455000.0	1631408.9	268	213
-0.335	-0.406	1783629.1	1816193.7	453849.3	1631793.9	1478	222
-0.406	-0.533	1816193.7	1873817.6	454422.4	1631561.0	860	230
-0.533	-0.645	1873817.6	1924452.9	454192.9	1631683.4	1120	230
-0.645	-0.631	1924452.9	1918035.0	463003.8	1626004.0	9364	263
-0.631	-0.698	1918035.0	1948435.3	453434.0	1632039.9	1951	329
-0.698	-0.685	1948435.3	1942342.0	463478.9	1625030.8	10298	307
-0.685	-0.646	1942342.0	1924632.8	457847.3	1628886.4	3474	298
-0.646	-0.657	1924632.8	1929551.9	444787.1	1637322.6	12075	294
-0.657	-0.529	1929551.9	1871260.1	455680.8	1630165.4	961	289
-0.529	-0.353	1871260.1	1791162.7	455385.8	1630321.4	628	284
-0.353	-0.205	1791162.7	1723875.2	455405.7	1630314.4	649	273
							274
							274

Apex (est.)

268 **299**
(Minimum) **(Average)**

Table K-14: Radius of curvature calculations for bend 5 (1985).

Bend	5
Year	1985
Depth (ft)	2.01 (avg.)

Bend id	Point id	GIS Coordinates (ft)		GIS Coordinates (ft)		Midpoint Slopes (ft/ft)	
		X _{CL}	Y _{CL}	X _{mid}	Y _{mid}	m	p
5 85	1 (u/s)	454515.4	1631942.6	454547.3	1631888.4	-1.700	-0.531
5 85	2	454579.2	1631834.2	454632.5	1631805.9	-0.531	-0.125
5 85	3	454685.8	1631777.6	454747.7	1631769.8	-0.125	0.011
5 85	4	454809.7	1631762.1	454871.2	1631762.8	0.011	0.052
5 85	5	454932.7	1631763.4	454993.4	1631766.6	0.052	-0.288
5 85	6	455054.1	1631769.7	455110.7	1631753.4	-0.288	-1.075
5 85	7	455167.3	1631737.0	455207.9	1631693.4	-1.075	-2.685
5 85	8	455248.5	1631649.9	455269.8	1631592.5	-2.685	-3.873
5 85	9	455291.2	1631535.1	455306.9	1631474.3	-3.873	-7.706
5 85	10	455322.6	1631413.4	455330.4	1631353.2	-7.706	4.365
5 85	11	455338.2	1631293.0	455325.0	1631235.0	4.365	1.908
5 85	12	455311.7	1631177.0	455283.0	1631122.3	1.908	1.763
5 85	13	455254.4	1631067.6	455224.1	1631014.2	1.763	0.762
5 85	14	455193.8	1630960.8	455144.9	1630923.6	0.762	1.025
5 85	15	455096.0	1630886.3	455052.9	1630842.2	1.025	1.122
5 85	16	455009.9	1630798.0	454969.0	1630752.2	1.122	1.004
5 85	17	454928.1	1630706.3	454884.5	1630662.5	1.004	1.336
5 85	18	454840.8	1630618.7	454804.1	1630569.6	1.336	7.931
5 85	19	454767.3	1630520.5	454759.8	1630461.1		
5 85	20 (d/s)	454752.4	1630401.6				

input (GIS)

Tangent Slopes (ft/ft)		Tangent Intercepts (ft)		Centroid Coordinates (ft)		R (ft)	width (ft)
a	c	b	d	x _c	y _c		
0.588	1.882	1364579.2	775998.8	454734.9	1631998.7	227	165
1.882	8.000	775998.8	-2006212.1	454789.1	1632100.8	339	147
8.000	-93.144	-2006212.1	44000255.9	454861.3	1632678.7	918	120
-93.144	-19.407	44000255.9	10461981.8	454839.0	1634763.8	3002	154
-19.407	3.467	10461981.8	53850.3	455011.8	1631410.2	362	174
3.467	0.930	53850.3	1208179.9	455051.5	1631547.9	222	176
0.930	0.372	1208179.9	1462017.2	454985.6	1631486.6	309	262
0.372	0.258	1462017.2	1513916.6	454151.5	1631175.9	1195	235
0.258	0.130	1513916.6	1572263.1	454340.2	1631224.7	1000	388
0.130	-0.229	1572263.1	1735554.9	454997.6	1631310.0	341	413
-0.229	-0.524	1735554.9	1869710.9	454868.4	1631339.6	472	430
-0.524	-0.567	1869710.9	1889278.6	452013.8	1632835.5	3691	437
-0.567	-1.312	1889278.6	2228232.5	454962.9	1631162.4	306	416
-1.312	-0.975	2228232.5	2074660.5	455652.5	1630257.5	840	362
-0.975	-0.892	2074660.5	2036359.7	457019.8	1628923.8	2748	335
-0.892	-0.996	2036359.7	2083781.9	453307.1	1632233.8	2227	288
-0.996	-0.748	2083781.9	1970978.0	455502.6	1630046.8	875	179
-0.748	-0.126	1970978.0	1687798.5	454987.5	1630432.4	237	167
							180
							175

Apex (est.)

222 **260**
(Minimum) **(Average)**

Table K-15: Radius of curvature calculations for bend 5 (1992).

Bend	5
Year	1992
Depth (ft)	2.02 (avg.)

Bend id	Point id	GIS Coordinates (ft)		GIS Coordinates (ft)		Midpoint Slopes (ft/ft)	
		X _{CL}	Y _{CL}	X _{mid}	Y _{mid}	m	p
5_92	1 (u/s)	454718.4	1631942.6	454757.7	1631905.9	-0.933	-0.853
5_92	2	454797.0	1631869.2	454837.8	1631834.5	-0.853	-0.597
5_92	3	454878.5	1631799.7	454923.8	1631772.6	-0.597	-0.475
5_92	4	454969.2	1631745.5	455017.0	1631722.8	-0.475	-0.444
5_92	5	455064.8	1631700.1	455113.9	1631678.3	-0.444	-0.598
5_92	6	455163.1	1631656.6	455208.0	1631629.7	-0.598	-1.414
5_92	7	455252.9	1631602.8	455283.7	1631559.3	-1.414	-3.652
5_92	8	455314.5	1631515.8	455328.5	1631464.7	-3.652	-7.129
5_92	9	455342.4	1631413.7	455349.9	1631360.5	-7.129	8.768
5_92	10	455357.4	1631307.3	455351.4	1631254.9	8.768	4.138
5_92	11	455345.4	1631202.4	455332.9	1631150.5	4.138	1.971
5_92	12	455320.3	1631098.6	455296.7	1631052.0	1.971	0.973
5_92	13	455273.0	1631005.4	455234.9	1630968.3	0.973	1.022
5_92	14	455196.7	1630931.2	455159.2	1630892.8	1.022	1.115
5_92	15	455121.7	1630854.5	455086.4	1630815.2	1.115	1.004
5_92	16	455051.2	1630775.9	455013.8	1630738.4	1.004	2.073
5_92	17	454976.5	1630701.0	454953.3	1630652.7	2.073	3.023
5_92	18	454930.0	1630604.5	454913.4	1630554.3	3.023	3.794
5_92	19	454896.8	1630504.2	454883.3	1630452.9		
5_92	20 (d/s)	454869.8	1630401.6				

input (GIS)

Tangent Slopes (ft/ft)		Tangent Intercepts (ft)		Centroid Coordinates (ft)		R (ft)	width (ft)
a	c	b	d	x _c	y _c		
1.072	1.172	1144559.3	1098910.4	456409.7	1633676.3	2422	551
1.172	1.674	1098910.4	870264.2	455247.7	1632314.8	634	578
1.674	2.107	870264.2	672958.5	455491.9	1632723.6	1109	588
2.107	2.254	672958.5	605766.6	456805.0	1635490.4	4171	562
2.254	1.673	605766.6	870153.9	454759.6	1630879.5	876	533
1.673	0.707	870153.9	1309554.9	455079.6	1631415.0	256	467
0.707	0.274	1309554.9	1506793.6	455037.3	1631385.0	306	446
0.274	0.140	1506793.6	1567484.8	454525.4	1631244.9	834	477
0.140	-0.114	1567484.8	1683189.7	454935.1	1631302.3	422	450
-0.114	-0.242	1683189.7	1741188.5	454498.5	1631352.1	860	460
-0.242	-0.507	1741188.5	1862047.0	454893.1	1631256.8	456	488
-0.507	-1.028	1862047.0	2098768.5	455013.7	1631195.6	322	516
-1.028	-0.979	2098768.5	2076369.1	458293.4	1627825.3	4386	511
-0.979	-0.897	2076369.1	2039097.0	456911.4	1629177.9	2452	510
-0.897	-0.996	2039097.0	2083930.3	453578.0	1632168.5	2027	453
-0.996	-0.482	2083930.3	1850113.0	455237.6	1630515.6	320	369
-0.482	-0.331	1850113.0	1781043.1	455689.4	1630297.6	819	311
-0.331	-0.264	1781043.1	1750338.8	456539.5	1630016.4	1714	321
							380
							243

Apex (est.)

256 **461**
(Minimum) **(Average)**

Table K-16: Radius of curvature calculations for bend 6 (1985).

Bend	6
Year	1985
Depth (ft)	2.36 (avg.)

Bend id	Point id	GIS Coordinates (ft)		GIS Coordinates (ft)		Midpoint Slopes (ft/ft)	
		X _{CL}	Y _{CL}	X _{mid}	Y _{mid}	m	p
6_85	1 (u/s)	454698.4	1629520.2	454708.8	1629462.6	-5.573	-4.871
6_85	2	454719.1	1629405.0	454730.7	1629348.6	-4.871	-4.617
6_85	3	454742.3	1629292.2	454753.9	1629238.7	-4.617	-4.617
6_85	4	454765.5	1629185.1	454777.8	1629128.2	-4.617	-6.399
6_85	5	454790.1	1629071.2	454798.6	1629017.2	-6.399	15.851
6_85	6	454807.0	1628963.2	454803.4	1628905.7	15.851	7.948
6_85	7	454799.8	1628848.3	454792.9	1628793.4	7.948	1.927
6_85	8	454786.0	1628738.4	454760.2	1628688.7	1.927	1.492
6_85	9	454734.4	1628639.1	454703.0	1628592.3	1.492	1.104
6_85	10	454671.7	1628545.5	454633.3	1628503.1	1.104	0.976
6_85	11	454594.9	1628460.8	454555.1	1628421.9	0.976	0.880
6_85	12	454515.3	1628383.0	454472.9	1628345.7	0.880	0.497
6_85	13	454430.5	1628308.3	454380.2	1628283.3	0.497	0.400
6_85	14	454330.0	1628258.3	454277.4	1628237.3	0.400	0.523
6_85	15	454224.9	1628216.3	454174.2	1628189.8	0.523	0.523
6_85	16	454123.5	1628163.3	454073.3	1628137.1	0.523	0.625
6_85	17	454023.2	1628110.9	453975.9	1628081.3	0.625	0.722
6_85	18	453928.6	1628051.7	453883.1	1628018.9	0.722	0.740
6_85	19	453837.6	1627986.0	453793.1	1627953.1		
6_85	20 (d/s)	453748.5	1627920.1				

input (GIS)

Tangent Slopes (ft/ft)		Tangent Intercepts (ft)		Centroid Coordinates (ft)		R (ft)	width (ft)
a	c	b	d	x _c	y _c		
0.179	0.205	1547871.5	1535990.9	459290.0	1630284.7	4655	152
0.205	0.217	1535990.9	1530748.3	464925.5	1631441.6	10408	144
0.217	0.217	1530748.3	1530626.2	8738678.6	3423367.3	8475984	164
0.217	0.156	1530626.2	1557940.5	452884.3	1628718.0	1938	189
0.156	-0.063	1557940.5	1657598.1	454291.8	1628938.0	516	186
-0.063	-0.126	1657598.1	1686015.1	452990.8	1629020.1	1817	193
-0.126	-0.519	1686015.1	1864693.7	454483.6	1628832.3	317	311
-0.519	-0.670	1864693.7	1933283.2	453868.5	1629151.5	1006	359
-0.670	-0.905	1933283.2	2040172.6	454056.2	1629025.7	781	323
-0.905	-1.024	2040172.6	2094028.1	453275.4	1629732.7	1833	353
-1.024	-1.136	2094028.1	2144510.1	453032.9	1629981.1	2180	357
-1.136	-2.011	2144510.1	2542135.9	454188.8	1628668.3	434	280
-2.011	-2.498	2542135.9	2763228.7	453758.8	1629533.2	1397	242
-2.498	-1.913	2763228.7	2497219.8	454696.4	1627190.5	1129	304
-1.913	-1.913	2497219.8	2496949.7	5039580.4	-7145659.0	9899817	456
-1.913	-1.599	2496949.7	2354151.0	454747.1	1626847.8	1456	522
-1.599	-1.385	2354151.0	2256642.5	454866.4	1626657.0	1681	499
-1.385	-1.352	2256642.5	2241451.0	459557.9	1620159.4	9694	453
							420
							340

Apex (est.)

317 **312**
(Minimum) **(Average)**

Table K-17: Radius of curvature calculations for bend 6 (1992).

Bend	6
Year	1992
Depth (ft)	2.36 (avg.)

Bend id	Point id	GIS Coordinates (ft)		GIS Coordinates (ft)		Midpoint Slopes (ft/ft)	
		X _{CL}	Y _{CL}	X _{mid}	Y _{mid}	m	p
6_92	1 (u/s)	454692.0	1629519.7	454698.6	1629462.7	-8.554	-4.769
6_92	2	454705.3	1629405.7	454717.0	1629350.0	-4.769	-4.641
6_92	3	454728.7	1629294.3	454740.3	1629240.5	-4.641	-4.965
6_92	4	454751.9	1629186.7	454762.8	1629132.3	-4.965	-52.895
6_92	5	454773.8	1629077.9	454774.8	1629022.6	-52.895	4.226
6_92	6	454775.9	1628967.3	454763.4	1628914.8	4.226	3.115
6_92	7	454751.0	1628862.3	454733.7	1628808.5	3.115	3.245
6_92	8	454716.5	1628754.7	454700.2	1628701.8	3.245	1.968
6_92	9	454683.8	1628648.8	454659.4	1628600.7	1.968	1.152
6_92	10	454634.9	1628552.6	454598.1	1628510.2	1.152	0.541
6_92	11	454561.3	1628467.8	454512.3	1628441.3	0.541	0.395
6_92	12	454463.4	1628414.8	454411.9	1628394.4	0.395	0.842
6_92	13	454360.4	1628374.1	454319.6	1628339.7	0.842	0.527
6_92	14	454278.7	1628305.3	454230.5	1628279.8	0.527	0.438
6_92	15	454182.2	1628254.4	454131.2	1628232.1	0.438	0.891
6_92	16	454080.3	1628209.7	454039.6	1628173.5	0.891	1.066
6_92	17	453998.9	1628137.2	453960.1	1628095.9	1.066	0.932
6_92	18	453921.3	1628054.5	453881.0	1628017.0	0.932	0.778
6_92	19	453840.8	1627979.5	453798.0	1627946.2		
6_92	20 (d/s)	453755.3	1627912.9				

input (GIS)

Tangent Slopes (ft/ft)		Tangent Intercepts (ft)		Centroid Coordinates (ft)		R (ft)	width (ft)
a	c	b	d	x _c	y _c		
0.117	0.210	1576304.2	1533998.2	455954.8	1629609.6	1266	214
0.210	0.215	1533998.2	1531258.7	474552.2	1633509.3	20267	223
0.215	0.201	1531258.7	1537536.2	446717.0	1627511.7	8208	222
0.201	0.019	1537536.2	1620424.9	454160.6	1629011.0	617	213
0.019	-0.237	1620424.9	1736534.2	454342.4	1629014.4	436	287
-0.237	-0.321	1736534.2	1774790.2	453390.8	1629239.6	1412	388
-0.321	-0.308	1774790.2	1768834.1	463850.9	1625881.7	9576	472
-0.308	-0.508	1768834.1	1859661.0	454091.1	1628889.5	640	526
-0.508	-0.868	1859661.0	2023174.2	454260.1	1628803.6	451	560
-0.868	-1.848	2023174.2	2468577.0	454366.1	1628711.6	312	583
-1.848	-2.530	2468577.0	2778045.3	454070.7	1629257.5	930	555
-2.530	-1.187	2778045.3	2167749.2	454534.3	1628084.8	338	533
-1.187	-1.897	2167749.2	2489819.1	453996.9	1628722.7	504	497
-1.897	-2.282	2489819.1	2664371.5	453518.2	1629630.8	1528	560
-2.282	-1.123	2664371.5	2137857.0	454270.5	1627914.2	351	620
-1.123	-0.938	2137857.0	2053940.9	454864.4	1627247.5	1241	671
-0.938	-1.073	2053940.9	2115086.7	452747.9	1629233.0	1663	690
-1.073	-1.285	2115086.7	2211020.7	453043.0	1628916.4	1231	559
							480
							380

Apex (est.)

312 **462**
(Minimum) **(Average)**

Table K-18: Radius of curvature calculations for bend 7 (1972).

Bend	7
Year	1972
Depth (ft)	3.01 (avg.)

Bend id	Point id	GIS Coordinates (ft)		GIS Coordinates (ft)		Midpoint Slopes (ft/ft)	
		X _{CL}	Y _{CL}	X _{mid}	Y _{mid}	m	p
7_72	1 (u/s)	447970.3	1621337.2	447918.9	1621348.0	-0.211	-0.119
7_72	2	447867.5	1621358.8	447816.5	1621364.9	-0.119	-0.095
7_72	3	447765.6	1621371.0	447714.8	1621375.8	-0.095	-0.023
7_72	4	447664.1	1621380.6	447613.0	1621381.8	-0.023	0.007
7_72	5	447561.9	1621382.9	447510.2	1621382.6	0.007	0.009
7_72	6	447458.5	1621382.2	447407.8	1621381.7	0.009	0.047
7_72	7	447357.1	1621381.3	447304.9	1621378.8	0.047	0.213
7_72	8	447252.7	1621376.3	447205.0	1621366.2	0.213	0.560
7_72	9	447157.3	1621356.0	447112.7	1621331.0	0.560	0.870
7_72	10	447068.1	1621306.1	447028.9	1621271.9	0.870	1.319
7_72	11	446989.6	1621237.8	446959.1	1621197.6	1.319	1.383
7_72	12	446928.6	1621157.4	446898.8	1621116.1	1.383	1.314
7_72	13	446869.0	1621074.8	446837.3	1621033.3	1.314	1.272
7_72	14	446805.7	1620991.7	446775.0	1620952.7	1.272	1.273
7_72	15	446744.4	1620913.7	446713.2	1620873.9	1.273	1.251
7_72	16	446681.9	1620834.2	446650.1	1620794.3	1.251	1.117
7_72	17	446618.2	1620754.4	446583.1	1620715.3	1.117	1.117
7_72	18	446548.1	1620676.2	446514.6	1620638.8	1.117	1.116
7_72	19	446481.2	1620601.4	446447.2	1620563.5	1.116	1.117
7_72	20	446413.3	1620525.7	446378.9	1620487.3	1.117	0.948
7_72	21	446344.6	1620448.9	446308.8	1620415.0		
7_72	22 (d/s)	446273.0	1620381.1				

input (GIS)

Tangent Slopes (ft/ft)		Tangent Intercepts (ft)		Centroid Coordinates (ft)		R (ft)	width (ft)
a	c	b	d	x _c	y _c		
4.742	8.390	-502754.4	-2136015.1	447678.9	1620209.9	1164	349
8.390	10.502	-2136015.1	-3080324.5	447305.5	1617076.6	4319	310
10.502	44.400	-3080324.5	-18252635.4	447581.3	1619973.2	1410	306
44.400	-141.671	-18252635.4	65020708.6	447534.8	1617907.8	3475	278
-141.671	-109.032	65020708.6	50403266.6	447852.4	1572912.4	48471	260
-109.032	-21.097	50403266.6	11058156.8	447432.5	1618686.0	2696	285
-21.097	-4.695	11058156.8	3720940.8	447334.3	1620759.2	623	307
-4.695	-1.786	3720940.8	2419669.8	447273.7	1621043.6	333	339
-1.786	-1.150	2419669.8	2135220.9	447357.2	1620894.4	503	383
-1.150	-0.758	2135220.9	1960168.5	447354.0	1620898.1	498	406
-0.758	-0.723	1960168.5	1944180.0	450484.3	1618524.1	4425	369
-0.723	-0.761	1944180.0	1961163.2	443514.0	1623563.0	4177	353
-0.761	-0.786	1961163.2	1972063.9	441590.9	1625026.8	6594	288
-0.786	-0.786	1972063.9	1971826.7	965405.8	1213371.6	659621	252
-0.786	-0.799	1971826.7	1977756.0	437124.2	1628407.4	12194	209
-0.799	-0.895	1977756.0	2020620.0	445206.9	1621947.7	1848	204
-0.895	-0.896	2020620.0	2020500.8	-2853147.9	4575547.3	4429363	198
-0.896	-0.896	2020500.8	2020450.6	-262863.8	2255900.2	952247	200
-0.896	-0.895	2020450.6	2020175.8	892992.5	1220588.7	599485	218
-0.895	-1.055	2020175.8	2091339.5	445463.1	1621307.3	1230	238
							262
							267

Apex (est.)

333 **285**
(Minimum) (Average)

Table K-19: Radius of curvature calculations for bend 7 (1985).

Bend	7
Year	1985
Depth (ft)	3.54 (avg.)

Bend id	Point id	GIS Coordinates (ft)		GIS Coordinates (ft)		Midpoint Slopes (ft/ft)	
		X _{CL}	Y _{CL}	X _{mid}	Y _{mid}	m	p
7_85	1 (u/s)	447970.3	1621157.4	447914.9	1621172.5	-0.273	-0.522
7_85	2	447859.5	1621187.7	447809.4	1621213.8	-0.522	-0.661
7_85	3	447759.4	1621239.9	447713.1	1621270.5	-0.661	-0.383
7_85	4	447666.8	1621301.1	447614.2	1621321.3	-0.383	-0.204
7_85	5	447561.6	1621341.4	447506.5	1621352.6	-0.204	-0.088
7_85	6	447451.4	1621363.9	447395.5	1621368.8	-0.088	-0.048
7_85	7	447339.6	1621373.7	447282.5	1621376.4	-0.048	-0.030
7_85	8	447225.5	1621379.2	447170.2	1621380.9	-0.030	0.154
7_85	9	447114.9	1621382.5	447059.5	1621374.0	0.154	0.291
7_85	10	447004.1	1621365.4	446951.1	1621350.0	0.291	0.494
7_85	11	446898.2	1621334.6	446847.6	1621309.6	0.494	0.591
7_85	12	446797.0	1621284.6	446748.2	1621255.8	0.591	0.970
7_85	13	446699.4	1621227.0	446659.7	1621188.4	0.970	1.345
7_85	14	446619.9	1621149.9	446586.1	1621104.5	1.345	1.705
7_85	15	446552.3	1621059.0	446523.7	1621010.2	1.705	1.793
7_85	16	446495.1	1620961.5	446467.7	1620912.4	1.793	5.693
7_85	17	446440.3	1620863.3	446430.8	1620809.0	5.693	14.582
7_85	18	446421.3	1620754.7	446417.4	1620698.3	14.582	12.188
7_85	19	446413.5	1620642.0	446408.9	1620586.0	12.188	10.168
7_85	20	446404.3	1620530.0	446398.8	1620473.4	10.168	4.289
7_85	21	446393.2	1620416.8	446381.0	1620364.5		
7_85	22 (d/s)	446368.8	1620312.3				

input (GIS)

Tangent Slopes (ft/ft)		Tangent Intercepts (ft)		Centroid Coordinates (ft)		R (ft)	width (ft)
a	c	b	d	x _c	y _c		
3.664	1.916	-19898.7	763305.3	448054.1	1621682.5	532	421
1.916	1.513	763305.3	943662.6	448312.8	1622178.2	1089	392
1.513	2.608	943662.6	454061.6	447431.0	1620843.7	515	358
2.608	4.911	454061.6	-576477.0	447371.0	1620687.1	681	286
4.911	11.400	-576477.0	-3478757.8	447309.0	1620382.7	991	228
11.400	20.678	-3478757.8	-7627324.5	447142.9	1618488.8	2892	251
20.678	33.006	-7627324.5	-13137904.9	446981.4	1615149.2	6235	242
33.006	-6.475	-13137904.9	4516031.8	447151.9	1620775.8	608	200
-6.475	-3.436	4516031.8	3157091.5	447189.9	1620529.7	856	169
-3.436	-2.025	3157091.5	2526354.7	447128.5	1620740.7	637	164
-2.025	-1.692	2526354.7	2377279.2	447514.2	1619959.4	1507	175
-1.692	-1.031	2377279.2	2081880.5	446988.2	1620849.6	475	189
-1.031	-0.744	2081880.5	1953196.4	447141.6	1620691.4	694	175
-0.744	-0.587	1953196.4	1882959.8	447419.5	1620484.7	1040	163
-0.587	-0.558	1882959.8	1869889.1	450977.4	1618397.5	5164	163
-0.558	-0.176	1869889.1	1699223.2	446755.4	1620751.9	334	198
-0.176	-0.069	1699223.2	1651312.3	447472.8	1620625.9	1059	183
-0.069	-0.082	1651312.3	1657212.1	438023.5	1621273.9	8414	170
-0.082	-0.098	1657212.1	1664375.6	439440.9	1621157.7	6992	165
-0.098	-0.233	1664375.6	1724433.3	445560.5	1620555.8	844	153
							150
							159

Apex (est.)

334 216
(Minimum) (Average)

Table K-20: Radius of curvature calculations for bend 7 (1992).

Bend	7
Year	1992
Depth (ft)	3.54 (avg.)

Bend id	Point id	GIS Coordinates (ft)		GIS Coordinates (ft)		Midpoint Slopes (ft/ft)	
		X _{CL}	Y _{CL}	X _{mid}	Y _{mid}	m	p
7_92	1 (u/s)	447970.3	1621146.6	447919.3	1621173.4	-0.524	-0.752
7_92	2	447868.3	1621200.1	447822.9	1621234.2	-0.752	-0.767
7_92	3	447777.5	1621268.4	447732.6	1621302.7	-0.767	-0.292
7_92	4	447687.8	1621337.1	447633.4	1621353.0	-0.292	-0.070
7_92	5	447578.9	1621369.0	447523.7	1621372.8	-0.070	-0.117
7_92	6	447468.4	1621376.7	447411.3	1621383.3	-0.117	-0.136
7_92	7	447354.2	1621390.0	447297.4	1621397.7	-0.136	0.000
7_92	8	447240.5	1621405.5	447184.3	1621405.4	0.000	0.132
7_92	9	447128.2	1621405.4	447072.6	1621398.1	0.132	0.311
7_92	10	447016.9	1621390.8	446963.2	1621374.0	0.311	0.515
7_92	11	446909.5	1621357.3	446860.2	1621331.9	0.515	0.665
7_92	12	446811.0	1621306.6	446762.8	1621274.5	0.665	1.055
7_92	13	446714.6	1621242.5	446675.7	1621201.5	1.055	1.657
7_92	14	446636.8	1621160.5	446608.0	1621112.7	1.657	2.274
7_92	15	446579.2	1621064.9	446556.3	1621012.8	2.274	3.300
7_92	16	446533.4	1620960.7	446517.0	1620906.7	3.300	6.485
7_92	17	446500.6	1620852.6	446491.9	1620796.1	6.485	6.282
7_92	18	446483.2	1620739.6	446474.3	1620684.2	6.282	12.047
7_92	19	446465.5	1620628.7	446460.8	1620572.3	12.047	2.672
7_92	20	446456.1	1620515.8	446436.5	1620463.4	2.672	1.287
7_92	21	446416.9	1620411.0	446383.7	1620368.2		
7_92	22 (d/s)	446350.5	1620325.5				

input (GIS)

Tangent Slopes (ft/ft)		Tangent Intercepts (ft)		Centroid Coordinates (ft)		R (ft)	width (ft)
a	c	b	d	x _c	y _c		
1.908	1.330	766709.6	1025580.6	448246.7	1621798.0	708	422
1.330	1.305	1025580.6	1037198.9	455117.5	1630937.0	12139	380
1.305	3.420	1037198.9	90567.9	447548.4	1621062.3	308	325
3.420	14.317	90567.9	-4785983.6	447487.4	1620854.0	523	274
14.317	8.558	-4785983.6	-2207773.4	447692.5	1623789.5	2423	263
8.558	7.366	-2207773.4	-1673364.6	448127.2	1627510.3	6169	277
7.366	-11235.000	-1673364.6	5025737404.5	447184.4	1620565.6	842	263
-11235.000	-7.571	5025737404.5	5006245.5	447184.4	1620551.2	856	250
-7.571	-3.212	5006245.5	3057001.2	447158.6	1620746.4	660	238
-3.212	-1.942	3057001.2	2489160.2	447153.9	1620761.7	644	210
-1.942	-1.505	2489160.2	2293475.7	447326.7	1620426.0	1020	198
-1.505	-0.948	2293475.7	2044511.3	447042.1	1620854.3	508	210
-0.948	-0.603	2044511.3	1890591.7	447052.2	1620844.7	522	230
-0.603	-0.440	1890591.7	1817415.3	447357.7	1620660.4	877	266
-0.440	-0.303	1817415.3	1756203.6	447419.3	1620633.3	945	285
-0.303	-0.154	1756203.6	1689651.4	447286.0	1620673.6	806	345
-0.154	-0.159	1689651.4	1691756.2	423410.8	1624355.5	23354	334
-0.159	-0.083	1691756.2	1657632.3	447958.2	1620448.0	1504	309
-0.083	-0.374	1657632.3	1787541.8	446055.8	1620605.9	410	319
-0.374	-0.777	1787541.8	1967201.7	446098.2	1620590.0	366	317
							264
							227

Apex (est.)

308 **282**
(Minimum) **(Average)**

APPENDIX L:
Radius of Curvature Dataset (Nanson and Hickin Methodology)

Table L-1: Mean radius of curvature calculation for bend 1 (1972).

Bend	1
Year	1972

Bend id	FID	GIS Coordinates (ft)		GIS Coordinates (ft)		Midpoint Slopes (ft/ft)	
		X _{BL}	Y _{BL}	X _{mid}	Y _{mid}	m	p
1_72	1	458229.8	1641150.0	458162.4	1641070.7	1.176	1.673
1_72	0	458094.9	1640991.4	458041.7	1640902.4		
1_72	2	457988.5	1640813.3				
1_72	3	458377.9	1641290.7	458236.4	1641141.0	1.058	1.995
1_72	0	458094.9	1640991.4	458003.2	1640808.4		
1_72	4	457911.5	1640625.4				

input (GIS)

Tangent Slopes (ft/ft)		Tangent Intercepts (ft)		Centroid Coordinates (ft)		
a	c	b	d	x _c	y _c	R (ft)
-0.850	-0.598	2030619.9	1914729.4	459115.0	1640260.7	1255
-0.945	-0.501	2074386.9	1870410.7	459248.5	1640184.1	1408

1331
(Average)

Table L-2: Mean radius of curvature calculation for bend 1 (1985).

Bend	1
Year	1985

Bend id	FID	GIS Coordinates (ft)		GIS Coordinates (ft)		Midpoint Slopes (ft/ft)	
		X _{BL}	Y _{BL}	X _{mid}	Y _{mid}	m	p
1_85	1	458177.7	1641303.3	458048.0	1641281.4	0.169	1.138
1_85	0	457918.3	1641259.4	457833.6	1641163.1		
1_85	2	457748.9	1641066.7				
1_85	3	458442.9	1641240.6	458180.6	1641250.0	-0.036	6.342
1_85	0	457918.3	1641259.4	457883.7	1641040.0		
1_85	4	457849.1	1640820.6				

input (GIS)

Tangent Slopes (ft/ft)		Tangent Intercepts (ft)		Centroid Coordinates (ft)		
a	c	b	d	x _c	y _c	R (ft)
-5.904	-0.879	4345568.4	2043635.6	458109.0	1640920.9	389
27.905	-0.158	-11144426.7	1713243.0	458171.5	1640994.6	366

377
(Average)

Table L-3: Mean radius of curvature calculation for bend 1 (1992).

Bend	1
Year	1992

Bend id	FID	GIS Coordinates (ft)		GIS Coordinates (ft)		Midpoint Slopes (ft/ft)	
		X _{BL}	Y _{BL}	X _{mid}	Y _{mid}	m	p
1_92	1	458123.7	1641297.3	457994.9	1641279.0	0.143	1.523
1_92	0	457866.1	1641260.6	457795.9	1641153.7		
1_92	2	457725.8	1641046.9				
1_92	3	458378.5	1641259.5	458122.3	1641260.1	-0.002	1.909
1_92	0	457866.1	1641260.6	457746.4	1641032.1		
1_92	4	457626.7	1640803.5				

input (GIS)

Tangent Slopes (ft/ft)		Tangent Intercepts (ft)		Centroid Coordinates (ft)		R (ft)
a	c	b	d	x _c	y _c	
-7.012	-0.657	4852728.1	1941801.9	458035.2	1640996.6	313
488.019	-0.524	-221931143.6	1880772.0	458121.4	1640835.6	496

405
(Average)

Table L-4: Mean radius of curvature calculation for bend 2 (1972).

Bend	2
Year	1972

Bend id	FID	GIS Coordinates (ft)		GIS Coordinates (ft)		Midpoint Slopes (ft/ft)	
		X _{BL}	Y _{BL}	X _{mid}	Y _{mid}	m	p
2_72	1	457421.0	1640027.6	457354.2	1639946.2	1.218	0.495
2_72	0	457287.4	1639864.9	457194.2	1639818.7		
2_72	2	457100.9	1639772.5				
2_72	3	457498.6	1640224.2	457393.0	1640044.5	1.701	0.711
2_72	0	457287.4	1639864.9	457119.0	1639745.2		
2_72	4	456950.7	1639625.6				

input (GIS)

Tangent Slopes (ft/ft)		Tangent Intercepts (ft)		Centroid Coordinates (ft)		R (ft)
a	c	b	d	x _c	y _c	
-0.821	-2.019	2015299.8	2562719.4	456978.0	1640254.9	498
-0.588	-1.407	1908927.8	2282993.9	456557.2	1640535.9	992

745
(Average)

Table L-5: Mean radius of curvature calculation for bend 2 (1985).

Bend	2
Year	1985

Bend id	FID	GIS Coordinates (ft)		GIS Coordinates (ft)		Midpoint Slopes (ft/ft)	
		X _{BL}	Y _{BL}	X _{mid}	Y _{mid}	m	p
2_85	1	457470.2	1640327.7	457482.6	1640218.0	-8.845	1.201
2_85	0	457495.0	1640108.3	457424.6	1640023.8		
2_85	2	457354.2	1639939.3				
2_85	3	457421.3	1640550.0	457458.2	1640329.2	-5.995	0.975
2_85	0	457495.0	1640108.3	457336.8	1639954.1		
2_85	4	457178.6	1639799.8				

input (GIS)

Tangent Slopes (ft/ft)		Tangent Intercepts (ft)		Centroid Coordinates (ft)		R (ft)
a	c	b	d	x _c	y _c	
0.113	-0.833	1588496.8	2021039.6	457226.2	1640189.0	281
0.167	-1.026	1564017.1	2109046.0	457039.2	1640259.3	480

380
(Average)

Table L-6: Mean radius of curvature calculation for bend 2 (1992).

Bend	2
Year	1992

Bend id	FID	GIS Coordinates (ft)		GIS Coordinates (ft)		Midpoint Slopes (ft/ft)	
		X _{BL}	Y _{BL}	X _{mid}	Y _{mid}	m	p
2_92	1	457456.4	1639846.2	457416.2	1639723.8	3.044	0.436
2_92	0	457375.9	1639601.3	457254.5	1639548.4		
2_92	2	457133.2	1639495.4				
2_92	3	457502.0	1640103.7	457438.9	1639852.5	3.987	0.277
2_92	0	457375.9	1639601.3	457121.8	1639531.1		
2_92	4	456867.6	1639460.8				

input (GIS)

Tangent Slopes (ft/ft)		Tangent Intercepts (ft)		Centroid Coordinates (ft)		R (ft)
a	c	b	d	x _c	y _c	
-0.329	-2.291	1789991.8	2687272.3	457138.1	1639815.1	320
-0.251	-3.616	1754590.1	3292427.2	457002.6	1639962.0	519

419
(Average)

Table L-7: Mean radius of curvature calculation for bend 3 (1972).

Bend	3
Year	1972

Bend id	FID	GIS Coordinates (ft)		GIS Coordinates (ft)		Midpoint Slopes (ft/ft)	
		X _{BL}	Y _{BL}	X _{mid}	Y _{mid}	m	p
3_72	1	456492.1	1637729.3	456460.4	1637648.1	2.567	1.221
3_72	0	456428.8	1637566.9	456372.7	1637498.4		
3_72	2	456316.6	1637429.9				
3_72	3	456462.9	1637883.6	456445.8	1637725.3	9.300	1.275
3_72	0	456428.8	1637566.9	456320.2	1637428.4		
3_72	4	456211.5	1637289.9				

input (GIS)

Tangent Slopes (ft/ft)		Tangent Intercepts (ft)		Centroid Coordinates (ft)		R (ft)
a	c	b	d	x _c	y _c	
-0.390	-0.819	1815474.5	2011357.6	455944.8	1637849.0	560
-0.108	-0.784	1686806.2	1995365.6	455861.6	1637788.1	609

584
(Average)

Table L-8: Mean radius of curvature calculation for bend 3 (1985).

Bend	3
Year	1985

Bend id	FID	GIS Coordinates (ft)		GIS Coordinates (ft)		Midpoint Slopes (ft/ft)	
		X _{BL}	Y _{BL}	X _{mid}	Y _{mid}	m	p
3_85	1	456646.3	1637437.7	456632.8	1637295.0	10.579	0.398
3_85	0	456619.4	1637152.4	456488.1	1637100.2		
3_85	2	456356.8	1637048.0				
3_85	3	456551.0	1637698.3	456585.2	1637425.4	-7.985	0.385
3_85	0	456619.4	1637152.4	456354.1	1637050.3		
3_85	4	456088.9	1636948.1				

input (GIS)

Tangent Slopes (ft/ft)		Tangent Intercepts (ft)		Centroid Coordinates (ft)		R (ft)
a	c	b	d	x _c	y _c	
-0.095	-2.514	1680457.6	2784614.4	456401.9	1637316.9	273
0.125	-2.596	1580246.6	2821672.8	456226.9	1637380.5	454

363
(Average)

Table L-9: Mean radius of curvature calculation for bend 3 (1992).

Bend	3
Year	1992

Bend id	FID	GIS Coordinates (ft)		GIS Coordinates (ft)		Midpoint Slopes (ft/ft)	
		X _{BL}	Y _{BL}	X _{mid}	Y _{mid}	m	p
3_92	1	456381.8	1637233.2	456342.8	1637155.3	2.002	0.919
3_92	0	456303.9	1637077.4	456238.2	1637016.9		
3_92	2	456172.4	1636956.5				
3_92	3	456431.1	1637400.6	456367.5	1637239.0	2.541	0.762
3_92	0	456303.9	1637077.4	456164.3	1636970.9		
3_92	4	456024.6	1636864.5				

input (GIS)

Tangent Slopes (ft/ft)		Tangent Intercepts (ft)		Centroid Coordinates (ft)		R (ft)
a	c	b	d	x _c	y _c	
-0.500	-1.088	1865107.1	2133382.6	455914.2	1637369.4	487
-0.394	-1.312	1816860.5	2235369.1	455785.2	1637468.2	649

568
(Average)

Table L-10: Mean radius of curvature calculation for bend 4 (1972).

Bend	4
Year	1972

Bend id	FID	GIS Coordinates (ft)		GIS Coordinates (ft)		Midpoint Slopes (ft/ft)	
		X _{BL}	Y _{BL}	X _{mid}	Y _{mid}	m	p
4_72	1	456029.0	1636594.0	455966.9	1636485.2	1.752	4.584
4_72	0	455904.8	1636376.4	455878.2	1636254.5		
4_72	2	455851.6	1636132.7				
4_72	3	456188.6	1636784.3	456046.7	1636580.3	1.437	12.814
4_72	0	455904.8	1636376.4	455885.6	1636131.3		
4_72	4	455866.5	1635886.2				

input (GIS)

Tangent Slopes (ft/ft)		Tangent Intercepts (ft)		Centroid Coordinates (ft)		R (ft)
a	c	b	d	x _c	y _c	
-0.571	-0.218	1896813.2	1735706.6	456675.6	1636080.6	826
-0.696	-0.078	1953893.4	1671708.8	456793.9	1636060.4	944

885
(Average)

Table L-11: Mean radius of curvature calculation for bend 4 (1985).

Bend	4
Year	1985

Bend id	FID	GIS Coordinates (ft)		GIS Coordinates (ft)		Midpoint Slopes (ft/ft)	
		X _{BL}	Y _{BL}	X _{mid}	Y _{mid}	m	p
4_85	1	456046.9	1636642.7	455959.2	1636612.3	0.346	2.609
4_85	0	455871.6	1636582.0	455838.7	1636496.2		
4_85	2	455805.8	1636410.4				
4_85	3	456226.8	1636679.1	456049.2	1636630.6	0.274	5.092
4_85	0	455871.6	1636582.0	455836.5	1636403.4		
4_85	4	455801.5	1636224.9				

input (GIS)

Tangent Slopes (ft/ft)		Tangent Intercepts (ft)		Centroid Coordinates (ft)		R (ft)
a	c	b	d	x _c	y _c	
-2.887	-0.383	2952760.1	1811181.2	456024.1	1636425.1	219
-3.656	-0.196	3303913.7	1725923.8	456126.9	1636346.4	347

283
(Average)

Table L-12: Mean radius of curvature calculation for bend 4 (1992).

Bend	4
Year	1992

Bend id	FID	GIS Coordinates (ft)		GIS Coordinates (ft)		Midpoint Slopes (ft/ft)	
		X _{BL}	Y _{BL}	X _{mid}	Y _{mid}	m	p
4_92	1	455652.2	1636562.3	455563.6	1636510.9	0.581	4.156
4_92	0	455475.1	1636459.5	455452.3	1636364.8		
4_92	2	455429.5	1636270.2				
4_92	3	455838.4	1636628.1	455656.7	1636543.8	0.464	15.487
4_92	0	455475.1	1636459.5	455462.8	1636269.1		
4_92	4	455450.5	1636078.6				

input (GIS)

Tangent Slopes (ft/ft)		Tangent Intercepts (ft)		Centroid Coordinates (ft)		R (ft)
a	c	b	d	x _c	y _c	
-1.722	-0.241	2420945.0	1745944.8	455680.3	1636310.0	254
-2.154	-0.065	2617956.2	1665678.8	455794.2	1636247.6	383

318
(Average)

Table L-13: Mean radius of curvature calculation for bend 5 (1972).

Bend	5
Year	1972

Bend id	FID	GIS Coordinates (ft)		GIS Coordinates (ft)		Midpoint Slopes (ft/ft)	
		X _{BL}	Y _{BL}	X _{mid}	Y _{mid}	m	p
5_72	1	455018.4	1631811.2	455089.4	1631638.6	-2.431	2.007
5_72	0	455160.4	1631466.0	455079.4	1631303.4		
5_72	2	454998.4	1631140.9				
5_72	3	454730.4	1632041.7	454945.4	1631753.8	-1.339	1.729
5_72	0	455160.4	1631466.0	454976.5	1631148.2		
5_72	4	454792.7	1630830.4				

input (GIS)

Tangent Slopes (ft/ft)		Tangent Intercepts (ft)		Centroid Coordinates (ft)		R (ft)
a	c	b	d	x _c	y _c	
0.411	-0.498	1444471.4	1858038.3	454715.4	1631484.8	445
0.747	-0.578	1291985.1	1894327.4	454502.0	1631422.7	660

553
(Average)

Table L-14: Mean radius of curvature calculation for bend 5 (1985).

Bend	5
Year	1985

Bend id	FID	GIS Coordinates (ft)		GIS Coordinates (ft)		Midpoint Slopes (ft/ft)	
		X _{BL}	Y _{BL}	X _{mid}	Y _{mid}	m	p
5_85	1	454933.5	1631669.4	455029.3	1631645.2	-0.252	-5.579
5_85	0	455125.1	1631621.1	455142.8	1631522.5		
5_85	2	455160.4	1631423.9				
5_85	3	454735.2	1631703.3	454930.2	1631662.2	-0.211	-173.456
5_85	0	455125.1	1631621.1	455126.2	1631425.0		
5_85	4	455127.4	1631229.0				

input (GIS)

Tangent Slopes (ft/ft)		Tangent Intercepts (ft)		Centroid Coordinates (ft)		R (ft)
a	c	b	d	x _c	y _c	
3.966	0.179	-173213.2	1549946.8	454991.5	1631495.4	183
4.740	0.006	-524886.0	1628801.2	454879.8	1631423.6	315

249
(Average)

Table L-15: Mean radius of curvature calculation for bend 5 (1992).

Bend	5
Year	1992

Bend id	FID	GIS Coordinates (ft)		GIS Coordinates (ft)		Midpoint Slopes (ft/ft)	
		X _{BL}	Y _{BL}	X _{mid}	Y _{mid}	m	p
5_92	1	454864.4	1631480.0	454985.3	1631449.8	-0.249	12.822
5_92	0	455106.2	1631419.7	455096.6	1631296.7		
5_92	2	455087.0	1631173.6				
5_92	3	454650.9	1631605.9	454878.6	1631512.8	-0.409	3.711
5_92	0	455106.2	1631419.7	455042.9	1631184.7		
5_92	4	454979.6	1630949.7				

input (GIS)

Tangent Slopes (ft/ft)		Tangent Intercepts (ft)		Centroid Coordinates (ft)		R (ft)
a	c	b	d	x _c	y _c	
4.011	-0.078	-193548.6	1666789.2	454950.0	1631308.1	192
2.445	-0.270	519185.7	1753819.1	454774.0	1631257.2	370

281
(Average)

Table L-16: Mean radius of curvature calculation for bend 6 (1985).

Bend	6
Year	1985

Bend id	FID	GIS Coordinates (ft)		GIS Coordinates (ft)		Midpoint Slopes (ft/ft)	
		X _{BL}	Y _{BL}	X _{mid}	Y _{mid}	m	p
6_85	1	454663.1	1628897.7	454616.9	1628803.5	2.042	0.929
6_85	0	454570.8	1628709.3	454495.0	1628638.9		
6_85	2	454419.3	1628568.5				
6_85	3	454686.5	1629074.7	454628.6	1628892.0	3.160	1.205
6_85	0	454570.8	1628709.3	454446.4	1628559.3		
6_85	4	454321.9	1628409.4				

input (GIS)

Tangent Slopes (ft/ft)		Tangent Intercepts (ft)		Centroid Coordinates (ft)		R (ft)
a	c	b	d	x _c	y _c	
-0.490	-1.076	1851454.8	2117876.5	454112.8	1629050.4	571
-0.316	-0.830	1772763.4	2005786.9	453686.4	1629190.2	1007

789
(Average)

Table L-17: Mean radius of curvature calculation for bend 6 (1992).

Bend	6
Year	1992

Bend id	FID	GIS Coordinates (ft)		GIS Coordinates (ft)		Midpoint Slopes (ft/ft)	
		X _{BL}	Y _{BL}	X _{mid}	Y _{mid}	m	p
6_92	1	454520.6	1628938.8	454439.4	1628816.3	1.509	1.032
6_92	0	454358.2	1628693.7	454257.8	1628590.2		
6_92	2	454157.5	1628486.7				
6_92	3	454641.5	1629193.5	454499.9	1628943.6	1.764	0.534
6_92	0	454358.2	1628693.7	454118.5	1628565.9		
6_92	4	453878.9	1628438.0				

input (GIS)

Tangent Slopes (ft/ft)		Tangent Intercepts (ft)		Centroid Coordinates (ft)		R (ft)
a	c	b	d	x _c	y _c	
-0.662	-0.969	1929878.4	2068873.2	453128.8	1629684.5	1579
-0.567	-1.874	1886606.6	2479574.2	453664.1	1629417.4	1003

1291
(Average)

Table L-18: Mean radius of curvature calculation for bend 7 (1972).

Bend	7
Year	1972

Bend id	FID	GIS Coordinates (ft)		GIS Coordinates (ft)		Midpoint Slopes (ft/ft)	
		X _{BL}	Y _{BL}	X _{mid}	Y _{mid}	m	p
7_72	1	447538.8	1621254.9	447386.1	1621198.8	0.367	0.695
7_72	0	447233.4	1621142.8	447101.3	1621051.0		
7_72	2	446969.3	1620959.3				
7_72	3	447856.9	1621204.9	447545.1	1621173.9	0.100	0.860
7_72	0	447233.4	1621142.8	446989.7	1620933.3		
7_72	4	446746.0	1620723.8				

input (GIS)

Tangent Slopes (ft/ft)		Tangent Intercepts (ft)		Centroid Coordinates (ft)		R (ft)
a	c	b	d	x _c	y _c	
-2.724	-1.439	2839938.8	2264570.9	447820.1	1620016.4	1270
-10.032	-1.163	6110736.9	2140904.5	447645.1	1620170.8	1056

1163
(Average)

Table L-19: Mean radius of curvature calculation for bend 7 (1985).

Bend	7
Year	1985

Bend id	FID	GIS Coordinates (ft)		GIS Coordinates (ft)		Midpoint Slopes (ft/ft)	
		X _{BL}	Y _{BL}	X _{mid}	Y _{mid}	m	p
7_85	1	447006.4	1621285.4	446920.8	1621241.0	0.518	0.653
7_85	0	446835.2	1621196.6	446754.0	1621143.5		
7_85	2	446672.7	1621090.4				
7_85	3	447193.4	1621296.2	447014.3	1621246.4	0.278	1.091
7_85	0	446835.2	1621196.6	446711.2	1621061.3		
7_85	4	446587.2	1620925.9				

input (GIS)

Tangent Slopes (ft/ft)		Tangent Intercepts (ft)		Centroid Coordinates (ft)		R (ft)
a	c	b	d	x _c	y _c	
-1.929	-1.530	2483357.5	2304802.9	447805.5	1619534.3	1925
-3.597	-0.916	3229160.1	2030360.9	447187.0	1620625.3	671

1298
(Average)

Table L-20: Mean radius of curvature calculation for bend 7 (1992).

Bend	7
Year	1992

Bend id	FID	GIS Coordinates (ft)		GIS Coordinates (ft)		Midpoint Slopes (ft/ft)	
		X _{BL}	Y _{BL}	X _{mid}	Y _{mid}	m	p
7_92	1	447201.3	1621278.5	447059.1	1621264.8	0.096	1.186
7_92	0	446916.8	1621251.2	446825.5	1621142.7		
7_92	2	446734.1	1621034.3				
7_92	3	447479.1	1621224.2	447197.9	1621237.7	-0.048	1.839
7_92	0	446916.8	1621251.2	446784.9	1621008.6		
7_92	4	446653.0	1620766.0				

input (GIS)

Tangent Slopes (ft/ft)		Tangent Intercepts (ft)		Centroid Coordinates (ft)		R (ft)
a	c	b	d	x _c	y _c	
-10.410	-0.843	6275226.7	1997753.1	447092.4	1620917.7	377
20.877	-0.544	-7715119.4	1863922.5	447176.8	1620795.5	525

451
(Average)

**APPENDIX M:
Migration Dataset
(Graphical and Quantifiable Results)**

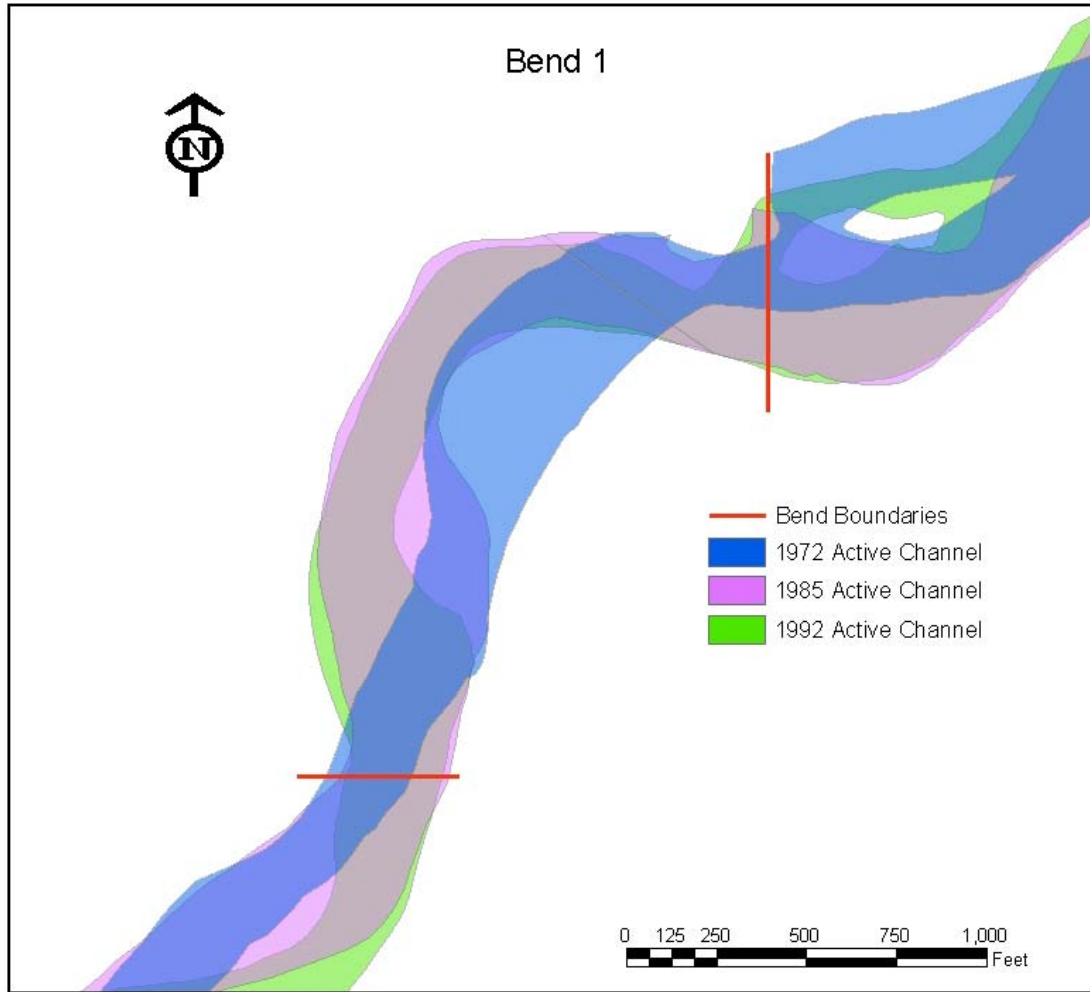


Figure M-1: Migration of bend 1 (1972-1992).

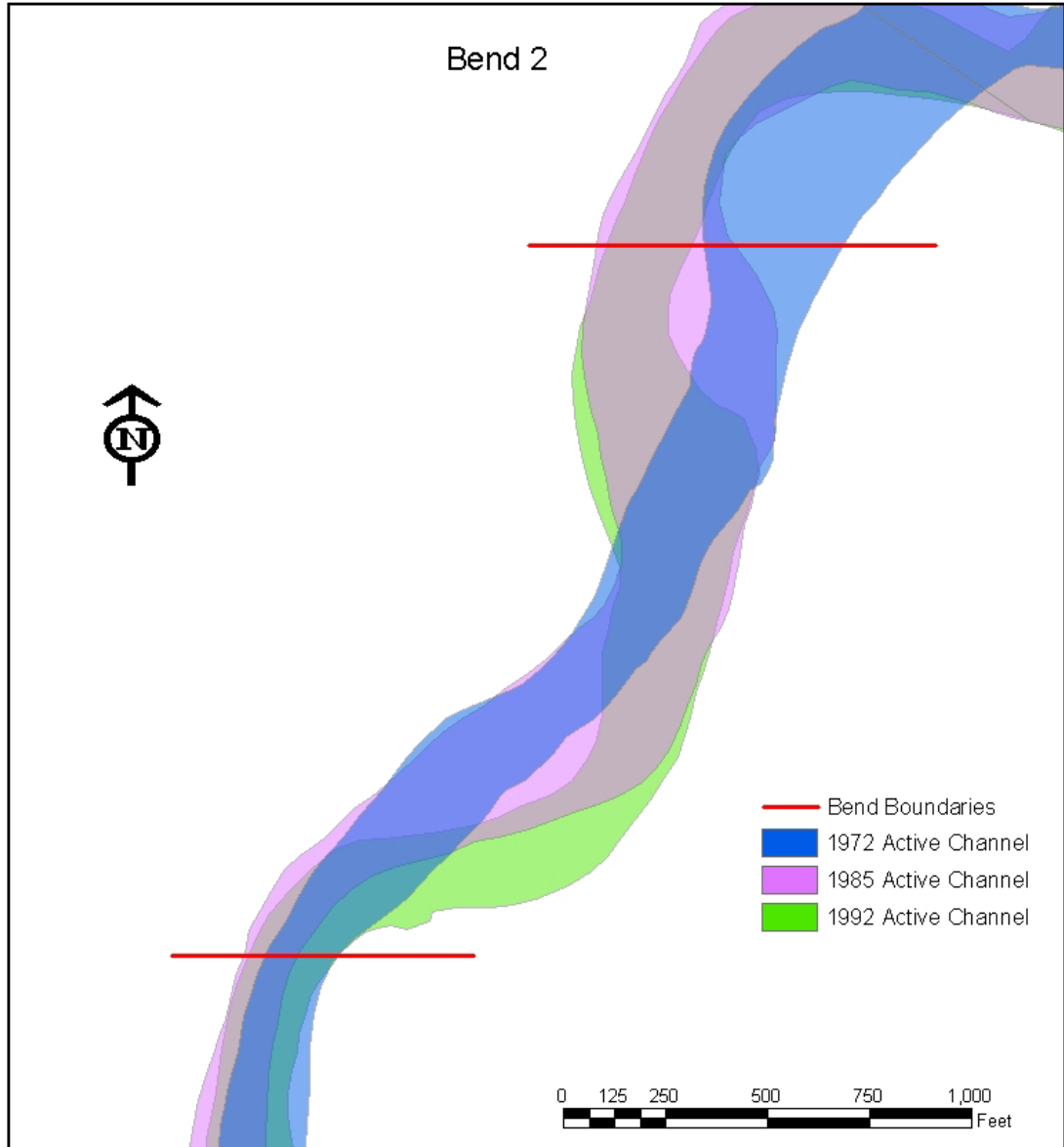


Figure M-2: Migration of bend 2 (1972-1992).

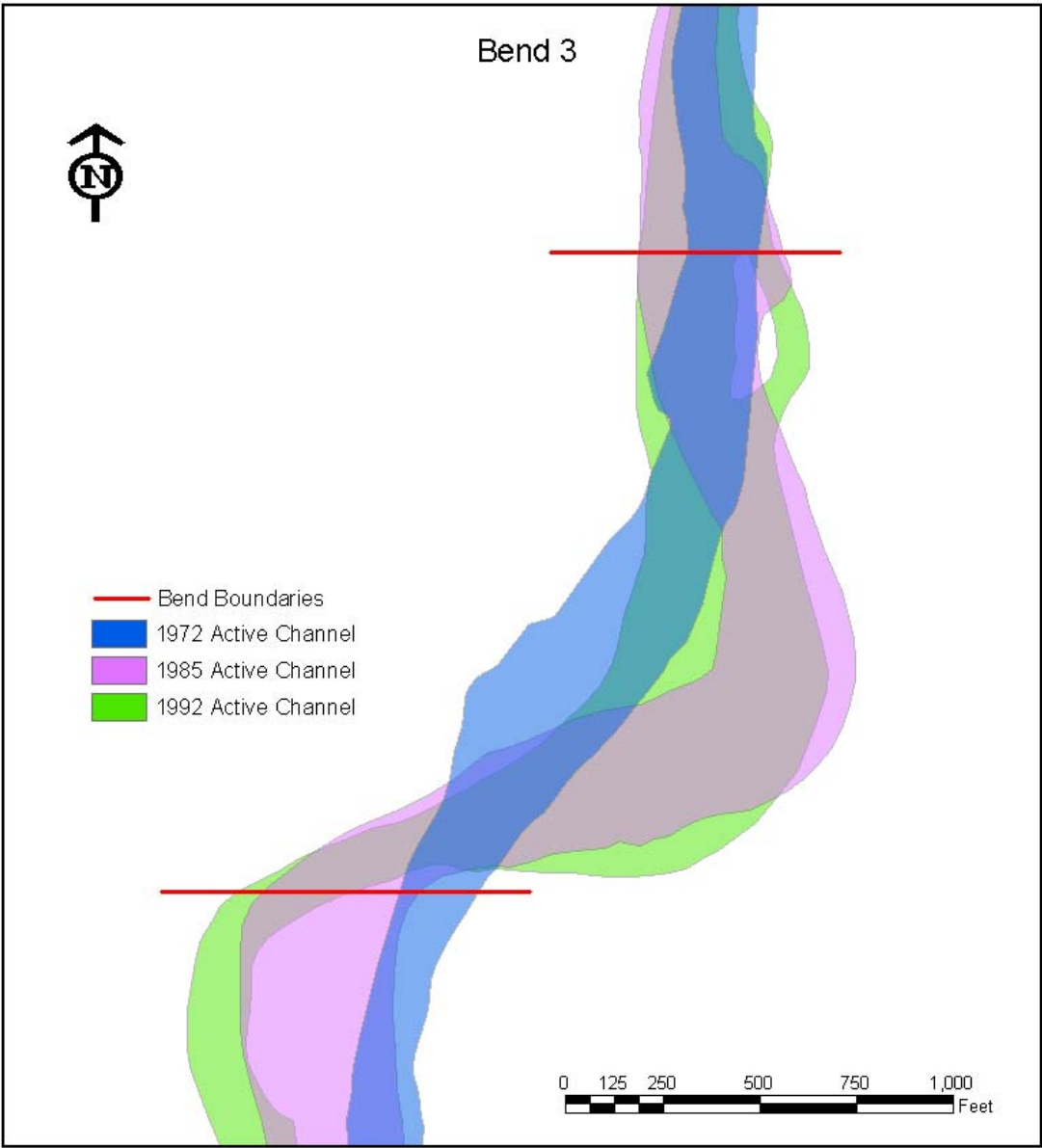


Figure M-3: Migration of bend 3 (1972-1992).

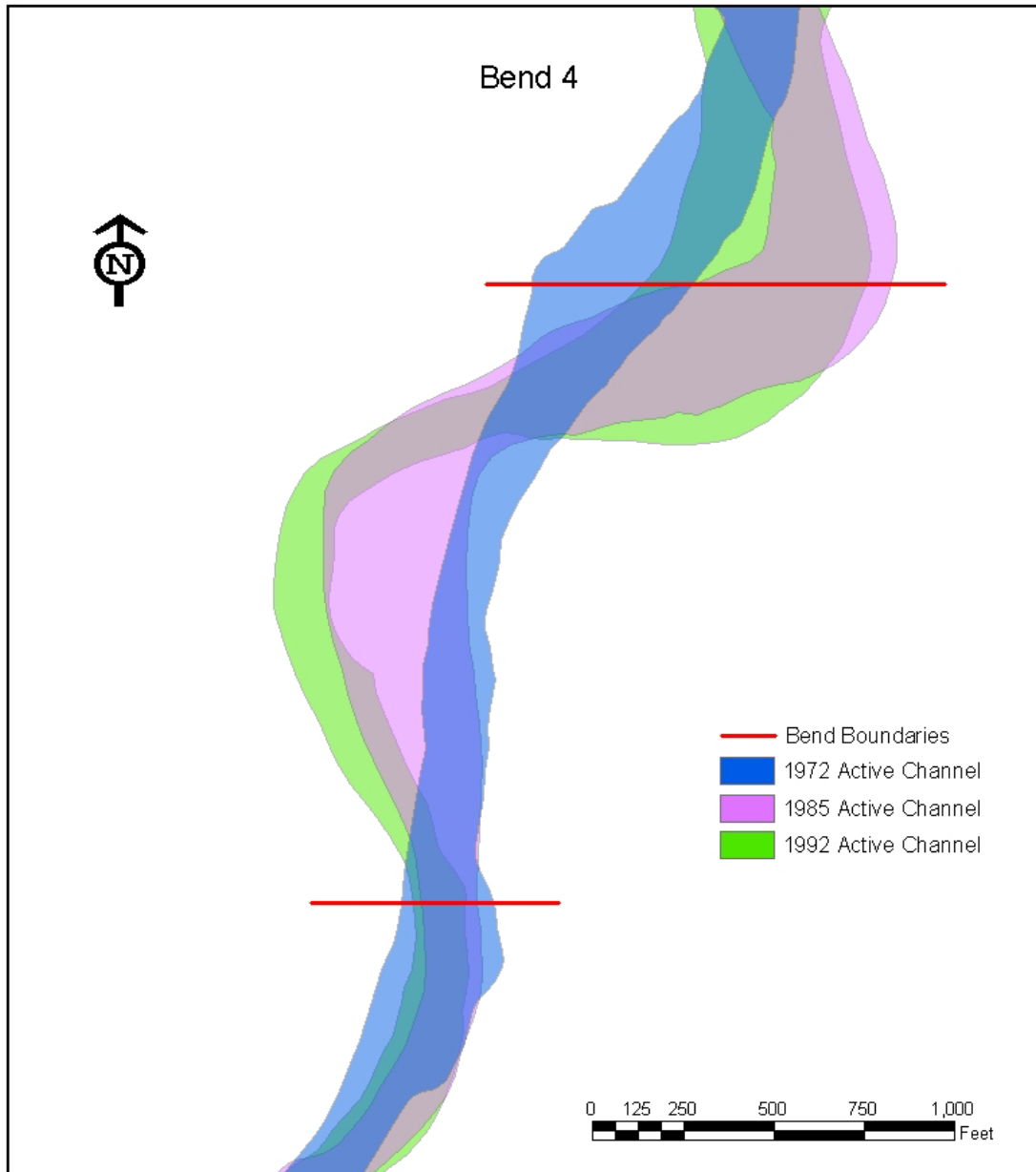


Figure M-4: Migration of bend 4 (1972-1992).

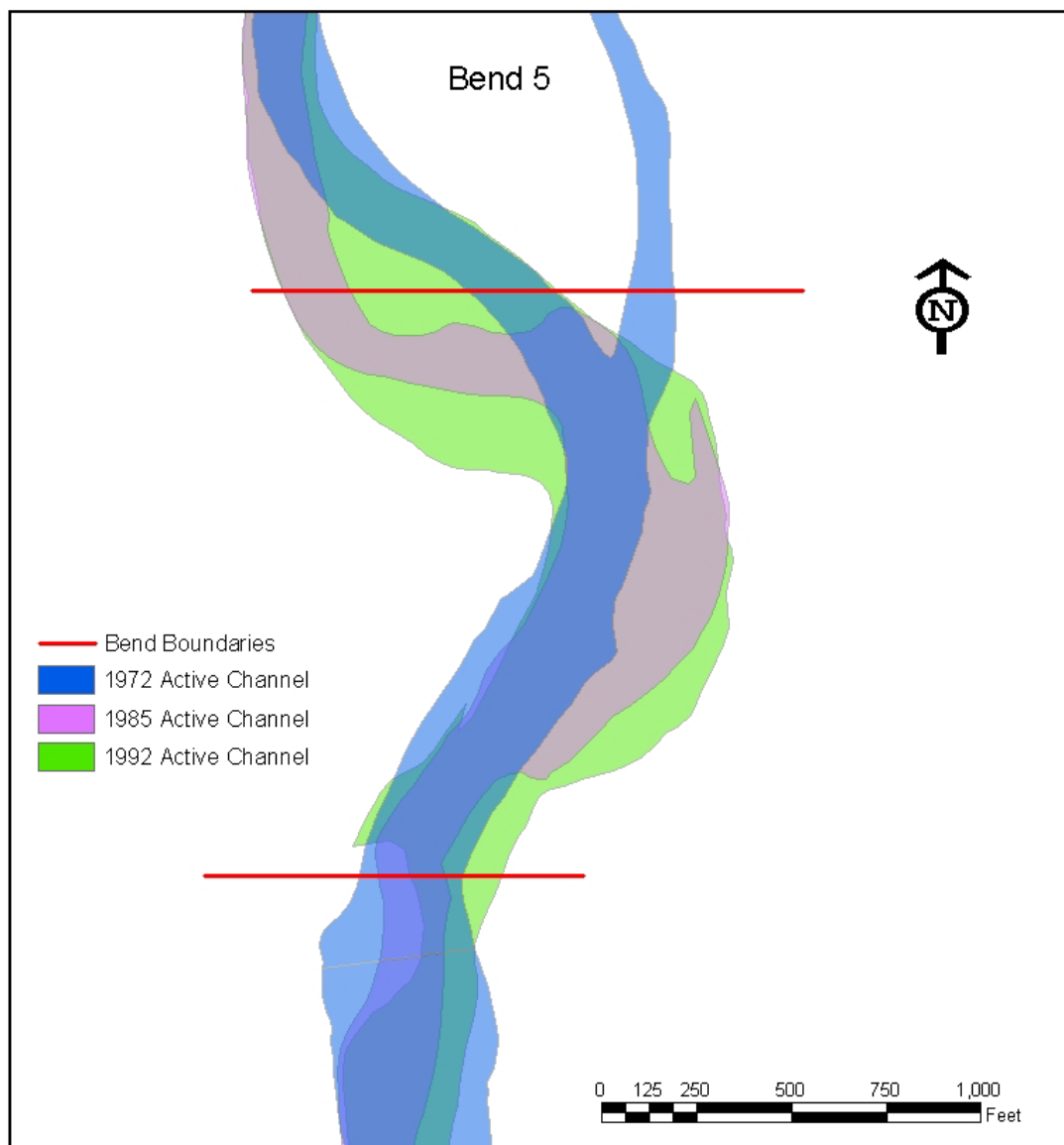


Figure M-5: Migration of bend 5 (1972-1992).

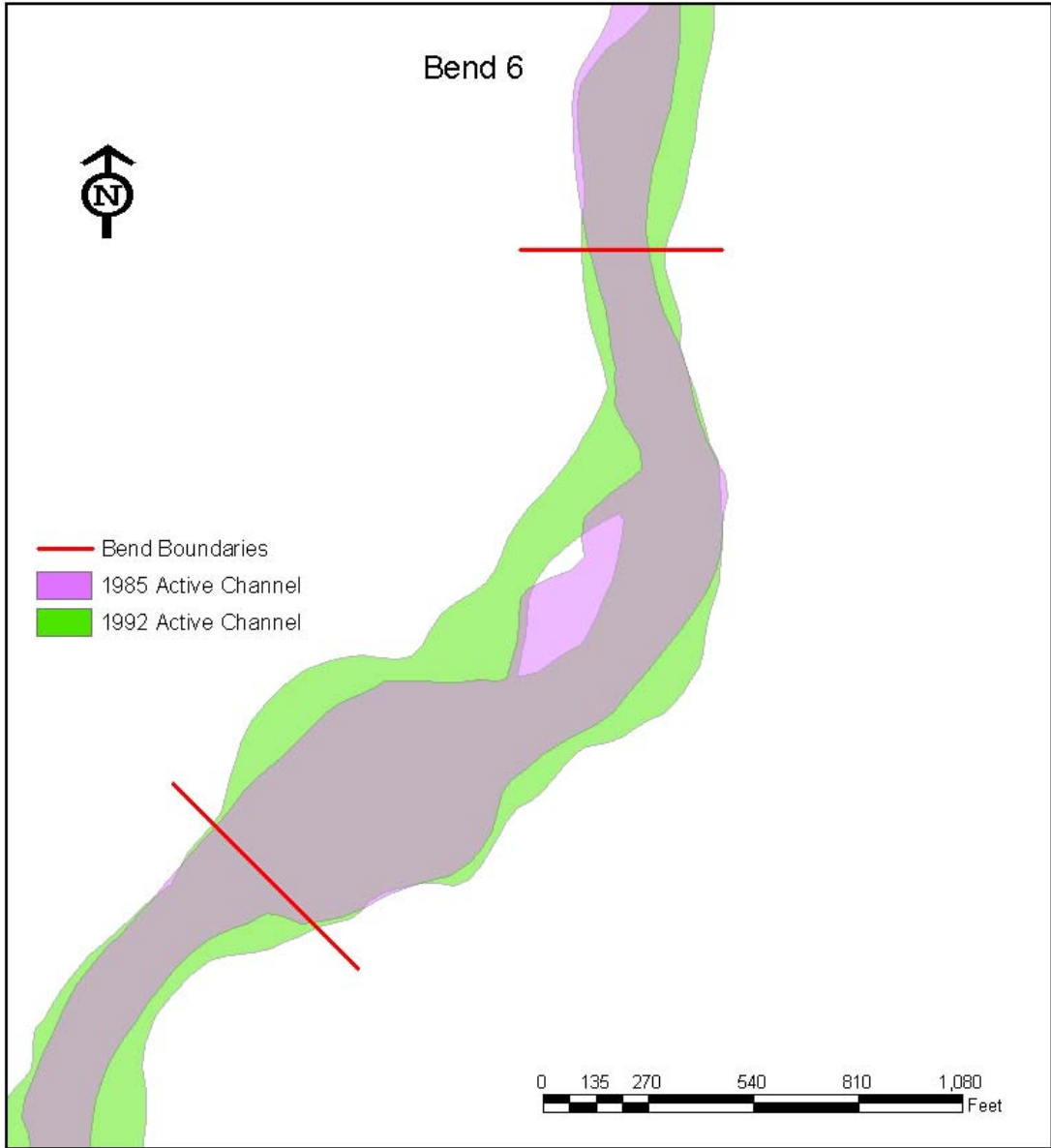


Figure M-6: Migration of bend 6 (1985-1992).

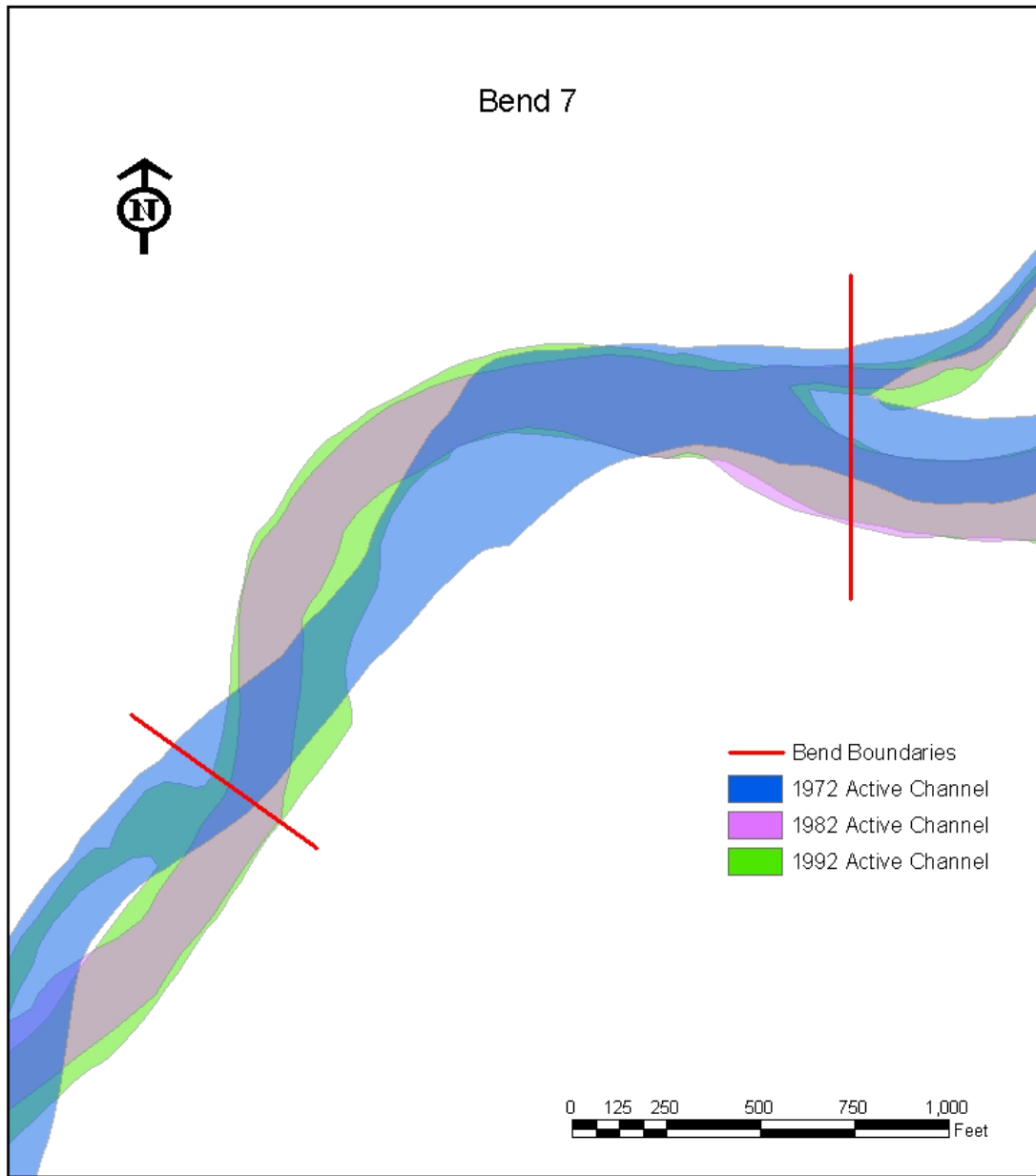


Figure M-7: Migration of bend 7 (1972-1992).

Table M-1: Migration rate input data for bend 1 (1972).

Bend 1
Year 1972
Depth (ft) 2.92 (avg.)

Bend id	Point id	GIS Coordinates (ft)		GIS Coordinates (ft)		width (ft)
		x _r	y _r	x _L	y _L	
1_72	1 (u/s)	458460.6	1641511.7	458461.9	1641347.9	164
1_72	2	458316.7	1641561.1	458397.5	1641305.0	269
1_72	3	458185.0	1641542.9	458346.5	1641265.0	322
1_72	4	458081.1	1641490.6	458299.4	1641223.3	345
1_72	5	457975.0	1641435.9	458243.0	1641165.6	381
1_72	6	457886.2	1641360.9	458197.0	1641112.3	398
1_72	7	457811.7	1641281.8	458136.7	1641039.2	406
1_72	8	457746.0	1641181.8	458089.5	1640984.3	396
1_72	9	457708.6	1641059.7	458049.0	1640919.7	368
1_72	10	457703.5	1640944.3	458006.3	1640845.2	319
1_72	11	457719.5	1640823.4	457961.1	1640757.1	250
1_72	12	457713.4	1640715.1	457926.8	1640672.6	218
1_72	13	457676.9	1640618.2	457898.9	1640577.7	226
1_72	14	457644.9	1640527.7	457880.2	1640480.5	240
1_72	15	457601.3	1640442.2	457868.6	1640376.4	275
1_72	16	457558.2	1640354.9	457800.6	1640286.2	252
1_72	17	457512.3	1640263.0	457738.7	1640207.9	233
1_72	18	457478.4	1640166.6	457692.5	1640118.7	219
1_72	19 (d/s)	457443.6	1640072.3	457659.6	1640024.4	221
input (GIS)						290
						(Average)

Table M-2: Migration rate input data for bend 1 (1985).

Bend 1
Year 1985
Depth (ft) 2.75 (avg.)

Bend id	Point id	GIS Coordinates (ft)		GIS Coordinates (ft)		width (ft)
		x _r	y _r	x _L	y _L	
1_85	1 (u/s)	458460.4	1641481.8	458462.9	1641234.1	247
1_85	2	458319.2	1641544.8	458416.3	1641246.8	282
1_85	3	458175.4	1641560.1	458340.8	1641274.6	256
1_85	4	458030.3	1641551.7	458238.4	1641298.7	249
1_85	5	457869.8	1641541.6	458088.8	1641321.0	240
1_85	6	457724.1	1641489.6	457975.7	1641290.3	296
1_85	7	457667.8	1641390.7	457873.9	1641237.1	256
1_85	8	457598.9	1641264.8	457776.2	1641163.3	205
1_85	9	457530.4	1641132.9	457745.9	1641045.9	233
1_85	10	457470.6	1641019.6	457785.0	1640917.0	314
1_85	11	457441.5	1640898.6	457869.0	1640780.8	419
1_85	12	457420.2	1640773.1	457883.8	1640681.2	471
1_85	13	457408.5	1640668.0	457883.3	1640578.4	480
1_85	14	457417.2	1640572.5	457882.0	1640479.9	465
1_85	15	457439.4	1640482.0	457846.9	1640383.7	419
1_85	16	457458.3	1640384.5	457821.5	1640279.6	368
1_85	17	457482.2	1640271.0	457798.9	1640192.1	318
1_85	18	457504.7	1640161.2	457782.8	1640098.3	283
1_85	19 (d/s)	457477.9	1640066.3	457755.7	1640001.5	291
input (GIS)						321
						(Average)

Table M-3: Migration rate input data for bend 1 (1992).

Bend 1
 Year 1992
 Depth (ft) 2.73 (avg.)

Bend id	Point id	GIS Coordinates (ft)		GIS Coordinates (ft)		width (ft)
		x _r	y _r	x _L	y _L	
1_92	1 (u/s)	458461.4	1641400.0	458461.4	1641240.7	159
1_92	2	458352.0	1641449.2	458415.5	1641251.3	165
1_92	3	458198.6	1641521.0	458346.5	1641267.1	205
1_92	4	458051.8	1641525.2	458251.8	1641282.3	236
1_92	5	457891.3	1641518.6	458111.6	1641299.2	228
1_92	6	457755.6	1641464.1	457972.2	1641292.3	248
1_92	7	457687.2	1641376.8	457851.7	1641253.5	205
1_92	8	457613.7	1641257.9	457779.3	1641162.2	191
1_92	9	457550.6	1641125.9	457727.9	1641052.4	192
1_92	10	457503.7	1641008.7	457688.6	1640950.0	194
1_92	11	457458.6	1640893.2	457643.1	1640844.5	191
1_92	12	457422.8	1640772.2	457619.5	1640734.1	200
1_92	13	457394.1	1640671.4	457661.4	1640622.1	272
1_92	14	457384.4	1640579.9	457799.7	1640496.4	358
1_92	15	457391.1	1640492.9	457836.7	1640385.9	437
1_92	16	457407.4	1640399.7	457816.1	1640280.7	413
1_92	17	457442.4	1640280.0	457788.2	1640194.8	349
1_92	18	457489.2	1640162.7	457766.3	1640100.3	279
1_92	19 (d/s)	457493.4	1640060.4	457743.3	1640006.1	258

input (GIS)

252
 (Average)

Table M-4: Migration rate input data for bend 2 (1972).

Bend 2
 Year 1972
 Depth (ft) 3.13 (avg.)

Bend id	Point id	GIS Coordinates (ft)		GIS Coordinates (ft)		width (ft)
		x _r	y _r	x _L	y _L	
2_72	1 (u/s)	457703.7	1640950.1	458039.1	1640903.8	339
2_72	2	457716.8	1640843.3	457982.1	1640802.0	269
2_72	3	457717.5	1640737.2	457937.9	1640706.0	223
2_72	4	457683.3	1640648.3	457905.6	1640605.1	227
2_72	5	457658.0	1640549.5	457882.9	1640504.6	229
2_72	6	457611.9	1640460.8	457875.0	1640398.1	271
2_72	7	457565.2	1640370.2	457807.9	1640298.3	253
2_72	8	457518.5	1640278.1	457744.1	1640214.3	235
2_72	9	457482.7	1640178.7	457697.8	1640135.3	219
2_72	10	457446.8	1640080.9	457659.7	1640024.7	220
2_72	11	457408.9	1640008.1	457589.9	1639936.2	195
2_72	12	457361.0	1639937.5	457516.0	1639847.8	179
2_72	13	457299.4	1639874.8	457441.2	1639762.5	181
2_72	14	457215.9	1639821.7	457347.6	1639686.6	190
2_72	15	457127.6	1639783.7	457272.3	1639610.0	227
2_72	16	457032.8	1639720.1	457194.6	1639548.1	236
2_72	17	456953.3	1639629.1	457132.0	1639476.5	235
2_72	18	456891.5	1639553.2	457069.5	1639411.3	228
2_72	19	456825.7	1639472.9	456995.8	1639335.6	219
2_72	20	456760.2	1639394.5	456920.8	1639270.8	202
2_72	21	456706.3	1639308.4	456845.9	1639213.8	168
2_72	22 (d/s)	456654.4	1639218.7	456797.5	1639158.8	155

input (GIS)

223
 (Average)

Table M-5: Migration rate input data for bend 2 (1985).

Bend 2
Year 1985
Depth (ft) 3.21 (avg.)

Bend id	Point id	GIS Coordinates (ft)		GIS Coordinates (ft)		width (ft)
		X _r	Y _r	X _L	Y _L	
2_85	1 (u/s)	457457.9	1640984.5	457768.2	1640940.3	306
2_85	2	457439.8	1640886.0	457847.9	1640823.0	398
2_85	3	457421.3	1640779.5	457884.9	1640713.4	463
2_85	4	457410.1	1640697.7	457882.7	1640610.8	474
2_85	5	457413.5	1640599.1	457883.5	1640503.0	466
2_85	6	457432.6	1640503.0	457859.4	1640400.7	433
2_85	7	457454.5	1640404.5	457824.2	1640292.5	372
2_85	8	457477.4	1640292.9	457799.9	1640198.2	320
2_85	9	457504.9	1640174.9	457786.5	1640115.7	288
2_85	10	457480.4	1640071.1	457753.8	1639997.4	279
2_85	11	457425.6	1639999.9	457701.4	1639892.6	292
2_85	12	457355.1	1639940.2	457658.5	1639766.1	349
2_85	13	457289.3	1639881.4	457593.3	1639642.2	387
2_85	14	457209.7	1639825.1	457470.6	1639558.2	374
2_85	15	457134.4	1639771.2	457351.3	1639513.1	340
2_85	16	457046.1	1639705.1	457259.6	1639481.9	307
2_85	17	456958.1	1639624.0	457157.5	1639459.4	250
2_85	18	456883.0	1639559.9	457057.7	1639420.9	215
2_85	19	456802.8	1639491.0	456932.2	1639388.2	164
2_85	20	456720.2	1639426.3	456839.2	1639333.6	151
2_85	21	456652.2	1639343.6	456770.8	1639262.4	144
2_85	22 (d/s)	456594.9	1639244.6	456720.1	1639190.2	137
input (GIS)						314

(Average)

Table M-6: Migration rate input data for bend 2 (1992).

Bend 2
Year 1992
Depth (ft) 3.21 (avg.)

Bend id	Point id	GIS Coordinates (ft)		GIS Coordinates (ft)		width (ft)
		X _r	Y _r	X _L	Y _L	
2_92	1 (u/s)	457492.2	1640981.0	457690.1	1640953.6	200
2_92	2	457455.4	1640884.3	457647.6	1640855.9	194
2_92	3	457424.6	1640778.2	457618.5	1640751.7	196
2_92	4	457400.0	1640699.8	457643.2	1640654.2	241
2_92	5	457384.4	1640605.7	457727.6	1640536.4	308
2_92	6	457388.7	1640512.7	457835.5	1640407.6	421
2_92	7	457403.4	1640419.6	457820.7	1640294.3	421
2_92	8	457433.6	1640304.5	457790.8	1640201.7	355
2_92	9	457482.9	1640179.4	457770.0	1640119.6	281
2_92	10	457496.4	1640068.1	457742.1	1640001.9	257
2_92	11	457473.1	1639982.7	457710.2	1639889.8	252
2_92	12	457456.7	1639879.9	457671.9	1639758.4	234
2_92	13	457454.1	1639753.9	457618.5	1639624.9	202
2_92	14	457400.6	1639630.4	457529.0	1639497.6	183
2_92	15	457310.8	1639563.5	457447.9	1639399.9	214
2_92	16	457218.9	1639522.2	457379.2	1639350.0	233
2_92	17	457118.5	1639492.2	457319.9	1639323.5	236
2_92	18	456994.2	1639473.0	457209.1	1639297.9	213
2_92	19	456847.0	1639454.5	457055.5	1639287.7	241
2_92	20	456755.7	1639397.7	456948.7	1639247.3	215
2_92	21	456679.6	1639324.3	456850.2	1639213.3	200
2_92	22 (d/s)	456615.3	1639232.7	456798.7	1639157.9	195
input (GIS)						250

(Average)

Table M-7: Migration rate input data for bend 3 (1972).

Bend 3
Year 1972
Depth (ft) 3.12 (avg.)

Bend id	Point id	GIS Coordinates (ft)		GIS Coordinates (ft)		width (ft)
		x _r	y _r	x _L	y _L	
3 72	1 (u/s)	456556.8	1638236.0	456740.3	1638222.5	184
3 72	2	456528.9	1638142.1	456734.2	1638118.9	207
3 72	3	456500.3	1638046.1	456739.0	1638017.0	240
3 72	4	456468.5	1637957.6	456728.8	1637920.5	263
3 72	5	456469.1	1637859.5	456720.5	1637821.1	255
3 72	6	456504.3	1637758.0	456711.2	1637720.7	210
3 72	7	456468.4	1637673.7	456696.6	1637615.3	236
3 72	8	456442.8	1637590.4	456650.4	1637514.4	221
3 72	9	456384.2	1637516.2	456619.7	1637408.9	258
3 72	10	456329.8	1637448.1	456589.8	1637301.6	298
3 72	11	456274.2	1637371.8	456542.8	1637208.9	314
3 72	12	456218.5	1637295.3	456486.1	1637135.1	312
3 72	13	456128.2	1637239.4	456415.4	1637044.8	347
3 72	14	456077.6	1637175.1	456345.5	1636963.3	341
3 72	15	455996.3	1637110.0	456280.9	1636897.8	355
3 72	16	455972.3	1636995.5	456221.7	1636826.4	302
3 72	17	455948.7	1636896.5	456157.0	1636757.3	251
3 72	18	455915.4	1636787.0	456096.3	1636680.1	210
3 72	19	455858.3	1636692.6	456050.3	1636624.0	204
3 72	20 (d/s)	455823.0	1636600.7	456002.1	1636547.2	187

input (GIS)

260
(Average)

Table M-8: Migration rate input data for bend 3 (1985).

Bend 3
Year 1985
Depth (ft) 2.94 (avg.)

Bend id	Point id	GIS Coordinates (ft)		GIS Coordinates (ft)		width (ft)
		x _r	y _r	x _L	y _L	
3 85	1 (u/s)	456432.8	1638244.7	456812.8	1638216.2	374
3 85	2	456430.0	1638154.0	456807.6	1638110.8	389
3 85	3	456443.6	1638053.2	456741.2	1638016.6	297
3 85	4	456463.0	1637959.5	456744.9	1637917.4	276
3 85	5	456484.9	1637858.4	456780.0	1637811.6	273
3 85	6	456525.0	1637754.9	456825.9	1637699.5	271
3 85	7	456575.4	1637646.8	456873.8	1637571.5	260
3 85	8	456647.5	1637515.0	456932.0	1637411.2	262
3 85	9	456656.8	1637392.0	456985.0	1637243.9	318
3 85	10	456641.4	1637273.6	456981.4	1637083.9	363
3 85	11	456623.2	1637159.2	456939.5	1636967.5	373
3 85	12	456533.5	1637105.0	456885.8	1636894.1	399
3 85	13	456400.9	1637056.2	456764.6	1636809.1	404
3 85	14	456270.5	1637023.9	456593.1	1636765.0	401
3 85	15	456169.4	1636979.8	456515.2	1636725.5	407
3 85	16	456057.5	1636939.3	456400.8	1636703.7	370
3 85	17	455971.8	1636882.3	456264.8	1636684.0	322
3 85	18	455867.6	1636815.3	456141.9	1636653.4	277
3 85	19	455704.9	1636745.5	456008.3	1636638.3	219
3 85	20 (d/s)	455580.8	1636671.3	455874.8	1636584.1	263

input (GIS)

326
(Average)

Table M-9: Migration rate input data for bend 3 (1992).

Bend 3
Year 1992
Depth (ft) 2.93 (avg.)

Bend id	Point id	GIS Coordinates (ft)		GIS Coordinates (ft)		width (ft)
		x _r	y _r	x _L	y _L	
3 92	1 (u/s)	456437.2	1638245.1	456792.7	1638218.5	347
3 92	2	456429.8	1638155.8	456843.6	1638104.9	400
3 92	3	456425.8	1638054.7	456871.0	1637999.8	441
3 92	4	456426.5	1637965.2	456857.9	1637902.4	446
3 92	5	456426.7	1637866.2	456801.3	1637808.1	384
3 92	6	456437.3	1637769.6	456782.4	1637708.8	336
3 92	7	456461.1	1637677.6	456810.0	1637586.0	340
3 92	8	456453.4	1637584.6	456844.9	1637443.8	380
3 92	9	456448.6	1637487.3	456887.8	1637286.4	431
3 92	10	456428.5	1637392.5	456918.6	1637119.5	515
3 92	11	456396.8	1637298.3	456884.1	1637001.1	552
3 92	12	456373.6	1637202.0	456851.4	1636915.1	547
3 92	13	456328.1	1637105.4	456771.7	1636803.3	542
3 92	14	456258.5	1637031.9	456667.5	1636707.5	530
3 92	15	456186.0	1636967.6	456596.5	1636661.6	512
3 92	16	456104.0	1636907.9	456512.2	1636627.4	469
3 92	17	456011.4	1636857.0	456367.7	1636616.3	387
3 92	18	455900.5	1636797.4	456193.1	1636626.4	252
3 92	19	455731.2	1636737.1	456029.7	1636631.7	149
3 92	20 (d/s)	455577.7	1636672.5	455795.8	1636609.0	140

input (GIS)

405
(Average)

Table M-10: Migration rate input data for bend 4 (1972).

Bend 4
Year 1972
Depth (ft) 3.47 (avg.)

Bend id	Point id	GIS Coordinates (ft)		GIS Coordinates (ft)		width (ft)
		x _r	y _r	x _L	y _L	
4 72	1 (u/s)	456004.5	1637120.8	456389.7	1637011.4	400
4 72	2	455980.0	1637031.4	456311.6	1636927.2	348
4 72	3	455960.8	1636954.2	456247.5	1636862.8	300
4 72	4	455941.2	1636861.7	456181.1	1636776.7	254
4 72	5	455908.7	1636775.4	456111.4	1636701.7	216
4 72	6	455859.9	1636695.2	456046.8	1636620.8	201
4 72	7	455825.6	1636608.0	455999.7	1636542.9	186
4 72	8	455795.9	1636509.8	455946.7	1636461.4	158
4 72	9	455766.3	1636408.6	455908.3	1636385.2	144
4 72	10	455740.7	1636311.9	455891.3	1636293.0	152
4 72	11	455716.9	1636217.3	455868.8	1636199.9	153
4 72	12	455696.4	1636118.9	455851.5	1636107.2	156
4 72	13	455683.6	1636017.9	455870.2	1636015.3	186
4 72	14	455679.6	1635924.5	455873.0	1635919.4	194
4 72	15	455682.6	1635826.3	455860.5	1635825.6	178
4 72	16	455676.5	1635732.7	455853.8	1635722.8	178
4 72	17	455661.1	1635637.4	455846.1	1635631.8	185
4 72	18	455643.3	1635540.1	455830.5	1635537.0	187
4 72	19	455630.1	1635448.6	455835.9	1635439.7	205
4 72	20 (d/s)	455620.0	1635356.1	455877.1	1635345.4	257

input (GIS)

212
(Average)

Table M-11: Migration rate input data for bend 4 (1985).

Bend 4
Year 1985
Depth (ft) 3.14 (avg.)

Bend id	Point id	GIS Coordinates (ft)		GIS Coordinates (ft)		width (ft)
		x _r	y _r	x _L	y _L	
4 85	1 (u/s)	456302.3	1637036.3	456866.3	1636874.3	390
4 85	2	456161.8	1636976.3	456731.2	1636795.4	382
4 85	3	456033.7	1636929.6	456575.9	1636758.1	377
4 85	4	455943.1	1636861.3	456379.9	1636704.5	312
4 85	5	455841.1	1636801.6	456197.4	1636672.1	254
4 85	6	455720.9	1636752.0	456003.6	1636637.7	207
4 85	7	455608.6	1636689.7	455880.9	1636588.3	255
4 85	8	455497.2	1636607.4	455823.7	1636502.8	334
4 85	9	455407.7	1636466.6	455804.7	1636401.6	401
4 85	10	455405.2	1636355.5	455800.0	1636305.0	396
4 85	11	455405.4	1636254.5	455802.2	1636208.3	397
4 85	12	455416.7	1636140.0	455806.1	1636110.4	386
4 85	13	455446.5	1636025.1	455816.0	1636016.3	366
4 85	14	455472.3	1635930.6	455826.2	1635920.7	350
4 85	15	455506.2	1635827.2	455836.9	1635826.1	328
4 85	16	455543.0	1635740.9	455843.9	1635723.8	296
4 85	17	455593.9	1635638.7	455838.8	1635633.0	242
4 85	18	455638.2	1635541.1	455835.7	1635536.3	197
4 85	19	455662.6	1635447.0	455830.7	1635441.3	168
4 85	20 (d/s)	455674.4	1635354.7	455830.3	1635346.9	156

input (GIS)

310
(Average)

Table M-12: Migration rate input data for bend 4 (1992).

Bend 4
Year 1992
Depth (ft) 3.18 (avg.)

Bend id	Point id	GIS Coordinates (ft)		GIS Coordinates (ft)		width (ft)
		x _r	y _r	x _L	y _L	
4 92	1 (u/s)	456272.8	1637045.2	456836.5	1636882.7	567
4 92	2	456185.4	1636967.1	456757.9	1636785.4	576
4 92	3	456104.3	1636908.1	456689.9	1636721.6	573
4 92	4	455990.3	1636845.0	456559.4	1636641.4	533
4 92	5	455881.2	1636786.2	456334.8	1636619.7	351
4 92	6	455745.2	1636742.7	456020.8	1636630.1	150
4 92	7	455613.6	1636688.5	455811.4	1636612.9	147
4 92	8	455473.3	1636615.5	455647.2	1636558.6	130
4 92	9	455318.5	1636480.2	455472.6	1636455.4	147
4 92	10	455284.3	1636371.5	455435.2	1636352.0	151
4 92	11	455269.1	1636269.0	455427.0	1636251.5	159
4 92	12	455271.8	1636150.6	455426.6	1636138.9	151
4 92	13	455308.7	1636028.2	455487.4	1636024.4	168
4 92	14	455348.9	1635932.2	455550.7	1635927.5	196
4 92	15	455399.8	1635827.7	455591.1	1635827.1	185
4 92	16	455439.5	1635745.5	455633.0	1635735.1	182
4 92	17	455508.2	1635641.0	455683.4	1635636.9	158
4 92	18	455582.5	1635542.1	455712.2	1635538.3	123
4 92	19	455632.3	1635448.2	455762.7	1635443.5	120
4 92	20 (d/s)	455652.6	1635354.8	455795.9	1635349.0	145

input (GIS)

246
(Average)

Table M-13: Migration rate input data for bend 5 (1972).

Bend 5
Year 1972
Depth (ft) 2.58 (avg.)

Bend id	Point id	GIS Coordinates (ft)		GIS Coordinates (ft)		width (ft)
		x _r	y _r	x _L	y _L	
5 72	1 (u/s)	454945.9	1631897.9	455428.5	1632234.7	535
5 72	2	455010.3	1631822.0	455435.2	1632112.5	430
5 72	3	455054.9	1631748.1	455439.0	1631973.0	385
5 72	4	455089.9	1631682.4	455444.5	1631837.3	322
5 72	5	455109.2	1631623.2	455411.5	1631670.4	306
5 72	6	455145.0	1631544.2	455374.1	1631560.2	229
5 72	7	455159.7	1631453.8	455372.3	1631464.3	213
5 72	8	455144.1	1631387.3	455364.5	1631360.2	222
5 72	9	455114.9	1631311.0	455337.7	1631253.8	230
5 72	10	455085.5	1631228.9	455307.6	1631167.8	230
5 72	11	455037.5	1631168.4	455281.1	1631071.0	263
5 72	12	454972.2	1631102.4	455263.9	1630958.7	325
5 72	13	454924.3	1631033.6	455196.6	1630893.9	307
5 72	14	454874.0	1630951.7	455141.1	1630818.8	298
5 72	15	454824.6	1630875.2	455088.7	1630745.7	294
5 72	16	454770.7	1630798.0	455028.9	1630668.1	289
5 72	17	454726.6	1630712.5	454988.0	1630600.5	284
5 72	18	454682.5	1630611.4	454944.7	1630534.3	273
5 72	19	454638.8	1630515.0	454908.6	1630462.2	275
5 72	20 (d/s)	454613.6	1630410.9	454887.1	1630397.9	274

input (GIS)

299
(Average)

Table M-14: Migration rate input data for bend 5 (1985).

Bend 5
Year 1985
Depth (ft) 2.01 (avg.)

Bend id	Point id	GIS Coordinates (ft)		GIS Coordinates (ft)		width (ft)
		x _r	y _r	x _L	y _L	
5 85	1 (u/s)	454682.7	1631716.0	454885.6	1631857.1	174
5 85	2	454814.5	1631688.3	455029.5	1631832.0	196
5 85	3	454921.5	1631670.0	455241.1	1631857.0	291
5 85	4	455042.7	1631661.6	455320.6	1631782.9	265
5 85	5	455119.8	1631626.0	455360.7	1631662.8	236
5 85	6	455150.6	1631542.7	455531.4	1631572.1	382
5 85	7	455158.5	1631454.1	455562.3	1631474.0	404
5 85	8	455162.2	1631386.6	455586.3	1631332.5	426
5 85	9	455152.0	1631300.6	455574.9	1631195.1	435
5 85	10	455122.4	1631217.4	455546.6	1631102.6	439
5 85	11	455089.1	1631146.6	455482.4	1630990.0	423
5 85	12	455045.2	1631065.8	455387.8	1630898.0	382
5 85	13	454988.4	1630999.2	455306.3	1630838.7	356
5 85	14	454938.2	1630920.2	455233.0	1630771.8	330
5 85	15	454901.5	1630837.2	455167.6	1630707.7	296
5 85	16	454842.4	1630764.5	455019.5	1630673.1	199
5 85	17	454786.2	1630686.4	454941.6	1630619.5	169
5 85	18	454721.7	1630601.2	454894.0	1630548.3	180
5 85	19	454666.2	1630511.1	454851.6	1630474.7	188
5 85	20 (d/s)	454661.2	1630409.7	454840.2	1630401.9	179

input (GIS)

298
(Average)

Table M-15: Migration rate input data for bend 5 (1992).

Bend **5**
Year **1992**
Depth (ft) **2.02 (avg.)**

Bend id	Point id	GIS Coordinates (ft)		GIS Coordinates (ft)		width (ft)
		x _r	y _r	x _L	y _L	
5 92	1 (u/s)	454597.6	1631655.0	455081.7	1631991.6	589
5 92	2	454672.1	1631591.6	455162.5	1631923.0	592
5 92	3	454728.7	1631558.3	455241.9	1631859.4	596
5 92	4	454759.2	1631538.0	455346.5	1631793.7	616
5 92	5	454717.5	1631565.5	455508.3	1631684.8	595
5 92	6	454784.7	1631516.1	455547.2	1631572.1	538
5 92	7	455069.3	1631449.0	455562.4	1631474.0	460
5 92	8	455118.2	1631391.8	455578.8	1631332.9	459
5 92	9	455118.9	1631310.1	455590.8	1631192.1	485
5 92	10	455101.8	1631223.8	455585.7	1631091.3	502
5 92	11	455079.4	1631149.5	455551.3	1630963.9	507
5 92	12	455039.3	1631069.5	455496.8	1630844.8	511
5 92	13	455000.5	1630993.5	455425.1	1630780.1	475
5 92	14	454957.3	1630911.2	455352.3	1630713.0	441
5 92	15	454886.2	1630844.7	455243.3	1630670.4	369
5 92	16	454832.2	1630769.3	455109.6	1630626.3	312
5 92	17	454769.7	1630693.6	455065.5	1630567.6	322
5 92	18	454665.9	1630618.3	455032.5	1630505.6	384
5 92	19	454614.9	1630522.1	455003.8	1630443.1	397
5 92	20 (d/s)	454745.7	1630406.1	454985.8	1630394.3	240
input (GIS)						469

(Average)

Table M-16: Migration rate input data for bend 6 (1985).

Bend **6**
Year **1985**
Depth (ft) **2.36 (avg.)**

Bend id	Point id	GIS Coordinates (ft)		GIS Coordinates (ft)		width (ft)
		x _r	y _r	x _L	y _L	
6 85	1 (u/s)	454601.3	1629515.6	454753.2	1629523.1	152
6 85	2	454632.7	1629400.0	454775.8	1629411.3	144
6 85	3	454654.9	1629281.9	454817.4	1629303.1	164
6 85	4	454666.3	1629177.1	454854.3	1629196.8	189
6 85	5	454696.5	1629058.5	454881.9	1629084.8	187
6 85	6	454734.6	1628957.6	454927.0	1628979.5	193
6 85	7	454640.0	1628879.5	454946.4	1628824.2	312
6 85	8	454582.9	1628790.9	454931.4	1628704.4	359
6 85	9	454571.0	1628709.5	454868.0	1628583.8	322
6 85	10	454490.6	1628666.7	454784.2	1628474.8	352
6 85	11	454420.6	1628592.7	454707.0	1628380.1	357
6 85	12	454403.5	1628467.9	454630.8	1628303.5	281
6 85	13	454342.3	1628408.3	454502.3	1628229.0	241
6 85	14	454228.2	1628402.6	454403.5	1628154.8	304
6 85	15	454077.1	1628406.3	454358.8	1628047.4	456
6 85	16	453978.7	1628358.8	454293.9	1627942.5	522
6 85	17	453889.5	1628294.3	454185.7	1627891.2	500
6 85	18	453800.7	1628206.0	454091.8	1627859.0	453
6 85	19	453717.3	1628130.3	453991.2	1627810.1	420
6 85	20 (d/s)	453647.1	1628041.5	453865.7	1627780.8	341
input (GIS)						312

(Average)

Table M-17: Migration rate input data for bend 6 (1992).

Bend **6**
Year **1992**
Depth (ft) **2.36 (avg.)**

Bend id	Point id	GIS Coordinates (ft)		GIS Coordinates (ft)		width (ft)
		x _r	y _r	x _L	y _L	
6_92	1 (u/s)	454580.0	1629514.6	454794.4	1629525.0	214
6_92	2	454590.4	1629396.8	454812.4	1629413.8	223
6_92	3	454617.2	1629280.0	454837.1	1629304.5	221
6_92	4	454644.5	1629174.7	454857.1	1629196.3	214
6_92	5	454588.0	1629041.5	454892.7	1629086.4	300
6_92	6	454516.1	1628933.3	454929.4	1628980.0	393
6_92	7	454491.7	1628905.4	454941.1	1628823.7	456
6_92	8	454425.4	1628828.5	454939.4	1628703.1	539
6_92	9	454396.4	1628783.3	454907.2	1628565.5	565
6_92	10	454378.0	1628737.5	454867.7	1628420.1	583
6_92	11	454331.7	1628658.1	454788.8	1628321.0	567
6_92	12	454233.5	1628589.9	454688.5	1628262.6	531
6_92	13	454205.8	1628559.8	454536.2	1628190.3	496
6_92	14	454164.6	1628493.3	454445.7	1628094.2	486
6_92	15	454027.2	1628470.4	454377.1	1628025.1	566
6_92	16	453909.2	1628449.1	454311.7	1627917.7	667
6_92	17	453812.5	1628397.2	454188.6	1627884.3	636
6_92	18	453726.5	1628295.8	454085.8	1627864.3	561
6_92	19	453678.9	1628175.6	453996.5	1627801.4	490
6_92	20 (d/s)	453639.5	1628050.8	453881.8	1627761.9	377
input (GIS)						454
						(Average)

Table M-18: Migration rate input data for bend 7 (1972).

Bend **7**
Year **1972**
Depth (ft) **3.01 (avg.)**

Bend id	Point id	GIS Coordinates (ft)		GIS Coordinates (ft)		width (ft)
		x _r	y _r	x _L	y _L	
7_72	1 (u/s)	447970.3	1621517.8	447970.3	1621168.0	349
7_72	2	447867.9	1621510.8	447865.6	1621199.8	310
7_72	3	447768.8	1621519.6	447766.5	1621212.2	306
7_72	4	447661.3	1621524.9	447661.2	1621244.0	278
7_72	5	447559.2	1621519.6	447558.8	1621258.1	260
7_72	6	447455.3	1621526.6	447461.5	1621240.4	285
7_72	7	447341.7	1621524.7	447376.9	1621219.2	307
7_72	8	447221.9	1621513.0	447287.6	1621182.0	339
7_72	9	447095.6	1621502.3	447233.7	1621142.2	383
7_72	10	446974.4	1621452.4	447189.3	1621110.1	405
7_72	11	446899.4	1621344.8	447133.7	1621059.5	369
7_72	12	446826.1	1621253.4	447085.9	1621014.9	353
7_72	13	446768.2	1621156.9	446992.8	1620974.8	288
7_72	14	446712.4	1621059.7	446920.0	1620912.4	252
7_72	15	446677.1	1620965.0	446844.6	1620837.3	209
7_72	16	446615.2	1620881.1	446783.4	1620760.4	204
7_72	17	446552.4	1620810.4	446703.2	1620685.7	198
7_72	18	446481.2	1620729.8	446639.2	1620606.5	200
7_72	19	446407.9	1620660.3	446570.7	1620519.5	218
7_72	20	446332.4	1620602.6	446509.2	1620443.4	238
7_72	21	446243.8	1620533.4	446449.6	1620366.1	262
7_72	22 (d/s)	446172.0	1620465.5	446377.0	1620292.0	267
input (GIS)						285
						(Average)

Table M-19: Migration rate input data for bend 7 (1985).

Bend 7
Year 1985
Depth (ft) 3.54 (avg.)

Bend id	Point id	GIS Coordinates (ft)		GIS Coordinates (ft)		width (ft)
		x _r	y _r	x _L	y _L	
7 85	1 (u/s)	447971.0	1621464.5	447971.5	1621044.0	421
7 85	2	447866.8	1621465.5	447864.5	1621071.9	393
7 85	3	447768.8	1621468.6	447765.4	1621107.7	361
7 85	4	447661.7	1621454.9	447662.4	1621165.3	289
7 85	5	447559.4	1621462.4	447558.5	1621231.8	231
7 85	6	447456.5	1621479.2	447461.5	1621225.3	254
7 85	7	447344.8	1621496.1	447375.5	1621241.3	250
7 85	8	447228.1	1621488.2	447271.2	1621274.1	210
7 85	9	447107.5	1621472.6	447175.2	1621298.3	177
7 85	10	446976.8	1621446.7	447072.5	1621298.7	164
7 85	11	446847.1	1621408.1	446962.7	1621266.9	183
7 85	12	446721.8	1621348.4	446867.9	1621217.4	196
7 85	13	446624.9	1621272.8	446765.8	1621159.7	180
7 85	14	446537.2	1621181.8	446670.3	1621088.3	163
7 85	15	446482.4	1621114.1	446615.7	1621011.5	168
7 85	16	446418.5	1621021.5	446578.2	1620907.1	196
7 85	17	446377.0	1620953.7	446527.0	1620831.9	190
7 85	18	446345.3	1620835.2	446511.3	1620706.6	173
7 85	19	446341.5	1620718.5	446500.8	1620579.4	167
7 85	20	446342.8	1620591.3	446485.9	1620462.8	152
7 85	21	446335.8	1620457.3	446468.4	1620350.3	151
7 85	22 (d/s)	446310.8	1620348.0	446435.9	1620241.2	167
input (GIS)						220

(Average)

Table M-20: Migration rate input data for bend 7 (1992).

Bend 7
Year 1992
Depth (ft) 3.54 (avg.)

Bend id	Point id	GIS Coordinates (ft)		GIS Coordinates (ft)		width (ft)
		x _r	y _r	x _L	y _L	
7 92	1 (u/s)	447970.7	1621473.2	447971.5	1621053.1	419
7 92	2	447867.0	1621461.1	447864.6	1621087.6	374
7 92	3	447767.6	1621466.2	447766.2	1621143.4	323
7 92	4	447661.7	1621474.7	447661.5	1621202.1	273
7 92	5	447559.7	1621493.3	447558.2	1621224.7	269
7 92	6	447456.4	1621502.7	447461.5	1621224.6	277
7 92	7	447342.4	1621517.2	447374.2	1621241.2	267
7 92	8	447220.3	1621525.9	447270.8	1621269.8	252
7 92	9	447090.5	1621516.0	447181.3	1621280.7	239
7 92	10	446956.4	1621481.1	447078.6	1621288.5	210
7 92	11	446832.9	1621424.4	446964.7	1621266.0	198
7 92	12	446709.7	1621359.5	446874.7	1621208.4	219
7 92	13	446604.1	1621289.6	446791.7	1621139.0	241
7 92	14	446514.9	1621198.5	446736.8	1621041.2	272
7 92	15	446465.3	1621125.2	446715.2	1620935.8	301
7 92	16	446401.9	1621035.9	446685.5	1620830.0	349
7 92	17	446366.7	1620962.1	446641.4	1620737.1	333
7 92	18	446340.7	1620839.1	446628.0	1620613.6	309
7 92	19	446325.0	1620731.9	446617.5	1620478.6	326
7 92	20	446317.3	1620615.1	446559.3	1620397.6	309
7 92	21	446297.8	1620489.9	446503.7	1620322.1	257
7 92	22 (d/s)	446270.8	1620381.8	446440.6	1620237.7	221
input (GIS)						284

(Average)

Table M-21: Migration rate calculations for bend 1 (1972-1992).

Bend 1 Point id	1972 - 1985					1985 - 1992				
	Δr (ft)	Δl (ft)	Δw (ft)	Δt (yrs)	M (ft/yr)	Δr (ft)	Δl (ft)	Δw (ft)	Δt (yrs)	M (ft/yr)
1 (u/s)	29.9	113.9	83.1	13	4.7	81.8	6.8	-88.3	7	25.3
2	16.5	61.2	12.7	13	5.0	101.0	4.6	-116.6	7	31.7
3	19.7	11.2	-66.0	13	7.5	45.5	9.4	-50.6	7	15.1
4	79.5	96.9	-96.4	13	21.0	34.1	21.1	-12.4	7	9.7
5	149.1	218.9	-140.5	13	39.1	31.4	31.6	-12.2	7	10.7
6	207.0	284.0	-102.3	13	45.6	40.6	4.0	-48.1	7	13.2
7	180.4	329.0	-149.7	13	50.7	23.9	27.6	-50.8	7	14.6
8	168.9	360.9	-191.0	13	55.4	16.4	3.3	-13.9	7	4.8
9	192.6	328.3	-135.5	13	50.5	21.4	19.1	-40.8	7	11.6
10	244.8	232.7	-5.1	13	37.1	34.9	101.9	-119.7	7	36.6
11	288.0	95.0	168.3	13	16.5	17.9	234.8	-228.0	7	68.7
12	298.9	43.9	252.9	13	6.9	2.7	269.5	-270.3	7	77.5
13	273.0	15.6	254.5	13	2.6	14.8	226.2	-208.0	7	64.1
14	232.0	1.9	225.9	13	0.6	33.6	84.0	-107.3	7	32.1
15	166.7	22.9	144.0	13	3.5	49.6	10.4	17.4	7	6.1
16	104.2	21.9	116.1	13	0.8	53.2	5.5	45.2	7	1.9
17	31.1	62.2	85.4	13	0.6	40.8	11.0	31.3	7	2.9
18	26.9	92.6	64.0	13	4.3	15.7	16.6	-4.6	7	5.3
19 (d/s)	34.8	98.7	70.3	13	4.9	16.6	13.2	-33.1	7	9.0
	31				19	-69				23
	(Average)				(Average)	(Average)				(Average)

Point id	1972 - 1992				
	Δr (ft)	Δl (ft)	Δw (ft)	Δt (yrs)	M (ft/yr)
1 (u/s)	111.7	107.3	-5.2	20	11.2
2	117.3	56.7	-103.9	20	13.9
3	25.8	2.1	-116.6	20	7.2
4	45.3	75.8	-108.8	20	11.5
5	117.7	187.4	-152.7	20	22.9
6	166.4	288.0	-150.5	20	30.2
7	156.5	356.6	-200.6	20	35.7
8	152.6	357.6	-205.0	20	35.8
9	171.3	347.4	-176.3	20	34.7
10	209.9	334.6	-124.7	20	33.5
11	270.1	329.8	-59.6	20	33.0
12	296.1	313.5	-17.4	20	31.4
13	287.7	241.6	46.5	20	24.1
14	265.6	82.1	118.6	20	11.5
15	216.3	33.3	161.4	20	4.4
16	157.4	16.4	161.2	20	0.6
17	71.9	51.2	116.7	20	0.3
18	11.4	76.1	59.4	20	1.4
19 (d/s)	51.2	85.6	37.3	20	5.0
	-38				18
	(Average)				(Average)

- Apex early year
- Apex late year
- Apex same year

Table M-22: Migration rate calculations for bend 2 (1972-1992).

Bend 2 Point id	1972 - 1985					1985 - 1992				
	Δr (ft)	Δl (ft)	Δw (ft)	Δt (yrs)	M (ft/yr)	Δr (ft)	Δl (ft)	Δw (ft)	Δt (yrs)	M (ft/yr)
1 (u/s)	248.2	273.4	-33.3	13	42.7	34.5	79.1	-106.2	7	31.4
2	280.3	135.9	128.6	13	22.1	15.7	202.9	-203.5	7	60.3
3	299.2	53.6	240.5	13	8.6	3.6	269.1	-267.6	7	77.2
4	277.6	23.6	247.6	13	4.1	10.3	243.4	-233.6	7	69.6
5	249.5	1.6	236.2	13	1.1	29.9	159.4	-157.4	7	49.5
6	184.2	15.9	162.5	13	2.9	45.0	24.8	-12.0	7	11.7
7	115.9	17.3	118.9	13	1.1	53.3	3.9	48.8	7	1.2
8	43.7	58.1	85.7	13	1.2	45.3	9.8	34.4	7	3.0
9	22.5	90.9	68.5	13	3.5	22.4	17.0	-7.2	7	6.7
10	35.0	97.9	59.0	13	5.7	16.3	12.5	-21.8	7	7.2
11	18.6	119.6	96.7	13	3.2	50.5	9.3	-39.2	7	14.1
12	6.5	164.3	170.3	13	0.0	118.1	15.5	-115.9	7	35.6
13	12.1	193.9	205.9	13	0.0	208.4	30.6	-184.8	7	60.5
14	7.1	177.8	184.0	13	0.1	272.6	84.1	-191.0	7	78.2
15	14.2	125.1	113.4	13	2.0	272.5	148.8	-126.2	7	78.2
16	20.2	92.7	70.8	13	3.2	251.6	178.1	-74.5	7	72.0
17	7.0	30.7	14.8	13	1.8	207.5	211.7	-14.0	7	61.9
18	10.8	15.2	-12.2	13	2.9	141.1	195.1	-2.1	7	48.3
19	29.2	82.5	-54.3	13	12.8	57.3	159.1	76.3	7	20.0
20	51.1	103.0	-51.6	13	15.8	45.6	139.5	64.9	7	17.2
21	64.5	89.4	-24.6	13	13.7	33.5	93.3	55.9	7	10.1
22 (d/s)	65.0	83.5	-18.4	13	12.8	23.7	85.0	58.2	7	7.2
	91				7.3			-64		37
	(Average)				(Average)			(Average)		(Average)

Point id	1972 - 1992				
	Δr (ft)	Δl (ft)	Δw (ft)	Δt (yrs)	M (ft/yr)
1 (u/s)	213.7	352.5	-139.5	20	35.3
2	264.7	338.8	-74.9	20	33.9
3	295.7	322.7	-27.1	20	32.3
4	287.9	267.0	14.0	20	27.0
5	279.3	158.5	78.9	20	17.9
6	229.2	40.6	150.5	20	6.0
7	169.1	13.5	167.7	20	0.7
8	88.9	48.3	120.0	20	0.9
9	0.7	73.9	61.3	20	0.7
10	51.2	85.4	37.1	20	5.0
11	69.0	129.0	57.5	20	7.0
12	111.7	179.7	54.5	20	11.8
13	196.3	224.4	21.1	20	20.0
14	265.9	261.9	-7.0	20	26.7
15	286.4	273.9	-12.8	20	28.7
16	271.8	270.8	-3.8	20	27.3
17	214.5	242.3	0.8	20	22.8
18	130.3	179.9	-14.3	20	16.2
19	28.1	76.5	22.0	20	4.1
20	5.6	36.5	13.3	20	1.4
21	31.0	4.3	31.3	20	0.2
22 (d/s)	41.5	1.5	39.8	20	0.2
	27				15
	(Average)				(Average)

- Apex early year
- Apex late year
- Apex same year

Table M-23: Migration rate calculations for bend 3 (1972-1992).

Bend 3		1972 - 1985					1985 - 1992				
Point id	Δr (ft)	Δl (ft)	Δw (ft)	Δt (yrs)	M (ft/yr)	Δr (ft)	Δl (ft)	Δw (ft)	Δt (yrs)	M (ft/yr)	
1 (u/s)	124.3	72.8	190.3	13	0.5	4.4	20.2	-27.6	7	7.5	
2	99.6	73.8	182.3	13	-0.7	1.8	36.6	11.2	7	3.9	
3	57.1	2.2	56.9	13	0.2	17.9	131.0	143.8	7	0.7	
4	5.8	16.4	13.5	13	0.7	36.9	114.0	169.8	7	-2.7	
5	15.8	60.3	18.6	13	4.4	58.7	21.6	110.8	7	-4.4	
6	21.0	116.7	60.9	13	5.9	89.0	44.5	65.1	7	9.8	
7	110.3	182.5	24.5	13	20.6	118.4	65.4	79.7	7	14.9	
8	218.1	300.0	41.4	13	36.7	206.2	93.0	117.9	7	25.9	
9	299.6	400.9	60.3	13	49.2	229.0	106.1	112.1	7	31.9	
10	357.1	448.1	65.1	13	56.9	243.9	72.2	151.8	7	23.5	
11	408.6	464.4	59.1	13	62.6	265.7	64.8	178.7	7	21.7	
12	368.1	466.8	87.8	13	57.5	187.1	40.4	147.9	7	11.4	
13	328.6	421.3	56.9	13	53.3	87.9	9.2	138.2	7	-5.9	
14	245.1	317.2	59.2	13	38.7	14.4	94.1	129.8	7	-3.0	
15	216.6	290.8	52.1	13	35.0	20.6	103.3	105.0	7	2.7	
16	102.1	217.1	68.7	13	19.3	56.1	135.0	99.0	7	13.1	
17	27.2	130.4	71.5	13	6.6	47.0	123.2	64.7	7	15.1	
18	55.6	52.9	66.8	13	3.2	37.4	57.8	-24.9	7	17.2	
19	162.2	44.3	15.1	13	14.7	27.6	22.4	-70.4	7	17.2	
20 (d/s)	252.4	132.6	76.0	13	23.8	3.3	82.8	-122.9	7	29.9	
	66				24					79	12
	(Average)				(Average)		(Average)			(Average)	

1972 - 1992					
Point id	Δr (ft)	Δl (ft)	Δw (ft)	Δt (yrs)	M (ft/yr)
1 (u/s)	119.9	52.6	162.7	20	0.5
2	100.1	110.4	193.5	20	0.8
3	75.0	133.1	200.7	20	0.4
4	42.7	130.4	183.3	20	-0.5
5	42.9	81.8	129.4	20	-0.2
6	68.0	72.2	125.9	20	0.7
7	8.3	117.1	104.2	20	1.1
8	12.0	207.0	159.2	20	3.0
9	70.6	294.8	172.4	20	9.6
10	113.2	375.9	216.9	20	13.6
11	142.9	399.6	237.8	20	15.2
12	181.0	426.4	235.7	20	18.6
13	240.6	430.4	195.1	20	23.8
14	230.7	411.3	189.0	20	22.6
15	237.2	394.1	157.1	20	23.7
16	158.1	352.1	167.8	20	17.1
17	74.1	253.5	136.2	20	9.6
18	18.2	110.7	41.9	20	4.3
19	134.6	21.9	-55.3	20	10.6
20 (d/s)	255.7	215.4	-46.9	20	25.9
	145				10
	(Average)				(Average)

- Apex early year
- Apex late year
- Apex same year

Table M-24: Migration rate calculations for bend 4 (1972-1992).

Bend 4 Point id	1972 - 1985					1985 - 1992						
	Δr (ft)	Δl (ft)	Δw (ft)	Δt (yrs)	M (ft/yr)	Δr (ft)	Δl (ft)	Δw (ft)	Δt (yrs)	M (ft/yr)		
1 (u/s)	309.5	495.9	-10.3	13	62.7	30.8	31.0	177.1	7	-16.5		
2	190.0	439.8	34.6	13	45.8	25.4	28.5	194.2	7	-20.1		
3	76.9	344.6	76.7	13	26.5	73.8	119.7	195.5	7	-0.3		
4	2.0	211.5	57.8	13	12.0	49.9	190.3	221.3	7	2.7		
5	72.5	90.9	38.6	13	9.6	43.0	147.1	96.7	7	13.3		
6	150.2	46.4	6.1	13	14.7	26.0	18.9	-56.9	7	14.5		
7	231.8	127.1	69.4	13	22.3	5.1	73.7	-108.4	7	26.8		
8	314.2	129.7	175.5	13	20.7	25.3	185.1	-203.8	7	59.2		
9	363.2	104.9	257.3	13	16.2	90.2	336.4	-254.2	7	97.3		
10	338.4	92.0	244.5	13	14.3	121.9	367.8	-245.5	7	105.0		
11	313.7	67.1	243.9	13	10.5	137.1	377.7	-238.0	7	107.5		
12	280.5	45.5	230.6	13	7.3	145.3	380.5	-234.7	7	108.6		
13	237.2	54.2	179.9	13	8.6	137.8	328.8	-198.1	7	95.0		
14	207.4	46.8	157.0	13	7.5	123.4	275.6	-154.4	7	79.1		
15	176.4	23.6	150.2	13	3.8	106.5	245.8	-142.9	7	70.7		
16	133.8	10.0	118.8	13	1.9	103.6	211.3	-113.9	7	61.2		
17	67.3	7.4	57.4	13	1.3	85.7	155.4	-84.8	7	46.6		
18	5.2	5.2	9.6	13	0.1	55.8	123.5	-74.2	7	36.2		
19	32.5	5.5	-37.1	13	5.8	30.3	68.1	-48.6	7	21.0		
20 (d/s)	54.5	46.8	-101.4	13	15.6	21.9	34.6	-11.0	7	9.6		
	98				15		-64				46	
	(Average)				(Average)		(Average)				(Average)	

Point id	1972 - 1992					
	Δr (ft)	Δl (ft)	Δw (ft)	Δt (yrs)	M (ft/yr)	
1 (u/s)	278.7	465.0	166.8	20	28.8	
2	215.2	468.3	228.9	20	22.7	
3	150.8	464.3	272.2	20	17.1	
4	51.9	401.7	279.1	20	8.7	
5	29.5	237.9	135.3	20	6.6	
6	124.2	27.6	-50.9	20	10.1	
7	226.7	200.8	-39.1	20	23.3	
8	339.5	314.8	-28.4	20	34.1	
9	453.5	441.3	3.0	20	44.6	
10	460.3	459.9	-1.0	20	46.1	
11	450.8	444.8	5.9	20	44.5	
12	425.8	426.0	-4.2	20	42.8	
13	375.0	383.0	-18.2	20	38.8	
14	330.8	322.4	2.6	20	32.5	
15	282.9	269.5	7.2	20	27.3	
16	237.3	221.2	4.9	20	22.7	
17	153.0	162.8	-27.4	20	17.2	
18	60.9	118.4	-64.5	20	12.2	
19	2.2	73.4	-85.7	20	8.1	
20 (d/s)	32.6	81.4	-112.4	20	11.3	
	34				25	
	(Average)				(Average)	

- Apex early year
- Apex late year
- Apex same year

Table M-25: Migration rate calculations for bend 5 (1972-1992).

Bend 5 Point id	1972 - 1985					1985 - 1992				
	Δr (ft)	Δl (ft)	Δw (ft)	Δt (yrs)	M (ft/yr)	Δr (ft)	Δl (ft)	Δw (ft)	Δt (yrs)	M (ft/yr)
1 (u/s)	320.0	661.3	-361.0	13	103.3	104.7	237.8	415.5	7	-10.4
2	237.2	493.3	-234.4	13	74.2	172.0	161.1	396.0	7	-9.0
3	154.6	229.4	-93.7	13	36.7	222.8	2.5	304.2	7	-11.3
4	51.6	135.3	-57.3	13	18.8	309.3	28.1	351.8	7	-2.1
5	10.9	51.4	-69.8	13	10.2	406.8	149.2	359.1	7	28.1
6	5.7	157.8	152.8	13	0.8	366.9	15.8	155.6	7	32.4
7	1.2	190.3	191.3	13	0.0	89.4	0.1	55.9	7	4.8
8	18.2	223.6	204.0	13	2.9	44.4	7.5	32.7	7	2.7
9	38.6	244.4	205.1	13	6.0	34.5	16.2	50.2	7	0.1
10	38.7	247.7	208.8	13	6.0	21.6	40.7	62.6	7	0.0
11	55.9	217.0	160.1	13	8.7	10.1	73.6	83.6	7	0.0
12	81.7	138.0	56.4	13	12.6	7.0	121.3	129.2	7	-0.1
13	72.7	122.8	49.6	13	11.2	13.3	132.5	118.5	7	3.9
14	71.5	103.3	32.1	13	11.0	21.2	133.0	111.2	7	6.1
15	85.8	87.5	1.4	13	13.2	17.1	84.4	73.0	7	4.1
16	79.2	10.7	-90.4	13	13.9	11.3	101.5	113.6	7	-0.1
17	65.0	50.1	-114.9	13	17.7	18.0	134.4	152.4	7	0.0
18	40.5	52.7	-92.7	13	14.3	58.3	145.0	203.4	7	0.0
19	27.7	58.4	-86.1	13	13.2	52.5	155.5	208.5	7	-0.1
20 (d/s)	47.6	47.1	-94.4	13	14.5	84.6	145.8	60.3	7	24.3
			-1.7		19			172		3.7
			(Average)		(Average)			(Average)		(Average)

Point id	1972 - 1992				
	Δr (ft)	Δl (ft)	Δw (ft)	Δt (yrs)	M (ft/yr)
1 (u/s)	424.6	423.5	54.4	20	39.7
2	409.2	332.2	161.6	20	29.0
3	377.4	227.5	210.5	20	19.7
4	360.9	107.2	294.5	20	8.7
5	396.0	97.8	289.3	20	10.2
6	361.4	173.5	308.4	20	11.3
7	90.5	190.4	247.1	20	1.7
8	26.3	216.1	236.7	20	0.3
9	4.1	260.5	255.3	20	0.5
10	17.1	288.4	271.4	20	1.7
11	45.9	290.6	243.6	20	4.6
12	74.8	259.3	185.6	20	7.4
13	86.1	255.3	168.1	20	8.7
14	92.7	236.3	143.3	20	9.3
15	68.8	172.0	74.4	20	8.3
16	67.9	90.9	23.2	20	6.8
17	47.0	84.3	37.5	20	4.7
18	18.0	92.3	110.7	20	0.0
19	25.0	97.1	122.5	20	0.0
20 (d/s)	132.1	98.8	-34.1	20	13.3
			170		9.3
			(Average)		(Average)

- Apex early year
- Apex late year
- Apex same year

Table M-26: Migration rate calculations for bend 6 (1985-1992).

Bend 6	1985 - 1992				
Point id	Δr (ft)	Δl (ft)	Δw (ft)	Δt (yrs)	M (ft/yr)
1 (u/s)	21.3	41.2	62.2	7	0.0
2	42.3	36.7	78.9	7	0.0
3	37.8	19.7	57.2	7	0.0
4	21.9	2.9	24.5	7	0.0
5	109.8	11.0	113.5	7	1.0
6	219.8	2.4	199.3	7	3.3
7	150.6	5.4	144.5	7	1.6
8	161.9	8.1	180.0	7	-1.4
9	189.6	43.3	242.7	7	-1.4
10	133.0	99.9	231.0	7	0.3
11	110.4	101.0	210.2	7	0.2
12	209.3	70.6	250.3	7	4.2
13	203.9	51.5	254.4	7	0.1
14	110.8	73.8	181.7	7	0.4
15	81.3	28.8	110.2	7	0.0
16	113.9	30.4	144.2	7	0.0
17	128.5	7.5	136.4	7	-0.1
18	116.4	8.0	108.2	7	2.3
19	59.4	10.3	69.6	7	0.0
20 (d/s)	12.0	24.9	36.6	7	0.0
	142				0.5
	(Average)				(Average)




-  Apex early year
-  Apex late year
-  Apex same year

Table M-27: Migration rate calculations for bend 7 (1972-1992).

Bend 7 Point id	1972 - 1985					1985 - 1992				
	Δr (ft)	Δl (ft)	Δw (ft)	Δt (yrs)	M (ft/yr)	Δr (ft)	Δl (ft)	Δw (ft)	Δt (yrs)	M (ft/yr)
1 (u/s)	53.3	124.0	72.3	13	8.1	8.7	9.1	-2.0	7	2.8
2	45.3	127.9	83.4	13	6.9	4.3	15.7	-19.0	7	5.6
3	51.1	104.5	55.4	13	7.7	2.6	35.7	-38.4	7	11.0
4	70.0	78.7	10.6	13	10.6	19.8	36.8	-16.3	7	10.4
5	57.2	26.3	-29.7	13	8.7	31.0	7.1	38.1	7	0.0
6	47.4	15.1	-31.3	13	7.2	23.5	0.8	23.0	7	0.2
7	28.8	22.1	-57.2	13	8.3	21.2	1.3	17.5	7	0.7
8	25.6	93.6	-129.8	13	19.2	38.5	4.3	42.7	7	0.0
9	32.0	166.7	-206.6	13	31.2	46.6	18.6	62.2	7	0.4
10	6.1	221.8	-241.5	13	36.1	39.9	11.8	46.4	7	0.8
11	82.1	268.8	-186.1	13	41.3	21.6	2.2	15.0	7	1.3
12	141.0	297.5	-157.3	13	45.8	16.5	11.3	23.9	7	0.6
13	184.3	292.7	-107.6	13	45.0	26.7	33.2	60.3	7	-0.1
14	213.6	305.4	-89.5	13	46.8	27.9	81.5	109.1	7	0.0
15	245.3	287.7	-41.5	13	44.2	20.4	125.1	132.7	7	1.8
16	241.6	252.2	-7.5	13	38.6	22.0	132.1	152.7	7	0.2
17	226.5	229.0	-7.7	13	35.6	13.4	148.6	142.9	7	2.7
18	172.0	162.4	-27.0	13	27.8	6.0	149.3	136.7	7	2.7
19	88.3	92.0	-50.4	13	17.7	21.3	154.1	159.3	7	2.3
20	15.3	30.3	-85.4	13	10.1	34.9	98.2	156.4	7	-3.3
21	119.3	24.6	-111.7	13	19.7	50.1	45.1	106.7	7	-1.6
22 (d/s)	181.8	77.9	-99.8	13	27.7	52.3	5.8	53.9	7	0.6
		-66		25		64		1.8		
		(Average)		(Average)		(Average)		(Average)		

Point id	1972 - 1992				
	Δr (ft)	Δl (ft)	Δw (ft)	Δt (yrs)	M (ft/yr)
1 (u/s)	44.6	114.9	70.3	20	4.5
2	49.7	112.2	64.4	20	4.9
3	53.4	68.7	16.9	20	5.3
4	50.2	41.9	-5.7	20	4.9
5	26.2	33.4	8.4	20	2.6
6	24.0	15.8	-8.3	20	2.4
7	7.5	22.1	-39.7	20	3.5
8	13.0	89.4	-87.1	20	9.5
9	14.6	148.1	-144.4	20	15.4
10	33.9	210.0	-195.1	20	22.0
11	103.7	266.8	-171.1	20	27.1
12	157.6	286.4	-133.4	20	28.9
13	211.0	259.6	-47.3	20	25.9
14	241.5	223.9	19.5	20	22.3
15	265.6	162.6	91.2	20	16.9
16	263.5	120.1	145.2	20	11.9
17	239.9	80.4	135.3	20	9.2
18	178.1	13.2	109.7	20	4.1
19	109.6	62.1	108.9	20	3.1
20	19.7	67.9	71.0	20	0.8
21	69.3	69.7	-5.0	20	7.2
22 (d/s)	129.5	83.7	-45.9	20	13.0
		-1.9		11	
		(Average)		(Average)	

- Apex early year
- Apex late year
- Apex same year

**APPENDIX N:
Curvature Plots**

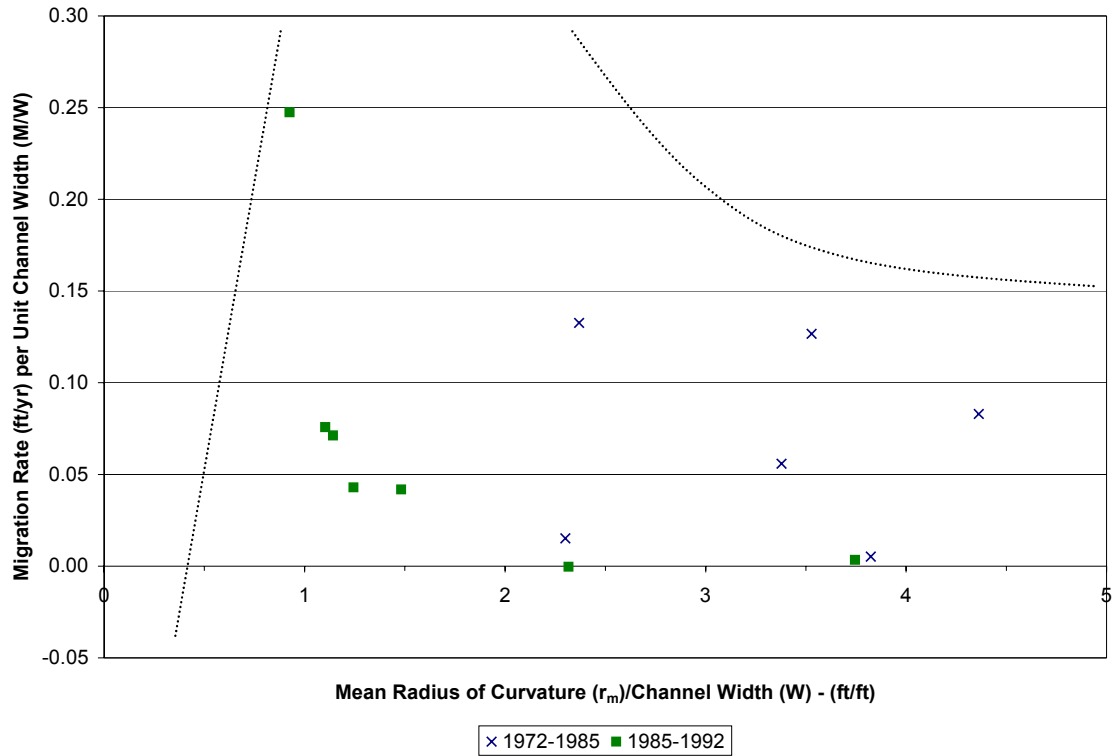


Figure N-1: Relative migration rate versus r_m/W (apex area averaged).

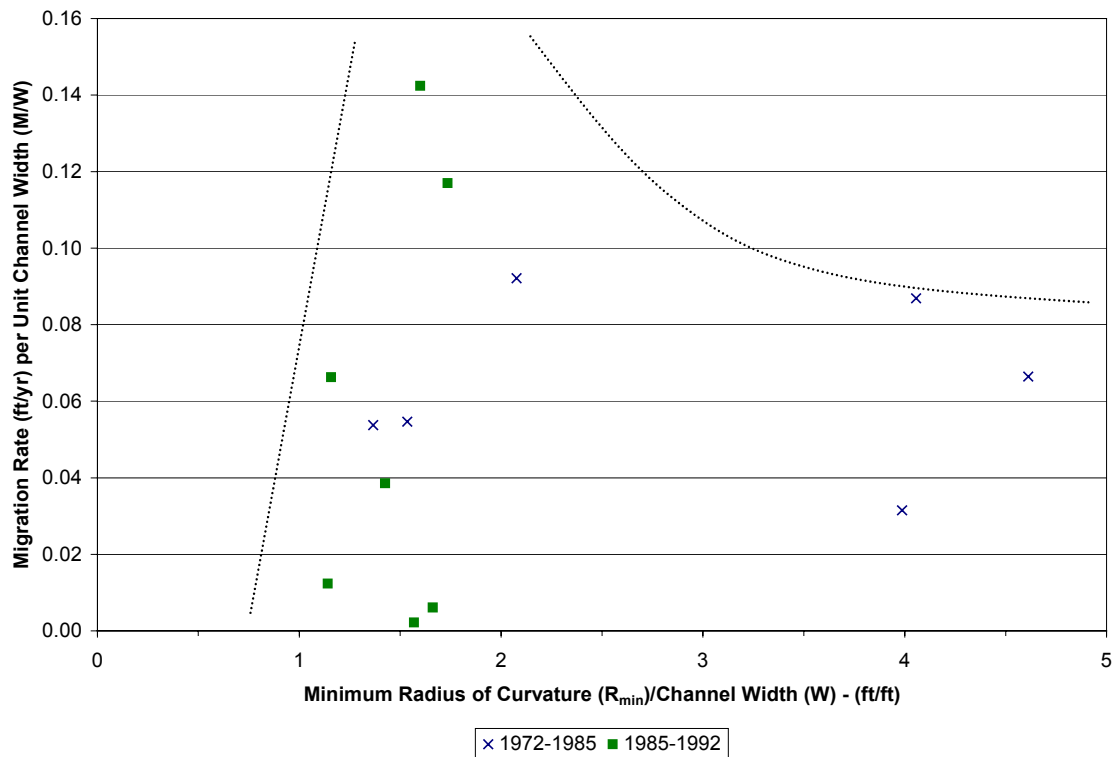


Figure N-2: Relative migration rate versus R_{min}/W (bend averaged).

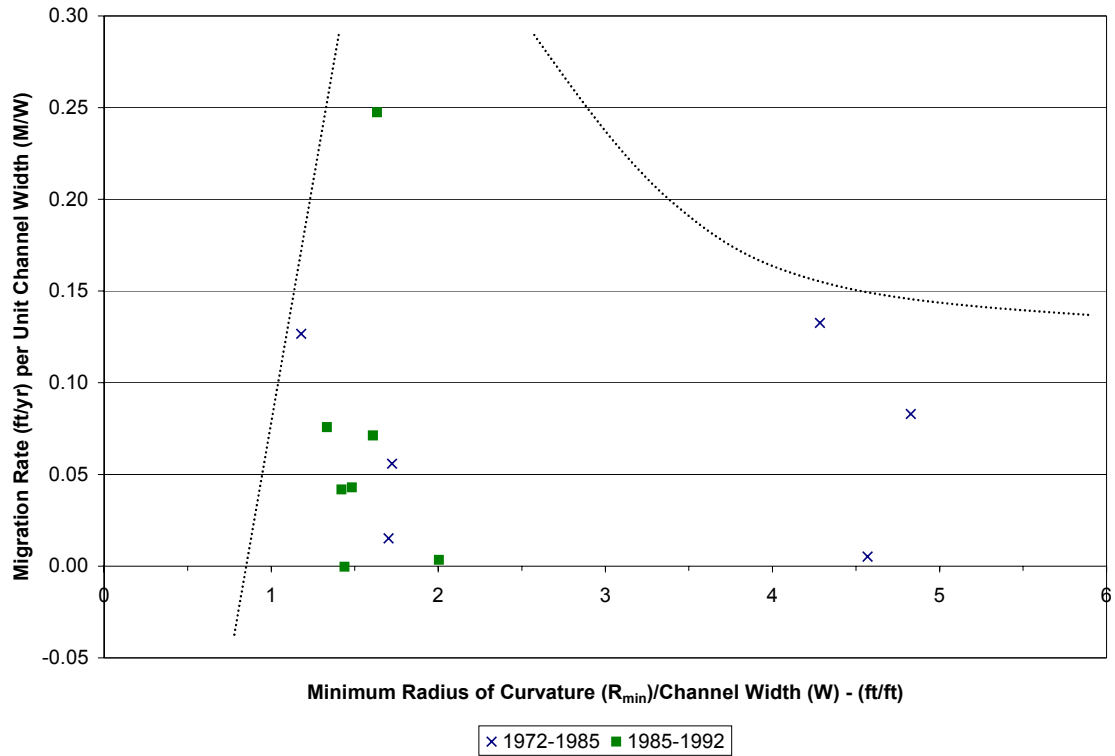


Figure N-3: Relative migration rate versus R_{min}/W (apex area averaged).

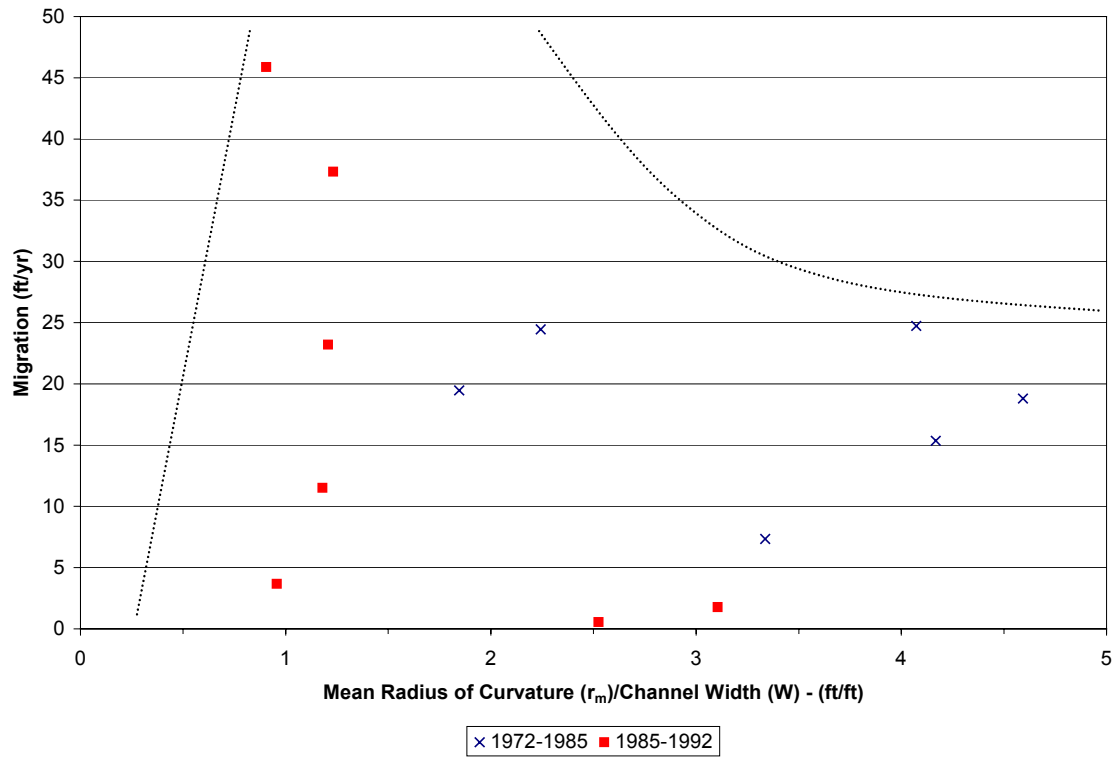


Figure N-4: Migration rate versus r_m/W (bend averaged).

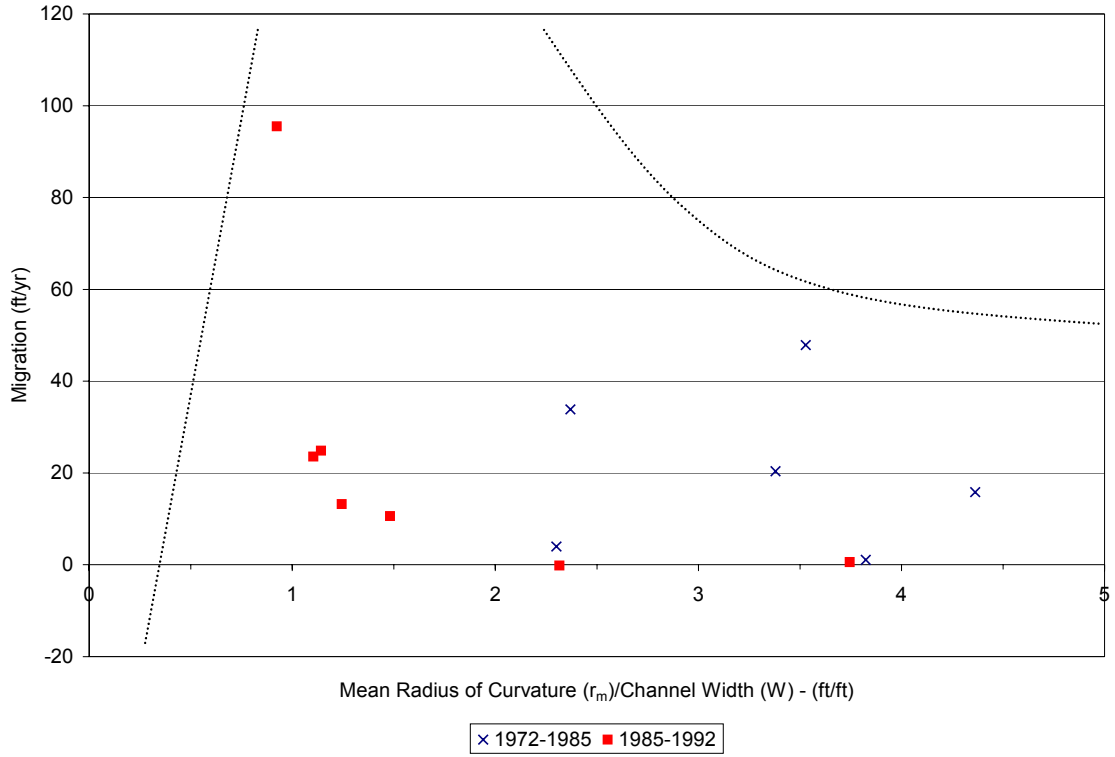


Figure N-5: Migration rate versus r_m/W (apex area averaged).

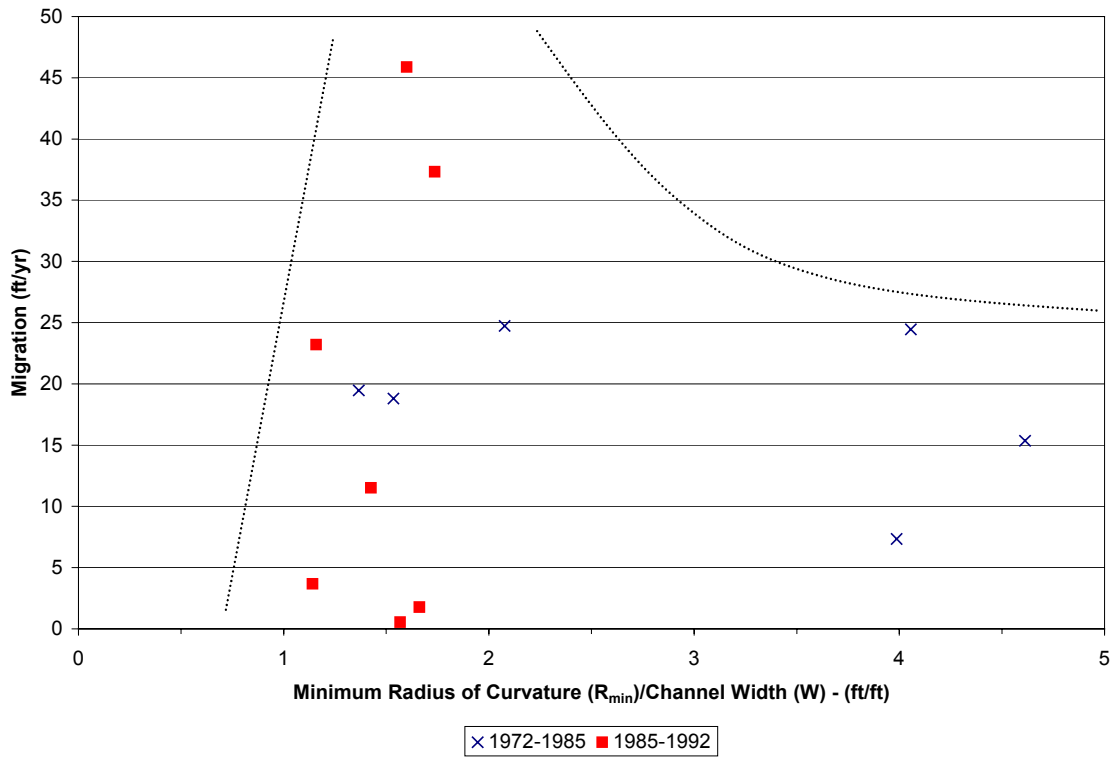


Figure N-6: Migration rate versus R_{min}/W (bend averaged).

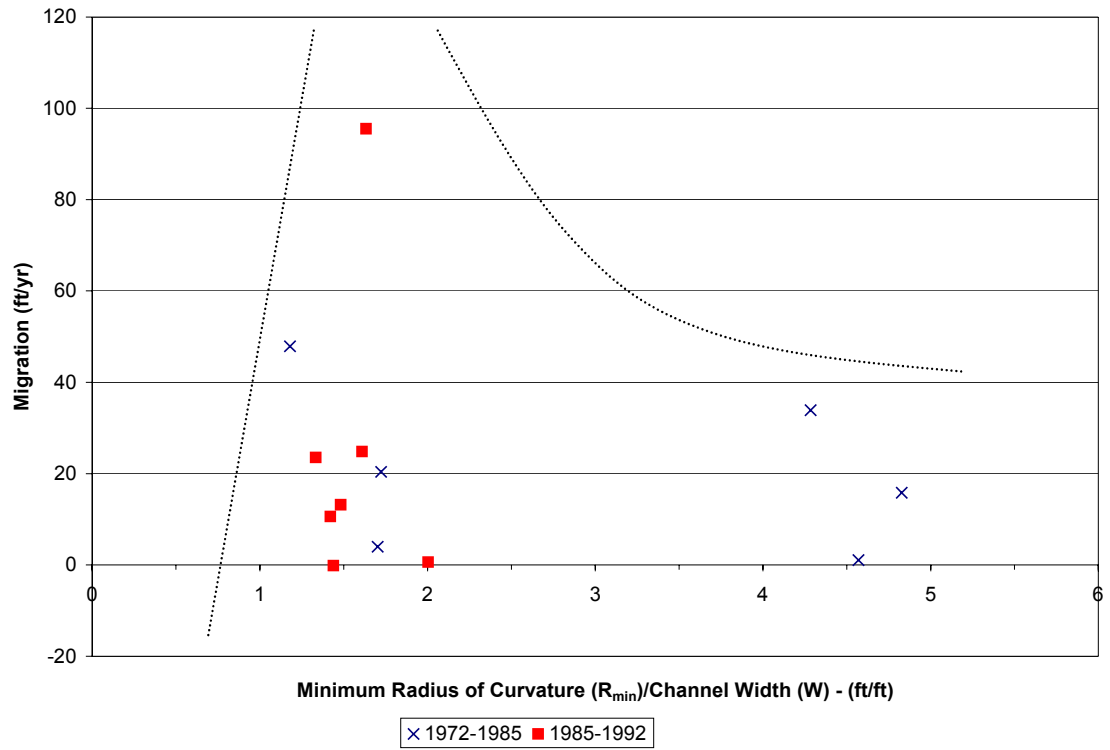


Figure N-7: Migration rate versus R_{min}/W (apex area averaged).

APPENDIX O:
Sine Generated Curves

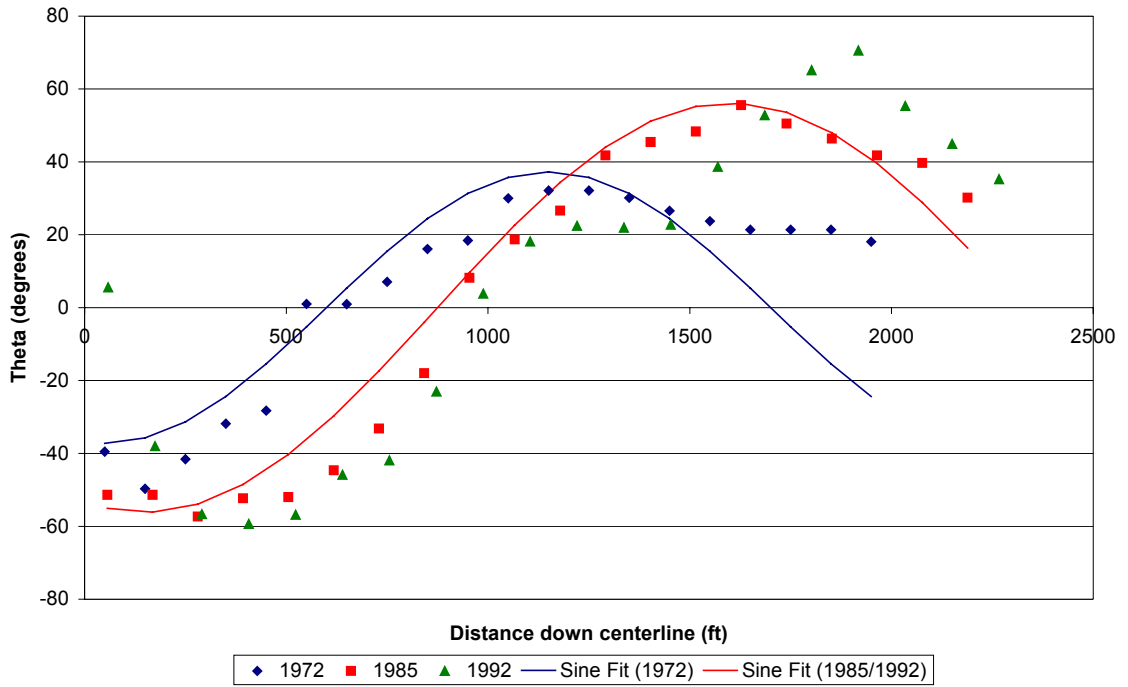


Figure O-1: Sine generated curves for bend 1 (1972, 1985 and 1992).

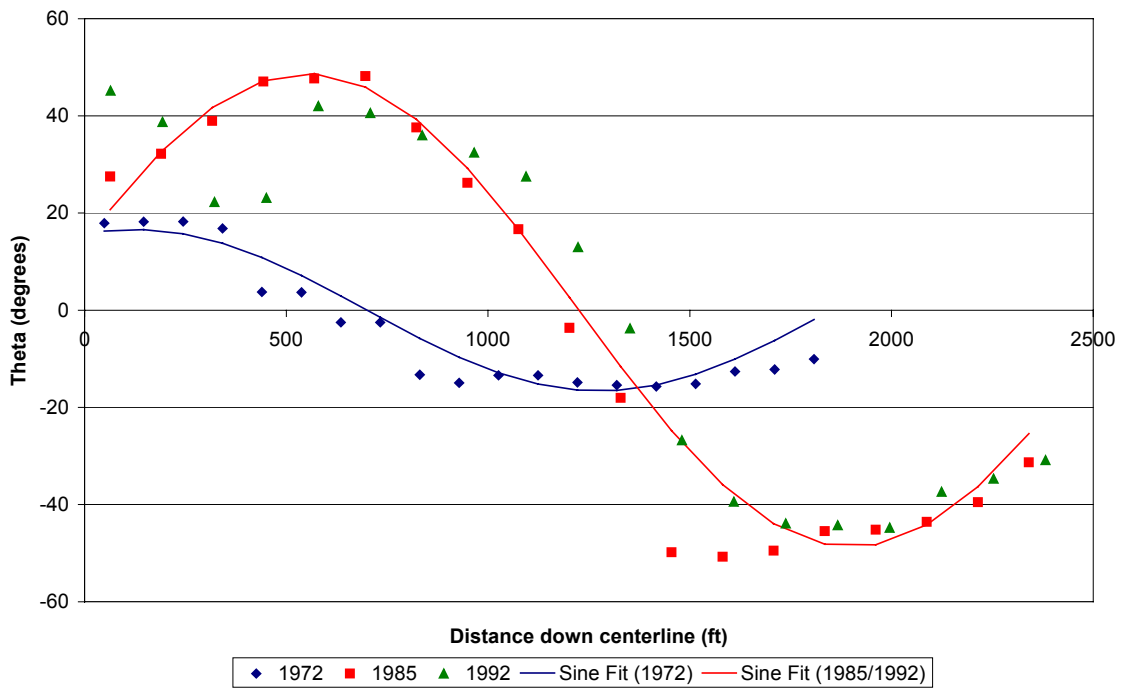


Figure O-2: Sine generated curves for bend 3 (1972, 1985 and 1992).

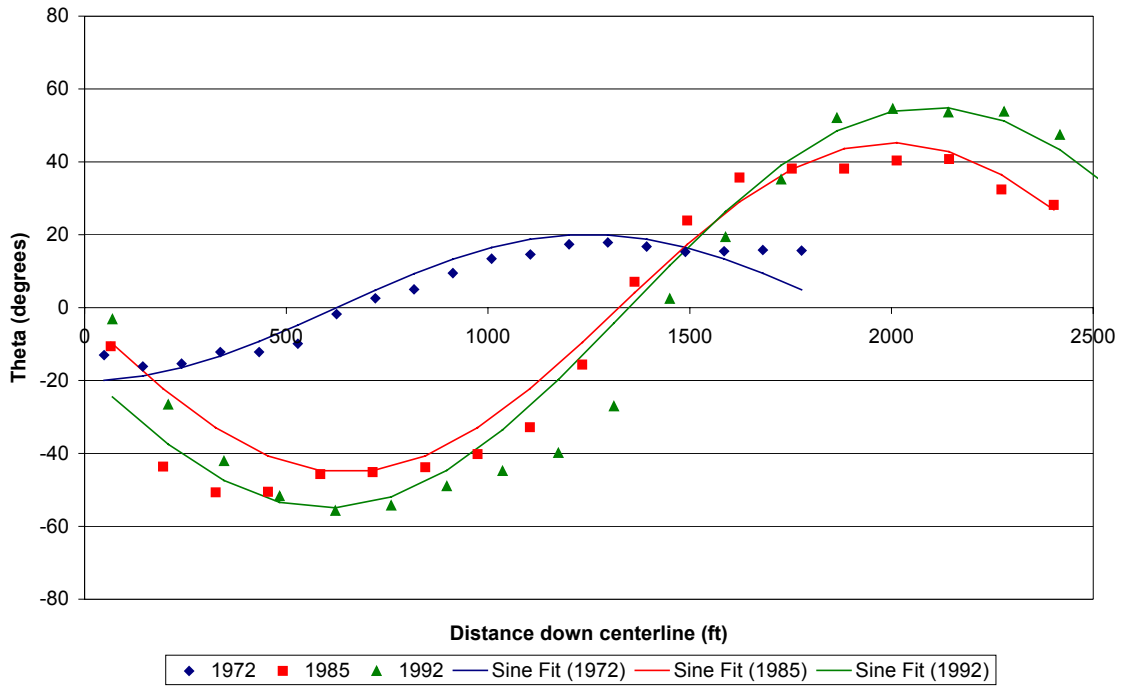


Figure O-3: Sine generated curves for bend 4 (1972, 1985 and 1992).

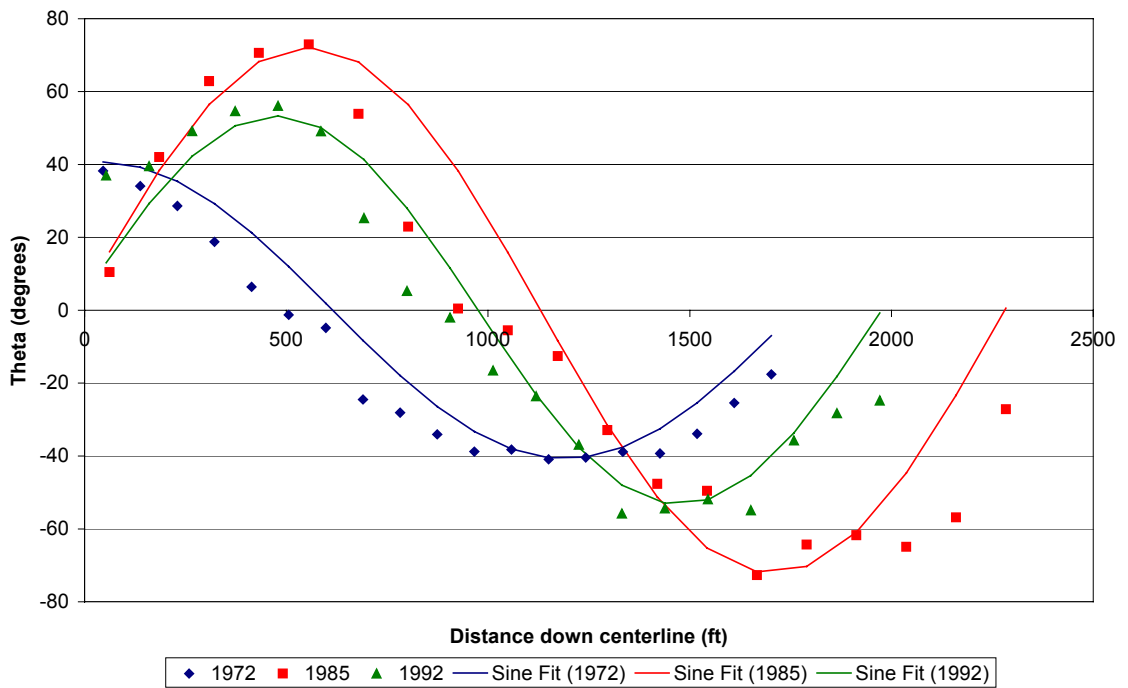


Figure O-4: Sine generated curves for bend 5 (1972, 1985 and 1992).

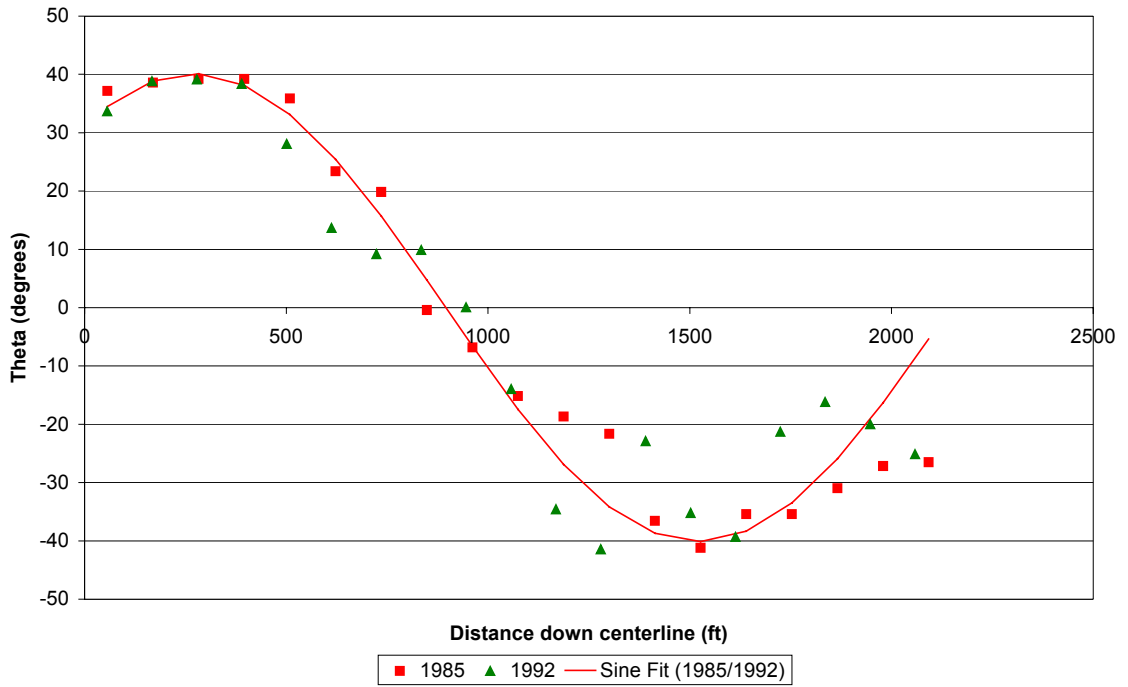


Figure O-5: Sine generated curves for bend 6 (1985 and 1992).

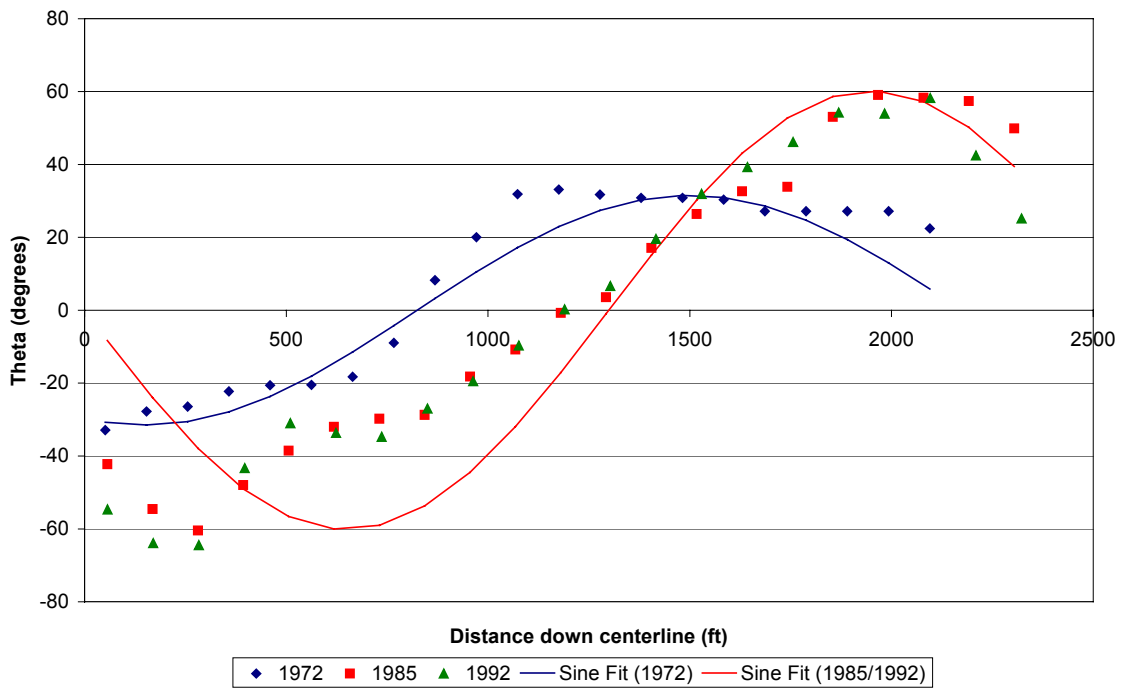


Figure O-6: Sine generated curves for bend 7 (1972, 1985 and 1992).

APPENDIX P:
Migration (M) and Width-to-Depth (W/h) Ratio Trends

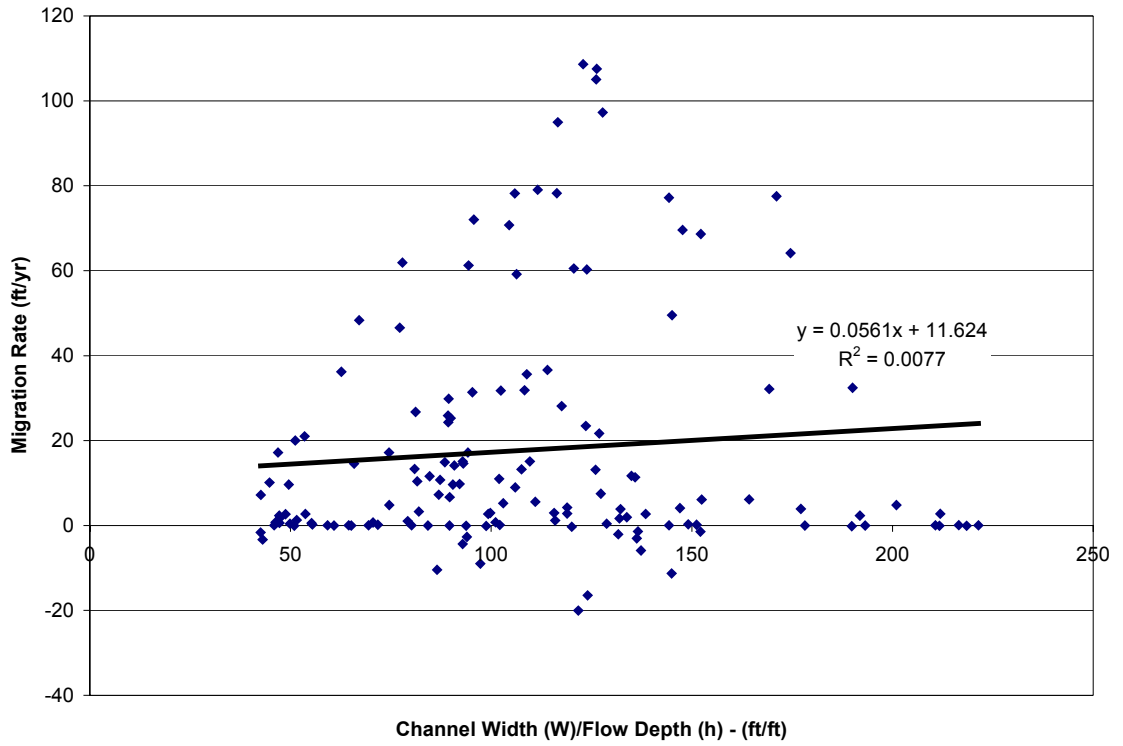


Figure P-1: M versus W/h for 1985-1992 time period (Galisteo Reach).

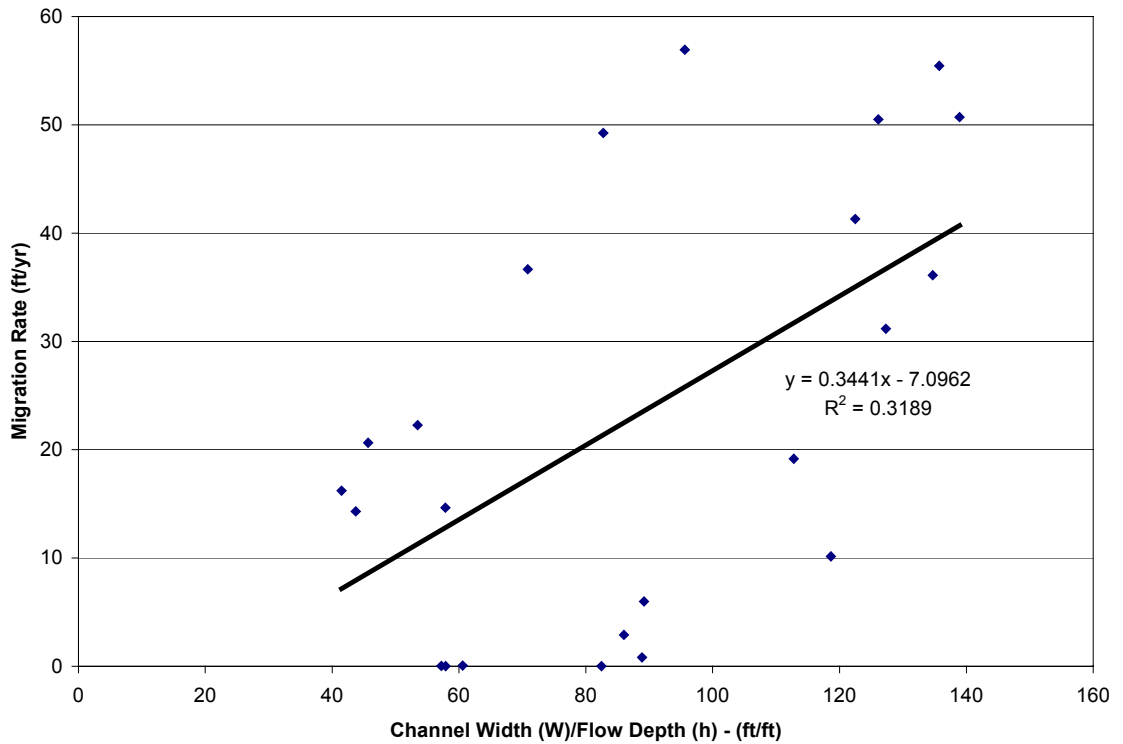


Figure P-2: M versus W/h for 1972-1985 time period (apex area).

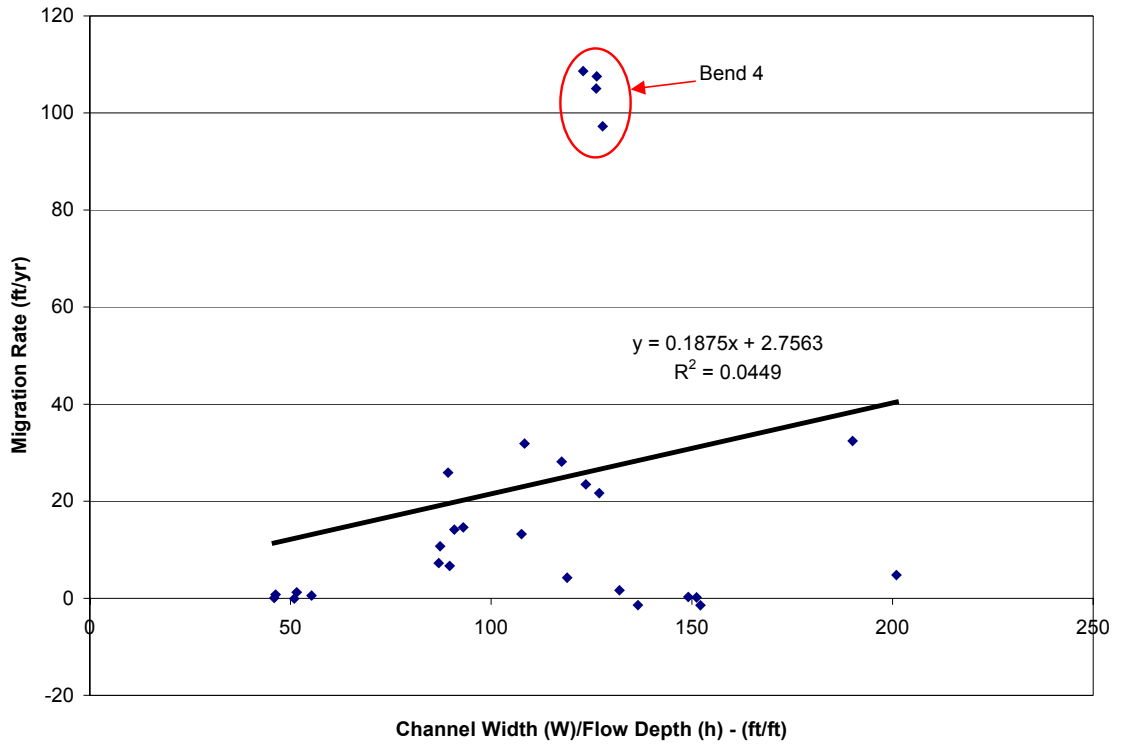


Figure P-3: M versus W/h for 1985-1992 time period (apex area).

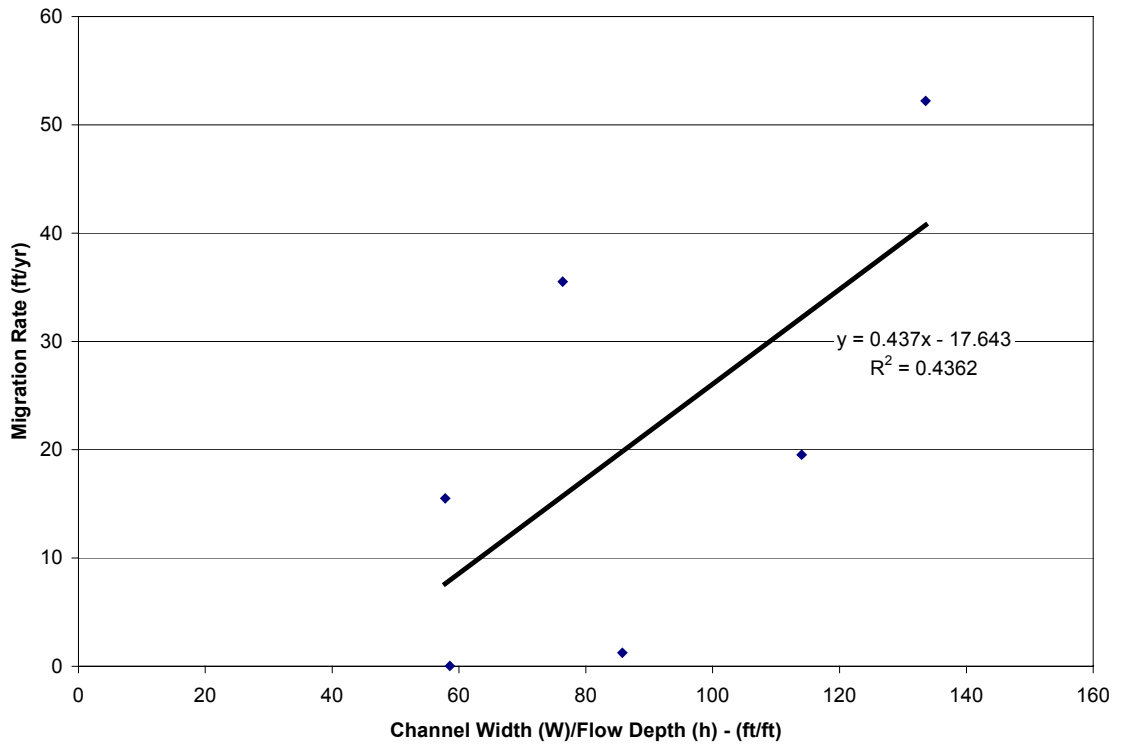


Figure P-4: M versus W/h for 1972-1985 time period (bends 1,2,3,4,5 and 7).

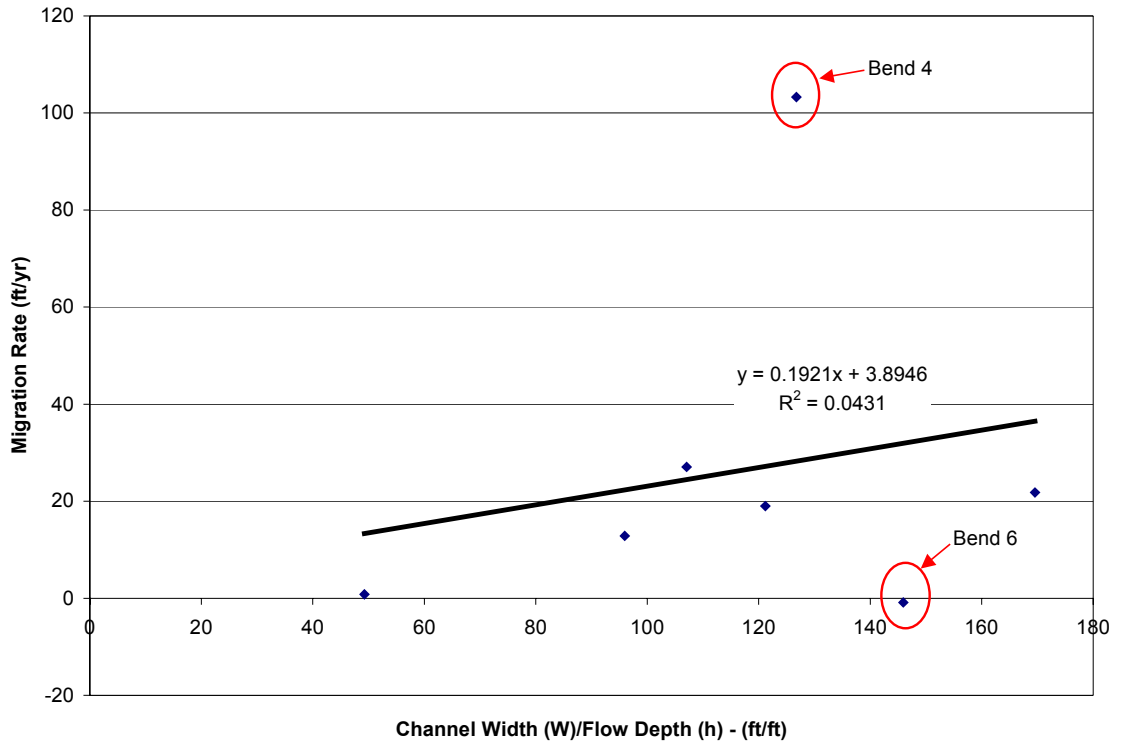


Figure P-5: M versus W/h for 1985-1992 time period (all bends).

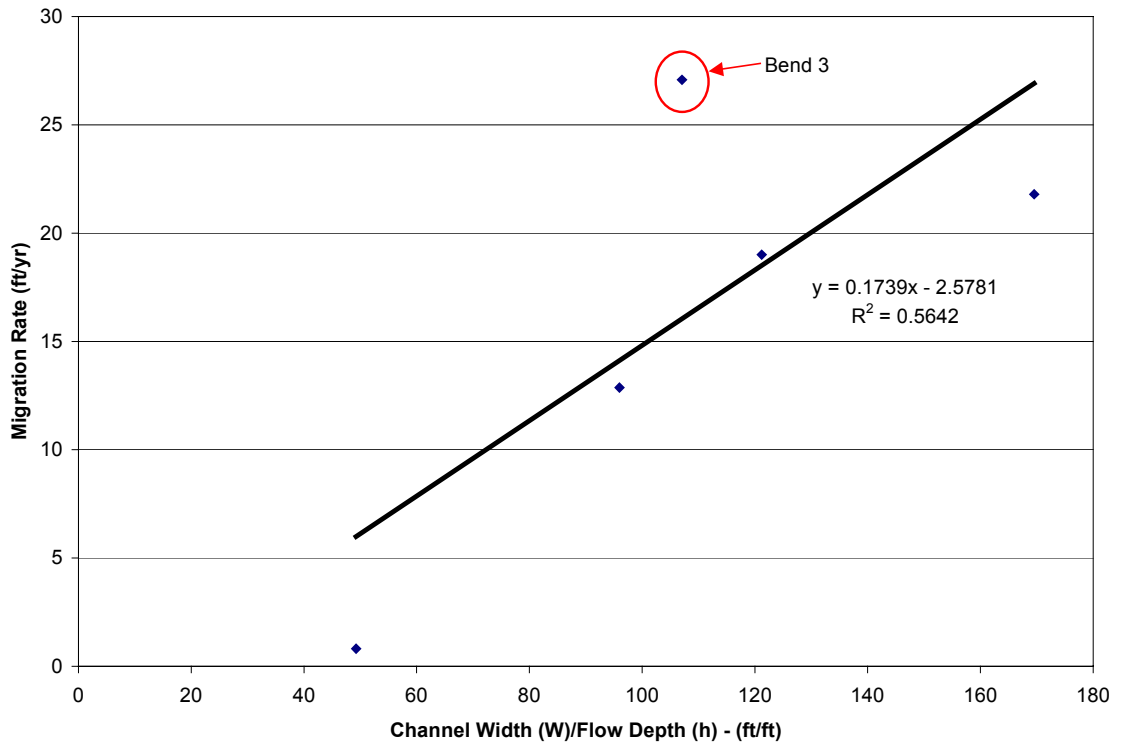


Figure P-6: M versus W/h for 1985-1992 time period (bends 1,2,3,5 and 7).

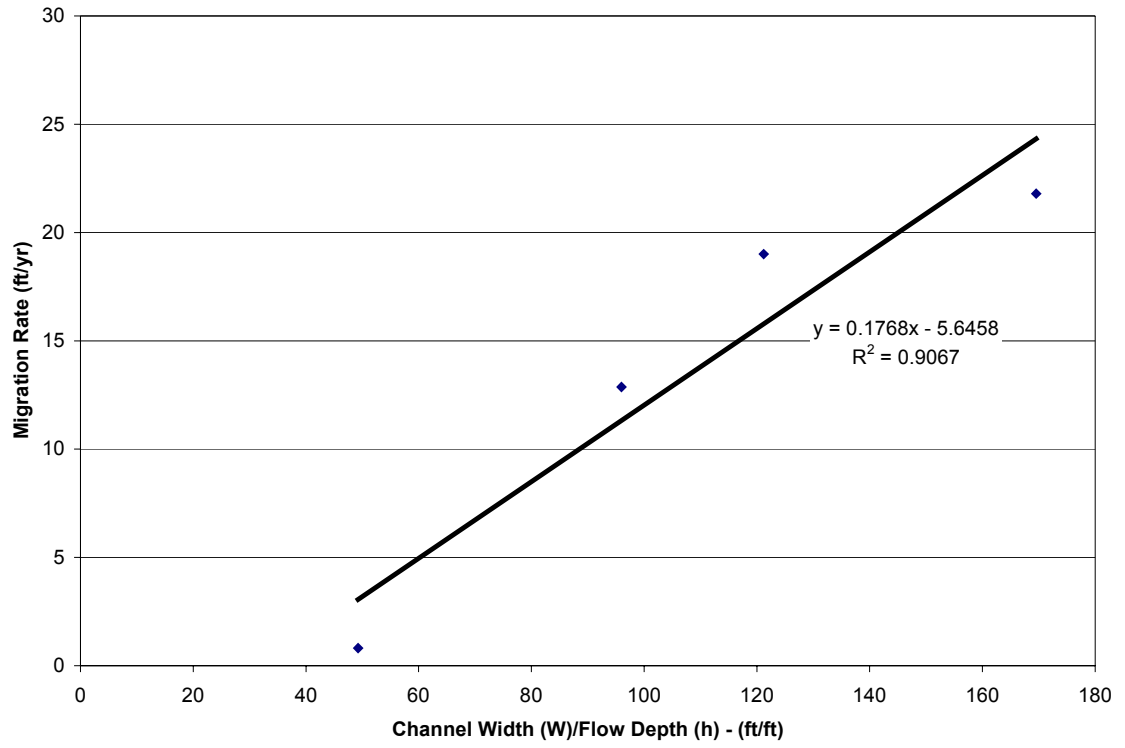


Figure P-7: M versus W/h for 1985-1992 time period (bends 1,2,5 and 7).